The autism and schizophrenia associated genes CYFIP1 and Ahi1 in synaptic signalling and neuronal development

Elizabeth Claire Davenport

A thesis submitted to University College London for the degree of Doctor of Philosophy

27th August 2015

Department of Neuroscience, Physiology and Pharmacology
University College London

I, Elizabeth Claire Davenport, confirm that the work presented in this thesis is my own. Where information has been derived from other sources, I confirm that this has been indicated in the thesis.

Abstract

Correct regulation of synaptic function is essential for normal brain activity. Disrupted synaptic signalling can result in a loss of neuronal contacts and altered morphology, leading to deficits in network activity and transmission; features of neuropsychiatric disorders. Indeed, defects in neuronal and synapse morphology are detected in autism and schizophrenia and thought to contribute to the characteristic behavioural abnormalities observed in these conditions. In this thesis the role of two neuropsychiatric disease associated proteins, CYFIP1 and Ahi1, in the regulation of synaptic function and neuronal morphology were investigated. First, this study revealed that CYFIP1 and CYFIP2 were enriched at excitatory synapses. Altering CYFIP1 gene dosage to model disease states showed that CYFIP1 affected dendritic complexity, spine morphology and spine actin dynamics. Inhibitory synapse integrity was also disrupted with increased CYFIP1 or CYFIP2 dosage. Secondly, genetic studies revealed a significant association of CYFIP1 with schizophrenia, contributing to the evidence that CYFIP1 is a risk locus for this condition. However, CYFIP1 schizophrenia-associated mutations identified here did not interfere with CYFIP1 localisation or protein interactions. Novel CYFIP1 knockout (KO) systems were characterised to further understand CYFIP1 function. Initial observations revealed CYFIP1 KO reduced viability and impaired F-actin levels in fast dividing cells while conditional KO of CYFIP1 in adult CA1 neurons disrupted dendritic complexity. Lastly, a novel Ahi1/HAP1/KIF5 trafficking complex was identified in brain. However, the trafficking of $GABA_A$Rs, known HAP1/KIF5 cargo, was unaffected by altered Ahi1 expression. Nevertheless, Ahi1 was localised to synapses and Ahi1 knockdown enhanced dendritic complexity. In summary, this thesis provides evidence that altered expression or disease associated mutations in CYFIP1 and Ahi1 led to changes in synapse integrity and dendritic complexity, both of which may contribute to the development of the neurological symptoms observed in autism and schizophrenia.

Acknowledgements

I could not have written this thesis without the guidance, help and support of a rather long list of people, I therefore have a number of people to thank. Firstly, I would like to thank my supervisor Josef Kittler for allowing me work in the lab, his guidance and support over the last five years have been invaluable. I would like to thank Manav for his contributions to the CYFIP project and Andrew McQuillin, Dave Curtis, Alessia and Niamh for their contributions and help with the SNP genotyping project.

Secondly, I would like to say a big thank you all the members of the Kittler lab, past and present. In particular, Kate, Ali, Lorena and Guillermo for teaching me such a lot in the beginning. A special mention goes to Victoria (my rotation and office buddy) for much fun and laughter in the early years and to the rest of our 'group' Ramona, Terri and Roz. A huge thank you to Nathalie and Nicol for your great friendship. Nathalie, I can always rely on you to be ready with a brew and gossip when I need it the most. Nicol, your Italian ways never stop making me smile and have made life at the bench so much fun.

My housemates in London need an enormous shout out. I never quite feel like I've got everything off my chest until it has been talked through over some trash TV! Anna, Catherine and Louisa thank you all so much for listening, giving me advice and being proof that you can do it. I am lucky to have such incredible friends. I must thank my family. Mum and Dad, thank you for supporting my choices and for always being at the end of the phone. Natalie and Chris, between the jokes about forever being a student, thank you for your support too.

Lastly, I want to thank Pete. His constant support, especially over the last two years, has been tireless. He has helped me though the highs and the lows with his motivational pep talks and patience. Together, and a large number of train journeys later, we've got to this point. With that, there is only one thing left to say; what's the next challenge?!

'The greatest rewards in life come from doing the things that challenge you the most'.

Publications

Publications related to this work:

Pathania, M.*, **Davenport, E.C.***, Muir, J., Sheehan, D.F., López-Doménech, G., and Kittler, J.T. (2014). The autism and schizophrenia associated gene CYFIP1 is critical for the maintenance of dendritic complexity and the stabilization of mature spines. *Translational Psychiatry*. *4*, e374.

*these authors contributed equally to this work.

Other publications:

Smith, K.R., **Davenport, E.C.**, Wei, J., Li, X., Pathania, M., Vaccaro, V., Yan, Z., and Kittler, J.T. (2014). GIT1 and βPIX Are Essential for GABAA Receptor Synaptic Stability and Inhibitory Neurotransmission. *Cell Reports*. *9*, 298–310.

Contents

List of Figures and Tables

Abbreviations

aa	Amino acid
Abi	Abelson-interacting protein
ABP	Actin binding protein
ADHD	Attention defecit hyperactive disorder
Ahi1	Abelson helper integration site 1
AMPA	α-amino-3-hydroxy-5-methyl-4-isoxazolepropionic acid
Arc	Activity-regulated cytoskeletal associated protein
ASD	Autism spectrum disorder
BDNF	Brain derived neurotrophic factor
bp	Base pair
CA	Consitutively active
Cb	Colybistin
CC	Coiled-coil domain
CHC	Clathrin heavy chain
cKO	Conditional knock out
CNS	Central nervous system
CNV	Copy number variation
CYFIP1/2	Cytoplasmic FMRP interacting protein1/2
DH	Dbl homolgy
DHPG	(s)-3,5-dihydrooxyphenyl glycine
DN	Dominant negative
E/I	Excitatory/inhibitory
ER	Endoplasmic reticulum
FMRP	Fragile X mental retardation protein
FRAP	Fluorescence recovery after photobleaching
FXS	Fragile X syndrome
GABA	Gamma-aminobutyric acid
$GABA_AR$	GABA type A receptor
GAD	Glutamic acid decarboxylase
GAP	GTPase activating protein
GBD	GTPase binding domain
GEF	Guanine nucleotide exchange factor
GFP	Green fluorescent protein
GlyR	Glycine receptor
GPCR	G-protein coupled receptor
GWAS	Genome wide association study

HAP1	Huntingtin associated protein 1
ID	Intelectual disability
iGluR	Ionotropic glutamate receptor
JS	Joubert's syndrome
KIF	Kinesin super family
KLC	Kinesin light chain
KO	Knock out
LTD	Long term depression
LTP	Long term potentiation
MAF	Minor allele frequency
mGluR	Metabotropic glutamate receptor
mIPSC	Mini inhibitory postsynaptic current
MR	Mental retardation
MT	Microtubule
mTOR	Mammalian target of rapamycin
NL	Neuroligin
NMDA	N-methyl-D-aspartate receptor
NMJ	Neuromuscular juction
nNOS	Neuronal nitric oxide synthase
NPF	Neuclear promoting factor
Nrxn	Neurexin
NS	Non-synonomous
PDZ	PSD-95/Dlg/ZO-1
PH	Plextrin homolgy
PSD	Post synaptic density
RBP	RNA binding protein
RNAi	RNA interference
RS	Rett's syndrome
SCZ	Schizophrenia
SE	Status epelipticus
SH3	Src homology
SNP	Single nucleotide polymorphism
Sra1	Specific Rac1 associated protein
TARP	Transmembrane AMPA receptor regulatory protein
TGN	Trans golgi network
TM	Transmemrane
Trk	Tyrosine receptor kinase
TS	Tuberous sclerosis
TZ	Transition zone

VCA	verprolin-homology/ cofilin-homology/acidic domain
vGAT	Vesicular GABA transporter
vGlut	Vesicular glutamate transporter
WASP	Wiskott–Aldrich syndrome protein
WAVE	WASP-family verprolin homologous protein 1
WHD	WAVE homology domain
WIP	WASP interacting proteins
WIRS	WRC interacting receptor sequence
WRC	WAVE regulatory complex
WT	Wild-type
XLMR	X-linked mental retardation
Y2H	Yeast two-hybrid
YFP	Yellow fluorescent protein

Chapter 1

Introduction

1.1 Neurons, synapses and transmission

Early studies of neuronal anatomy over 200 years ago proposed that the brain was not a continuous entity, as previously thought, and was in fact composed of many individual neurons capable of communicating with each other. Many years of research later and it is now known that the human brain is made up of a complex network of an estimated 100 billion neurons. In order for our brains to function in memory processing, decision-making and learning these neurons have had to evolve to become highly sophisticated signalling units. They are adapted for long-range intracellular signalling within the cell and short-range intercellular signalling between neurons. A typical neuron consists of a complex architecture of dendrites designed to receive signals from neighbouring cells, a cell soma, which contains the nucleus, and an axon, which in large mammals can extend up to meters in length to reach its target.

Neurons communicate by generating an electrical signal, known as an action potential, which can be propagated along the length of one cell and transmitted to the next at specialised sites. These sites of communication are known as synapses. There are two classes of synapses within the central nervous system (CNS), the chemical synapse, which is the major type of synapse in the brain, and the electrical synapse. In the electrical synapse ion channels, called gap junctions, connect the membranes between two neighbouring cells allowing the passing of ions between cells for fast bidirectional signalling. In a chemical synapse the signal transmission is directional. The electrical impulse from the transmitting cell is converted into a chemical signal at axonal presynaptic boutons which then activates the postsynaptic site on the dendrites of the receiving cell. Upon reaching the presynapse the electrical action potential activates voltage-gated calcium channels, which results in a local rise in intracellular Ca^{2+}. This triggers the fusion of chemical neurotransmitter filled vesicles with the plasma membrane resulting in the release of neurotransmitter into the synaptic cleft. The synaptic cleft is a 20-40nm gap between the pre and postsynapse.

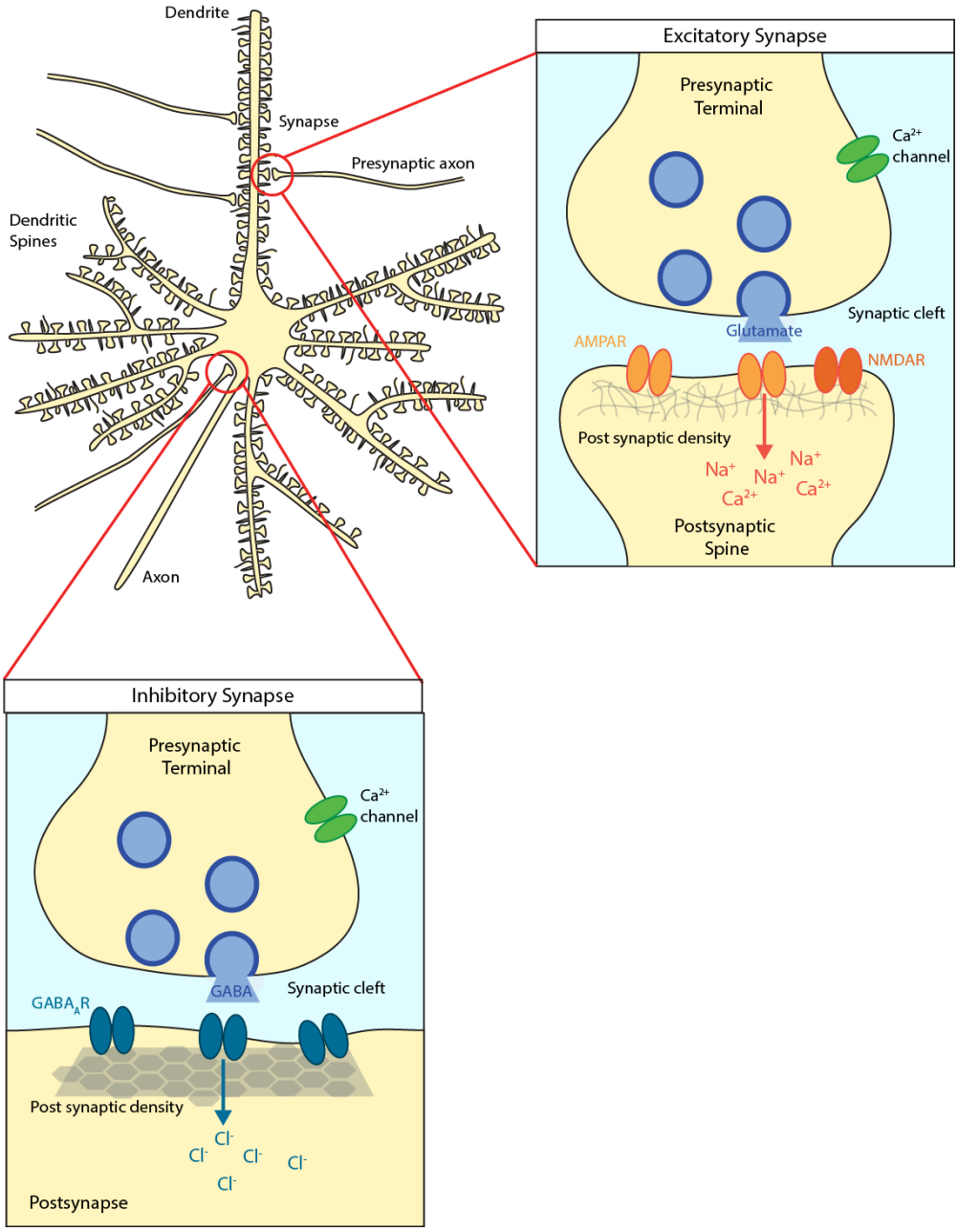

Figure 1.1: Excitatory and inhibitory chemical synapses.

The arrival of an action potential at an axon terminal allows the influx of calcium through voltage-dependent calcium channels, which triggers synaptic vesicle fusion with the plasma membrane releasing neurotransmitter into the synaptic cleft. The main excitatory neurotransmitter is glutamate, which binds to and activates the glutamate ligand-gated ion channel receptors such as NMDA and AMPA receptors that are permeable to sodium and calcium. The main inhibitory neurotransmitter is GABA, which binds to and activates $GABA_A$ receptors which are permeable to chloride ions.

Neurotransmitter diffuses across the cleft and binds to ionotrophic receptors anchored in the membrane of the postsynaptic cell. When stimulated by neurotransmitter these receptors allow the flow of ions into the postsynaptic cell, which either promote or inhibit the firing of a new action potential.

Early electron microscopy studies discovered key differences in the structure of chemical synapses within the vertebrate CNS. Synapses were classified as type 1 (asymmetric) and type 2 (symmetric) based on the width of their electron dense postsynaptic density (PSD) (Gray, 1959). Later, with the identification of synapse type specific neurotransmitters combined with immunohistochemistry, the different structures were labelled excitatory and inhibitory synapses respectively. In mature neurons, excitatory synapses contain ionotropic receptors that are activated by the binding of excitatory neurotransmitters such as glutamate. Upon activation the receptor channels open allowing the fast influx of positively charged ions, such as sodium (Na^+) and calcium (Ca^{2+}) ions, into the postsynaptic cell. This lowers the membrane potential of the cell making it more excitable and increases the likelihood of an action potential firing. In comparison, upon activation of inhibitory synapses, mediated predominantly by the neurotransmitter GABA (γ-aminobutyric acid) in the CNS, ionotropic GABA type A receptors ($GABA_ARs$) open and allow the flow of negatively charged chloride (Cl^-) ions into the cell. In mature neurons, where intracellular chloride is generally low, this increases the membrane potential in the postsynaptic cell, leaving it in a hyperpolarised state, decreasing the chances of an action potential firing. Conversely, in immature neurons in which GABAergic synapses are the first functional synapses to be formed, GABA acts as an excitatory neurotransmitter eliciting membrane depolarisation. This is because young neurons express the Na-K-Cl cotransporter (NKCC1). This enables Cl^- ions to accumulate intracellularly so that when $GABA_ARs$ are activated, Cl^- ions flow out of the cell and cause subsequent membrane depolarisation (Lu et al., 1999; Vardi et al., 2000). It is not until later in development (post-natal days 3-12) that GABA elicits inhibitory effects due to a switch in the transmembrane Cl^- gradient during the maturation of the neurons caused by the expression of the K-Cl cotransporter (KCC2) (Ben-Ari, 2002, 2014). Excitatory and inhibitory synapses act together to modulate neuronal communication and any disruption or damage to this signalling system can impact detrimentally on normal brain function (Figure 1.1).

1.2 The excitatory synapse

Excitatory synapses bring about the depolarisation of the postsynaptic cell, if the appropriate threshold is met, resulting in a new action potential and the transmission of a nerve impulse from one neuron to another. This is the fundamental mechanism of neuronal connectivity and is essential for normal brain function. The main excitatory neurotransmitter within the CNS is glutamate, thus making glutamatergic synapses the main excitatory synapse within the brain. Glutamate binds and activates the ionotropic NMDA, kainate and AMPA receptors and the metabotropic mGluR receptors. NMDA and AMPA receptors have been most intensely studied due to their abundance at glutamatergic synapses and their roles in synaptic plasticity. Synaptic plasticity is the ability of synapses to strengthen or weaken over time in response to increases or decreases in their activity. This strengthening or weakening in synaptic transmission effects response to future stimuli and is thought to underlie learning and memory.

1.2.1 Dendritic spines and excitatory synaptic structure

1.2.1.1 Structure and composition of dendritic spines

Dendritic spines are actin rich, dynamic, membrane protrusions that decorate the shafts of neuronal dendrites. These structures were first described over 100 years ago by Ramón y Cajal in his beautiful descriptive drawings of neuronal architecture (Ramón y Cajal, 1888; Yuste, 2015). He proposed that dendritic spines could serve as the contact sites between neurons. This proposal was later confirmed with the emergence of electron microscopy (Gray, 1959). Dendritic spines are now known to compartmentalise the excitatory postsynaptic density (PSD) and spatially confine biochemical signals for efficient neuronal transmission (Bourne and Harris, 2008; Kennedy et al., 2005). The PSD is the term given to the vast collection of proteins that make up the post excitatory synapse discussed in more detail below. By electron microscopy the PSD appears as an electron dense thickening on spine heads opposed to the presynaptic active zone (Gray, 1959; Sheng and Kim, 2011). Packaging of the PSD into spines allows ions and signalling molecules to become concentrated following synaptic activation for the efficient propagation of neuronal inputs.

During development dendrites produce numerous filopodia, thin actin dependent membrane extensions. Many of these filopodia will develop into spines, thought to be

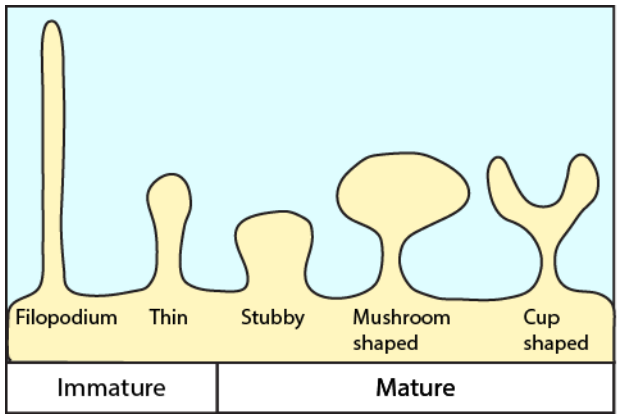

Figure 1.2: Spine morphology classification.

Dendritic spines come in a wide variety of shapes and sizes, with a volume ranging from 0.01 to 0.8μm^3. On the basis of detailed anatomical studies of fixed brain tissue, dendritic spines have been classified by shape as long thin, stubby, mushroom and cup-shaped. Spines begin as actin based protrusions called filopodia, then throughout development progress from immature long, thin spines to mature mushroom, branched, stubby or cup-shaped spines. This maturation process relies on network activity to strengthen the synapse and induce mature spine formation. Spine morphology is stabilised by expression of structural proteins and actin dynamics. However, the speed in which spine structure can change is calling this static view of spine morphology into question. Adapted from (Hering and Sheng, 2001).

stabilised by the formation of synapses, while others will retract and form synapses on the dendritic shaft. These shaft synapses may eventually re-emerge on spines or may be eliminated during synaptic pruning later in development (Bourne and Harris, 2008). Due to their actin rich nature, dendritic spines are highly dynamic structures and can continuously adapt their morphology, even throughout adulthood (Ebrahimi and Okabe, 2014; Sala and Segal, 2014). In particular, their shape varies dramatically during development from an immature spine with weak synaptic connections to a mature spine with stronger stable connections. During development increased sensory inputs will strengthen a synapse and influence progression to a mature spine structure (Alvarez and Sabatini, 2007; Fischer et al., 2000). Additionally, recent work using 2 photon microscopy and glutamate uncaging has revealed that glutamate alone is sufficient to induce *de novo* spine formation in the mouse cortex (Kwon and Sabatini, 2011). Considerable literature addressing spine morphology has risen with advancements in imaging techniques, and has resulted in the formation of common spine classifications used to describe the different spine morphologies observed (Figure 1.2) (Bellot et al., 2014; Bourne and Harris, 2008). However, this static view of spine classification is being reconsidered as more recent live imaging studies demonstrate *in vivo* spines can change size and shape within minutes (Sala and Segal, 2014). Importantly, the correct modulation of these small membrane protrusions is critical as defects in spine morphology and regulation are hallmarks of neurological disorders (Penzes et al., 2011).

1.2.1.2 Dendritic spine plasticity

An essential adaptation of dendritic spines is their ability to undergo structural and functional changes in response to synaptic plasticity. One form of synaptic plasticity is long-term potentiation (LTP), the persistent, long lasting strengthening of synapses in response to recent patterns of high-frequency stimulation. At excitatory postsynapses this form of plasticity is characterised by increased spine volume as well as alterations in PSD size and increased AMPAR surface expression. Conversely, during long-term depression (LTD), the long-lasting weakening of synapses following low-frequency stimulation, there is a reduction in spine volume, PSD size and a decrease in AMPARs (Kasai et al., 2010; Matsuzaki, 2007; Sala and Segal, 2014; Shepherd and Huganir, 2007). Advanced live cell imaging has demonstrated these alterations in spine morphology in response to LTP and LTD stimulation protocols (Hill and Zito, 2013; Oh et al., 2013; Zito et al., 2009). Enhancing or reducing synaptic strength in this way requires numerous cellular processes such as changes in the

composition of surface receptors and the PSD (Chater and Goda, 2014; Makino and Malinow, 2009; Sheng and Kim, 2011), changes in actin dynamics (Hanley, 2014; Hotulainen and Hoogenraad, 2010), altered exocytosis and endocytosis and regulation of protein turnover including the redistribution of polyribosomes and proteasomes (Bourne and Harris, 2008). Indeed, recycling endosomes, exocytosis and endocytosis are critical for the regulation of spine shape as these processes add or remove membrane from the spine during activity-dependent growth or shrinkage (Park et al., 2006). Blocking the recycling endosome trafficking pathway abolishes LTP-induced spine formation (Park et al., 2006). Likewise, local protein translation at spines is upregulated during LTP to provide the necessary proteins for PSD expansion and spine growth while, proteosomes are redirected to spines to regulate protein turnover (Bourne et al., 2007; Kelleher et al., 2004).

1.2.1.3 The actin cytoskeleton and its regulation

Regulation of the actin cytoskeleton is fundamental to dendritic spine development and plasticity (Bellot et al., 2014; Hotulainen and Hoogenraad, 2010). Actin filaments are capable of extending and retracting in a process known as actin treadmilling. This process generates forces within the cell necessary for changes in cell morphology, membrane curvature and movement of organelles within the cytoplasm (Pollard and Cooper, 2009). Dendritic spines undergo all these actin driven processes which is reflected in the highly actin-rich nature of spines.

A description of the actin assembly machinery and the main proteins involved will therefore be given prior to a discussion of the evidence that actin is vital for dendrite spine formation and maintenance.

Actin assembly: The actin structure is highly dynamic and made up of monomeric globular (G)-actin that polymerises to form filamentous actin (F-actin). In response to appropriate signalling new actin filaments are generated by proteins including the actin related protein (Arp2/3) complex and formins (Pollard, 2007). Proteins are required for this process because G-actin polymerisation is unfavourable due to the incredibly unstable nature of actin oligomers. Filament elongation however, is much more stable. During elongation actin monomers bind to filaments at the fast growing plus (barbed) end whereas depolymerisation of actin involves the loss of actin monomers from the minus (pointed) end of filaments (Lee and Dominguez, 2010). G-actin binds to ATP and ATP can regulate actin formation. ADP-bound actin

dissociates from filaments more rapidly than ATP-bound actin suggesting that ATP hydrolysis promotes actin disassembly (Pollard, 1986).

Rho GTPases: Rho GTPases are found in all eukaryotic cells and are best documented for their important signalling roles in regulating the actin cytoskeleton, which implicate the proteins in many cellular processes such as cell polarity, motility and trafficking (Jaffe and Hall, 2005). The family comprises of 20 molecules however, the most well described members of the family are RhoA, Rac1 and cdc42. In the mammalian system both Rac1 and cdc42 have been shown to induce the formation of membrane protrusions known as lamellopodia and filopodia, while RhoA is more critical for cellular trafficking (Heasman and Ridley, 2008; Ridley et al., 1992).

Rho family proteins can bind to both GTP and GDP and have intrinsic GTPase activity. These proteins are often called molecular switches because in their active GTP-bound forms they can activate downstream effector proteins and drive cellular mechanisms. The activity of Rho proteins is regulated by two classes of proteins known as the guanine exchange factors (GEFs) and the GTPase activating proteins (GAPs). GEFs promote the exchange of GDP to GTP by stimulating GDP release and therefore regulate the activation of Rho GTPases while GAPs stimulate the intrinsic GTPase activity of the proteins leading to hydrolysis of GTP back to GDP and deactivation (Jaffe and Hall, 2005).

Rho GTPases bring about changes at the plasma membrane by activating actin polymerisation. They are often recruited and consequently locally activated by GEFs (Rossman et al., 2005). Indeed, post-translational modifications of the Rho GTPases at basic regions within the C-terminus of Rho proteins allow the molecules to directly interact with the plasma membrane. An intriguing class of proteins known as the guanine-nucleotide dissociation inhibitors (GDIs) can bind to Rho GTPases and are capable of masking their interaction with the membrane and downstream effectors adding another level of regulation to these critical global regulatory molecules (Heasman and Ridley, 2008; Jaffe and Hall, 2005).

Formins: Formins are a major group of actin nucleators known to produce unbranched filaments and are present in almost all eukaryotes. These proteins play critical roles in many aspects of cell function including, cytokinesis, cell polarity, migration and morphogenesis (Breitsprecher and Goode, 2013). The defining feature

of all formins is the presence of the C-terminal formin homology domains 1 and 2 (FH1 and FH2). These domains are capable of binding to actin and are thought to bring about nucleation *in vivo* by capturing and stabilising G-actin monomers (Breitsprecher and Goode, 2013). Indeed, FH2 domains are sufficient to trigger nucleation of purified actin (Chesarone et al., 2010). During elongation, FH2 domains are active as a homodimer and bind processively to the elongating barbed end of actin filaments to protect against capping proteins attempting to terminate elongation. The FH1 domain is proline rich and recruits profilin-actin complexes. This recruitment dramatically accelerates actin elongation; thought to be due to a rise in local G-actin concentration. The N-terminus of formins are more variable, functioning mainly to direct protein localisation via signalling and protein interactions. It is this sequence diversity that primarily leads to the different biochemical and cellular activities of individual formins (Campellone and Welch, 2010).

Arp2/3 complex: The Arp2/3 complex initiates the formation of branched daughter actin filaments on the side of existing mother filaments. It functions by anchoring the pointed end of the daughter filament to the mother filament as the free barbed end grows away from the complex (Pollard, 2007). This intrinsically inactive seven subunit complex contains two actin related proteins, Arp2 and Arp3 and 5 other subunit proteins: ARPC1-5. An actin monomer, as well as an actin regulatory molecule known as a nucleation promoting factor (NPF) and actin filaments come together to cooperatively activate the Arp2/3 complex.

Nucleation promoting factors (NPFs): These proteins have been identified as scaffolding molecules that act upstream of the Arp2/3 complex and bring about its activation. NPFs all share a common C-terminus and have been classified into four different families based on their different N-terminal domains. The WASP and WAVE families are the most described and more recently the WHAMM/JMY and WASH families have also been identified (Derivery and Gautreau, 2010; Padrick and Rosen, 2010; Pollitt and Insall, 2009; Takenawa and Suetsugu, 2007). The common C-terminal region of NPFs contains a VCA domain that consists of the verprolin-homology domain (V; also known as the WASP-homology-2-domain (WH2)) the cofilin-homology domain (C; also known as the central domain) and the acidic domain (A). The V domain binds to the actin monomer while the CA domain interacts with Arp2/3 resulting in Arp2/3 complex activation and actin polymerisation. The initiation of a new actin branch requires the nucleation of three actin monomers. The

Arp2/3 complex provides two actin related molecules, therefore the binding of another actin monomer to the V domain mimics the three actin molecules necessary for *de novo* filament formation (Machesky and Insall; Machesky et al., 1999; Pollard, 2007; Takenawa and Suetsugu, 2007).

The VCA domain alone can activate the Arp2/3 complex however; full-length WASP with a partial deletion of an internal basic region has been shown to activate Arp2/3 with higher efficiency in pure systems (Suetsugu et al., 2001). This demonstrates how other regions beyond the VCA domain of NPFs are important in contributing to Arp2/3 activation and regulation. Indeed, the N-terminal regions of NPFs either contain regulatory domains that are important for the autoinhibition of the VCA domain or interact with other proteins and in this way provide inhibition of the VCA domain. This tight control of actin nucleation is necessary for normal cellular function. One class of proteins known to regulate NPFs are the Rho GTPases.

WASP: WASP (Wiskott-Aldrich syndrome protein) was originally identified as the gene mutated in Wiskott-Aldrich syndrome, an immunodeficiency disease (Derry et al., 1994). Later N-WASP was identified to interact with growth factor receptor-bound protein 2 (GRB2) and was named neural-WASP due to its enriched expression in neuronal tissue but the protein has since been shown to be expressed in other tissue types (Miki et al., 1996). WASP and N-WASP are both NPFs and share very similar protein structure. Both proteins contain an N-terminal WI domain followed by a basic region, a GTPase binding domain (GBD) and a proline-rich domain before the C-terminal VCA region. Early experiments demonstrated that under resting conditions WASP proteins were retained in an autoinhibited state, an intramolecular interaction between the N-terminal GBD and C region of the C-terminal VCA domain occluded the VCA domain from binding Arp2/3 and initiating actin polymerisation rendering the protein inactive.

Cdc42, among other Cdc42 related GTPases, in its GTP-bound form has been shown to competitively interact with the GBD, relieving WASP autoinhibition and regulating its activity (Derivery and Gautreau, 2010; Padrick and Rosen, 2010; Takenawa and Suetsugu, 2007). WASP proteins are also known to be activated by phosphorylation or by the binding of SH3 domain containing proteins to their proline rich region (Ho et al., 2004; Suetsugu et al., 2002). Additionally, the autoinhibited conformation of WASP is reasonably weak and binding of WASP interacting proteins (WIP) proteins

to the WI domain of WASP has been shown to intensify its autoinhibition (Martinez-Quiles et al., 2001). Importantly, most of the mutations associated with WASP are found within the WI domain, highlighting the significance of the WIP interactions for normal WASP regulation and function. Lastly, phosphinositides have been shown to interact with the basic region of WASPs and are thought to target them to the membrane to locally regulate actin dynamics. Taken together, the activation of WASP proteins and hence Arp2/3 is tightly modulated by various types of signalling molecules (Takenawa and Suetsugu, 2007).

WAVE: On the other hand, WASP family Verprolin-homologous proteins (WAVE), another large class of NPFs, are structurally distinct from WASP proteins and behave differently with regards to their activation and native complex formation. Indeed, unlike the WASP family WAVE proteins are constitutively active (Machesky et al., 1999). WAVE1 was identified from a screen of proteins that shared sequence homology with the VCA domain of WASP (Miki et al., 1998). Further screening identified the mammalian homologs WAVE2 and WAVE3 (Suetsugu et al., 1999). WAVE proteins have a different N-terminal structure to WASP and N-WASP, they contain a WAVE homology domain (WHD) and a basic region. The basic region can interact with phosphoinosides and is important for the localisation of WAVE proteins while the WHD is important for WAVE complex formation. The WAVE complex was first identified by purifying WAVE1 from bovine brain lysate (Eden et al., 2002). Four other proteins were found in a complex with WAVE1 in a 1:1:1:1:1 stoichiometry. The complex was later confirmed by the purification of WAVE2 from HeLa cells (Gautreau et al., 2004; Innocenti et al., 2004). Since then, all three WAVE proteins have been identified in the same pentameric heterocomplex complex with Nap1, CYFIP1 (also known as Sra1 or the closely related CYFIP2/PIR121), Abi (Abelson-interacting protein) and HSPC300 (also known as BRICK). The pentameric heterocomplex is known as the WAVE regulatory complex (WRC) and like WASP proteins has been implicated in many actin regulatory functions due to its ability to activate Arp2/3 and promote actin polymerisation.

WAVE Regulatory Complex (WRC): Although the interactions between members of the WRC have been known for many years, there has been much debate about how the WRC is regulated and the role it plays in activating the Arp2/3 complex. WAVE is known to bind to Abi1/2 in a 1:1 protein complex. HSPC300 also interacts directly with WAVE. Nap1 and CYFIP1 form a homodimer, which interacts with

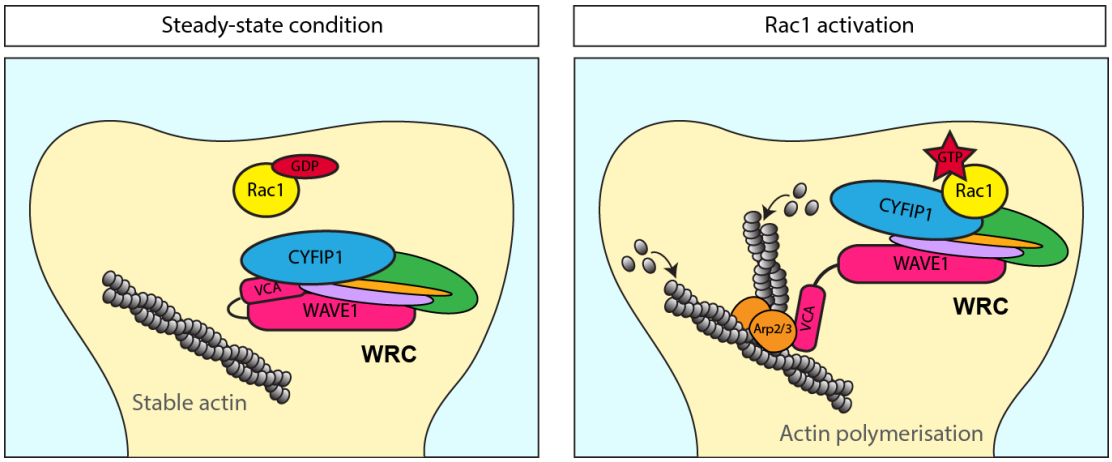

Figure 1.3: Schematic representation of WAVE regulatory complex regulation.

The WAVE regulatory complex (WRC) consists in five components, CYFIP1 or CYFIP2 (blue), NAP1 (green), Abi (purple), HSPC300 (orange) and WAVE (pink). Under steady-state conditions CYFIP1 maintains the WRC in an inactive state by binding and occluding the active VCA domain of WAVE. Following Rac1 activation, where GDP is exchanged for GTP, active GTP-bound Rac1 interacts with CYFIP1 causing a conformational change in the protein which relieves its repression of the VCA domain. The VCA domain can then interact with Arp2/3 and bring about actin polymerisation and branching.

WAVE via a Nap1 Abi interaction (Innocenti et al., 2004). Nap1 can interact with the membrane anchor Nck (Kitamura et al., 1996) and CYFIP1 is known for its specific binding to activated Rac1 (Kobayashi et al., 1998), both of these interactions are thought to contribute to the regulation of the WRC. In addition, the WRC has been reported to be activated by phospholipids cooperatively at the membrane and can undergo phosphorylation at many sites of which some have been shown to enhance signalling activity (Takenawa and Suetsugu, 2007).

It was initially suggested that the WRC maintains WAVE in an inactive state and that GTP-Rac1 binding to CYFIP1 could stimulate the dissociation of WAVE and HSPC300 from the complex resulting in WAVE activation (Eden et al., 2002). However, this was followed by the suggestion that Rac1 can bind to the WRC without promoting its dissociation and that WAVE was active and could stimulate Arp2/3 within the complex with or without Rac1 binding (Innocenti et al., 2004). More recent structural experiments and the publication of the 2.3-angstrom WRC crystal structure have revealed the true mechanism of WRC regulation (Chen et al., 2010b; Ismail et al., 2009). CYFIP1 and Nap1 share homologous structures and were described to interact extensively and form a pseudo-symetric dimer that provides a platform for binding of the trimer consisting of WAVE:Abi:HSPC300. Importantly, the C-terminus of WAVE including the VCA domain interacts with CYFIP1; an interaction that is central to the regulation of the complex activity. As previously described the V domain is critical for actin binding. In the WRC, the helical region of the V domain which would normally recruit an actin monomer is buried in the CYFIP1 interface making it inaccessible to actin. Furthermore, the C domain, which is necessary for Arp2/3 binding, is also masked by its interaction with CYFIP1. When amino acid residues of these interactions are mutated, the WRC becomes constitutively active, highlighting that these interactions are critical for WRC inhibition. Studies into the affinity of the WRC for Rac1 revealed that active Rac1 interacts with the WRC competitively with the VCA domain. Therefore, active Rac1 is thought to bind to the WRC via CYFIP1 resulting in conformational changes allowing the VCA domain to be accessible to recruit monomeric actin and activate Arp2/3 (Figure 1.3) (Chen et al., 2010b; Ismail et al., 2009).

1.2.1.4 The actin cytoskeleton and dendritic spines

Within dendritic spines both F-actin and G-actin have been detected. The actin network within the head of the spine is branched whereas in the spine neck the actin

forms long tight bundles (Hotulainen and Hoogenraad, 2010). Compared to other cellular regions, actin turnover in the spine is extremely high with actin filaments in the head being replaced every minute (Honkura et al., 2008; Star et al., 2002). This property of spine actin is consistent with the knowledge that spine morphology can change in a time scale of seconds to minutes. Indeed, actin polymerisation has been shown to be associated with spine enlargement while actin depolymerisation is linked with spine shrinkage (Sala and Segal, 2014). Furthermore, synaptic activity has been shown to modulate spine head size via actin mechanisms (Star et al., 2002). Evidence for a role of actin in spine stability was provided by Allison and colleagues who demonstrated that acute depolymerisation of actin filaments with the drug latrunculin A resulted in loss of AMPA receptor positive dendritic spines in primary hippocampal neurons (Allison et al., 1998). The observations that actin dynamics are intimately linked to spine morphology and synapse activity has driven research into this field.

More recently, as well as being shown to alter spine shape, changes in spine actin dynamics have been shown to contribute to the organisation of the PSD. PSDs fluorescently labelled with GFP-tagged PSD-95 have been shown to undergo rapid dynamic structural changes driven by actin dynamics both under steady-state conditions and in response to synaptic activity (Blanpied et al., 2008). Furthermore, super-resolution imaging studies have shown that the PSD is more complex than just one protein rich domain. It is in fact made up of smaller subsynaptic domains that rearrange during plasticity (MacGillavry et al., 2013; Nair et al., 2013) in response to actin redistribution (Kerr and Blanpied, 2012). Indeed, it has been proposed that actin filaments contact the PSD at its interior face and perisynaptically (Burette et al., 2012; Frost et al., 2010a) and that this contact is critical for structural and functional synaptic plasticity (Kerr and Blanpied, 2012). Interestingly, upon closer inspection using photoactivation localisation microscopy (PALM), movements of individual actin molecules within the spine have been measured. These experiments revealed that actin has heterogeneous polymerisation rates within the spine. The molecular velocity of the actin varied between different subdomains of the spine head and neck demonstrating the diverse functions of actin within the spine (Frost et al., 2010a).

Another role for actin within spines is in the trafficking of AMPARs, particularly during synaptic plasticity. Actin is necessary to propel recycling endosomes towards the membrane for insertion of receptors during LTP, but is also critical for the

generation of membrane curvature during the endocytosis and exocytosis of AMPARs following LTD or LTP respectively (Hanley, 2014). Manipulating actin dynamics with drugs has demonstrated a role for actin in the AMPA trafficking process. Treatment of cultured neurons with the actin stabilising drug jasplakinolide blocked glutamate-induced AMPAR internalisation (Zhou et al., 2001). Furthermore, both the depolymerising drug latrunculin B and phalloidin (another actin-stabilising drug) were shown to block LTP (Kim and Lisman, 1999). These finding indicate dynamic F-actin is necessary for LTP and the stabilisation of AMPARs at synapses while depolymerisation of actin is required for AMPAR endocytosis. There are numerous actin associated proteins and actin binding proteins (ABPs) that have been implicated in the regulation of AMPAR trafficking within the synapse such as RIL, cofilin, PICK1 and ARC (Hanley, 2014). Many of these molecules interact with the intracellular tail of AMPAR subunits and couple them directly or via associated proteins to the actin cytoskeleton. Indeed, PICK1 has been shown to interact with the GluA2 subunit and regulate actin dynamics through inhibition of Arp2/3 during AMPAR internalisation. Upstream of PICK1, the GTPase Arf1 in its active form was shown to limit PICK1-mediated inhibition of Arp2/3. Loss of Arf1 resulted in increased PICK1 inhibition, AMPAR internalisation and spine shrinkage. Interestingly, NMDA-induced LTD down-regulated Arf1 activation and GluA2-PICK1 binding (Rocca et al., 2013). Of note, others have reported depolymerising actin with drugs has little or no effect on the synaptic stability of all, or a subpopulation, of synaptic AMPARs. This suggests that instead the role of actin on AMPAR trafficking may be more important at extrasynaptic sites (Kerr and Blanpied, 2012; Kim and Lisman, 2001). Additionally, conditional knockout of the actin filament disassembly protein n-cofilin in the forebrain of postnatal mice reduced the lateral mobility of AMPARs within the membrane extrasynaptically but not at synaptic sites (Rust et al., 2010).

As well as regulating receptor trafficking, ABPs are known to influence dendritic spine structure, function and plasticity. The Arp2/3 complex is an ABP that brings about *de novo* actin branch formation by acting as a catalyst to nucleate free G-actin (Pollard, 2007). Upstream actin regulators such as Rac1, WASP and WAVE, which themselves are tightly regulated, control both spatially and temporally the activation of this complex. Indeed, altered expression of Rac1 and WAVE impact on spine morphology, highlighting how critical these signalling pathways are for the maintenance of dendritic spines (Corbetta et al., 2009; Kim et al., 2006). In the context of dendritic spines, conditional KO of Arp2/3 in mouse forebrain results in a defect in spine

structural plasticity, significant loss of dendritic spines and behavioural abnormalities demonstrating the importance for this protein in spine structure and function (Kim et al., 2013). Furthermore, inhibition of the Arp2/3 complex by PICK1 is required for AMPAR internalisation (Rocca et al., 2008) and a mutant version of PICK1, that cannot bind and inhibit Arp2/3, was shown to block CA1 LTD in hippocampal slices (Nakamura et al., 2011) indicating how Arp2/3 regulation is critical for synaptic plasticity. In addition to Arp2/3, the formin ABPs promote unbranched actin filament formation (Breitsprecher and Goode, 2013) and are critical to the establishment of filopodia (Mellor, 2010) and hence dendritic spine formation. Furthermore, electron microscopy studies demonstrate that the spine neck contains bundles of unbranched actin filaments (Landis and Reese, 1983) therefore, formins are thought to have a role in spine neck formation and maintenance. Indeed, it has been shown that filopodia elongation at both the root and tip is regulated by the small GTPase Rif acting on the formin mDia2 during spinogenesis (Hotulainen et al., 2009).

On the other hand, cofilin is a ubiquitous ABP that reorganises actin filaments by causing minus end depolymerisation and F-actin severing. This reduces the ratio of F to G-actin, therefore increasing F-actin turnover. Cofilin is deactivated by LIM kinase mediated phosphorylation and activated by the slingshot phosphatases (SSH1) (Sarmiere and Bamburg, 2004). Pontrello et al. demonstrated a role for cofilin in synaptic plasticity. They showed upon NMDAR activation, active calcineurin causes dephosphorylation of cofilin, active cofilin is then translocated into spines and brings about remodelling (Pontrello et al., 2012). Additionally, conditional loss of cofilin in neurons results in a greater proportion of F-actin, increased spine density and area resulting in altered synaptic plasticity and impaired associative learning (Rust et al., 2010).

Many other actin regulatory proteins have been shown to be important in spine morphology and synaptic receptor trafficking. The Rho GTPases are all fundamental regulators of actin dynamics and impact on spine morphology (Negishi and Katoh, 2005; Newey et al., 2004). Furthermore, Rho GTPase GAPs and GEFs have also been implicated in spine structure. Altered expression of the Rac1 GEFs PIX and Kalirin7 are both associated with defects in spine morphology (Penzes et al., 2001; Zhang, 2005). Other synaptically localised ABPs such as α-actinin, calponin, profilin, neurabin1 and VASP are involved in the building of F-actin (reviewed by (Bellot et al., 2014)). Additionally, actin capping proteins, which bind plus ends and inhibit F-actin

extension, impact spine morphology. Indeed, loss of the capping protein Eps8 results in increased filopodia and immature spines as well as impaired synaptic plasticity (Menna et al., 2013; Stamatakou et al., 2013). Taken together, these finding have illustrated the critical role for ABPs and actin regulatory proteins in spine structural and functional maintenance and plasticity.

1.2.2 The postsynaptic density and glutamate receptors

The excitatory PSD is a dynamic structure containing hundreds of proteins, many of which have been identified to be critical for brain function. The PSD is a morphological specialisation of the postsynaptic membrane located largely at the tips of dendritic spines. However, certain spines have been described to contain more than one synapse and therefore PSD, and in some cases PSDs have also been identified on dendritic shafts. Functionally, the PSD spatially localises postsynaptic elements directly opposed to the presynaptic active zone. The principal functional components of the PSD are the ionotropic glutamate receptors, which are embedded in a vast, dense protein network of scaffolding proteins, signalling molecules, cytoskeletal elements and membrane proteins. Importantly, this network couples activation of glutamate receptors to biochemical signals within the postsynaptic cell (Figure 1.4) (Sheng and Kim, 2011).

Research into the PSD began in the 1970s when detergents were used to purify the PSD. Changes in conformation and concentration of proteins were correlated with learning and memory; evidence for the importance of the plastic PSD in neurological function (Davis and Bloom, 1973; Siekevitz, 1985). It was not until the 1990s and the emergence of peptide sequencing that the first PSD proteins, CAMKII and PSD95 were identified and cloned. However, it was much later when these proteins were shown to be the most abundant molecules of the PSD (Cheng et al., 2006; Cho et al., 1992; Peng et al., 2004). Yeast two-hybrid (Y2H) screens were also popular in the 90s with researchers using known molecules of the PSD, such as receptor subunits as 'bait' to identify novel PSD proteins.

More recently, mass spectrometry has allowed further characterisation of novel PSD proteins. An estimate for the number of PSD proteins now ranges from a few hundred to 2000. False positives can be identified in all these methods, plus rare or loosely bound PSD proteins can go undetected indicating the need for caution when

interpreting the great number of screens available in this field. Nevertheless, many PSD proteins have now been robustly characterised and classified into functional categories (Sheng and Kim, 2011).

1.2.2.1 Glutamate receptors

The vast majority of excitatory transmission in the CNS is mediated by the ubiquitous amino acid glutamate. This neurotransmitter is packed into presynaptic vesicles by specialised vesicular transporters (vGLUTs). Following presynaptic stimulation glutamate is released and diffuses across the synaptic cleft to activate glutamate receptors (GluRs) positioned in the postsynaptic membrane. GluRs are the most functionally critical membrane proteins of the PSD consisting of ionotropic (iGluR) and metabotropic (mGluR) glutamate receptors. The fast-acting iGluRs open upon ligand binding, resulting in an influx of cations, membrane depolarisation and production of a subsequent action potential. mGluRs on the other hand, are G-protein-coupled receptors and have a slower response to glutamate. In particular, goup I mGluRs (mGluR-I) including mGluR1 and 5 are enriched postsynaptically at glutamatergic synapses and localise to perisynaptic zones on the periphery of the PSD (Luján et al., 1997). They signal though G-proteins to produce a canonical signalling cascade which triggers the mobilisation of Ca^{2+} and the activation of various downstream effector pathways (Bellone and Mameli, 2012). mGluR-I are known to modulate NMDAR activity and are often found in close proximity to these receptors via scaffolding proteins of the PSD (Tu et al., 1999). Additionally, they are important in the regulation of protein translation and can modulate synaptic strength by inducing LTP and LTD in various brain regions (Lüscher and Huber, 2010). Conversely, mGluR-II are predominantly found presynaptically and have different signalling properties. Mammalian iGluRs are encoded by 18 genes and form four receptor families: AMPA, NMDA, kainate and delta receptors (AMPARs, NMDAs, kainateR and deltaRs). AMPARs and NMDARs typically mediate excitatory post synaptic currents and are vital in the production of synaptic plasticity and therefore will be discussed in more detail.

Both AMPA and NMDARs are made up of four subunits which form a tetrameric complex within the membrane. Four genes encode the AMPAR subunits (GluA1-4) while 7 genes are known to encode the NMDAR subunits (GluN1, GluN2A-D, GluN3A-B). AMPAR subunits can form homo and heteromers however, the latter are more prominent *in vivo*. Indeed, AMPARs are said to be a product of a dimer of

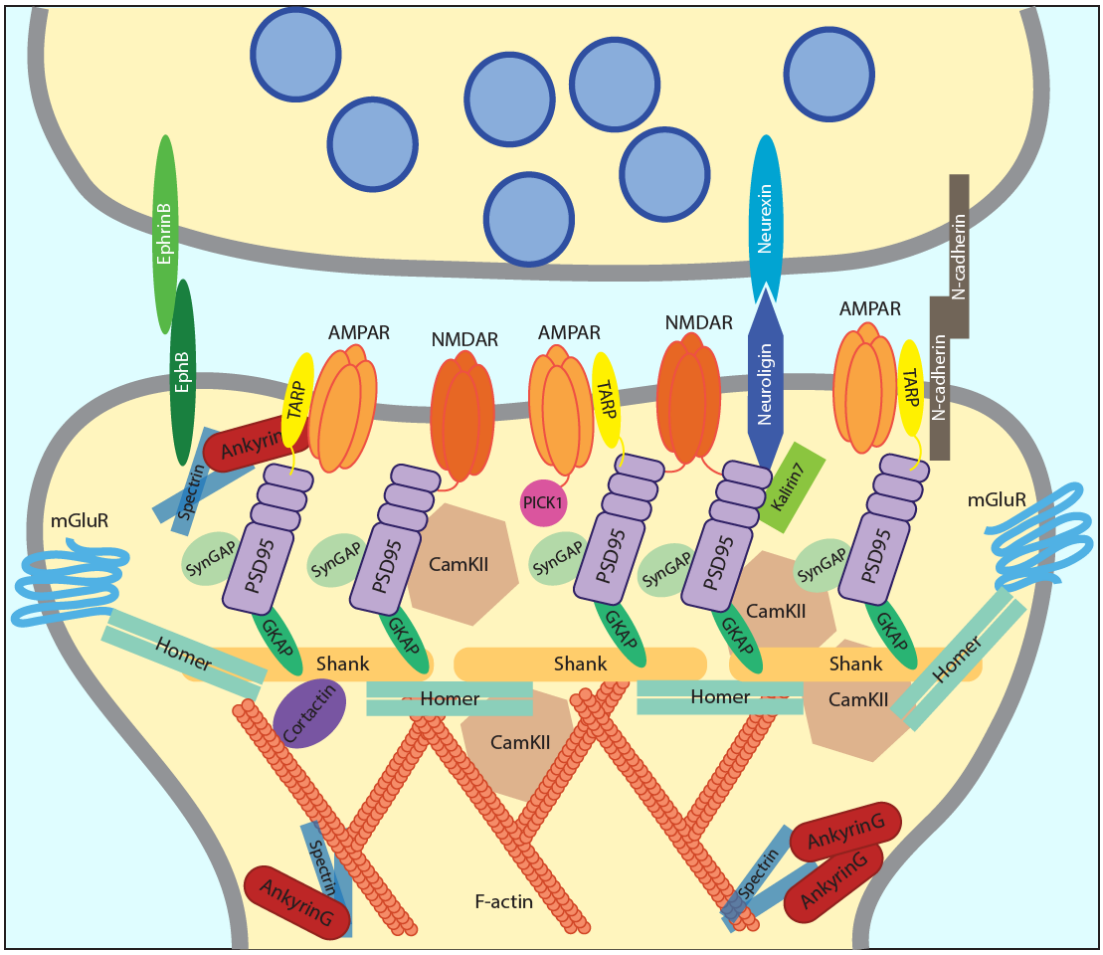

Figure 1.4: Molecular composition of the excitatory postsynaptic density.

A schematic diagram depicting proteins know to localise or function within the postsynaptic density (PSD) contained within a dendritic spine discussed in this introduction. Protein interactions indicated by direct contacts or overlaps between the proteins. Adapted from (Sheng and Kim, 2011).

dimers formed during transit through the secretory pathway (Ayalon and Stern-Bach, 2001). NMDARs are made up of two GluN1 subunits and either two GluN2 subunits or a combination of GluN2 and GluN3 subunits.

AMPA receptors are activated by glutamate alone with one ligand binding to each subunit. Two ligand bound subunits is sufficient to allow ion influx through the channel and flux is increased as more binding sites are occupied. Interestingly, subunits can undergo splicing, post-translational modifications and RNA editing to alter the channel properties adding diversity to the receptor properties (Smart and Paoletti, 2012). For instance, RNA editing of the GluA2 subunit mRNA results in an amino acid change at residue 607 from a neutral glutamine to a positively charged arginine within the channel pore (Sommer et al., 1991). This positive charge renders the channel impermeable to calcium (Ca^{2+}). AMPAR permeability to cations is therefore governed by the GluA2 subunit which is the most abundant subunit in the CNS and is required for proper receptor conformation (Sans et al., 2003). GluA2 is commonly found in its edited form hence, the principle ions gated by AMPARs are sodium and potassium, distinguishing AMPARs from NMDARs which also permit calcium influx. NMDARs have a more complicated activation process. Efficient channel opening requires glutamate and the co-agonist glycine or D-serine to interact with the GluN2 and GluN1/3 subunits respectively. This has to occur simultaneously with membrane depolarisation to relieve the Mg^{2+} block from within the channel pore that exists at resting potential (Smart and Paoletti, 2012). More often than not NMDARs and AMPARs are found together within excitatory PSDs. In response to glutamate NMDAR activation will occur following AMPAR activation and membrane depolarisation. Indeed, synapses only containing NMDARs are considered 'silent' synapses as they do not response to glutamate due to the Mg^{2+} block not being removed.

Numerous intracellular proteins within the PSD, such as scaffolding and cytoskeletal molecules, can interact with the GluRs via their intracellular regions. These interactions have been shown to control the transport and clustering of GluRs as well as the recruitment of multiple signalling molecules (Smart and Paoletti, 2012). Both AMPARs and NMDARs contain C-terminal PDZ-binding domains which allow binding with many core PSD PDZ-containing proteins. For example AMPARs can bind GRIP and PICK1 while NMDARs interact with PSD95, SAP102, SAP97, and PSD93 (also known as chapsyn110). These scaffold molecules play key roles in the structural and functional changes that excitatory synapses experience during

development, plasticity, and disease (Elias and Nicoll, 2007; Montgomery et al., 2004). Interestingly, AMPARs do not directly interact with PSD95, the most abundant scaffold within the PSD but bind to it indirectly via the AMPA receptor auxiliary subunits (TARPs) (Bats et al., 2007). TARPs are membrane proteins which modulate AMPAR activity and are important in the trafficking and stabilisation of the receptor. GluR trafficking, mediated by intracellular protein interactions, is thought to be one of the major underlying mechanisms of synaptic plasticity. Indeed, rapid insertion or removal of AMPARs from the post synaptic membrane resulting in synaptic strengthening or weakening correlate with LTP and LTD respectively (Shepherd and Huganir, 2007).

1.2.2.2 Adhesion molecules

Adhesion molecules are another class of PSD membrane proteins, which function mainly by interacting with presynaptic binding partners to align and stabilise the synapse. Adhesion molecules form a trans-synaptic link across the cleft allowing signals to be propagated from intracellular contacts on one side of the synapse to the other. The best described example of a trans-synaptic link is between the presynaptic neurexins (Nrxns) and the postsynaptic neuroligins (NLs). Nrxns are a highly diverse family of type-I membrane proteins. The human genome has three Nrxn genes each of which encodes an α- and β-Nxrn from different promoters. These transcripts can also undergo extensive alternative splicing resulting in thousands of Nrxn isoforms (Südhof, 2008). Neuroligins (NLs) were first identified as endogenous Nrxn ligands and are also type-I membrane proteins. There are 4 known NL proteins in mammals each containing a large extracellular domain, a transmembrane region and a short intracellular tail, interactions with cytosolic proteins via this tail region are critical for synapse formation and stability. Intriguingly, NL1 and NL2 have been shown to be synapse specific and are detected at glutamatergic and GABAergic/glycinergic synapses respectively. NL1 binds to the excitatory scaffold molecule PSD95 through its C-terminal intracellular PDZ domain-binding motif targeting it to excitatory synapses (Irie et al., 1997). By contrast, NL3 has been reported to be present at both excitatory and inhibitory synapses, while NL4 has been detected to a lesser extent at glycinergic synapses (Südhof, 2008). NLs have recently been shown to form constitutive dimers, including homomers and heteromers. This finding raises the question as to the distinct roles of different NL heteromers (Poulopoulos et al., 2012). Other trans-synaptic complexes such as EphB-EphrinB binding and N-cadherin homophilic contacts are also found in the PSD (Sheng and Kim, 2011).

Different expression patterns of these adhesion molecules, many of which have numerous family members and splice forms, are thought to contribute to synapse diversity (Shen and Scheiffele, 2010; Sheng and Kim, 2011). It is clear that a large number of Nxrn and NL variants are generated from the many genes and complex alternative splicing processes. Researchers are now trying to understand the importance of such a varied family of proteins. It has been proposed that a combinational interaction code generated by these variants may determine synapse identity and network connectivity (Krueger et al., 2012). Indeed, different Nrxn3 splice isoforms deferentially regulate AMPA receptor trafficking, while loss of Nrxn3 from different brains regions reveal distinct circuit-dependent functions for the protein (Aoto et al., 2013, 2015).

Many synaptic adhesion molecules have synaptogenic properties (Craig and Kang, 2007). Over expression of NL1 in cultured neurons promotes excitatory synapse formation, whereas, silencing NL1 reduced synapse number (Chen et al., 2010a; Chih et al., 2005). Furthermore, expression of either Nrxn1β or NL1 in heterologous cells cocultured with dissociated neurons led to the induction of post and presynapses respectively on neighbouring neurons and the formation of hemisynapses (Graf et al., 2004; Scheiffele et al., 2000). An interesting experiment using microspheres coated with antibodies against NL1 or Nrxn1β protein showed that these beads could induce clustering of NL1 and hemisynapase formation. This suggests the clustering of NL1 is important for its synaptogenic properties and the recruitment of scaffold proteins (Barrow et al., 2009).

1.2.2.3 Scaffold proteins

Scaffold proteins are characterised by highly conserved, multiple protein-protein interacting domains that are important for the facilitation of protein binding and the formation of complex protein networks. These proteins can interact with multiple binding partners simultaneously to link different components of the PSD.

PSD95: PSD95 is the most abundant and most widely-studied scaffold protein of the PSD (Cheng et al., 2006; Peng et al., 2004). The main function of PSD95 and its family members (PSD93/Chapsyn110, SAP97 and SAP102) is to bind and tether membrane proteins and signalling molecules in the PSD. Like many PSD proteins PSD95 and its family proteins contains PDZ binding domains. PDZ domains were named after their occurrence in three related scaffold proteins **P**SD95/**D**lg/**Z**O-1. These domains

commonly interact with short peptide motifs often found at the very C-terminus of proteins. PSD95 was notably shown to interact with the GluN2 subunit of the NMDAR and stabilise these receptors at the surface (Kornau et al., 1995; Roche et al., 2001). However, these experiments were mostly carried out using an overexpression system in heterologous cells and it is still unclear if the same mechanism occurs *in vivo*. A clearer role for PSD95 is in the coupling of receptor activity with downstream signalling molecules. PSD95 can bind to a variety of signalling molecules such as Kalirin7, SynGAP and AKAP97 recruiting them to membrane-tethered receptors for localised signalling (Kim and Sheng, 2004). Furthermore, PSD95 can interact with TARPs to recruit AMPARs to synapses and regulate AMPAR surface trafficking, thereby regulating synaptic strength (Bats et al., 2007). Indeed, overexpression of PSD95 increases excitatory synaptic transmission while RNAi knockdown of PSD95 decreases it (El-Husseini et al., 2000; Elias et al., 2006). It has been shown that PSD95 is intimately linked with synaptic plasticity too as overexpression of PSD95 occludes increased AMPAR LTP in slice culture and LTD is impaired in PSD95 mutant mice (Ehrlich et al., 2007; Migaud et al., 1998; Stein et al., 2003). PSD95 can also interact with adhesion molecules within the synapse such as the neuroligins (Irie et al., 1997). Taken together, this diverse molecule acts as a synaptic hub by interacting simultaneously with glutamate receptors, signalling proteins and adhesion molecules for efficient synaptic function.

Shank, Homer and GKAP: These three proteins form another abundant scaffolding complex deep within the PSD. Shank interacts with Homer via its PDZ domain while GKAP binds on the one hand to Shank and on the other to PSD95 acting as a bridge between this tripartite complex and membrane proteins via PSD95. There are three Shank proteins (1-3), which are large with many protein interacting partners. Shank proteins have been shown to promote spine growth and synaptic transmission (Sala et al., 2001). Furthermore, mutations in Shank proteins have been strongly associated with autism spectrum disorders (ASD) and KO mice show synaptic and spine defects highlighting the importance of Shank function in the PSD (Durand et al., 2012; Peça et al., 2011; Sato et al., 2012). The Homer family of proteins (Homer1-3) couple Shanks to group I mGluRs which indirectly creates an interaction between NMDARs and mGluRs via Shank, GKAP and PSD-95 (Tu et al., 1999). Homer also interact with dynamin3 linking the PSD with endocytic zones, specialised regions for endocytosis located proximal to the PSD for plasticity induced receptor trafficking (Lu et al., 2007).

Other scaffolding components: IRSp53 has been identified in the PSD and interacts with both PSD95 and Shank. This molecule acts as a Rac1 effector to regulate actin dynamics in spines (Choi et al., 2005; Soltau et al., 2004). AKAP79 binds to PSD95 and recruits AKAP associated enzymes to the PSD such as PKA and calcineurin. AKAP proteins are thought to bring these kinases and phosphatases closer to their specific substrates within the synapse (Bhattacharyya et al., 2009; Tavalin et al., 2002). Other scaffolding proteins have been shown to be important in the targeted transport of AMPARs within the synapse such as GRIP1 and PICK1 (Hanley and Henley, 2005; Mao et al., 2010; Setou et al., 2002). These trafficking molecules are present throughout the cell and are not selectively enriched in the PSD suggesting they function elsewhere within the trafficking pathway as well. Cytoplasmic signalling molecules such as kinases (CAMKIIα and β, PKA) and phosphatases (calcineurin, PP1) are recruited by scaffold proteins and enriched within the PSD for downstream regulation. CAMKIIα interacts with NMDARs and is activated by Ca^{2+} influx when NMDARs are stimulated. Active CAMKIIα brings about synaptic AMPAR delivery and is critical for LTP (Sheng and Kim, 2011).

1.3 The inhibitory synapse

GABA mediated inhibitory neurotransmission is the main form of inhibition in the brain, is critical for maintaining the correct balance between neuronal excitation and inhibition and is necessary for normal brain function (Smith and Kittler, 2010). GABA neurotransmitter largely acts through $GABA_A$Rs within the CNS. In addition, to the fast action of GABA on ionotropic $GABA_A$Rs, GABA also activates metabotropic $GABA_B$Rs that alter neuronal activity on a slower scale (Gassmann and Bettler, 2012). The inhibitory neurotransmitter glycine acts on a different subset of inhibitory synapses, via glycine receptors (GlyRs), which are important for mediating inhibition in the spinal cord, brainstem and retina (Betz et al., 1999; Dutertre et al., 2012). $GABA_A$R expression, trafficking and function modulate the strength of GABAergic synapses, implicating $GABA_A$Rs in the regulation of virtually all aspects of neuronal information processing and brain development.

1.3.1 GABA and $GABA_A$ receptors

$GABA_A$Rs are expressed ubiquitously throughout the whole CNS. They are heteropentameric GABA-gated chloride channels that belong to the Cys-loop ligand

gated ion channel family and respond to the neurotransmitter GABA. GABA was first identified in 1950 (Awapara et al., 1950; Roberts and Frankel, 1950). This identification lead to a large body of research suggesting GABA was acting as an inhibitory neurotransmitter (Bloom and Iversen, 1971). This data accumulated in the discovery that GABA localised to inhibitory nerve terminals in the brain. GABA is derived from glutamate by two glutamic acid decarboxylase isoforms found presynaptically, GAD65 and GAD67 (Erlander et al., 1991) and is loaded into synaptic vesicles by the vesicular GABA transporter (vGAT).

There are 19 $GABA_AR$ subunits, which have been classed into 8 different groups based on sequence homology (α1-6, β1-3, γ1-3, δ, ε, θ, π, ρ1-3). Each individual subunit consists of an N-terminal extracellular region, four transmembrane (TM) domains and a large cytoplasmic loop between TM3 and TM4. This loop is the site of most intracellular interactions between the subunit and cytosolic proteins important in signalling and trafficking. $GABA_ARs$ with different subunit compositions give rise to different receptor subtypes that are structurally and functionally distinct (Luscher et al., 2011a; Möhler, 2006). Recently, the first 3D X-ray structure for the $GABA_AR$ was described using a human β3 homopentamer. The structure revealed architectural elements unique to eukaryotic Cys-loop receptors and is vital for a complete understanding of the $GABA_AR$ and of the consequences of human disease mutations (Miller and Aricescu, 2014).

The most common subtypes that are found enriched in at least one area of the brain are made up of 2α and 2β subunits as well as a single γ2 or δ subunit. Other subunit combinations exist leading to less common subtypes with more limited distribution within the brain (Olsen and Sieghart, 2008). The major $GABA_AR$ subtypes that localise to the synapse are made up of two α1, α2 or α3 subunits, together with two β2 or β3 subunits and one γ2 subunit. Indeed, the γ2 subunit is essential for the postsynaptic clustering of these subtypes (Essrich et al., 1998). Within the synapse γ2 subunit-containing receptors characteristically have a lower affinity for GABA than extrasynaptic receptors and hence respond selectively to high levels of GABA released into the synaptic cleft during inhibitory synaptic transmission resulting in transient rapidly-desensitising postsynaptic responses (Perrais and Ropert, 1999).

$GABA_ARs$ also exist extrasynaptically and are known to be important in mediating tonic inhibition. This persistent form of GABAergic conductance is thought to shape

neuronal excitability and synaptic plasticity (Brickley and Mody, 2012). The most common nonsynaptic $GABA_AR$ subtypes consist of α4βδ in the forebrain and α6βδ in the cerebellum while α1βδ is important for tonic inhibition in the hippocampus. The δ-containing receptor subtypes have a high affinity for GABA allowing activation even in the presence of ambient GABA concentrations, often the result of residual GABA overspill from the synapse (Lee and Maguire, 2014; Luscher et al., 2011a). The necessity of δ-containing receptors for normal regulation of neuronal circuits is highlighted by the fact that changes in expression patterns and levels of δ-subunit containing receptors are associated with neurological disease phenotypes (Whissell et al., 2014). Interestingly, $GABA_ARs$ made up of specific subunit compositions are also detected along axons and within the axon initial segment (AIS) where they play a role in modulating action potential conductance and neurotransmitter release (Kullmann et al., 2005; Luscher et al., 2011a; Nusser et al., 1996).

1.3.2 Inhibitory synaptic structure

For efficient inhibitory synaptic transmission to take place it is vital that inhibitory neurotransmitter receptors are targeted to synapses opposing GABA or glycine releasing presynaptic terminals. Synaptic targeting and clustering of both $GABA_A$ and glycine receptors is mediated by the interaction of the intracellular domains of these receptor subunits with the cytoskeleton and the inhibitory PSD (Moss and Smart, 2001). Within the inhibitory PSD the proteins organise around one critical scaffold molecule, gephyrin. Gephyrin forms multimeric complexes by auto-aggregation and becomes the core of the PSD onto which other key proteins can interact. $GABA_ARs$, GlyRs, NLs and collybistin (Cb) are all known to interact with gephyrin and contribute to the integrity of the PSD (Figure 1.5) (Sheng and Kim, 2011; Tyagarajan and Fritschy, 2014).

How the inhibitory PSD forms and is maintained is still not well understood. Unlike, the excitatory PSD which is compartmentalised within dendritic spines, GABAergic synapses are found on the cell soma, dendritic shafts and within the AIS. Therefore, association of inhibitory PSD proteins with cytoskeletal components and extracellular molecules probably contribute to the formation and stabilisation of these synapses (Tyagarajan and Fritschy, 2014). Indeed, the inhibitory PSD interacts with the presynapse via trans-synaptic protein complexes, which implies a presynaptic contribution to the formation and maintenance of inhibitory synapses (Craig and

Kang, 2007; Zhang et al., 2010). The formation of hemisynapses on neurons co-cultured with heterologous cells overexpressing proteins of interest has provided an elegant method for determining the synaptogenic properties of a protein. Currently, presynaptic Nrxns and postsynaptic NL2, Slitrk3 and $GABA_A$Rs themselves have all been shown to promote inhibitory synapse formation in this way (Chih et al., 2006; Fuchs et al., 2013; Kang et al., 2008; Siddiqui and Craig, 2011; Takahashi et al., 2012).

1.3.2.1 Gephyrin

Gephyrin is considered to be the principle inhibitory postsynaptic scaffold protein which can auto-aggregate and form a lattice-like structure. The 93kDa molecule was the first identified protein to localise at inhibitory synapses (Triller et al., 1985) and was known to interact directly with GlyRs via the β-subunit (Pfeiffer et al., 1982). Since these early findings work has focused on characterising the role of gephyrin at inhibitory synapses and how the protein impacts on inhibitory synaptic structure and function (Tyagarajan and Fritschy, 2014). Gephyrin has two functional domains, G and E, joined by an unstructured linker region that contains most gephyrin regulatory sites and protein binding sites. The crystal structures of the G and E domains have been solved which has allowed models to be developed regarding the aggregated structure of gephyrin. Through the formation of trimers and dimers, gephyrin is thought to generate a hexagonal structural network capable of anchoring GlyRs and $GABA_A$Rs within the inhibitory synapse (Xiang et al., 2001). However, recently these models have been called into question following structural analysis of gephyrin and super-resolution imaging of gephyrin and GlyRs. Quantitative single molecule imaging has revealed endogenous gephyrin clusters at a density of 5,000-10,000 molecules/μm^2 and molecules are in approximately a 1:1 stoichiometry with GlyRs consistent with a model whereby all gephyrin molecules can bind receptors rather than binding as dimers and trimers (Specht et al., 2013). The inability to solve the structure of the linker region of gephyrin means accurately determining the mechanism of gephyrin auto-aggregation remains an obstacle within the field (Sander et al., 2013; Tyagarajan and Fritschy, 2014).

Although a robust interaction between gephyrin and GlyRs has been described an interaction between $GABA_A$Rs and gephyrin has been difficult to obtain (Meyer et al., 1995; Pfeiffer et al., 1982). It was not until more recently that a detergent-sensitive interaction between gephyrin and the α2 subunit was described, which was later shown for the α1 and α3 subunits (Maric et al., 2011; Saiepour et al., 2010; Tretter et

al., 2008, 2011). Others have shown using *in vitro* assays that gephyrin is capable of binding the intracellular loop of $GABA_AR$ β2 and β3 subunits too (Kowalczyk et al., 2013). Interestingly, the binding sites of the α-subunits on gephyrin overlap and compete with the binding of the GlyR β-subunit within the E domain, however, the affinity of the $GABA_AR$ subunits are ~500 fold less than the GlyR subunits (Maric et al., 2011). Of note, the α-subunits, together with the γ2 and δ subunits have been shown to play a direct role in the synaptic versus extrasynaptic localisation of $GABA_ARs$. Indeed, expression of α2β3γ2 receptors in HEK cells co-cultured with neurons produced fast GABAergic events consistent with synaptic localisation. Substitution of the α2 subunit for α6 resulted in very slow events that could not be explained by changes in receptor kinetics but instead were due to the loss of synaptic targeting potentially due to lack of gephyrin binding (Wu et al., 2012). Recently, the synaptic localisation of α5 subunit containing $GABA_ARs$, through an interaction with gephyrin, has been reported. The levels of these receptors, commonly known to be extrasynaptic, within the synapse have been shown to regulate dendritic outgrowth and spine maturation (Brady and Jacob, 2015). Although the interaction between gephyrin and $GABA_ARs$ appears to be subunit specific, gephyrin still serves as a reliable postsynaptic marker for all GABAergic synapses.

Gephyrin has been shown to be required for the synaptic clustering of $GABA_ARs$ in a subtype specific manner. In the absence of gephyrin α2βγ2 and α3βγ2 receptors no longer cluster at synapses (Essrich et al., 1998; Kneussel et al., 1999). However, α1βγ2 receptors have been shown to cluster at synapses independently of gephyrin. This is interesting as gephyrin has been shown to be essential for GlyR clustering (Lévi et al., 2004). Furthermore, this finding points towards other, potentially unknown inhibitory PSD scaffold proteins being sufficient to stabilise synapses independent of gephyrin. Intriguingly, the relationship between the $GABA_ARs$ and gephyrin appears to be bi-directional. Loss of postsynaptic receptor clustering in $GABA_AR$ subunit KO mice results in synaptic gephyrin declustering and the formation of large gephyrin aggregates within the soma, coupled with these cells failing to produce GABAergic currents (Peden et al., 2008). Taken together, these data indicate that the exact role of gephyrin at synapses is receptor and receptor subtype specific.

Recent biochemical studies have revealed that post-translational modifications of gephyrin are integral to its role in regulating $GABA_AR$ clustering and inhibitory synaptic transmission. Phosphorylation of gephyrin at serine 270 and serine 268 by

GSK3β and ERK respectively was shown to regulate the density of GABAergic synapses and the frequency of GABAergic postsynaptic currents (Tyagarajan et al., 2011a, 2013). Furthermore, a homeostatic increase in perisomatic inhibitory synapses and spontaneous GABAergic currents following NMDA-receptor dependent LTP was shown to be dependent on CamKII phosphorylation of gephyrin at serine 305 in slices (Flores et al., 2015). Additionally, in dissociated neuronal culture palmitoylation of gephyrin at cysteine 212 and cystine 284 has been shown to enhance gephyrin clustering and potentiate GABAergic transmission (Dejanovic et al., 2014). Lastly, gephyrin has been reported to interact with neuronal nitric oxide synthase (nNOS) and be S-nitrosylated *in vivo*. S-nitrosylation had a negative effect on gephyrin clustering as inhibition of nNOS resulted in larger gephyrin clusters and more surface $GABA_A$Rs (Dejanovic and Schwarz, 2014). It remains to be fully determined what the upstream regulators of these modifications are. However, Wuchter and colleagues carried out a screen to identify kinases required for gephyrin clustering and identified 12 hits including FGFR1, TrkB, TrkC, MAPK and mTOR pathways (Wuchter et al., 2012).

1.3.2.2 Neuroligin 2

Neuroligins (NLs) have already been discussed with respect to the excitatory synapse, however, the synapse specificity of NL2 has led to it being intensely studied as a potential molecular determinant for GABAergic synapse formation (Krueger et al., 2012; Varoqueaux et al., 2004). Co-culture experiments have revealed that heterologous cells overexpressing NL2 can induce presynaptic development of GABAergic synapses on neighbouring neurons (Chih et al., 2005; Scheiffele et al., 2000). NL2 has also been shown to interact with gephyrin (Poulopoulos et al., 2009), therefore, can drive the clustering of gephyrin and $GABA_A$Rs at new postsynaptic sites. Recently, binding of Nrxn1β to NL1 was shown to stimulate the interaction between NL1 and PSD95 and promote phosphorylation of NL1 at tyrosine 782 in its intracellular domain. This phosphorylation prevented gephyrin binding to NL1 suggesting that ligand-dependent tyrosine 782 phosphorylation provides a mechanism to control the balance between excitatory and inhibitory scaffold assembly (Giannone et al., 2013). The corresponding residue in NL2, tyrosine 770, when mutated to a phospho-null residue abolished the interaction between NL2 and gephyrin (Poulopoulos et al., 2009). However, physiological phosphorylation of this site or the signalling molecules involved have not been identified for NL2. It remains to be determined if tyrosine 770 phosphorylation could provide a mechanism for

modulating inhibitory synapse formation. In line with this notion, NL2 was recently shown to undergo proline-directed phosphorylation which led to the recruitment of the peptidyl-proline *cis-trans* isomerase Pin1 and a loss of gephyrin binding. Indeed, in Pin1 KO mice, NL2, gephyrin and $GABA_AR$ accumulation was enhanced at inhibitory synapses and amplitude of spontaneous GABAergic currents were increased (Antonelli et al., 2014).

Interestingly, NL2 knock-out mice can still form GABAergic synapses although the animals show region specific alterations in GABAergic synapse distribution and function. This implies that NL2 is not essential for GABAergic synapse formation and that there are likely compensatory mechanisms in place using other adhesion molecules or NL family members. Nevertheless, NL2 KO mice show selective loss of gephyrin and $GABA_AR$ clusters, a decrease in inhibitory transmission in the cerebral cortex and exhibit increased-anxiety behaviour demonstrating the importance of NL2 at inhibitory synapses (Blundell et al., 2009; Gibson et al., 2009; Hoon et al., 2009). Furthermore, conditional NL2 KO in the medial prefrontal cortex of mice has shown that local disruption of synaptic inhibition by loss of NL2 can also lead to cognitive impairments. These mice displayed complete loss of NL2 in the medial prefrontal cortex within 2-3 weeks and by 6-7 weeks showed major reductions in inhibitory synaptic transmission along with impaired anxiety, fear memory and social interactions (Liang et al., 2015). Triple NL1, NL2 and NL3 KO mice showed severely altered GABAergic and glycinergic synapses in the brainstem but not a total lack of inhibitory synapses suggesting that other so far unknown inhibitory synaptogenic complexes probably exist (Tyagarajan and Fritschy, 2014).

1.3.2.3 Collybistin

Collybistin (Cb), encoded by the gene *Arhgef9*, is another protein localised to the inhibitory synaptic PSD in rodent brain. It was first identified to bind to gephyrin in a Y2H screen and can modulate gephyrin clustering. When overexpressed in non-neuronal cells gephyrin appears diffuse in the cytoplasm, however, coexpression of Cb induces the translocation of gephyrin to the cell surface and drives the formation of gephyrin clusters (Kins et al., 2000). In neurons, endogenous Cb colocalises with gephyrin and $GABA_AR$ clusters and is recruited to synapses early in development. Intriguingly, Cb is only detected at a subset of gephyrin positive puncta within the cerebellar cortex (Patrizi et al., 2012). Mutations in *Arhgef9*, are a rare cause of intellectual disability (ID), with associated features such as seizures, increased anxiety

and aggressive behaviour, thought to be caused, at least in part, by mislocalised gephyrin and altered inhibitory synapse formation (Harvey et al., 2004, 2008).

Cb is a specific Rho GTPase GEF and its crystal structure revealed it to be selective for Cdc42 (Xiang et al., 2006). The protein has an N-terminal SH3 domain as well as a catalytic DBL homology (DH) domain and a pleckstrin homology (PH) domain. There are three known isoforms of Cb (Cb1-3) and numerous splice variants of each. By studying Cb splice variants with and without the SH3 domain (SH3+, SH3-), this motif was shown to negatively regulate the translocation and submembrane clustering of gephyrin (Harvey et al., 2004). More recently Cb splice variants were shown to differentially interact with Cdc42 and gephyrin to regulate gephyrin clustering. Cdc42, gephyrin and $Cb2_{SH3-}$ but not $Cb2_{SH3+}$ could form a ternary complex and explained the increased gephyrin clustering in neurons observed with $Cb2_{SH3-}$ compared to $Cb2_{SH3+}$ overexpression (Tyagarajan et al., 2011b). That said, shRNA mediated knockdown of Cb in hippocampal cultures impaired GABAergic signalling which could be rescued by any of the Cb isoforms (Körber et al., 2012). Therefore, the relevance for these numerous splice isoforms still remains unclear (Papadopoulos and Soykan, 2011).

Cb has been shown to drive gephyrin clustering and inhibitory synapse stability via interactions with $GABA_ARs$ and NL2, as well as its interaction with Cdc42. Indeed, gephyrin and Cb both interact with the α2 $GABA_AR$ subunit forming a trimeric complex. This complex can be disrupted by a disease associated mutation in Cb (G55A), highlighting the importance for Cb in α2 subunit-containing $GABA_AR$ clustering (Saiepour et al., 2010). Interestingly, a recently discovered epilepsy and intellectual disability (ID) associated mutation in Cb (R290H) was shown to alter the strength of an intramolecular interaction in Cb between the DH and PH domains. This mutation reduced the phosphatidylinositol 3-phosphate lipid-binding affinity of Cb and consequently affected inhibitory synapse formation (Papadopoulos et al., 2015). NL2 has been shown to specifically activate Cb and drive the cell autonomous clustering of $GABA_ARs$ in the presence of gephyrin and $Cb2_{SH3+}$. This mechanism has been suggested to be more physiological as only Cb isoforms containing the SH3 domain have been detected *in vivo* (Poulopoulos et al., 2009). KO mouse studies provide more evidence for the role of Cb in gephyrin clustering and GABAergic synapse formation. *Arhgef9* KO mice show Cb is not essential for gephyrin and GlyR clustering at glycinergic synapses, however, alterations were seen at GABAergic

synapses. Furthermore, the animals showed reduced GABAergic transmission in the hippocampus. Behaviourally, they were more anxious than WT animals and had impaired spatial learning, consistent with reduced inhibitory transmission (Papadopoulos et al., 2007). These defects in inhibitory transmission could also be induced upon conditional postnatal KO of Cb in mice demonstrating that Cb in required for GABAergic maintenance as well as development (Papadopoulos et al., 2008).

1.3.2.4 Other scaffolding components

Including, gephyrin, NL2, Cb and $GABA_A$Rs themselves, there have been a number of other inhibitory synaptic molecules identified however the function of many of these proteins remain largely unknown (Tyagarajan and Fritschy, 2014). The scaffold molecule S-CAM is known to be enriched at inhibitory synapses and although an interaction with gephyrin has not yet been described it can bind to NL2 via its protein interacting domains (Sumita et al., 2007). Likewise, MAM domain-containing GPI anchor proteins MDGA1 and MGDA2 interact in *cis* with NL2 but not other NLs. Loss of these proteins reduce inhibitory synapses in a NL2 dependent manner (Lee et al., 2013). The large cytoskeletal protein dystrophin has been shown to selectively localise to a subset of GABAergic synapses and in dystrophin KO mice $GABA_A$R clustering was reduced in dystrophin-positive brain regions independent of gephyrin (Knuesel et al., 1999). Interestingly, dystroglycan, an adhesion molecule that links dystrophin to the extracellular matrix shows similar enrichment at a subset of synapses and is necessary for the synaptic targeting of dystrophin (Lévi et al., 2002). Lastly, the adhesion molecule neurofacin was shown to stabilise GABAergic terminals at the AIS and regulate gephyrin cluster size (Kriebel et al., 2011).

Gephyrin has been shown to interact with tubulin. Intriguingly, tubulin is found in very little quantities at inhibitory synapses therefore, the role for this interaction and whether it is important for inhibitory synapse structure is still not well understood. Gephyrin also interacts with motor proteins and acts as an adaptor in the transport of GlyRs and so the interaction between gephyrin and tubulin may be due to a trafficking function (Dumoulin et al., 2009). Actin is thought to be the more predominant cytoskeletal structure at inhibitory synapses and the actin binding proteins profilin1 and profilin2, have been shown to interact with gephyrin. Furthermore, this complex interacts with the ENA/VASP actin associated protein family, also regulators of actin dynamics (Giesemann et al., 2003). Interestingly, the ENA/VASP complex also

interact with the WRC (Chen et al., 2014b). In cultured neurons, profilin2A robustly colocalises with gephyrin at inhibitory postsynaptic sites. The gephyrin profilin interactions have been proposed to regulate changes in the actin cytoskeleton either up or downstream of gephyrin anchoring to the PSD (Murk et al., 2012). Recently, the scaffold protein GIT1, known to be important in the regulation of excitatory synaptic structure, has been identified as a new member of the inhibitory PSD. GIT1 localises to inhibitory synapses, interacts with gephyrin and $GABA_AR$s and was shown to be essential for inhibitory synaptic stability and transmission due to its role in an actin regulatory pathway involving βPIX and Rac1 (Smith et al., 2014).

1.3.3 $GABA_AR$ trafficking

Regulation of $GABA_AR$ trafficking may determine inhibitory synaptic strength and hence neuronal excitability. Indeed, $GABA_AR$s can be rapidly trafficked between synaptic and extrasynaptic sites and between surface and intracellular compartments (Petrini and Barberis, 2014). These processes are regulated by interactions with several $GABA_AR$-associated proteins, and by phosphorylation, palmitoylation and ubiquitination of receptors (Figure 1.5) (Luscher et al., 2011a).

Receptors are trafficked to the plasma membrane via the secretory pathway. Newly synthesised $GABA_AR$s assemble in the endoplasmic reticulum (ER); any unassembled receptors are targeted for degradation by ubiquitination. PLIC-1 interacts with correctly assembled receptors and inhibits their degradation, which in turn promotes translocation of the receptors from the ER to the Golgi (Bedford et al., 2001). The palmitoyltransferase GODZ palmityolates the γ2 $GABA_AR$ subunit and promotes the trafficking of receptors though the Golgi apparatus (Keller et al., 2004). The GEF BIG2 is thought to facilitate receptors exiting the Golgi (Charych et al., 2004). Upon exiting the Golgi, $GABA_AR$s interact with the kinesin motor KIF5A, via the GABA-receptor associated protein (GABARAP), which is known to bind to the $GABA_AR$ γ2 subunit (Wang et al., 1999), and are trafficked to the membrane (Nakajima et al., 2012). The less well characterised kinesin motor KIF21b has also been recently shown to drive the surface delivery of γ2 subunit containing $GABA_AR$s via an interaction with the γ2 subunit (Labonté et al., 2014). At the plasma membrane $GABA_AR$s are initially inserted extrasynaptically and laterally diffuse into synaptic sites where they become anchored by interactions with inhibitory synapse scaffold proteins (Bogdanov et al., 2006). Extrasynaptic receptors localise to endocytic zones or lipid rafts

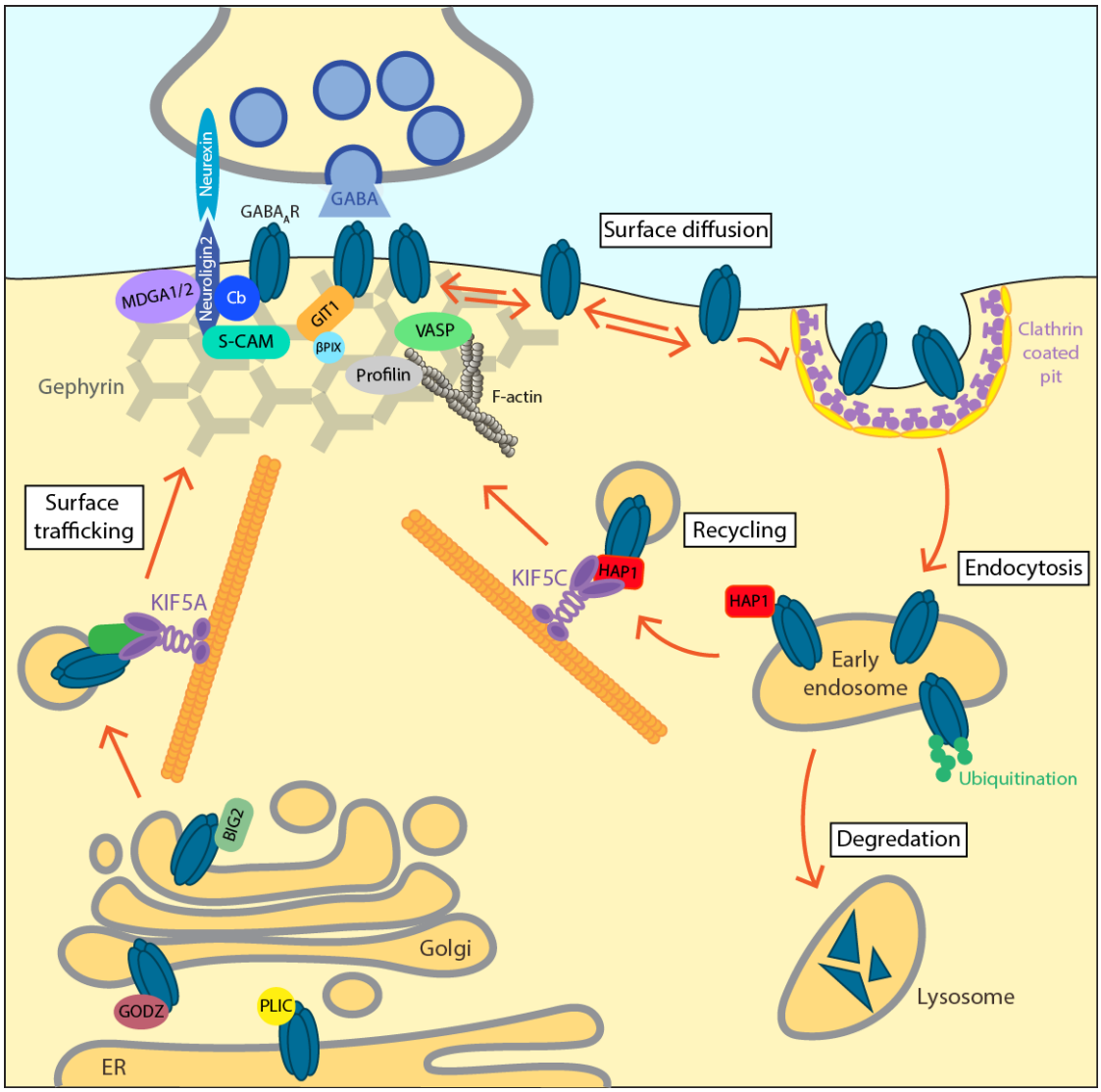

Figure 1.5: GABA$_A$ receptor trafficking and the inhibitory PSD.

GABA$_A$Rs are assembled in the endoplasmic reticulum (ER) and trafficked through the ER and Golgi via the adaptor proteins PLIC, GODZ and BIG2. Receptors are then coupled to the KIF5A kinesin motor and transported to the membrane. At the inhibitory synapse gephyrin, collybistin (Cb) and GIT1 tether GABA$_A$Rs within the PSD. Gephyrin/Cb/GABA$_A$R complexes interact with and are stabilised by the adhesion molecule neuroligin2 which in turn binds to presynaptic neurexin to aid pre and postsynaptic alignment. GABA$_A$Rs are endocytosed in a phospho-sensitive manner, dephosphorylation promotes AP2 binding and clathrin-dependent endocytosis. In early endosomes γ2 subunit ubiquitination leads to lysosomal degradation of internalised receptors. Otherwise, an interaction between HAP1 and the β3 subunit facilitate KIF5C dependent recycling of GABA$_A$Rs back to the plasma membrane. Adapted from (Luscher et al., 2011a).

(Hering et al., 2003; Kittler et al., 2000). A motif within the intracellular loop of the $GABA_AR$ β3 subunit mediates AP2 binding and stabilisation of receptors at endocytic zones (Smith et al., 2012).

Within the plasma membrane $GABA_ARs$ can be remarkably dynamic. With advancements in live cell imaging, receptor lateral diffusion has been analysed. Fluorescent recovery after photobleaching (FRAP) experiments of fluorescently labelled $GABA_ARs$ revealed that $GABA_AR$ lateral diffusion was confined at synaptic sites compared to extrasynaptic locations with the fluorescence recovery rates being slower and faster respectively. Recovery was faster at the edges of bleached regions consistent with replenishment of $GABA_ARs$ within the plane of the membrane rather than by insertion into the membrane from internal receptor pools. Interestingly, loss of gephyrin increased the fluorescence recovery rate at synaptic sites providing evidence for the role of gephyrin in $GABA_AR$ synaptic confinement (Jacob et al., 2005). More recently, single-particle tracking of $GABA_ARs$ with quantum dots has demonstrated that receptor diffusion dynamics are modulated by neuronal activity. $GABA_ARs$ were less clustered and more dynamic within the membrane following glutamate receptor activation (Bannai et al., 2009; Muir et al., 2010).

Internalisation of extrasynaptic $GABA_ARs$ occurs mainly via dynamin and clathrin-mediated mechanisms. Phosphorylation dependent interactions between the $GABA_AR$ β and γ2 subunits with endocytic proteins such as AP2 modulate this process and provide subtype-specific regulation (Kittler et al., 2005, 2008, 2000). Once internalised, $GABA_ARs$ are ubiquitinated and trafficked to the lysosomal pathway for degradation or rapidly re-inserted into the surface membrane facilitated by an interaction with the Huntingtin-associated protein 1 (HAP1) (Arancibia-Cárcamo et al., 2009; Kittler et al., 2004). HAP1 acts as an adaptor molecule coupling $GABA_ARs$ to the kinesin motor KIF5 allowing their recycling back to the synapses after internalisation (Kittler et al., 2004; Twelvetrees et al., 2010). Disrupting the HAP1-KIF5 interaction reduces the number of synaptic $GABA_ARs$ and physiologically decreases mini inhibitory postsynaptic currents (mIPSCs); hence HAP1 can regulate the strength of inhibitory synaptic transmission.

1.4 Neuropsychiatric disorders

1.4.1 Genetics

Neuropsychiatric disorders such as ASD, SCZ, ID and epilepsy are heterogeneous; patients present with a wide spectrum of symptoms ranging from mild to very severe. The varying disease phenotypes can make diagnosis and treatment challenging, therefore understanding the genetic basis of these disorders will help uncover more about the human physiology and disease aetiology so that more effective means of diagnosis, treatment and prevention can be developed.

Similar to cancer and diabetes, neuropsychiatric disorders are referred to as common or complex disorders. They arise from an accumulation of common genomic variations with small effect sizes, which are considered to be risk factors for the condition, in combination with lifestyle and environmental factors. The huge variety in the combination of genetic risk factors a patient may possess is thought to explain the large phenotypic heterogeneity observed in these disorders. Such genomic variations include, changes to individual nucleotides known as single nucleotide polymorphisms (SNPs). These polymorphisms can be common occurring in the population at a frequency >5% or can be rare with a frequency of <1-0.5%. Larger structural variations such as deletions, insertions, translocations, inversions and copy number variations (CNVs) may also contribute to the genetic basis of neuropsychiatric disorders (Frazer et al., 2009; Schork et al., 2009). It must be noted, that some monogenetic diseases do present with neuropsychiatric phenotypes. The defective genes in these diseases are more easily identified due to their large effect size allowing a targeted approach to studying the mechanisms of the disease but also the associated cognitive phenotypes.

Heritability is the proportion of phenotypic variance in a population attributable to additive genetic factors (Manolio et al., 2009). It is measured by estimating the relative contributions of genetic verses non-genetic factors to the total phenotypic variation. These estimates are important as they outline to what extent genetic factors influence disease phenotypes. Estimates of disease heritability are commonly derived from familial and twin studies. Familial studies compare the rates of disease in family members of an individual with the disease to the prevalence of the disease in the general population. As family members share genetic information, higher disease

rates within families with an affected member demonstrate an inherited genetic contribution to the disease. Twin studies on the other hand, compare the concordance rate, i.e. the presence of the same trait in both twins, of monozygotic twins to dizygotic twins. For example, if the concordance rate of a disease trait was higher in monozygotic twins who share almost 100% of their genetic material compared to dizygotic twins who share 50% of their DNA this implicates that genes play an important role in this trait. Monozygotic twins also provide a powerful tool to study environmental versus genetic contributions to a disease; differences in traits between monozygotic twins are most likely due to environmental factors. Early studies of twins to estimate ASD heritability showed ~90% concordance in ASD diagnosis in monozygotic pairs and ~10% in dizygotic twins suggesting a heritability of around 90% (Bailey et al., 1995). However, more recently population-based studies with larger sample sizes have resulted in a more refined estimate of ~50%, and suggest half of this heritability is due to common variants (Gaugler et al., 2014; De Rubeis and Buxbaum, 2015). In the case of SCZ, compiling available twin studies data has led to an estimate for heritability of 81% (Bienvenu et al., 2011; Sullivan et al., 2003).

There is a large proportion of heritability in many neuropsychiatric disorders (Bienvenu et al., 2011; De Rubeis and Buxbaum, 2015), and to this end identifying what genetic variations contribute to this heritability remains an important question. In the past, genetic linkage studies were used to identify disease-associated genes in affected families. By knowing the location of known genetic markers, this method could be used to narrow down the location of the genomic region-associated with disease. Genetic linkage has proven useful for single-gene disorders but is more challenging and less accurate for complex disorders that may arise from more than one alteration in the genome. Originally, to determine the genetics of complex disorders, associated SNPs were identified mainly through sequencing projects focusing on genes thought to be involved in pathways underlying the disorder. However, this candidate gene approach was often based on imperfect biological understanding, used small sample sizes and the number of SNPs assayed were limited. Over recent years, vast improvements in genomic sequencing has led to the emergence of large-scale screening techniques to identify genetic variations associated with complex disorders. These screens have been aided by the completion of the Human Genome Project and the HapMap Project which have identified regions of common genetic variation in the human genome. Genetic research in this way is able to shed more light on the contributing genetic risk factors for neuropsychiatric

disorders.

1.4.1.1 Genome-wide association studies

Genome-wide association studies (GWAS) provide a high throughput method of screening whole genomes for common SNPs and are therefore not candidate driven. This type of study is a powerful unbiased method of detecting genetic variants that contribute to complex disorders. The most common approach of GWAS is the case-control setup. Microarray chips containing common regions of genomic variation are used to screen DNA from a large patient group (cases) with a particular disorder and compared to a large group of healthy control individuals (controls). Common genetic variants that occur significantly more frequently in cases compared to controls are said to be associated with the disorder. For each genotyped SNP, the allele frequency is then calculated in the control and case cohort, this is the amount of a particular allele represented as a proportion of the total alleles at that particular genetic locus. Geneticists look for a significant difference in the allele frequency of a particular SNP between the case and control group. The odds ratio is often used to report the size of a genetic association in a GWAS. It is a ratio of the odds of having a disease with a specific allele verses the odds of having the disease without the specific allele. When the allele frequency is much greater in the cases compared to control the odds ratio will be higher than 1. Furthermore, a p-value for the significance of the odds ratio is often calculated using a chi-squared test. Odds ratios significantly different from 1 highlight SNPs that are associated with disease and is the main goal for GWAS. This type of genetic analysis is very useful in identifying the numerous genetic contributing factors to complex disorders such as ASD and SCZ (McCarroll et al., 2014). However, as these disorders are thought to arise from an accumulation of many different variants with small effect sizes, large sample numbers are needed to identify associated variants.

1.4.1.2 Rare variants studies

Although GWAS have proved essential in identifying genes and variants associated with neuropsychiatric disorders the studies are limited as they only focus on the contribution of common genetic variants to the condition in question. Common variants individually or in combination typically confer relatively small increments in risk explaining only a small proportion of heritability (Frazer et al., 2009), leaving a large amount of heritability for neuropsychiatric disorders unexplained. One explanation for this missing heritability is that there are a large number of common

variants with small effects yet to be found. Increasing the sample size of GWAS will improve their power to detect association and may reveal more implicated common variants. However, another explanation is that rare variants with larger effect sizes that are poorly detected with SNP arrays contribute risk (Manolio et al., 2009; Zuk et al., 2014). It is thought that the higher penetrance of these rare variant may result in a selective disadvantage and reduced fecundity in the affected individuals contributing to the low frequency of these alleles in the population. This idea has motivated geneticists to explore the contribution of rare mutations to disease. These mutations may infer greater risk but are less frequent in the population therefore harder to detect (Manolio et al., 2009).

In contrast to GWAS which mainly uses SNP arrays, rare variant association studies employ high-throughput whole genome or exome sequencing. With the improvements in the speed and the reduction in costs of such sequencing methods these studies are becoming increasingly widespread. Following genotyping, analysis is similar to that of GWAS determining whether a variant occurs significantly more frequently in cases than controls. Rare variant association studies have the ability to detect rare variants occurring in <0.5-1% of the population which are not included in common SNP arrays. A caveat to this technique is that the power to detect association of rare variants with disease is very low, even in large sample sizes, due to the rarity of variants. Strategies are being developed to assess the collective effect of multiple rare variants within target genomic regions (Bansal et al., 2010). As with GWAS the need to compile samples from numerous datasets is apparent and will improve the power to detect association.

1.4.1.3 Structural variation: copy number variation

In addition to the identification of common and rare SNPs contributing to complex diseases, there have been a number of studies investigating the contribution of rare structural variations, such as copy number variations (CNV), to human disease. CNV is the most common form of structural variation in the human genome and can result from deletions, duplications, triplications, insertions and translocations of DNA stretches ranging from 1 kilobase to several megabases. Depending on the genetic location of these structural variations an array of genes can be disrupted resulting in alternate gene products or changes in allelic expression. Moreover, disruption of genomic regulatory regions can result in dysregulated gene expression. Most CNVs are stable and inherited contributing to 13% of human genomic DNA, however, some

CNVs arise *de novo*. Like with SNPs, disease-associated CNVs detected so far include rare variants with large associated effect sizes and common variants with more modest effects but carried by a large proportion of the population.

As an extension of GWAS specialised SNP arrays have been designed which incorporate specific CNV probes so sample DNA can be screened for CNVs (McCarroll, 2008). However, many SNP arrays have sufficient information to permit CNV analysis already (Frazer et al., 2009; Manolio et al., 2009). Indeed, genetic screens have identified *de novo* CNVs within the genome that are strongly associated with neuropsychiatric disorders such as ASD, SCZ and ID (Lee and Lupski, 2006; Merikangas et al., 2009; Sebat et al., 2007; Shishido et al., 2014; Tam et al., 2009).

1.4.2 Molecular mechanisms of neuropsychiatric disorders: synapses and dendrites

Genetic studies as described above have identified numerous neuropsychiatric disorder associated SNPs and CNVs. By studying the function of the genes affected by these genomic variations it may be possible to elucidate some of the molecular and cellular mechanisms which become dysregulated in such conditions. Interestingly, genes implicated in the regulation of synaptic function and dendritic development are consistently emerging from genetic studies to be associated with disorders such as ASD, SCZ and MR. This is perhaps not surprising considering numerous studies report that many neuropsychiatric disorders are characterised by dendritic and synaptic pathology (Figure 1.6) (Kaufmann and Moser, 2000; Kulkarni and Firestein, 2012; Penzes et al., 2011).

Correct dendritic development requires the formation of dendritic branches and dendritic spines and is necessary for neurons to receive and convey information, is a critical step in neurogenesis and vital for normal brain function (Kulkarni and Firestein, 2012). Dendrites must satisfy particular physiological requirements to function efficiently. Firstly, dendrites need to cover the area (dendritic field) that includes the sensory and/or synaptic inputs of that neuron. Secondly, dendrites need to be complex and dense enough to sample and process all the signals that converge on the dendritic field. Finally, dendrites need to be flexible and capable of adjusting during development and in response to experience (Jan and Jan, 2010). In this way, dendritic development is a highly complex process and requires a large number of

organised and well-coordinated signalling pathways and mechanisms to occur.

Dendritic development occurs in stages. Human dendritic development begins with early polarisation, which occurs prenatally. The neurons then progress into a stage of dendritic and synapse expansion and growth, this stage occurs both pre and postnatally with dendritic complexity and synapse number approaching their maximum in early childhood. Following this, dendrites and synapses undergo remodelling and pruning during adolescence with the elimination of some processes. Finally, the remaining dendrites undergo differentiation and maturation until their mature structures are reached (Kaufmann and Moser, 2000). The molecular mechanisms that regulate dendritic morphogenesis can be broadly divided into cell-extrinsic and cell-intrinsic cues.

Cell extrinsic cues include chemoattractive and chemorepellent molecules such as ephrins and neurotrophins. Furthermore, neurotransmitters, growth factors and cell adhesion molecules influence dendritic development and guidance to their partner synapses (Parrish et al., 2007; Valnegri et al., 2015). Acetylcholine has been shown to impact on dendritic expansion while, activation of certain glutamate receptors has been implicated in dendritic pruning (Kaufmann and Moser, 2000). In addition, neurotrophins such as BDNF and NGF have been shown to modulate dendritic arborisation in cortical neurons in a layer specific manner (McAllister et al., 1995, 1997). These growth cues signal through tyrosine receptor kinases (Trks) (Trks reviewed by (Patapoutian and Reichardt, 2001)). Each trophic factor signals through a different subset of Trks such that the response of the neuron to neurotrophin signalling is determined by the pattern of receptors it expresses (Parrish et al., 2007). It is not fully understood how neurotrophins are delivered to growing neurons *in vivo*, however local delivery of BDNF in cultured cortex brain slices has been shown to enhance dendritic branching suggesting that where these factors are produced and delivered may allow for spatial regulation of dendritic growth (Cohen-Cory et al., 2010; Horch and Katz, 2002).

As well as secreted proteins and cell adhesion molecules, the expression of surface receptors, the formation of synapses and neuronal activity also contribute to extracellular growth cues (Valnegri et al., 2015). Live cell imaging has revealed dendritic branch formation is not a steady process of growth and extension as originally thought but is actually a dynamic process of extension and retraction.

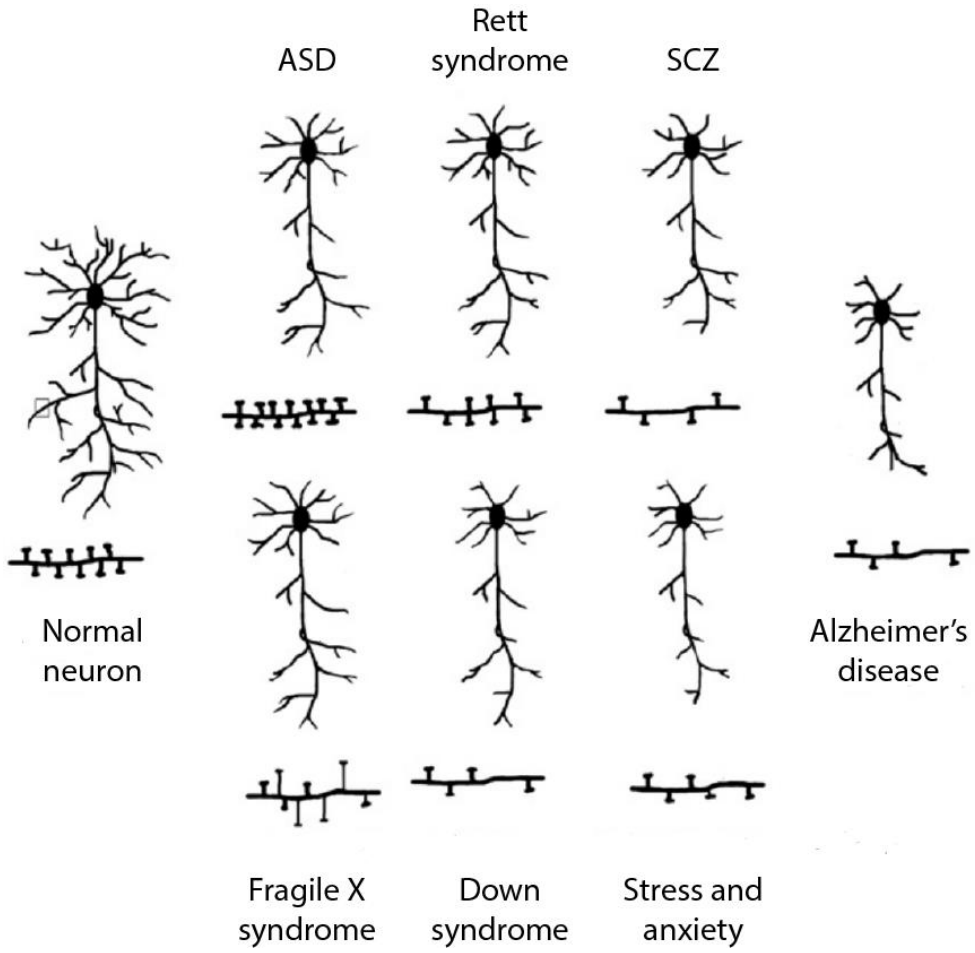

Figure 1.6: Dendritic and spine morphology in neuropsychiatric disorders.

Schematic representation of a neuron and dendritic processes containing spines in brains of individuals with neuropsychiatric disorders. Defects in dendritic development and morphology including changes in dendritic branching, fragmentation of dendrites, retraction or loss of branches and changes in spine morphology and number contribute to many neuropsychiatric disorders. In particular, neurons from subjects with autism spectrum disorder (ASD) show decreased dendritic complexity and higher spine density than normal. Similarly neurons from Rett's syndrome sufferers have decreased dendritic branching. Neurons from schizophrenia patients show reduced dendritic arbour and spine density. Finally, aberrant dendritic morphology and a high density of long, thin, immature dendritic spines is observed in fragile X syndrome. Down syndrome, stress and anxiety and Azheimer's disease all also impact on dendritic and spine morphology. Adapted from (Kulkarni and Firestein, 2012).

Dendrite branching begins with filopodia formation; these protrusions rapidly extend and contract several times per minute (Dailey and Smith, 1996). Many protrusions are lost during retraction while some are stabilised and form nascent branches. Synapses form on these newly extended dendritic filopodia and contribute to filopodia stabilisation, allowing them to mature into dendritic branches (Niell et al., 2004). Indeed, in the juvenile calsyntenin1 KO mouse, a protein important in the trafficking of receptors, synapses were less mature due to altered NMDAR subunit composition and transmission was depressed. KO neurons showed decreased dendritic development, an increased proportion of filopodia-like dendritic protrusions and more thin spines (Ster et al., 2014). This highlights the importance of synapse formation and maturation in the dendritic development. Synaptic activity is also important for dendritic growth. Indeed, two photon imaging of GFP-expressing pyramidal CA1 neurons revealed enhanced filopodia extension following high frequency stimulation (Maletic-Savatic et al., 1999). As the neuron matures and synapses develop, dendritic filopodia become less dynamic and are replaced by the formation of dendritic spines (Dailey and Smith, 1996; Kulkarni and Firestein, 2012). It is not surprising that due to the intimate relationship between synapse development and dendritic stabilisation loss of synapse function or stability can lead to defects in connectivity resulting in brain disease. This theory is being considered in the context of many neuropsychiatric disorders.

A vital role for cell-intrinsic factors in dendritic growth and development has been demonstrated by *in vitro* studies (Puram and Bonni, 2013). Even within the artificial environment of a culture dish, neurons develop different dendritic morphologies. It can therefore be assumed that the intrinsic factors within the neurons are influencing these differences in morphology (Bartlett and Banker, 1984). The major intracellular factors regulating dendritic morphogenesis comprise of transcriptional regulators, cytoskeletal mechanisms and regulators of protein trafficking and turnover including local protein translation (Puram and Bonni, 2013). *Drosophila* provide a simple system to study dendritic morphogenesis. Indeed, a genome-wide screen of transcription factors identified 78 fly genes that regulated different elements of dendritic outgrowth, from coverage, to outgrowth versus branching and specification of primary or secondary structures (Parrish 2006). It is thought that the different expression patterns of these transcription factors between neurons influence their dendritic morphology. Many of these genes have been shown to have conserved functions in mammals too. Other transcription factors are known to promote activity

dependent dendritic development in respond to Ca^{2+} regulation (Jan and Jan, 2010; Kulkarni and Firestein, 2012).

Similarly to the role of actin in dendritic spine morphology, discussed above on page 27, actin dynamics and actin regulators are vital for normal dendritic development. The small GTPases RhoA, Rac1 and Cdc42 are well known for their roles in regulating actin extension and retraction and are critical to neuronal development (Auer et al., 2011; Negishi and Katoh, 2005; Newey et al., 2004). In *Drosophila*, RhoA mutants show excessive dendritic growth while loss of all three Rac1 proteins reduces dendritic size and complexity in mushroom bodies (Lee et al., 2000; Ng et al., 2002). Furthermore, loss of Cdc42 in the fly visual system results in reduced dendritic branching and decreased spine density (Scott et al., 2003). In mouse brain, conditional KO of Rac1 impacts on neuronal migration and axonal growth resulting in developmental defects. However, Rac2 and Rac3 appear to compensate to some degree as the Rac1 KO and Rac3 brain specific conditional KO mouse shows more severe developmental effects on hippocampal development and spine morphology (Corbetta et al., 2009; Tahirovic et al., 2010).

Lastly, precise protein turnover, including protein formation, delivery and degradation is critical for dendritic formation. Without correct dendritic trafficking the building blocks required for outgrowth cannot be delivered to sites of extension. Indeed, loss of the neuronal motor KIF5 or the KIF5 adaptor protein GRIP1 by RNAi in rat hippocampal neurons results in reduced dendritic development due to a reduction in the delivery of key trophic signalling receptors to the membrane (Hoogenraad et al., 2005). Additionally, mice haploinsufficient for the dynenin reterograde motor adaptor protein LIS1 display reduced dendritic length and branching compared to WT pyramidal neurons. To enhance the efficiency of protein delivery to sites of extension dedicated mechanisms have been identified which target elements of the secretory pathway to dendrites. Indeed, Golgi outposts and local zones of complex dendritic ER have been identified in dendrites and are essential for dendritic development (Cui-Wang et al., 2012; Horton et al., 2005). Finally, irrespective of the efficient trafficking pathway in place, due to the high demand for proteins during dendritic extension and following neuronal activity there is a requirement for rapid local protein synthesis within dendrites. Many RNA binding proteins have been implicated in the regulation of local protein synthesis and are required for dendritic patterning (Puram and Bonni, 2013). The Fragile X mental

retardation protein (FMRP; discussed in detail below, page 62) regulates the trafficking and translation of dendritic mRNA and influences dendritic morphology however the exact mechanisms are unclear (Bagni and Greenough, 2005).

Consistent with neuropsychiatric disorder association studies highlighting genes involved in the regulation of dendritic development, genes vital for synapse formation stability and function have also been associated with neuropsychiatric disorders. Indeed, dendritic spine defects during development, maintenance and plasticity as well as alterations in both excitatory and inhibitory synapse structure and function have been implicated in major neurological disorders (Penzes et al., 2011; Smith and Kittler, 2010; Ting et al., 2012). A summary of what is understood about the dendritic and synaptic mechanisms of pathogenesis for selected neuropsychiatric disorders is discussed below.

1.4.2.1 Autism spectrum disorders

Autism spectrum disorders (ASD) form a heterogeneous neurodevelopmental syndrome characterised by deficits in social interactions, disruptions of verbal communication and the presence of repetitive behaviour. ASD effects ~1% of children, symptoms appear in early childhood and diagnosis occurs around 2-3 years of age. Across the core features there are significant differences in the extent and quality of the symptoms. For example, the degree of speech delay or whether the patient will present with mental retardation (MR) are variable. Furthermore, social impairments are expressed differently, some patients display aloof style behaviour while other individuals actively seek social interactions although often in an odd manner. This large variability in symptoms explains why the disorder is considered a spectrum. ASD research is an expanding field; attempts are being made to understand the etiology of ASD and what molecular factors influence the disorder and produce such symptom variability (Geschwind and Levitt, 2007).

Altered dendritic morphology is considered a hallmark of ASD. In fact ASD, and disorders that are often comorbid with ASD such as Rett's syndrome (RS) and Fragile X syndrome (FXS), are regularly associated with abnormal brain size. It is speculated this is due to defects during dendritic development or pruning. The primary behavioural abnormalities in ASD patients occur within the first three years of life consistent with the idea that defective dendritogenesis could be an underlying cause (Jan and Jan, 2010). In one of the first studies to describe the morphological effects

of ASD, Golgi staining of CA1 pyramidal neurons from post-mortem brains revealed decreased dendritic branching in ASD subjects compared to control samples (Raymond et al., 1996). Through similar methods an increase in spine density on apical dendrites of cortical pyramidal neurons has also been shown for patients with ASD (Hutsler and Zhang, 2010). The authors suggested spine density inversely correlated with cognitive function. Others have shown by morphometric analysis that the hippocampus and amygdala are enlarged in autistic brains (Schumann et al., 2004). These observations of reduced dendritic complexity and enhanced synaptic connections are consistent with the emerging theory that ASD involves short-range hyperconnectivity in local circuits and long-range hypoconnectivity between brain regions (Belmonte et al., 2004; Geschwind and Levitt, 2007).

Since the discovery of disrupted dendritic complexity and spine morphology in ASD patients, there has been increasing interest in understanding the underlying mechanisms of this disorder. Genetics have provided a powerful tool for identifying candidate ASD genes. Linkage and association studies have detected mutations in genes resulting in monogenic forms of ASD such as tuberous sclerosis (associated with TSC1 and TSC2 mutations), Rett's syndrome (associated with MECP2 mutations), and FXS (associated with FMR1 mutations). Mutations in FMR1 account for ~2% of ASD cases (Huguet et al., 2013). Additionally, genes that possess common SNPs, rare variants or CNVs which occur in patients with ASD significantly more frequently than in control patients are considered to be associated with ASD. Indeed, *de novo* CNVs are present in 10-20% of patients with ASD compared with 1-2% of the general population. The most frequent are located at chromosomal regions 7q11, 16p11, 22q11-13 and 15q11-13 (Huguet et al., 2013). The latter of which contains the gene encoding CYFIP1 and will be discussed in more detail in Chapter 3. Many of these ASD-associated genes have defined roles in pathways that regulate synaptic stabilisation and function providing evidence for synaptic dysfunction having a role in the etiology of ASD.

A number of mutations identified in Nrxns and NLs are associated with ASD and result in synaptic and dendritic defects (Südhof, 2008). Internal deletions in Nrxn1 are observed in patients with ASD and rare ASD-associated mutations in NL3 and NL4 have been discovered in individuals with X-linked autism. These mutations were shown in cell culture experiments to result in an increase in spine density (Chih et al., 2004). Chanda and colleagues demonstrated the NL4 ASD-associated mutation

R704C significantly impaired normal synaptic function. When the mutation was introduced into NL3, surface AMPARs at excitatory synapses were decreased and AMPAR mediated synaptic responses were impaired. Intriguingly, the same mutation in NL4 had the opposite effect elevating AMPAR-mediated synaptic responses (Chanda et al., 2015). Disruptions in NL function could therefore result in destabilised synaptic connections, loss of synapses and reduced dendritic complexity (Chen et al., 2010a). ASD-associated NL deficits also impact on inhibitory synaptic function. NL3 KO mice, NL3 knock-in mice, containing the autism mutation R451C, and NL2 overexpression all resulted in increased inhibitory transmission and social deficits in the mice (Hines et al., 2008; Radyushkin et al., 2009; Tabuchi et al., 2007). This altered inhibitory function due to disrupted $GABA_AR$ number and synapse stability may be an important factor underlying altered network activity in ASD. Indeed, condition knock-out (KO) of the inhibitory synapse specific NL2 in the prefrontal cortex of mice resulted in the animals developing behavioural deficits associated with neuropsychiatric disorders such as impaired anxiety, fear memory and social behaviours (Liang et al., 2015).

Another intensely studied family of ASD-associated proteins are the Shank family proteins (Guilmatre et al., 2014; Jiang and Ehlers, 2013). CNVs in the genes encoding Shank2 and Shank3 are associated with ASD (Berkel et al., 2010; Durand et al., 2007; Pinto et al., 2010). Additionally, patients with ASD have been identified with deletion mutations or nonsense point mutations in the genes encoding Shank1 and Shank3 (Durand et al., 2007; Sato et al., 2012). KO mouse studies have revealed that loss of any Shank protein results in spine defects and disrupted excitatory synaptic transmission. Moreover, ASD mutations in Shank3 result in modified spine morphology via actin mechanisms (Durand et al., 2012). Dendritic complexity is also altered in Shank2 knockdown neurons and cannot be rescued by ASD-associated Shank2 mutants (Berkel et al., 2012). This demonstrates the importance of Shank proteins in synaptic function and dendritic morphology and highlights why Shank mutations are so strongly associated with ASD. Indeed, Shank2 and Shank3 KO mice demonstrate ASD like behaviour such as deficits in social behaviour, abnormal vocalisation and repetitive compulsive actions (Peça et al., 2011; Schmeisser et al., 2012). Other synaptic molecules such as SAPAP2 and Epac2 have also been implicated in the molecular mechanisms of ASD (Srivastava et al., 2012).

1.4.2.2 Fragile X syndrome

Fragile X syndrome is the most common form of inherited intellectual disability (ID), severe mental retardation (MR) affects 25% of male cases and it is the most frequent known cause of ASD. The disorder is characterised by mild to severe cognitive impairment, physical abnormalities, attention deficit, autistic behaviour, childhood seizures and importantly abnormal immature dendritic spines within the brain (Bardoni et al., 2000; Comery et al., 1997). Most cases of FXS are a result of an unstable CGG repeat expansion in the 5' UTR promoter region of the gene FMR1. FMR1 encodes the fragile X mental retardation protein (FMRP). FMR1 expansion leads to hypermethylation and transcriptional silencing resulting in loss of FMRP expression. In addition, rare cases of FXS have been identified that are associated with deletions and point mutations in FMR1. Such as the rare isoleucine to asparagine mutation at position 304 (I304N) within the coding region found in a patient with severe FXS (Bagni and Greenough, 2005; Bardoni et al., 2000; Feng et al., 1997).

FMRP and its two other family members FXR1P and FXR2P are RNA binding proteins (RBPs) that are highly expressed in the brain. FMRP binds polyribosomes and mRNAs, although a precise RNA binding motif for FMRP family proteins has not been described (Brown et al., 1998; Rubeis and Bagni, 2011). Defects in the mRNA binding function of FMRP are important in the pathogenesis of FXS as the I304N mutation attenuates the association of FMRP with polyribosomes and mRNA (Feng et al., 1997). That said, the exact disease pathogenesis of FXS is still not clear.

Intense research has improved our understanding of FMRP function in an attempt to understand how disrupted expression and mutations in the protein result in FXS and give rise to neurological symptoms such as ID and ASD. In highly polarised cells such as neurons protein translation occurs not only in the soma but also at synapses, along the dendrites and in axons too. Indeed, local protein synthesis at synapses is critical for synaptic plasticity as protein translation blockers can abolish BDNF-induced LTP (Kang and Schuman, 1996). FMRP has been described to play a critical role in the stability, localisation, transport and local translation of target mRNA in neurons (Abekhoukh and Bardoni, 2014; Bagni and Greenough, 2005; Bassell and Warren, 2008; Rubeis and Bagni, 2011). When bound to mRNA FMRP has been shown to repress protein translation both *in vitro* and *in vivo* (Rubeis and Bagni, 2011). Over 200 FMRP target genes display abnormal distribution on actively transcribing polyribosomes in lymphoblastoid cells from FXS patients, suggestive of altered

translation (Brown et al., 2001). Furthermore, in FMR1 KO mice, FMRP target mRNAs are more localised to polyribosomes due to excessive translation and the levels of the translated proteins are increase. This result is also seen in synaptoneurosome fractions highlighting the importance of FMRP's repressive function at the synapse (Muddashetty et al., 2007; Zalfa et al., 2003). More recently high-throughput screening identified over 100 proteins whose expression was altered in purified synaptoneurosomes from FMR1 KO neurons, likely due to the effect of loss of FMRP on dendritic mRNA localisation and protein synthesis (Darnell et al., 2011; Liao et al., 2008).

Disrupted protein translation upon loss of FMRP has been shown to impact on synaptic plasticity, which is critical for normal neuronal function and could contribute to the neurological effects of FXS. mGluR5-dependent LTP is reduced in the cortex of FMR1 KO mice. In addition, mGluR-dependent LTD is amplified in the absence FMRP in the hippocampus whereas, NMDAR LTD is unchanged (Huber et al., 2002). The enhanced mGluR5 LTD in FMR1 KO mice was shown to be insensitive to protein synthesis inhibitors. It has therefore been suggested that the abnormality in expression of synaptic proteins following loss of FMRP is impacting on mGluR5 receptor activation. Indeed, in these mice mGluR5 receptors are less associated with the PSD protein homer, suggesting defects in downstream synaptic signalling (Abekhoukh and Bardoni, 2014; Giuffrida et al., 2005).

FMRP was shown by a Y2H screen to interact with CYFIP1 and CYFIP2 (**cy**toplasmic **F**MRP **i**nteracting **p**rotein **1** and **2**) (Schenck et al., 2001). Unlike FMRP, CYFIP proteins do not interact with mRNA; instead these proteins have been suggested to regulate the function of FMRP. It is thought that CYFIP proteins may control the affinity of FMRP for RNA or regulate the formation of FMRP family protein homo or heterodimers since the CYFIP binding site is also the site for FMRP to bind with itself or its paralogs FXR1P and FXR2P (Schenck et al., 2001). As CYFIP proteins have been suggested to regulate FMRP function there has been great interest in the FXS research field to understand more about CYFIP function.

Recently a role for CYFIP1 was described in the translational initiation complex. CYFIP1 was identified as a neuronal eukaryotic translation initiation factor (eIF4E)-binding protein (4E-BP) (Napoli et al., 2008). 4E-BPs function by sequestering eIF4E and repressing translation. The 4E-BPs and eIF4G, the scaffolding protein required

for the assembly of the active initiation complex, compete for the same binding site on e1F4E. Therefore, if a 4E-BP, such as CYFIP1, is bound to eIF4e then eIF4G cannot bind to form the initiation complex and translation is repressed. In brain and at synapses FMRP recruits CYFIP1 in a complex with eIF4e to its associated mRNA resulting in the repression of FMRP target mRNA due to the inability of eIF4G to bind (Napoli et al., 2008). The FMRP-CYFIP1-e1F4E complex has been shown to interact and regulate a variety of FMRP target transcripts including CamKII, Arc, APP and Map1b. Interestingly, the complex also contains BC1 RNA. This non-translated RNA enhances the FMRP-CYFIP1 interaction and can act as an adaptor to recruit a different subset of mRNAs to the FMRP-CYFIP1-eIF4E complex. Consistent with this, downregulation of CYFIP1 in cultured neurons or genetic depletion in mice results in a significant increase in the protein levels of FMRP target transcripts (Napoli et al., 2008; Rubeis and Bagni, 2011). It is of note that the FMRP-CYFIP1-eIF4E complex is present along dendrites and at synapses and its repressive function can be regulated by neuronal activity. Indeed, upon the stimulation of synaptoneurosomes with either BDNF or DHPG, the mGluR I agonist, CYFIP1 is released from e1F4E and the translational block is removed (Napoli et al., 2008).

Intriguingly, there has been some controversy as to the formation of the FMRP-CYFIP1-eIF4E complex. Iacoangeli and colleagues could not detect an interaction between FMRP and BC1 mRNA either *in vitro* or *in vivo* and interactions between BC1 mRNA and FMRP target mRNAs were found to be nonspecific (Iacoangeli et al., 2008a, 2008b). This data suggests that BC1 and FMRP act independently to regulate translation. Furthermore, the majority of the FRMP pool has been described to associate with transcribing polyribosomes implying that only a small proportion of FMRP functions with CYFIP1 in regulating translational initiation. Indeed, FMRP acts as a transcriptional brake and has recently been shown to reversibly stall ribosomes specifically on its target mRNA (Darnell et al., 2011). Therefore, as suggested when CYFIP1 and CYFIP2 were first identified, CYFIP proteins are also likely to interact with this larger pool of polyribosome-associated FMRP and contribute to the modulation of FMRP activity during active translation (Abekhoukh and Bardoni, 2014; Schenck et al., 2001).

As a final note, like ASD, patients with FXS also develop spine morphology defects. Post-mortem studies of Golgi labelled FXS patient brains and research into the FMR1 KO mice reveal in both cases neurons with long, thin tortuous spines (Comery et al.,

1997; Irwin et al., 2001; Rudelli et al., 1985). The altered translation of synapse specific proteins due to loss of FMRP is hypothesised to cause these spine defects. Indeed, changes in the mRNA levels of key PSD scaffold proteins and actin regulatory proteins, such as PSD95 and Arc have been shown in models of FXS (Ifrim et al., 2015; Napoli et al., 2008). Furthermore, loss of FMRP in KO mice, leads to overactive Rac1. Increased activity of this global actin regulator results in abnormal spine and dendritic development (Bongmba et al., 2011) suggesting another mechanism for the defects in neuronal morphology observed in FXS patients.

1.4.2.3 Joubert's syndrome

Joubert's syndrome (JS) is an autosomal recessive neurodevelopmental disorder characterised by multiple behavioural and neuroanatomical abnormalities, development delay and MR. Individuals with JS are considered to have a multisystem disease with abnormal breathing and eye movements, ataxia, hypotonia and cognitive difficulty as well as extra-neuronal features such as retinal degeneration and cystic kidney disease (Doherty, 2009; Ferland et al., 2004; Joubert et al., 1968, 1969; Louie and Gleeson, 2005). Physically, the disease is defined by abnormal cerebellar development and lack of midline fusion between the two hemispheres resulting in a 'molar tooth sign' on MRI scans. Furthermore, many features of ASD have been described in up to 40% of JS patients (Esmailzadeh and Jiang, 2011; Holroyd et al., 1991; Ozonoff et al., 1999). One study analysed the behaviour of two children with JS, both displayed autistic characteristics, one child met diagnostic criteria while the other showed autistic features including stereotypic behaviour and impaired social interaction and communication (Holroyd et al., 1991).

As JS is a monogenic disorder with neuropsychiatric phenotypes mutations in the genes known to cause the disease have been identified due to their high heritability and large effect size. The protein products of all 11 genes currently identified are localised to primary cilia (Doherty, 2009). Defects in ciliogenesis have been observed when proteins associated with cilia are mutated and result in multisystem disorders, characterised by brain malformations, retinal degeneration and kidney disease, known as ciliopathies (D'Angelo and Franco, 2009; Lee and Gleeson, 2010; Waters and Beales, 2011). A comparison of the human symptoms of JS has led to the characterisation of this disease as a ciliopathy (Doherty, 2009; Hsiao et al., 2009; Lancaster et al., 2009, 2011a; Louie and Gleeson, 2005; Simms et al., 2011; Waters and Beales, 2011; Westfall et al., 2010).

Cilia are dynamic, specialised membrane bound organelles that project out from the cell surface. They consist of a microtubule (MT) cytoskeleton (axoneme), which is anchored in the cell by the basal body, a structure composed of a pair of centrioles located under the cell surface (Figure 1.7) (Marshall, 2008; Reiter et al., 2012). Primary cilia are found on most cell types including renal epithelial cells, retinal photoreceptors, chondrocytes, fibroblasts and neurons. The membrane surrounding the protruding axoneme is specialised containing specific signalling receptors. The most proximal region of the axoneme is termed the transition zone (TZ). The elements of the TZ have been reported to act as gatekeepers, regulating the trafficking of molecules into the cilia (Figure 1.7) (Reiter et al., 2012).

Of note, loss of function mutations in the gene *Ahi1*, as a result of frame shifts or nonsense mutations, are known to cause JS (Dixon-Salazar et al., 2004; Ferland et al., 2004). Studies using Ahi1 KO mice have provided a useful tool for investigating Ahi1-mediated JS. Transgenic Ahi1 neuron-specific KO mice showed depressive phenotypes and remained significantly more immobile in the tail suspension test and the forced swim test compared to wild-type control animals (Xu et al., 2010). Furthermore, Ahi1 heterozygous animals (*Ahi1*$^{+/-}$) showed anxiolytic characteristics across different behavioural paradigms designed to test anxiety. *Ahi1*$^{+/-}$ mice showed a significant decrease in anxiety in the open field, elevated plus maze and light-dark box tests as well as during social interaction with other mice (Lotan et al., 2013). MRI imaging revealed reduced connectivity between the amygdala and other brain regions involved in the processing of antipanic stimuli and inhibitory avoidance learning (Lotan et al., 2014). The data suggests *Ahi1*$^{+/-}$ mice present with relative resistance to stress. Moreover, individuals with JS disease causing *Ahi1* mutations have the classic cerebellar vermis defects and limited involvement of the cerebral cortex. Indeed, MRI scans from these patients revealed the typical midbrain 'molar tooth' structure (Dixon-Salazar et al., 2004; Ferland et al., 2004). Mouse models of JS with mutations in *Ahi1* also display the malformation (Lancaster et al., 2011a). The evidence suggests that Ahi1 could be critical for neuronal development and function.

Mechanistically, primary cilia are vital in developmental signalling pathways and neuronal development is known to be impaired when primary cilia are disrupted (Waters and Beales, 2011). Therefore, research into the mechanisms of JS has focused on the role of JS causing genes in cilia formation and function. Indeed, Ahi1 has been

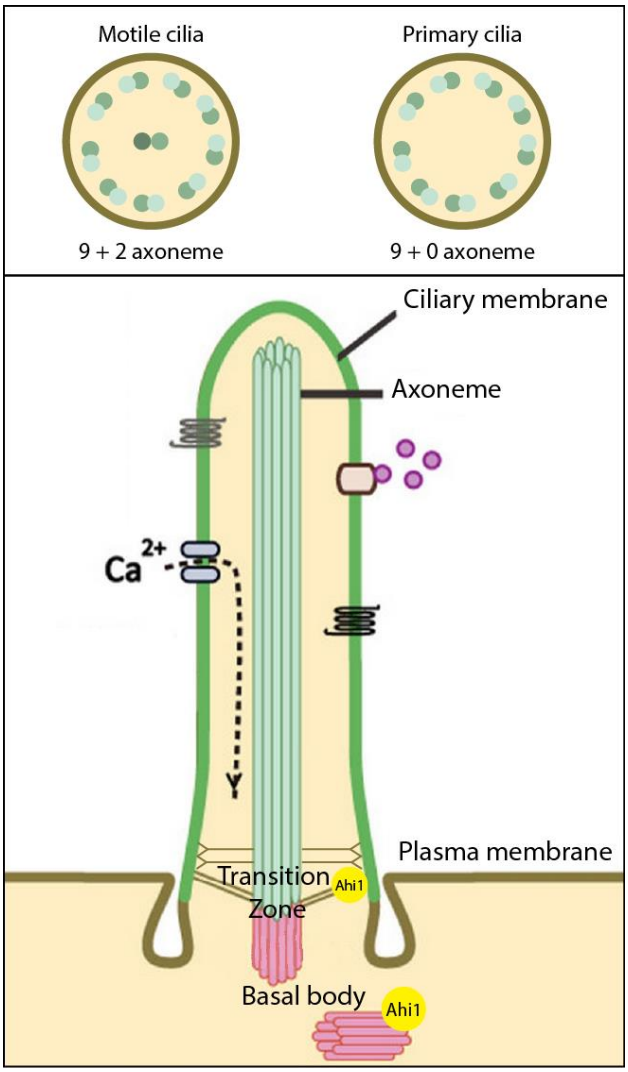

Figure 1.7: Structure of the primary cilia.

Cilia are classified into two categories based on their structure. The first, motile cilia, have their MTs arranged in a 9 + 2 circular pattern, consisting of a central MT pair surrounded by the 9 MT doubles. The second, primary cilia, lack the central 2 MTs (9 + 0 axoneme) and are usually non-motile (top panel). The core structure of primary cilia is composed of MT bundles forming the axoneme extending from the basal body, a microtubule-based structure derived from the mother centriole. The basal body can nucleate the MTs that form the axoneme. The transition zone (TZ) sits just above the basal body and contains the ciliary necklace. This is a ring structure of membrane proteins that encircles the base of the cilia. The TZ also contains Y-shaped linkers that span from the axoneme to the ciliary necklace and a growing number of cytosolic proteins. The ciliary membrane is continuous with the plasma membrane, but contains a unique protein composition, such as Ca^{2+} channels and receptors. Thus, primary cilia can function as a sensory organelle for receiving and transducing extracellular stimuli into cells. Ahi1 has been located at the basal body and TZ. Adapted from (Hsiao et al., 2012).

localised to the basal body and TZ (Hsiao et al., 2009; Lee et al., 2014). However, much less is known about how these mechanisms might result in neuropsychiatric phenotypes.

1.4.2.4 Schizophrenia

Schizophrenia (SCZ) is a chronic, severe heterologous brain disorder that effects about 0.5-1% of the population and is highly heritable (~80%). SCZ manifests itself through positive symptoms including delusions, hallucinations, altered thought and negative symptoms such as loss of emotional responses, apathy and social withdrawal. Cognitive symptoms include impaired attention, memory and executive functions (Andreasen, 1995; Lewis and Lieberman, 2000).

In contrast to mental disorders that develop in early childhood such as ASD discussed above, the onset of SCZ is associated with late adolescence and early adulthood. Therefore, SCZ could arise from over-pruning or failed maintenance of dendritic complexity later in life. Post-mortem studies and non-invasive imaging techniques have demonstrated one of the defining features of SCZ is grey matter loss, resulting in loss of connectivity (Harvey et al., 1993; Karlsgodt et al., 2008; Ruiz et al., 2013). Others have reported that decreased brain volume in SCZ is not due to loss of axons or cells bodies (Selemon et al., 1995) strengthening the theory that SCZ arises from a loss of dendritic architecture and spines. Consistent with this, decreased spine density has been observed in the brain regions most affected by grey matter loss illustrating changes in spine density may directly result in the reduced brain volume detected. Indeed, reduction of basal dendrites and dendritic spine density was identified in the prefrontal cortex (Broadbelt et al., 2002; Garey et al., 1998; Glantz and Lewis, 2000) a region of the brain severely affected in SCZ patients (Tan et al., 2007). Interestingly, histology and electron microscopy on SCZ post-mortem tissue revealed that hippocampal pyramidal neurons were reduced in size with less spines and synaptic contacts in the CA3 region (Arnold et al., 1995; Benes et al., 1991; Jönsson et al., 1999; Kolomeets et al., 2005).

Consistent with mechanisms thought to underlie ASD, genes encoding synaptic proteins appear to be strongly associated with SCZ. This raises an unanswered question in the field as to why two disorders that appear to share similar genetic and molecular mechanisms of pathogenesis have such different times of disease onsets. The synaptically targeted protein DISC1 plays a role in regulating spine morphology

and has been implicated in SCZ (Hayashi-Takagi et al., 2010; Penzes et al., 2011). Genetically, *DISC1* is truncated from intron 8 by a balanced translocation in a large Scottish pedigree and cosegregates with major mental illness including SCZ (St Clair et al., 1990). Evidence has now been provided for this protein having a role in dendritogenesis and maintenance of neuronal complexity too (Duan et al., 2007; Kvajo et al., 2011; Lepagnol-Bestel et al., 2013). Altered expression of PSD structural proteins have also been implicated in SCZ pathogenesis. PSD95 protein levels are reduced in post-mortem cortical samples from SCZ patients while other PSD proteins such as Shank3, PSD93 and SAP102 have altered mRNA levels (Föcking et al., 2014; Kristiansen et al., 2006). Indeed, Shank3 mutations have been associated with SCZ too (Gauthier et al., 2010). Loss or mutated synaptic scaffold proteins could be resulting in synapse and dendritic spine loss and defects in neurotransmission contributing to the etiology of SCZ.

Actin regulation is critical for synapse stability and spine morphology therefore it is not surprising that mutations in key actin regulators are associated with SCZ. Kalirin7 is a Rac GEF and mutations in conserved regions of the gene have been identified in SCZ patients and are thought to be functionally damaging (Kushima et al., 2012). Indeed, loss of kalirin7 correlates with cortical spine loss, a feature of SCZ (Hill et al., 2006). Kalirin7 has also been shown to mediate DISC1 effects on spine morphology as DISC1 anchors kalirin7 at spines so it can activate Rac1 (Hayashi-Takagi et al., 2010).

1.4.2.5 The excitatory/inhibitory balance

Neuronal homeostasis refers to the phenomenon where neurons alter their excitability to maintain stable levels of electrical activity during development and changes in environmental conditions. Neurons can regulate their excitability via finely tuned mechanisms that respond to changes in action potential firing and network activity. These mechanisms include modulation of synaptic strength, alterations in presynaptic release probability and adjustments in intrinsic membrane excitability via up- or down-regulation of excitatory and inhibitory receptors (Turrigiano, 2011). Too much excitability or inhibition due to defects in these mechanisms can result in pathological consequences. In fact, a leading hypothesis for ASDs is that they arise from an imbalance in excitation and inhibition in particular circuits. Indeed, pathological alterations in the excitatory/inhibitory (E/I) balance have been increasingly implicated in neuropsychiatric disorders such as FXS, RS,

tuberous sclerosis (TS) and epilepsies (Bateup et al., 2013; Chao et al., 2010; Paluszkiewicz et al., 2011; Pizzarelli and Cherubini, 2011).

The mammalian target of rapamycin (mTOR) pathway is strongly implicated in ASD and modifications in this pathway have been shown to disrupt the E/I balance. The mTOR pathway is activated in response to growth factors and signals through the mTOR complex to bring about protein synthesis and the regulation of cell growth and metabolism. Upstream of mTOR, mutations in the mTOR negative regulator PTEN occur in 1-5% of patients with ASD (Zhou and Parada, 2012). Downstream of mTOR, the eIF4e binding protein 2 (4E-BP2) is necessary to maintain the E/I balance. Mice lacking 4E-BP2 showed autistic-like behaviours, social interaction deficits and developed an increased ratio of excitatory to inhibitory synaptic inputs. The effects were shown to be due to disrupted expression of synapse stabilising proteins NL1 and NL2 (Gkogkas et al., 2013). Furthermore, neuronal loss of the mTOR negative regulator TSC1, a protein mutated in TS and a common target for mutations associated with ASD and epilepsy, weakened inhibition. This was caused by dysregulation of mTOR and altered the E/I balance leading to hippocampal excitability (Bateup et al., 2013). These examples of ASD-associated alterations in the E/I balance implicate modulation of mTOR signalling and consequently disrupted protein synthesis; emphasising its potential as a converging pathway in some forms of ASD.

GABAergic signalling enhances hyperpolarisation and is therefore essential for regulating the excitability of a neuron and maintaining the E/I balance of neuronal circuits (Smith and Kittler, 2010). Defects in $GABA_AR$ trafficking have been shown to alter the E/I balance in disorders such as epilepsy and Huntington's disease (Twelvetrees et al., 2010). Loss of surface $GABA_ARs$ results in a lack of intrinsic inhibition and is one of the major pathologies of status epilepticus (SE). During SE, the $GABA_AR$ β3 subunit was shown to be selectively dephosphorylated resulting in rapid internalisation of surface $GABA_ARs$ due to enhanced AP2 dependent clathrin-mediated endocytosis (Terunuma et al., 2008). KIF5A KO mice have impaired surface $GABA_AR$ trafficking and show epileptic phenotypes (Nakajima et al., 2012). Additionally, mutations is $GABA_AR$ subunits that have been identified in genetic epilepsies, rather than modifying channel properties, impair intracellular trafficking or impact on receptor degradation (Gallagher et al., 2007). A number of GABAergic scaffolding molecules involved in stabilising the synapse and tethering $GABA_ARs$ have

been associated with neuropsychiatric disorders. Mutations in the NLs have been identified in ASD patients (Südhof, 2008). Deleting NL3 in mice or overexpression of NL2 lead to an increase in inhibitory transmission and impaired social interactions (Hines et al., 2008; Tabuchi et al., 2007). While constitutive loss, or condition loss in the prefrontal cortex of NL2 in mice causes decreased inhibition and anxiety-like behaviour (Blundell et al., 2009; Liang et al., 2015). This behaviour was also observed in $GABA_AR$ γ2 KO mice or with loss of Cb dependent receptor clustering (Earnheart et al., 2007). Altered inhibitory homeostasis, due to disrupted $GABA_AR$ trafficking or changes in inhibitory synapse number by disrupted scaffolding molecules, may therefore be another important factor underlying aberrant network activity in psychiatric disorders.

1.5 Thesis Aims

Precise development and maintenance of dendritic complexity and efficient synaptic transmission is vital for normal neuronal connectivity and brain function. Alterations in these processes are thought to contribute to the etiology of neuropsychiatric disorders however, the precise mechanisms are still being understood. Given that the genes encoding the proteins CYFIP1 and Ahi1 have been robustly associated with neuropsychiatric disorders through genetic studies the aims of this thesis are as follows:

1. To investigate the possibility that CYFIP1, and its homologue CYFIP2, regulate dendritic morphology and synapse stability in an attempt to elucidate why altered dosage of these proteins have been associated with neuropsychiatric disorders.

2. To identify novel CYFIP1 SCZ-associated mutations and explore how these mutations impact on CYFIP1 function.

3. To characterise CYFIP1 genetic knockout systems to further understand the molecular functions of CYFIP1.

4. To investigate the possibility that Ahi1 is important in the trafficking of $GABA_AR$s at the inhibitory synapse and in the regulation of dendritic morphology.

Chapter 2

Materials and Methods

2.1 Antibodies

2.1.1 Non-commercial antibodies

The mouse monoclonal antibodies anti-myc (WB and IF, 1:100), anti-HA (WB and IF, 1:100), anti-KIF5A-C (WB, 1:100) and anti-GAD6 (IF, 1:100) were obtained from 9E10, 12CA5, SUK4 and GAD6 hybridoma cells respectively (acquired from the Development Studies Hybridoma Brank). All hybridoma antibodies were used directly as supernatant and diluted as described for western blotting and immunofluorescence. Monoclonal antibodies were produced by growing hybridoma cultures in Integra CL350 Bioreactor flasks. Cells were maintained in the cell compartment in DMEM with 20% FBS, 1% penicillin-streptomycin and 0.1% gentamicin. The nutrient compartment contained serum free DMEM containing penicillin-streptomycin and 0.1% gentamicin. Once confluent cells were harvested every 3-5 days by removal of 80% of the media from the cell compartment and replacement with fresh media. In addition nutrient media was changed with every harvest. Cells were spun down and the antibody containing supernatant was filtered through a 0.45µm filter and stored at -20°C. 9E10, 12CA5 and SUK4 antibodies were produced by Rosalind Norkett, GAD6 antibody was produced by Katharine Smith.

2.1.2 Commercial antibodies

For a list of all commercial antibodies and the concentrations at which they were used see Table 2.1. All Alexa Fluor fluorescent marker conjugated secondary antibodies were from Molecular Probes and used at 1:1000. Anti-rabbit and anti-mouse HRP conjugated secondary antibodies were from Rockland and BioRad respectively, used at 1:10 000.

Table 2.1: Commercial primary antibodies (dilutions for given experiments are indicated)

Antigen	Species	Company	Product code	Western blotting	Immuno-fluorescence	Immuno-precipitation	Immuno-histochemistry
Ahi1 (H-300)	rabbit	Santa Cruz	sc-98623	1:200	-	4µg	-
Ahi1	mouse	Abcam	ab93386	1:500	1:500	2µg	-
β-tubulin	mouse	Sigma	T5293	1:1000	-	-	-
Chapsyn 110 (N18/30)	mouse	Neuromab	73-057	1:50	-	-	-
c-Myc (A-14)	rabbit	Santa Cruz	sc-789	-	1:100	-	-
CYFIP1	rabbit	Millipore	07531	1:500	1:200	-	-
CYFIP1/Sra1	mouse	Synaptic Systems	309 011	1:500	1:200	-	-
$GABA_AR$ γ2 subunit	guinea pig	Synaptic Systems	224 004	-	1:500	-	-
Gephyrin	mouse	Synaptic Systems	147 011	-	1:500	-	-
Gephyrin	rabbit	Synaptic Systems	147 003	1:1000	-	-	-
GFP	rat	Nacalai-Tesque	04404-84	-	1:2000	-	1:500
GFP (FL)	rabbit	Santa Cruz	sc-8334	1:100	1:100	-	-
GFP (N86/8)	mouse	Neuromab	73-131	1:100	-	-	-
HAP1	mouse	BD Transduction	611 302	1:500	-	-	-
HAP1 (N18)	goat	Santa Cruz	sc-12556	-	-	2µg	-
Homer	rabbit	Synaptic Systems	160 002	1:500	1:500	-	-
NAP1	rabbit	Abcam	ab96715	1:500	-	-	-
Shank1-3 (N23B/49)	mouse	Neuromab	73-089	1:50	-	-	-
PSD-95 (K28/43)	mouse	Neuromab	75-028	1:500	1:500	-	-
Rac1	mouse	Millipore	23A8	1:500	-	-	-
RFP	rabbit	Abcam	62341	1:500	1:500	-	-
vGAT	rabbit	Synaptic Systems	131 003	-	1:1000	-	-
vGlut	guinea pig	Synaptic Systems	135 304	-	1:1000	-	-
WAVE2 (H-110)	rabbit	Santa Cruz	sc-33548	1:200	-	-	-

2.2 Animals

The *Cyfip1* KO mouse line (MDCK; EPD0555_2_B11; Allele: *Cyfip1*$^{tm2a(EUCOMM)Wtsi}$) was obtained from the Wellcome Trust Sanger Institute as part of the International Knockout Mouse Consortium (IKMC). Transgenic animals were generated following the Knockout-First strategy on C57BL/6N Taconic USA background (Skarnes et al., 2011; White et al., 2013). The Cre^{ERT} line (Feil et al., 1997) (B6N Tac Rosa26 CreERT2 (MJBA)) was also obtained from the Wellcome Trust Sanger Institute, again transgenic mice were bred on C57BL/6N Taconic USA background. The *camkcre4* (Cre$^{CAMKII\alpha}$) line has been described previously (Mantamadiotis et al., 2002) and the YFP Rosa26 reporter line (Ribeiro et al., 2013) was obtained from Prof. Alison Lloyd. Animals were maintained under controlled conditions (temperature 20 ± 2°C; 12 hour light-dark cycle). Food and water were provided *ad libitum*. The genotyping was carried out following distributors recommended procedures, DNA was extracted from ear biopsies and PCR reactions were performed. All experimental procedures were carried out in accordance with institutional animal welfare guidelines and the UK Animals (Scientific Procedures) Act 1986.

2.3 Molecular Biology

2.3.1 Constructs

Human CYFIP1 and CYFIP2 GFP and mCherry tagged constructs were generated using the Gateway Cloning System (Invitrogen) with the expression vectors pDEST47GFP (Invitrogen), pDEST-eGFP-N1 and pDEST-mCherry-N1 (Addgene, plasmid numbers 31796 and 31907 respectively). CYFIP1 mutant constructs were generated by site-directed reverse PCR mutagenesis on the pENTR221-CYFIP1 vector and cloned using the Gateway Cloning System into pDEST-eGFP-N1. Primers used for mutagenesis are listed in Table 2.6. pCAG-DsRed was purchased from Addgene (plasmid number 11151) and actin^{GFP} was a gift from Dr. Jonathan Hanley (University of Bristol).

All restriction enzymes used were from New England Biosciences (NEB). The human Ahi1 constructs tagged at the N-terminus with either GFP or DsRed were purchased from Addgene (plasmid numbers 30494 and 30495 respectively). The N-terminal GFP and myc tagged mouse Ahi1 constructs were generated by PCR amplification of

the mouse full-length Ahi1 cDNA from an untagged vector pSPORT6_msAhi1 (available from the Mammalian Gene Collection). The PCR product was cloned into pEGFP-C1 (Clontech) and a myc-tagged pRK5 vector using NotI/SalI and BglII/SalI restriction sites respectively. Ahi1 mutant constructs were generated by site directed reverse PCR mutagenesis on the human Ahi1^{GFP} vector. Primers used for mutagenesis are listed in Table 2.6. Full-length rat HAP1a was C-terminally tagged with an HA epitope (YPYDVPDYA) in a pRK5 vector and has been described previously (Kittler et al., 2004; Li et al., 1998). HAP1a^{GFP}, HAP1b^{GFP} and untagged HAP1b were a gift from X. J. Li. Rat HAP1a^{myc}153-599, 215-599, 329-599 and 371-599 were generated in the lab by Alison Twelvetrees using PCR to amplify the cDNA and then cloned into an N-terminal myc tagged pRK5 vector. Full-length mouse KIF5C was N-terminally myc tagged and cloned into the pRK5 vector by Mike Lumb.

2.3.2 Polymerase Chain Reaction (PCR)

PCR is a process of amplifying DNA in a thermocycler using DNA polymerase (Phusion, Finnzymes). The PCR reaction was assembled as described in Table 2.2 and subjected to a PCR programme with an appropriate annealing temperature and extension time (Table 2.3). The annealing temperature (Tm) is calculated for each set of primers using the online Thermoscientific Tm calculator and varies depending on GC content and length of the primers. The extension time and the number of repeats of the cycle depend on the length of the template DNA. 5µl of the resulting PCR product was ran on an agarose gel to confirm amplification and the rest of the product was purified using a DNA purification kit (Qiagen) following the manufacturer's instructions.

Primers were designed for PCR using a number of guidelines for efficient downstream reactions. Primers should be between 18-22pb long, with a G-C content in the range of 40-60%. The primers should have a melting temperature (Tm) between 42-65°C and the primer pairs should not differ my more than 5°C. Finally, primers should contain a C or G base at the 5' or 3' end for efficient binding to the specific DNA sequence due to the stronger bonding of G and C bases.

Table 2.2: Standard PCR reaction mix.

Standard PCR reaction	Stock conc.	Final conc.
10µl 5X HF buffer	5X	1X
2.5µl forward primer	10µM	0.5µM
2.5µl forward primer	10µM	0.5µM
1µl template DNA	-	-
1µl dNTP mix	10mM	200µM
0.5µl Phusion (DNA polymerase)	2U/µl	0.02U/µl
32.5µl ddH_2O	-	-

Table 2.3: PCR reaction and protocol.

Step	Temp (°C)	Time	
Melting	98	5 minutes	
Melting	98	30 seconds	
Annealing	X	30 seconds	Repeat x 25-35
Extension	72	1 minute per Kb	
Extension	72	10 minutes	
Hold	4	∞	

2.3.3 Genotyping by PCR

DNA was extracted from ear biopsies or tissue samples using the Hot Shot protocol (Truett et al., 2000) or from cell samples using the DNeasy Blood and Tissue Kit (Qiagen) following manufacturers guidelines. Genotyping PCR was carried out as a standard PCR reaction using the appropriate primers, to a final volume of 20µl (Table 2.4). However, Taq Polymerase (NEB) was used instead of Phusion as high-fidelity amplification was not required. Taq buffer (4X) was used which contained dNTPs therefore, extra were not added. 5µl of the PCR product was ran on a 1.2% agarose gel to determine the size of the PCR products.

Table 2.4: Genotyping PCR primers.

Primer Name	Sense	Symbol	Product Size (bp)	Sequence
Cyfip1_234230	forward	a^F	259 (WT)	tggaagtaatggaaccgaaca
	reverse	a^R	454 (floxed)	gtaactacctataatgcagacctgaag
CAS_R1_Term	forward	a^F	182	tggaagtaatggaaccgaaca
	reverse	a'^R		tcgtggtatcgttatgcgcc
LacZ_2_small	forward	Z^F	108	atcacgacgcgctgtatc
	reverse	Z^R		acatcgggcaaataatatcg
Cre recombinase	forward	C^F	233	catttgggccagctaaacat
	reverse	C^R		taagcaatccccagaaatgc
CYFIP1_deletion	Forward	d^F	499	tggtagccctcttcttgtgga
	reverse	d^R		ctccaagattccccccaaaac

2.3.4 Site-directed reverse PCR mutagenesis

Mutagenesis PCR was carried out as a standard PCR reaction using appropriately designed primers, care was made to make sure the extension time was adjusted to allow for amplification of the whole vector. After PCR and purification, the product was then 5' phosphorylated and ligated. 16µl of the purified PCR product was incubated at 65°C for 5 minutes and then on ice for 2 minutes to aid efficient phosphorylation. 2µl of T4 polynucleotide kinase (PNK) buffer and 1µl of PNK (NEB) was then added to the PCR product and the mixture was incubated at 37°C for 30 minutes. 1µl of T4 DNA ligase (NEB) was then added to the reaction to ligate the PCR product overnight.

2.3.5 Agarose gels

0.8-1.2% agarose gels were made by dissolving the appropriate mass of agarose (Melfords) in 1X TBE buffer (National Diagnostics). As the gel was poured, 1µl ethidium bromide was added to label the DNA bands. Gels were loaded with DNA samples diluted with 6X loading dye (Table 2.5), a 10 Kb ladder (Bioline) and were run at 90V in 1X TBE. Resolved DNA labelled with ethidium bromide was visualised using UV light.

2.3.6 Digestion and purification of DNA from agarose gels

10µl purified PCR product or 1µg plasmid were digested with 1µl restriction enzyme (and 1µl of different enzyme for double digests), 2µl 10X enzyme buffer (NEB), 1µl 20X BSA (NEB), and filtered ddH_2O to a 20µl final volume. Digestions were incubated at 37°C for 1-2 hours. Digestions were then run on an agarose gel as described above. DNA bands of interest were visualised by UV and excised using a scalpel. DNA was extracted from the gel using a gel extraction kit (Qiagen) following the manufacturer's instructions.

2.3.7 Ligations

Ligation reactions consisted of 2µl T4 DNA ligase buffer (NEB), 1µl T4 DNA ligase (NEB), 10µl insert, 2µl vector and 5µl ddH_20. An estimated 1:5 ratio of insert to vector was used and adjusted if necessary to optimise ligation efficiency. The reaction was incubated at 4°C overnight.

Table 2.5: Bacterial culture and molecular biology solutions

Solutions	Components
Luria-Bertani Broth (LB)	10g NaCl, 10g Tryptone 5g Yeast extract H2O up to 1L
Luria-Bertani Broth Agar (LB Agar)	10g NaCl, 10g Tryptone 5g Yeast extract 10g Agar, H2O up to 1L
TBE	89 mM Tris 89mM Boric acid pH 8.3 8.32mM Na_2EDTA
Loading dye (6X)	40% sucrose 0.25% bromophenol blue H2O
Ampicillin	100 µg/ml
Kanamycin	30 µg/ml
Chloramphenicol	30 µg/ml
Spectinomycin	100 µg/ml

2.3.8 Bacterial growth media and plates

Bacteria were grown at 37°C in LB or grown on plates made of LB agar. Each were supplemented with appropriate antibiotic depending on the resistance gene present on the plasmid being amplified (Table 2.5).

2.3.9 Production of chemically competent bacterial cells

Chemically competent TOP10 *E. coli* (Invitrogen) were produced in the lab by Nathalie Higgs. Briefly, cells from a single colony were cultured at 37°C overnight in 5ml LB. 1.5ml of this preculture was used to inoculate two flasks, each containing 150ml of LB. Flasks were incubated at 37°C until an OD_{600} of 0.6 was reached. Cells were then cooled on ice for 30 minutes before being harvested by centrifugation. Cells were slowly resuspended in 60ml buffer TfBI (a mix of Solution A: 30mM KAc, 100mM KCl, 10mM $CaCl_2.2H_2O$, dH_2O to a final volume of 700ml, autoclaved to sterilise and Solution B: 50mM $MnCl_2$, 15% glycerol, dH_2O to a final volume of 300ml and sterilised by filtration using a 0.45 um filter). Cells were harvested once more by centrifugation and very gently resuspended in 6ml buffer TfBII (a mix of Solution C: 10mM NaMOPS, 75mM $CaCl_2.2H_2O$, 10mM KCl, dH2O to a final volume of 70ml, autoclave to sterilise and Solution D: 15% glycerol, dH_2O to a final volume of 30ml and sterilised by filtration using a 0.45 um filter). Cells were aliquoted and immediately snap frozen in liquid nitrogen and stored at -80°C.

2.3.10 Transformation of chemically competent bacterial cells

In house produced chemically competent TOP10 *E.coli* or commercially available OneShot TOP10 *E.coli* (Invitrogen) were transformed using a heat shock protocol. 50µl of cells were thawed on ice for each transformation reaction. 2-10µl of ligation reaction, 2µl clonase reaction or ~50ng plasmid DNA was added to the cells and incubated on ice for 30 minutes. Cells were heat shocked at 42°C for 30 seconds then placed back on ice for 2 minutes. 200µl of SOC media (2% glucose in Luria-Bertani medium (LB), Table 2.5) was added to the cells and they were incubated at 37°C for 1 hour at 225 rpm to recover. Finally, cells were spread onto antibiotic selection LB agar plates and incubated overnight at 37°C. Bacterial colonies were picked and cultures inoculated the next day. For screening ligations, colonies were picked and grown in 5ml LB plus antibiotic overnight, plasmid DNA was extracted and analysed by restriction digest. Positive results were confirmed with DNA sequencing.

2.3.11 Maxi and mini preparation of plasmid DNA

Plasmid DNA was prepared from 3ml (mini) or 200ml (maxi) overnight bacterial cultures using the GelElute Plasmid Mini Prep Kit (Sigma) or the Endotoxin-free Maxiprep Kit (Promega), following manufacturer's protocols.

2.3.12 LR clonase reaction (Gateway Cloning System)

Entry vectors (pENTR) (Invitrogen) containing a specific gene of interest were purchased from commercial cDNA clone libraries. pENTR vectors contain the cDNA flanked by *att*L recombination sites, which are capable of recombining with *att*R sites present on destination (pDEST) vectors. Therefore, in the presence of the recombinase enzyme LR clonase (Invitrogen), the cDNA of a gene of interest in a pENTR vector can be easily cloned into a variety of pDEST vectors containing different N and C terminal tags to quickly generate many different expression clones. 300ng of pENTR vector and 150ng of pDEST vector were made up to a total volume of 9µl with TE buffer (1mM EDTA, 10mM TRIS pH 8), 1µl of LR clonase was added and the reaction was incubated overnight at room temperature. The clonase was then denatured with 1µl Proteinase K (Invitrogen) for 10 minutes at 37°C then stored at 4°C. 2µl of clonase reaction was then transformed into chemically competent OneShot TOP10 *E. coli* (Invitrogen).

pENTR and pDEST vectors commonly contain different antibiotic resistance genes therefore, pDEST vectors can be selected for over pENTR vectors following recombination by plating transformed bacteria onto the appropriate antibiotic. To confirm that the pDEST vectors have undergone recombination, positive colonies should die when grown in media containing chloramphenicol. pDEST vectors contain a chloramphenicol resistance gene between the *att*R sites which is lost upon recombination with a gene of interest. If the pENTR and pDEST vectors contained the same antibiotic resistance gene, following recombination the clonase reaction was digested with a specific restriction enzyme chosen to linearise only the pENTR vector prior to transformation. The Proteinase K was denatured for 20 minutes at 65°C. 2µl enzyme buffer (NEB) 1µl appropriate enzyme and 7µl filtered ddH_2O was added to the whole 10µl clonase reaction and incubated at 37°C for 2 hours. Restriction enzyme was then denatured for 20 minutes at 65°C before 5µl of the digestion was transformed into chemically competent OneShot TOP10 *E. coli* (Invitrogen).

Table 2.6: List of primers used for molecular biology.

Construct	Sense	Sequence
msAhi1_eGFP	forward	catcatcGCGGCCGCgagccagaaactccagagaag
	reverse	catcatGTCGACtcagttggtttgtgacttcgt
msAhi1_myc	forward	catcatAGATCTgagccagaaactccagagaag
	reverse	catcatGTCGACtcagttggtttgtgacttcgt
hAhi1_R351X	forward	cacTgaactgatagacttaagt
	reverse	aatgtaaactcccaagaca
hAhi1_R435X	forward	cttTgaggctctgatga
	reverse	caaatagggaaaattttcat
hAhi1_V433D	forward	aagAcatcctgttctttgag
	reverse	taggactctcatcagagcc
hAhi1_Y933C	forward	gctGcaatggaacatttc
	reverse	gtttgaacatttcagcctc
CYFIP1_SNP1(S431N)	forward	ccgacaAcgctgaagagtac
	reverse	ggcagtccttgttggagtact
CYFIP1_SNP2(R440C)	forward	acgTgctacaactacaccag
	reverse	ggcacgctcgtactctt
CYFIP1_SNP3(R766S)	forward	caatAgtctgatcacccagc
	reverse	aggtctattgatctgccga
CYFIP1_SNP4(Y777C)	forward	tccctagaactggcgattggac
	reverse	cttaCacatggctgctgagac
CYFIP1_SNP5(R826Q)	forward	gttccAggaggccaacca
	reverse	atggcgtcgaagccgt
CYFIP1_SNP2 KASPar	forward1	gaaggtgaccaagttcatgctgagtacgagcgtgccacgc
	forward2	gaaggtcggagtcaacggattaagagtacgagcgtgccacgt
	reverse	catcctcacctccactagggcaa
CYFIP1_SNP3 KASPar	forward1	gaaggtgaccaagttcatgctcggcagatcaatagacctcaatc
	forward2	gaaggtcggagtcaacggattctcggcagatcaatagacctcaata
	reverse	tgctgagacgcgctgggtgat
CYFIP1_SNP4 KASPar	forward1	gaaggtcggagtcaacggattgcgcgtctcagcagccatgta
	forward2	gaaggtgaccaagttcatgctcgcgtctcagcagccatgtg
	reverse	cactttcaaatcgtccaatcgccagtt
CYFIP1_SNP5 KASPar	forward1	gaaggtgaccaagttcatgctcacgttgtggttggcctccc
	forward2	gaaggtcggagtcaacggattacacgttgtggttggcctcct
	reverse	tggacggcttcgacgccatgtt

2.3.13 Generation of Ahi1 shRNA constructs

RNA interference (RNAi) enables the specific knockdown of mRNA by the introduction of short double stranded RNA molecules that are complementary to the gene of interest. These dsRNA molecules are cleaved to short 18-21 bp fragments by the enzyme, Dicer, and the resulting small interfering RNAs (siRNAs) are recruited to the RNA-Induced Silencing Complex (RISC). This effector complex is able to distinguish between the sense and antisense RNA strands, degrade the sense strand and utilise the antisense strand to target genes for silencing. Small hairpin RNAi (shRNAi) was developed to allow long-term knockdown of target proteins in cells by expressing the shRNA from a transfected DNA based vector.

The Ahi1 shRNA construct was made according to the pSUPER manufacturer's protocol (Oligoengine). The oligonucleotides used to create the Ahi1 shRNA construct correspond to the nucleotides 2503-2523 of mouse Ahi1 as described in (Hsiao et al., 2009) (5'-GAAACTGTCACAGAGGTGATA-3'). A scrambled sequence was used as a control (5'-GGAATCTTCCTGCTTTGGG-3'). The oligonucleotides were annealed with annealing solution (100 mM NaCl, 50 mM HEPES pH 7.4), digested with BamH1 and HindIII and cloned into the BglII and HindIII sites of pSUPERneoGFP (Oligoengine).

2.4 KASPar Genotyping

KASPar (KBiosciences Competitive Allele-Specific Polymerase Chain reaction) genotyping is a simple, quick and cost effective way to determine the allele frequency in a sample and control set. KASPar is a homogeneous, FRET bases, endpoint genotyping technology and consists of two main components. The first is the KASPar assay mix which is made up of competing, forward primers targeting the variant of choice, and one common reverse primer. Each forward primer has a unique tail sequence that corresponds with two universal FRET cassettes, one labelled with FAM™ dye and the other with HEX™ dye. The second component is the KASPar master mix, which contains the universal fluorescent FRET cassettes and Taq polymerase in an optimised buffer solution. The two forward competing primers, targeting the wild-type allele and variant allele. During PCR one of the allele-specific forward primers matches the genomic region and the target region is amplified with the common reverse primer. As PCR progresses the level of allele specific tails increase and the fluor-labelled part of the complementary FRET cassette gets incorporated. This releases the fluor from its 3' end quencher to produce a fluorescent

signal which indicates the genotype of the genomic sample.

2.4.1 Primer design and PCR optimisation

KASPar genotyping primers were designed to target the desired mutation by Dr. Andrew McQuillin using Primer Picker (K Bioscience, UK). Two almost identical primers were designed against the genomic region of each SNP. The primers differed in their last base, one contained the wild-type base while the other contained the rare variant base. Normal primer design guidelines were also considered (see page 76). Primers listed in Table 2.6. Optimisation of genotyping conditions was done using both the specific forward primers and the common reverse primer. The six different master mixes tested are outlined in Table 2.7 and the volumes of the allele mixtures are described in Table 2.8. The conditions used varied the concentration of $MgCl_2$ present in the reaction, and the addition or absence of DMSO. The addition of Mg^{2+} ions is essential as they remove phosphates from the dNTPs allowing the reaction to continue. The addition of organic additives such as DMSO, inhibit the formation of DNA secondary structures and aid amplification in GC-rich regions. DMSO also lowers the Tm of DNA by changing its conformation, facilitating the annealing of primers to the genomic DNA and enhancing amplification. Optimisation was carried out on wild-type DNA. Ideally, a positive sample containing the variant of interest would also be used to test the second forward primer however, a positive sample was not available in this case.

The optimised conditions were used to carry out case-control genotyping on DNA samples. DNA samples were aliquoted onto 384-well PCR plates and dried down prior to genotyping. The master mix for the PCR procedure was dispensed into each well of the plate using the Epmotion 5075 (Eppendorf, UK). The plate was then mixed and spun in a centrifuge at 1500rpm for 1 minute before loading into the LightCycler 480 (Roche Diagnostics, UK). The thermal cycling conditions for the endpoint genotyping are outlined in Table 2.9. For all SNPs genotyped, 17% were duplicated to detect error and confirm reproducibility of genotypes on a cross check plate consisting of case and control duplicates. All the data was analyses to confirm Hardy-Weinberg equilibrium (HWE) where possible i.e. all the variants genotyped occurred normally and were not being influenced by natural selection.

2.4.2 Endpoint genotyping

Endpoint genotyping was conducted using LC480 software (Roche Diagnostics, UK). Each fluorescent output was measured and samples were differentiated depending on the signal recorded (Figure 2.1). Any samples that did not cluster closely in the wild-type, heterozygous or homozygous mutant regions were manually labelled as unknown and regenotyped on the cross check plate. Additionally, samples which failed to amplify in the initial genotyping run were plated on the cross check plate from the stock genomic DNA sample following dilution to the appropriate concentration (33.3ng/µl).

Genotype data was accumulated and complied to confirm no differences were present between the original calls and the cross check plate. If such differences were present samples were either removed or sequenced to verify calls. As to be expected for each SNP genotyped there was a number of samples which failed both the original and cross check genotyping, these samples were removed.

2.4.3 KASPar statistical analysis

Allelic associations for SNPs were performed using the Chi-square test. A cut-off significance of $p<0.05$ was used. Minor allele frequency was calculated as the number of mutant alleles divided by the total number of alleles.

Table 2.7: Optimisation conditions for KASPar genotyping

Reagents	A 1.8mM $MgCl_2$	B 2.2mM $MgCl_2$	C 2.5mM $MgCl_2$	D 2.8mM $MgCl_2$	E 5% DMSO	F 10% DMSO
DNA	1	1	1	1	1	1
2X Rxn mix (+KTAQ)	2	2	2	2	2	2
Assay mix ½	0.11	0.11	0.11	0.11	0.11	0.11
$MgCl_2$ 1:10	0	0.32	0.56	0.8	0	0
Water	0.89	0.57	0.33	0.09	0.69	0.5
DMSO	0	0	0	0	0.2	0.4
Total	4	4	4	4	4	4

Table 2.8: Allele mix for KASPar assay.

Reagents	Concentration in Assay Mix (µM)	Volume in 1X Assay Mix (µl)
Allele specific primer 1 (100µM)	12	12
Allele specific primer 2 (100µM)	12	12
Common reverse primer (100µM)	30	30
Water/TrisHCL (10mM, pH8.3)		46
Total		100

Table 2.9: Thermocycling conditions for KASPar genotyping.

Programme	Target Temp (°C)	Hold	Ramp Rate °C/s	Cycles
Hot start activation	94	15 min	4.8	1
1st amplification	94	20 sec	2.5	10
	65	1min	2.5	
2nd amplification	94	20 sec	2.5	26
	57	1min	2.5	
Reading	37	1 sec	2.5	1
	38	1sec	0.06	
3rd amplification	94	20 sec	2.5	3
	57	1min	2.5	
Reading 1	37	1 sec	2.5	1
	38	1 sec	0.06	
4th amplification	94	20 sec	2.5	3
	57	1min	2.5	
Reading 2	37	1 sec	2.5	1
	38	1 sec	0.06	
Cooling	40	1 sec	2.5	1

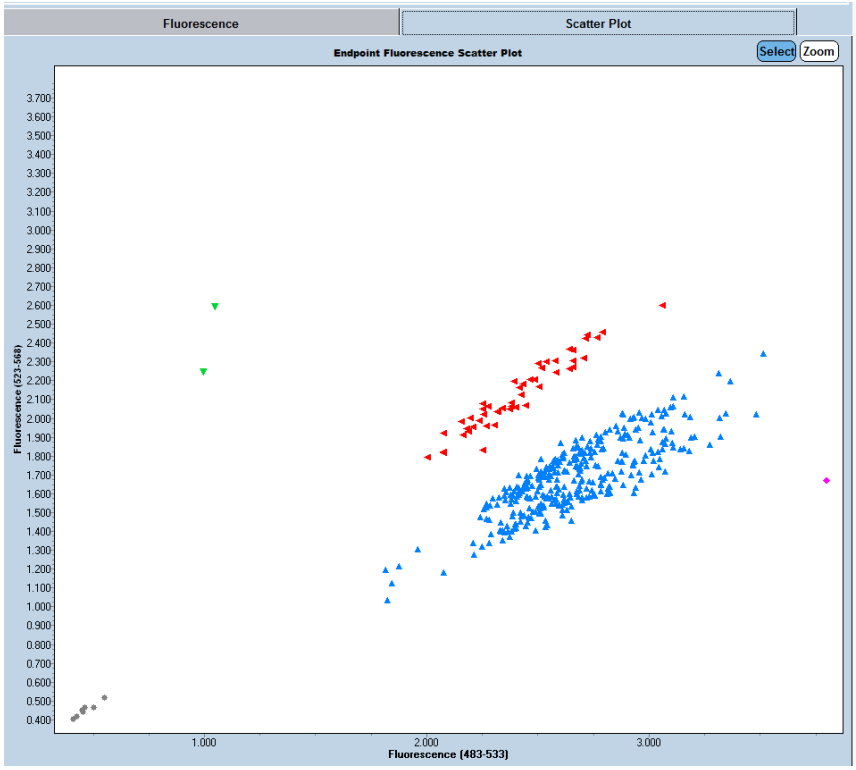

Figure 2.1: Example of KASPar endpoint genotyping.

An example of the KASPar endpoint genotyping output from one of the case control plates genotypes for a single variant of a gene. Wild-type alleles are represented by the blue triangles, heterozygous individuals are represented by the red triangles and individuals homozygous for the mutation are represented by the green triangles. Both the grey and pink circles are samples which have failed or are undefined and were repeated on the cross-check plate.

2.5 Cell Culture

2.5.1 Cell culture media and reagents

Table 2.10: Composition of cell culture solutions

Solutions	Components
Phosphate buffered saline (PBS)	137 mM NaCl, 2.7 mM KCl 10 mM Na_2HPO_4,2 mM KH_2PO_4
Trypsin solution	137 mM NaCl, 2.7 mM KCl 8 mM Na_2HPO_4, 1.5mM KH_2PO_4 2.5 µg/ml Trypsin (Sgima) 0.2 µg/ml EDTA, Phenol Red
Dissection media	HBSS (GIBCO) 10mM HEPES
Attachment media	Minimal Essential Media (GIBCO) 10% horse serum 1 mM sodium pyruvate 0.6% glucose
Maintenance media	Neurobasal (GIBCO) 2% B27 (GIBCO) 1% glutaMAX (GIBCO) 33 mM glucose
Cell line culture media	Dulbecco's Modified Eagle Medium (GIBCO) 10% foetal bovine serum (FBS) 1% penicillin/streptomycin
MEF culture media	Dulbecco's Modified Eagle Medium (GIBCO) 15% foetal bovine serum (FBS) 1% penicillin/streptomycin
Electroporation buffer	15 mM NaH_2PO_4 35 mM Na_2HPO_4, 5 mM KCl 10 mM $MgCl_2$, 11 mM Glucose 100 mM NaCl, 20 mM HEPES

2.5.2 COS-7, HEK and MEF cell culture

Cells were cultured in 10cm dishes with 10ml of culture media at 37°C in 5% CO_2 humidified atmosphere. When confluent, cells were briefly washed in PBS then detached using 1ml trypsin solution and pelleted at 1000 rpm for 2 minutes. Following resuspension cells were plated at an appropriate dilution into fresh dishes and media.

For biochemistry and immunofluorescence cells were transfected using Nucleofector® technology (Amaxa) following the manufacturer's protocol and plated into either fresh dishes or dishes containing 13mm glass coverslips. Briefly, cells to be nucleofected were detached from their dishes as above and pelleted. The cell pellet was resuspended in 100µl per transfection of electroporation buffer. 3-6µg of each plasmid required was added to each nucleofection cuvette followed by 100µl of the cell suspension. Cells were nucleofected and then immediately plated in complete culture media and incubated at 37°C in 5% CO_2.

2.5.3 Generation of transformed MEF lines

Mouse embryonic fibroblasts (MEFs) were cultured from E10.5 transgenic mouse embryos by Prof. Josef Kittler. Briefly, mice were crossed to generate litters of the appropriate genotype. Pregnant female mice were killed when embryos were E10.5 using schedule 1 methods following United Kingdom regulations. The uterus was removed and placed onto ice cold dissection media. The embryos within their placenta were harvested and placed into separate wells containing dissection media. Separately, embryos were carefully dissected from the placenta and the head and internal organs were removed. The remaining tissue was roughly cut to increase surface area and incubated with 30µl 0.125% trypsin for 10 minutes at 37°C. The trypsin was removed and tissue was washed twice with dissection media. Tissue was triturated in 1ml of warm MEF culture media by gently pipetting up and down with a 1ml pipette until a single cell suspension was achieved. Cells were counted using a hemocytomer and erythrosine B dye to exclude dead cells before being plated. Media was changed after 24 hours. Media was changed every two days in the first week following preparation and cells were split if necessary when almost confluent. Following repeated splitting cells gained immortal characteristics and spontaneously transformed. After 8-10 passages of the transformed culture the cells were amplified and frozen down slowly in FBS + 10% DMSO and stored at -80°C.

2.5.4 Primary neuronal cell cultures

2.5.4.1 Neuronal culture from E18 Sprague-Dawley rats

Cortical and hippocampal neurons were cultured from E18 Sprague-Dawley rats as previously described (Banker and Goslin, 1998). Briefly, timed pregnant rats were killed by a schedule 1 method following United Kingdom regulations. E18 embryos were removed and placed onto ice-cold dissection media. Brains were isolated, meninges were removed and hippocampi and cortices were dissected. Dissected tissue was then incubated in 0.125% trypsin diluted in dissection media (5 mL) for 15 minutes at 37°C. Tissue was washed twice in dissection media and triturated to a single cell suspension in attachment media using a fire-polished glass pasteur pipette. Following trituration, cells were counted using a hemocytomer and erythrosine B dye to exclude dead cells before being plated accordingly on pre-prepared poly-L-lysine (PLL) coated plates or 13mm glass coverslips in attachment media. PLL was incubated for a minimum of 3 hours with coverslips for hippocampal culture and plates for cortical culture at 500µg/ml and 50µg/ml respectively. Cells were incubated at 37°C in 5% CO_2 humidified atmosphere. The media was changed 4-6 hours later to neuronal maintenance media.

2.5.4.2 Neuronal culture from E16 WT or transgenic mice

Cortical and hippocampal neurons were cultured from wild-type or transgenic E16 mouse litters using the same protocol as described above for rat cultures. However, during transgenic preparations the tissue from individual embryos was dissected, triturated and plated separately to ensure no cross contamination of genotypes. A sample of remaining tissue from each embryo was retained for genotyping by PCR. To obtain mouse transgenic neuronal cultures appropriate animals were crossed to produce litters with the desired genotypes.

2.5.5 Lipofectamine transfection

Neurons were transfected at the appropriate age using Lipofectamine 2000 (Invitrogen). For 2 coverslips in individual wells of a 24 well plate, 1µg DNA was combined with 100µl unsupplemented Neurobasal (NB) and 2µl Lipofectamine with 100µl NB in separate tubes. Following 5 minutes incubation at RT the Lipofectaime solution was gently combined with the DNA and incubated for 30 minutes at RT to complex. 300µl pre-warmed NB + 0.6% glucose was added to the complex solution and gently mixed, then 250µl of this was dropped carefully onto each coverslip.

Coverslips were incubated at 37°C for 2 hours followed by replacing the transfection media with 1ml pre-warmed conditioned maintenance media. Volumes were scaled up for additional coverslips or larger dishes.

2.6 Biochemistry

2.6.1 Preparation of whole brain and brain region lysates

Adult rat or mouse whole brains were mechanically homogenised on ice in 10ml and 5ml HEPES buffer respectively (50mM HEPES pH 7.5, 0.5% Triton X-100, 150mM NaCl, 1mM EDTA, 1mM PMSF, 10µg/ml antipain, pepstatin and leupeptin) and solubilised for 1 hour rotating at 4°C. Solubilised material was ultracentrifuged at 38000 rpm for 40 minutes and the supernatant (solubilised protein) was collected and quantified using the Bradford assay following the manufacturer's protocol (BioRad).

For brain region lysates, cortex, hippocampus and cerebellum were dissected in HEPES buffered HBSS from P16 or P55 mouse brains. Samples were weighed and homogenised on ice in the appropriate volume of HEPES buffer (7µl/1mg) and solubilised for 1 hour rotating at 4°C. Solubilised material was then centrifuged at 14000 rpm for 10 minutes. The supernatant was collected and quantified as above.

2.6.2 Immunoprecipitation from brain lysate or transfected COS-7 cells

For immunoprecipitation (IP) from whole brain lysate, 2mg of brain lysate in a volume of 0.5mL HEPES buffer (see above) was incubated with 2-4µg antibody overnight, followed by a 1 hour incubation with 25µl of a 50% slurry of protein A or G beads (Generon), depending on the species of antibody. For IP from transfected COS-7 cells, a 10cm dish of transfected cells was solubilised in 0.5mL TRIS buffer for 1 hour (50mM Tris pH 7.5, 0.5% Triton, 150mM NaCl, 1mM EDTA, 1mM PMSF, 10µg/mL antipain, leupeptin, pepstatin) and centrifuged at 12 000 rpm for 10 minutes to pellet the cell debris. Supernatant was either incubated with 2µg antibody for 2 hours followed by 1 hour with 25µl of protein A or G beads (50% slurry), depending on the species of antibody, or 10µl of a 50% slurry of GFP TRAP beads (Chromotech) or myc agarose beads (SIGMA) for GFP and myc IPs respectively. All incubations were under rotation at 4°C. Finally, beads were washed 3-5 times with the appropriate buffer to remove any non-specific binding and analysed by SDS-PAGE and western blotting.

2.6.3 SDS-Polyacrylamide Gel Electrophoresis (SDS-PAGE)

All samples to be analysed by SDS-PAGE were denatured in 3X sample buffer (150mM Tris pH 8, 6% SDS, 0.3M DTT, 0.3% Bromophenol Blue, 30% glycerol) for 6 minutes at 100°C and either stored at -20°C or immediately loaded onto a polyacrylamide gel. Gels were formed of a 10% resolving gel (10% acrylamide mix (ProtoGel, National Diagnostics), 0.375M Tris pH 8.8, 1% SDS, 1% ammonium persulphate, 0.04% TEMED) and a 5% stacking gel (5% acrylamide mix, 0.125M Tris pH 6.8, 1% SDS, 1% ammonium persulphate, 0.1% TEMED) and cast in Novex 1.5mm cassettes (Invitrogen). Gels were submerged in running buffer (Table 2.11) (National Diagnostics) in a Novex XCell SureLock Mini-Cell system (Invitrogen) and electrophoresis was carried out at 120V for ~2 hours until the dye front reached the end of the cassette.

2.6.4 Transfer of SDS-PAGE gels

Samples subjected to SDS-PAGE were transferred onto Hybond-ECL nitrocellulose membrane (GE Healthcare) using the Novex Blot Module transfer system. The gel and pre-wetted membrane were sandwiched between pieces of 3mm filter paper (Whatmann) and sponges to fill the Blot Module. The system was run for 2 hours at 30V in 1X transfer buffer (Table 2.11) (National Diagnostics). Following transfer, the membrane was probed with Ponceau stain to reveal protein on the membrane.

2.6.5 Western blotting

Membranes were blocked for 1 hour with 4% milk in PBS-0.05% Tween (PBS-T). Blocked membranes were incubated over night at 4°C with primary antibodies, then washed 3 times with 4% milk PBS-T and incubated for 1 hour with HRP conjugated secondary antibodies diluted in blocking solution. After 3 times 10 minute washes with 4% milk PBS-T and one final wash with PBS-T the membranes were incubated with the Luminata Crescendo substrate (Millipore) for 1 minute. Bands were detected using an ImageQuant LAS 4000 CCD camera system (GE Healthcare). For western blot quantification densiometric analysis of protein bands was carried out using ImageJ (NIH, Bethesda, MD, USA).

2.6.6 Stripping

Membranes were washed two times with PBS-T for 10 minutes and then incubated in pre-warmed (37°C) stripping buffer for 30 minutes (Table 2.11). Membranes were

then washed in PBS-T 3 times for 10 minutes and blocked in 4% Milk in PBS-T for 1 hour before incubation with the primary antibody.

Table 2.11: SDS-PAGE and Western blotting buffers and solutions.

Solutions	Components
10% resolving gel	10% Protogel (acrylamide solution) 375 mM Tris pH 8.8 1% SDS 1% ammonium persulphate (APS) 0.04% TEMED
Stacking gel	5% Protogel (acrylamide solution) 125 mM Tris pH 6.8 1% SDS, 1% APS 0.004% TEMED
10x Running buffer	250 mM Tris 1.92 M glycine 1% SDS
10x Transfer buffer	250 mM Tris 1.92 M glycine 20% methanol 0.35% SDS
Ponceau stain	5% acetic acid 0.1% Ponceau S
Membrane blocking solution	4% non fat milk 0.05% Tween in 1x PBS
Stripping buffer	6.25 mM Tris pH 6.8 2% SDS 0.7% mercapto-ethanol in 1x PBS

2.7 Immunofluorescence and Microscopy

2.7.1 Confocal microscopy

All imaging was carried out using a Zeiss LSM700 upright confocal microscope unless otherwise stated. Objectives used are summarised in Table 2.12.

Table 2.12: Confocal microscope objectives.

Objective	Emersion media	Microscope	Numerical Aperture
63X	Oil	LSM700	1.4
40X	Oil	LSM700	1.3
63X	Water	LSM700	1.0
10X	Air	LSM700	0.3
5X	Air	LSM700	0.16
20X	Air	Neurolucida	0.45

2.7.2 Live FRAP imaging of dendritic spines

Transfected cells grown on 13mm glass coverslips were perfused with ACSF (10mM HEPES pH 7.4, 125mM NaCl, 10mM D-Glucose, 5mM KCl, 2mM $CaCl_2$, 1mM MgCl2 pH7.4) at 37°C and imaged with a 63X water objective. Movies were captured using the 488 laser at 2%, a 3.5X optical zoom and a 512x512 pixel resolution for 50 cycles (1.94 seconds/cycle). The pixel dwell time was set to 3.15µsec and pinhole size was set to 2µm. Bleaching of the spine head with 100% laser intensity for 10 iterations occurred after 10 cycles. Spines selected for photobleaching all had a clearly formed head. Movies were saved and analysed in ImageJ (NIH, Bethesda, MD, USA).

2.7.3 Immunocytochemistry

Neurons or cells lines grown on 13mm coverslips were removed from their media and immediately fixed in 4% PFA (PBS, 4% paraformaldehdye, 4% sucrose, pH 7) for 7 minutes. Coverslips were gently washed in PBS then blocked and permeablised for 10 minutes in block solution (PBS, 10% horse serum, 0.5% BSA, 0.2% Triton X-100). Coverslips were incubated with primary antibody diluted in block solution for 1 hour at RT. They were washed 5X in PBS then incubated for another hour with secondary

antibody. Finally they were washed 5 times in PBS then mounted onto glass slides using ProLong Gold antifade reagent (Invitrogen). Once the mount was set coverslips were sealed with nail varnish. For surface staining the protocol was the same however, block solution was used without detergent. Cells were visualised using a Zeiss LSM700 confocal microscope and a 63X oil immersion objective, images were digitally captured using LSM software.

2.7.4 Immunohistochemistry

2.7.4.1 Nissl and antibody staining

Adult mouse brains were dissected whole and fixed in 4% PFA for 24 hours at 4°C. Brains were then cryoprotected by incubating in PBS 30% sucrose for 24 hours at 4°C and could then be stored at -80°C indefinitely. For Nissl staining, brains were embedded in 2% agarose (SIGMA) and the agarose block was glued (Lotite) in place for sagittal sectioning on the slicing stage. 30µm slices were made using a vibratome (Leica); slices were carefully removed from the agarose and stored at -20°C in cryprotect solution (30% polyethylene glycol, 30% glycerol in PBS). Slices were washed, blocked and permeablised in PBS 0.5% Triton X-100 during the day. Following 2X 5 minute washes in PBS slices were incubated with Neurotrace Green Fluorescent Nissl Stain (1:200 with PBS, Molecular Probes) overnight at 4°C. Slices were washed for 10 minutes in PBS 0.5% Triton X-100, then twice for 5 minutes in PBS, followed by a final 2 hour wash with PBS.

For antibody staining cryoprotected brains were mounted and serially cryosected in a Bright OTF-AS Cryostat (Bright Instrument, Co. Ltd) at 30µm thickness. Again slices were stored at -20°C in cryoprotect solution (30% polyethylene glycol, 30% glycerol in PBS). Slices were washed blocked and permeablised in block buffer during the day (10% HRS, 0.2M glycine, 3% BSA, 0.5% Triton X-100). Slices were incubated with primary antibody diluted in block buffer overnight at 4°C before being washed 3X 30 minutes in PBS-0.5% Triton. Secondary antibody was incubated with slices for 4 hours at RT before 3X 30 minute final washes in PBS-0.5% Triton. All slices were carefully floated onto glass coverslips and mounted using ProLong Gold antifade reagent (Invitrogen). Slices were imaged using a Zeiss LSM700 confocal microscope and a 5X or 10X air objective. A series of overlapping images were taken and merge together on PhotoShop (Adobe) using the photomerge tool.

2.7.4.2 X-gal staining

Adult mouse brains were dissected whole and mounted using glue without fixation on the slicing stage. Brains were supported with blocks of 2% agarose. 300µm slices were made using a vibratome (Leica); slices were carefully transferred to a 12 well plate and stored in PBS. Slices were post-fixed in fix buffer (0.1M phosphate buffer pH7.3, 5mM EGTA pH 7.3 (Sigma), 2mM $MgCl_2$, 0.2% glutareldahyde, 0.4% PFA, 0.01% deoxycholate, 0.02% NP-40) for 15 minutes at RT. Slices were washes 3X 15 minutes with gentle rotation in wash buffer (0.1M phosphate buffer pH 7.3, 2mM $MgCl_2$, 0.01% deoxycholate, 0.02% NP-40). Slices were then incubated with filter sterilised staining solution (0.1M phosphate buffer pH 7.3, 2mM $MgCl_2$, 5mM potassium ferrocyanide, 5mM potassium ferricyanide, X-gal 1mg/ml added just before use) over night at 37°C with gentle rotation. Slices were washed another 3X 15 minutes, then dehydrated gradually in 50%, 70% and 100% ethanol. Slices can be stored in 100% ethanol until mounting.

2.8 Image Analysis

2.8.1 Synaptic enrichment and cluster analysis

Single confocal images were acquired with the 63X objective for cluster analysis and synaptic enrichment experiments. An image of the cell was captured using a 0.5X zoom. From this, 3-5 sections of primary or secondary dendrite, ~100µm from the soma, were imaged with a 3.5X zoom (equating to a 30µm length of dendrite). Acquisition settings and laser power were kept constant within experiments.

Synaptic enrichment and cluster analysis was carried out using Metamorph (Molecular Devices, Sunnyvale, CA, USA). Analysis was carried out on the zoomed images (3-5 per cell) and then averaged to give a value per cell. To quantify protein enrichment at synaptic sites, the length of dendrite was traced to generate the 30µm long dendritic region. A user-defined threshold was applied to the synaptic marker channel and regions were generated around the thresholded area within the traced dendrite. The dendrite and synaptic puncta regions were then transferred to the protein of interest channel. The fluorescence enrichment was measured as the average fluorescence intensity within the labelled synaptic puncta regions and normalised to the average intensity of the total dendritic process region. For cluster analysis, again the length of dendrite was traced to generate the 30µm long dendritic region. This region was applied to all cluster channels. A user-defined threshold was then applied

to all cluster channels and regions were generated around thresholded area within the traced dendrite. Number of regions and total area of regions per 30µm of dendrite were quantified as a readout for synaptic clusters. Clusters smaller than 0.01µm² were excluded from the number of regions analysis. Thresholds were set individually for each cluster channel and kept constant across treatment conditions within an experiment.

2.8.2 Fluorescence intensity analysis

To quantify fluorescence intensity for shRNA knockdown characterisation, cells were imaged in a single plain of focus with the 63X objective and a 0.5X zoom. An appropriate threshold was applied to the cell fill channel and a cell region was generated. This region was transferred to the channel of interest and average pixel intensity within the region was calculated using ImageJ (NIH, Bethesda, MD, USA). Data was normalised to the average control value to give a percentage change in fluorescence intensity from 100%. Confocal stacks (0.5µm step size) were taken of representative cells and max projected for figures.

Line scans used for protein localisation were performed in ImageJ using the PlotProfile function (NIH, Bethesda, MD, USA), pixel intensity was calculated as a function of distance along a manually drawn line and plotted on a graph.

2.8.3 Dendritic spine FRAP analysis

Movies were analysed using ImageJ (NIH, Bethesda, MD, USA). Initially, movies were subjected to the StackReg plugin to correct for drift between frames. A customised ImageJ plugin was then used to measure the fluorescence intensity of a manually selected ROI over the head of the spine normalised to the total fluorescence of the image to correct for photobleaching. These values were then normalised to the average of the first 10 frames and the lowest value in the data set was subtracted from all values to generate a set of data between ~1 and 0. Finally, the average recovery data points across all movies were plotted on a graph against time and fitted to an first order exponential recovery curve ($y = a*(1-\exp(-b*x))$) using Mathematica (Wolfram Research, Champaign, IL, USA). The average time constant was calculated as $\tau = 1/b$ where b is the rate constant. The mobile fraction was calculated as an average of the plateaued fluorescence level, taken as the last 20 frames, and presented as a percentage of the pre-bleached level.

2.8.4 Dendritic spine morphology analysis

Confocal image stacks were acquired for spine morphology analysis with voxel dimensions of 0.19µm x 0.19µm x 0.57µm. Spines were manually identified for analysis in Imaris software (Bitplane AG, Zurich, Switzerland). For spine classification custom parameters were used. Spines were classified into stubby, mushroom, long and thin, and filopodia categories using a ratio of spine head and neck diameters to spine length (Table 2.13). Classification was entirely automated until the final step where errors in classification were removed.

Table 2.13: List of spine classification Matlab parameters.

Spine Classification	Matlab Plugin Parameters
Stubby	length(spine) < 0.8 and min_width(spine) > 0.1
Mushroom	3 * max_width(head) > length(spine) and length(spine) > 0.8 and min_width(spine) > 0.1
Long, Thin	length(spine) >= 1.20 * max_width(head) and length(spine) < 3.5 and min_width(spine) > 0.1
Filopodia	length(spine) > 3.5 and min_width(spine) > 0.1

2.8.5 Sholl dendrite analysis

Confocal image stacks were captured using the 63X or the 40X objective for dendritic morphological analysis with voxel dimensions of 0.39µm x 0.39µm x 0.54µm and 0.63µm x 0.63µm x 1.0µm respectively. Neuronal arbors were reconstructed by semi-manual tracing using NeuronStudio (Wearne et al., 2005). Total dendritic length and total number of branch points per cell were calculated from the Sholl analysis output from NeuronStudio. To generate number of intersections as a function of distance from the soma the .swc trace file from NeuronStudio was imported into ImageJ (NIH, Bethesda, MD, USA) and this analysis was generated from the NeuroTracer plugin.

Dendritic morphology in adult mice were analysed using the FD Rapid Golgi Stain kit (FD NeuroTechnologies) and Neurolucida (MBF Bioscience). For Golgi-stained Sholl analysis, impregnated brains were sliced at 150µm using a vibratome (Leica). Well isolated hippocampal CA1 neurons were imaged at 20X using the Neurolucida

software system and an upright light microscope with a motorized stage (MBF Bioscience). The entire extent (apical and basal) of the dendritic tree was traced and reconstructed. Total dendritic length, total number of branch points (nodes) and intersections as a function of distance from the soma were calculated from the Neurolucida output file. Three males were analysed for each condition with a minimum of three cells traced per animal. When using animals from separate litters, each genotype was equally represented from each litter.

2.9 Statistics

All data were obtained using cells from at least three different preparations. Repeats for experiments are given in the figure legends as N numbers and refer to number of cells unless otherwise stated. All statistical analysis was carried out using GraphPad Prism (GraphPad Software, CA, USA) or Microsoft Excel. Data was tested for normal distribution with D'Agostino and Person to determine the use of parametric (unpaired student's t-test, one-way ANOVA, two-way ANOVA) or non-parametric (Mann-Whitney, Kruskal-Wallis) tests. Appropriate post-hoc tests were carried out in analyses with multiple comparisons. The Bonferroni's post hoc test and the Dunn's post hoc test were used to compare the data groups to their reference group or compare all the data groups for parametric and non-parametric analysis respectively. Data are shown as ± standard error of the mean (SEM). Data was considered significant if the p value was < 0.05. Stars represent p values as follows: *$p<0.05$, **$p<0.01$, ***$p<0.001$.

Chapter 3
CYFIP1 and CYFIP2 CNVs in neuronal morphology and synaptic maintenance

3.1 Introduction

The 15q11-13 region of the human genome is a common locus for genetic structural rearrangement and often results in abnormal neurological phenotypes. In particular, CNVs at the 15q11.2 locus have been associated with intellectual disability (ID) behavioural abnormalities, epilepsies, autism spectrum disorder (ASD) and schizophrenia (SCZ) (Table 3.1). This genetic locus encodes four genes *Tubgcp5, Cyfip1, Nipa1* and *Nipa2* and the non-coding mRNA *Whamml1*. Of the four genes, *Cyfip1* is highly expressed within the brain and has been robustly associated with a variety of neuropsychiatric disorders independent of its neighbouring genes.

Indeed, there is mounting evidence to suggest that *Cyfip1* is the dosage-sensitive gene within this genetic locus and that altered expression of this protein could be contributing to disease onset. Firstly, CNV of *Cyfip1* specifically has been linked to ASD and behavioural disturbances (Doornbos et al., 2009; Leblond et al., 2012). Genome wide expression profiling of patients with a 15q11-13 duplication has specifically demonstrated an up-regulation of *Cyfip1* mRNA in those that suffer from ASD (Nishimura et al., 2007). Furthermore, a direct deletion of the *Cyfip1* gene was identified in an autistic patient who also had a *SHANK2* deletion (Leblond et al., 2012). Additionally, a small screen with less than 100 cases and controls found an association of CNVs in *Cyfip1* with SCZ while genotyping in the Chinese Han population revealed a significant SCZ-associated SNP within *Cyfip1* (Tam et al., 2010; Zhao et al., 2013b). Taken together, *Cyfip1* is emerging as a candidate susceptibility gene for neuropsychiatric disorders. On the other hand, the homologue of CYFIP1, CYFIP2, has no direct association with neuropsychiatric disorders. However, the gene is located on chromosome 5 in the q33.3 region which has been identified as a susceptibility locus for SCZ and attention-deficit/hyperactive disorder (ADHD) via

linkage studies (Arcos-Burgos et al., 2004; Gurling et al., 2001).

Protein analysis has revealed human CYFIP1 and CYFIP2, share 88% amino acid sequence homology and the proteins are conserved across species. Mouse CYFIP1 and CYFIP2 share 98.7% and 99.9% amino acid sequence homology with human CYFIP1 and CYFIP2 respectively. Single CYFIP orthologs have also been identified in flies (*D. melanogaster*) and worms (*C. elegans*) sharing 67% and 51% amino acid identity respectively with the human proteins. Zebrafish (*D. rerio*), like mammalian species have two conserved CYFIP proteins (Pittman et al., 2010; Schenck et al., 2001). CYFIP proteins are widely expressed and enriched in brain (Schenck et al., 2001). dCYFIP mRNA was detected ubiquitously in flies and is present throughout the fly life cycle. During development the highest levels of dCYFIP mRNA expression were notably in the CNS and gut with expression in the CNS peaking towards the end of embryogenesis. This expression was mirrored by the protein levels (Schenck et al., 2003). Equally, in mice, CYFIP1 mRNA can be detected by native hybridisation ubiquitously throughout embryogenesis with most prominent hybridisation occurring in brain tissue. This continued into adulthood with the hippocampus and olfactory bulb showing higher mRNA expression levels than other brain regions (Köster et al., 1998). In addition, CYFIP1 protein can be detected at all ages in mouse brain with peak expression in the third post-natal week (Bonaccorso et al., 2015). In contrast, CYFIP2 is moderately expressed in 3 day old mice and increases after day 7. Interestingly, CYFIP1 has also been identified in synaptosomal fractions (Schenck et al., 2001).

Human CYFIP1 and CYFIP2 are both 1253 amino acid residues long and by western blot produce bands at ~145KDa (Saller et al., 1999; Schenck et al., 2001). As the whole length of CYFIP proteins are species conserved this suggests the proteins must be structurally and functionally important. It is then interesting to note that CYFIP proteins contain no particular structural domains such as SH3 and coiled-coil domains. They have however, been described to interact with several other proteins which has implicated them in multiple cellular processes (Figure 3.1).

3.1.1 Cellular functions of CYFIP proteins

CYFIP1 was originally identified as a target for the actin regulatory GTPase Rac1. The ~140KDa protein identified was purified from bovine brain cytosol with GTP-bound GST-Rac1, the human cDNA was cloned, characterised and named Sra1 (**s**pecific **R**ac1

associated protein) (Kobayashi et al., 1998). Later, the interaction between CYFIP1 and Rac1 was shown to be vital in modulating the activity of the Wave Regulatory Complex (WRC), a heteropentameric complex consisting of CYFIP1, NAP1, Abi, WAVE and HSPC300 and critical for actin regulation (see Figure 1.3) (Chen et al., 2010b; Eden et al., 2002; Ismail et al., 2009). The WRC complex is a downstream effector of Rac1 which brings about Arp2/3 activity resulting in actin nucleation, branching and polymerisation. In parallel, CYFIP2 was identified in a complex with WAVE and Rac1 and due to sequence similarity is considered to regulate the WRC similarly to CYFIP1 however, has been less studied (Eden et al., 2002).

This role in actin regulation implicates CYFIP proteins in a number of dynamic pathways. CYFIP1 along with other members of the WRC, NAP1 and Abi, are required for WAVE stability and localisation during the formation of actin based membrane protrusions. During lamellipodia formation, active Rac1 has been shown to translocate the WRC to the leading edge of migrating cells and induced actin polymerisation. However, following RNAi to CYFIP1 or Nap1 translocation and lamellipodia formation was lost (Kunda et al., 2003; Steffen et al., 2004). Interestingly, clathrin heavy chain (CHC) was also shown to control lamellipodia formation via an interaction with dCYFIP and by regulating the recruitment of the WRC to the membrane. Overexpression of CHC reduced the membrane targeting of the WRC and decreased cell migration, while membrane targeted CHC enhanced cell migration (Gautier et al., 2011). Recently, a small diverse class of membrane proteins including G-protein coupled receptors (GPCRs), protocadherins, neuroligins and ion channels were found to possess a **W**RC **i**nteracting **r**eceptor **s**equence (WIRS) that directly binds to a conserved surface, formed by CYFIP, of the WRC (Chen et al., 2014a). This motif has also been suggested to be important in recruiting the WRC complex to the membrane for actin polymerisation. Indeed, mutant flies expressing a form of dCYFIP that could no longer interact with WIRS domain containing membrane proteins were shown to have defects in actin organisation and egg morphology during oogenesis which led to female sterility (Chen et al., 2014a).

CYFIP1 and CYFIP2 have also been implicated in the regulation of intracellular membrane trafficking. During carrier biogenesis from the trans-Golgi network (TGN), activation of the GTPase Arf triggers the recruitment of AP1 and CHC. CHC, via its interaction with CYFIP1 or CYFIP2, then recruits a CYFIP1 or 2/Abi/Nap1 complex to the TGN membrane which, with Rac1 and N-WASP, promotes actin polymerisation

and tubule formation (Anitei et al., 2010). Moreover, CYFIP1 has been described to interfere with normal epithelial morphogenesis in cancer (Silva et al., 2009) and impair bristle development in flies, a process known to be highly dependent on actin dynamics (Bogdan et al., 2004).

3.1.2 CYFIP proteins and FMRP

Although arguably the most well described function for CYFIP proteins are as components of the WRC, CYFIP proteins can also interact with FMRP. Shortly after CYFIP1 was first identified, an independent Y2H screen, using FMRP as a bait, identified two human homologs, each with a mass of 145KDa, and named them CYFIP1 and CYFIP2 (**cy**toplasmic **F**MRP **i**nteracting **p**rotein1 and 2) (Schenck et al., 2001). Via this interaction, CYFIP1 has been shown to regulate synaptic mRNA translation in an activity-dependent manner (see section 1.4.2.2) (Napoli et al., 2008). *In vitro* RNAi to CYFIP1 in cultured mouse neurons demonstrated that reduced CYFIP1 expression altered the expression levels of FMRP target proteins such as ARC and CamKII. This disruption in protein expression of FMRP target transcripts was also observed in CYFIP haploinsufficient animals (*Cyfip1*$^{+/-}$) (Napoli et al., 2008; De Rubeis et al., 2013). Indeed, the physiology of CYFIP1 heterozygous mice phenocopies characteristics of FMRP KO mice (Bozdagi et al., 2012; Huber et al., 2002). The role for CYFIP2 and FMRP has been less well described however, CYFIP2 alone interacts with the FMRP family members FXR1P and FXR2P (Schenck et al., 2001) (Figure 3.1).

3.1.3 CYFIP proteins in neuronal development

The varied functions of CYFIP have implicated the proteins in neurodevelopmental processes. Indeed, dCYFIP is enriched in axons and motor terminals. Genetic deletion of dCYFIP was lethal and resulted in defects in axonal pathfinding with aberrant midline crossings, stalled axonal growth and abnormal branching, which mostly led to death during pupal life (Schenck et al., 2003). Furthermore, the organisation of the synaptic neuromuscular junction (NMJ) was effected in dCYFIP mutant flies. Schenck *et al.* first described NMJs of dCYFIP mutants to display synaptic undergrowth, disturbed bouton structure and supernumerary budding. Supernumerary budding describes the phenotype where buds arise from existing boutons and form intermediate structures towards the establishment of new boutons (Schenck et al., 2003, 2004). This finding was later confirmed with electron microscopy images of dCYFIP mutant NMJs (Zhao et al., 2013a). NMJs also displayed enlarged synaptic

vesicles and more cisternae characteristic of deficient endocytosis. These effects were suggested to be due to disrupted F-actin assembly detected at presynaptic NMJ terminals (Zhao et al., 2013a).

Others have also reported the involvement of dCYFIP in neuronal development. dCYFIP expression was detected in the growth cones of developing photoreceptors as well as in the eye imaginal disc cells. When dCYFIP expression was reduced photoreceptors exhibited pronounced axonal defects and eyes appeared smaller with a rough appearance (Bogdan et al., 2004). A study carried out in zebrafish characterised the *nevermind (nev)* mutant; *nev* encodes CYFIP2. In retinal ganglion cells of *nev* mutants, positional dorso-ventral information was not maintained by axons as they projected from the retina though the optic tract to the tectum during development. Interestingly, *nev* function is specific to retinal axons. This study highlights that CYFIP proteins have a conserved role in axonal guidance. Indeed, when morpholinos were used against CYFIP1, retinal axon pathfinding defects were also observed suggesting CYFIP1 too, is required in early axon development (Pittman et al., 2010). Equally, mouse hippocampal studies had previously described a role for CYFIP1 with CRMP-2 in axonal development. Knockdown of CYFIP1 by RNAi abolished CRMP-2 induced axonal outgrowth and multiple axon formation. CYFIP1 was found in a complex with CRMP-2 and kinesin-1 light chain (KLC1). When either KLC1 or CRMP-2 were knocked down CYFIP1 was mislocalised from the growth cone suggesting the importance of these trafficking molecules in targeting CYFIP1 to regulate axon formation (Kawano et al., 2005).

A clear role for CYFIP proteins in the regulation of actin dynamics during various cellular functions and in axonal development has been established. There is however, very little known about the role of CYFIP proteins in the regulation of dendritic morphology and synaptic structural stability. Actin cytoskeletal dynamics play a key role in the establishment and maintenance of dendritic arborisation and spines. Remodelling the actin cytoskeleton is also critical for the structural changes in spine shape that occur during synaptic plasticity (Hotulainen and Hoogenraad, 2010). To support this, knockout mice of key actin regulators such as Rac1, PAK3 and WAVE1 display defects in spine dynamics and disrupted neuronal development (Corbetta et al., 2009; Kim et al., 2006; Meng, et al., 2005; Soderling et al., 2007; Tahirovic et al., 2010). Moreover, there are a growing number of mental illness-associated actin regulatory molecules including DISC1, dysbindin1, PAK3 and SRGAP2 that have been

implicated in the regulation of dendritic development and spine morphology (Charrier et al., 2012; Hayashi et al., 2004; Hayashi-Takagi et al., 2010; Ito et al., 2010). Disrupted expression of these molecules leads to alterations in neuronal structure, spine morphology and cognitive function; characteristics of ASD and SCZ. This demonstrates that correct regulation of actin dynamics is a critical mechanism for neuronal development and normal brain function and defects in modulators of this pathway are associated with disease.

It can be hypothesised that CYFIP1, as a candidate ASD and SCZ gene and an actin regulator, may also play a role in the regulation of neuronal morphology in this way. Therefore, investigating the role of CYFIP1, and its homologue CYFIP2, in dendritic morphology and synaptic maintenance may shed light on the neuropsychiatric phenotypes associated with CNV at the CYFIP1 region of the genome. Additionally, how genomic microdeletions and microduplications affecting CYFIP1 expression, as a result of CNV, produce similar neuropsychiatric phenotypes has not yet been addressed (Bozdagi et al., 2012; Rubeis and Bagni, 2011).

In this chapter using fixed and live confocal imaging, CYFIP1 and CYFIP2 have been shown to localise to dendritic spines and are enriched at excitatory synapses. Overexpression of either protein in neurons altered dendritic complexity and spine morphology. On the other hand, employing a CYFIP1 haploinsufficient mouse model to study loss of CYFIP1 expression, revealed disruptions in neuronal morphology, altered synaptic protein expression and impacted on actin dynamics by disrupting F-actin assembly. Finally, CYFIP1 and CYFIP2 were also identified at inhibitory synapses and there, overexpression resulted in a reduction of inhibitory synapses but an increase in excitatory synapses. This demonstrates modelling CNV of CYFIP1 or CYFIP2 disrupts neuronal morphology and synaptic maintenance, potentially via altered actin dynamics, and suggests CYFIP mediated defects in neuronal complexity and synaptic function may contribute to the development of the neurological symptoms observed in ASD and SCZ.

Table 3.1: List of references that implicate *Cyfip1* in neuropsychiatric disorders.

Genetic locus	Genetic variation	Approach	Associated disorder	Reference
Cyfip1	CNV	CNV project	SCZ	(Tam et al., 2010)
Cyfip1	Microduplication	mRNA analysis	ASD	(Nishimura et al., 2007)
Cyfip1	Deleterious variants	whole exome sequencing	SCZ	(Purcell et al., 2014)
Cyfip1 15q11.2	Rare CNV and SNPs	SNP array, CNV analysis, qPCR	SCZ	(Zhao et al., 2013b)
15q11-13 *Cyfip1*	Type I deletion reduced mRNA levels	mRNA analysis	PWS	(Bittel et al., 2006)
SHANK2 *Cyfip1*	*De novo* deletion deletion	Genome wide SNP array	ASD	(Leblond et al., 2012)
15q11.2	Microduplication	SNP array	ASD	(van der Zwaag et al., 2010)
15q11.2	Microdeletion	CGH array	ASD, ADHD, OCD	(Doornbos et al., 2009)
15q11.2	Microdeletion	Genome wide SNP array	SCZ	(Stefansson et al., 2008)
15q11.2	Microdeletion		SCZ, ASD	(Stefansson et al., 2014)
15q11.2	CNV	CGH array	ASD	(Levy et al., 2011)
15q11-13	CNV	Dense genotyping arrays	ASD	(Pinto et al., 2010)
15q11.2	CNV	SNP array and CNV analysis	SCZ	(Kirov et al., 2012)
15q11.2	Microdeletion	SNP array, qPCR, CGH	epilepsy	(de Kovel et al., 2010)
15q11.2	Microdeletion	CGH array	ASD, ID	(Madrigal et al., 2012)
15q11.2	Microdeletion	CGH	Behavioural problems	(von der Lippe et al.)
15q11.2	CNV	SNP array and CGH	Developmental delay	(Burnside et al., 2011)
15q11.2	Microduplication	SNP array and CNV analysis	AD	(Ghani et al., 2012)
15q11.2	Microdeletion	SNP array and CNV analysis	epilepsy	(Lal et al., 2015)
15q11-13	Microduplication	SNP array and CNV analysis	Psychotic illness	(Ingason et al., 2011)
15q11-13	Paternal duplication	Array CGH, MLPA analysis	ID, epilepsy	(Marini et al., 2013)

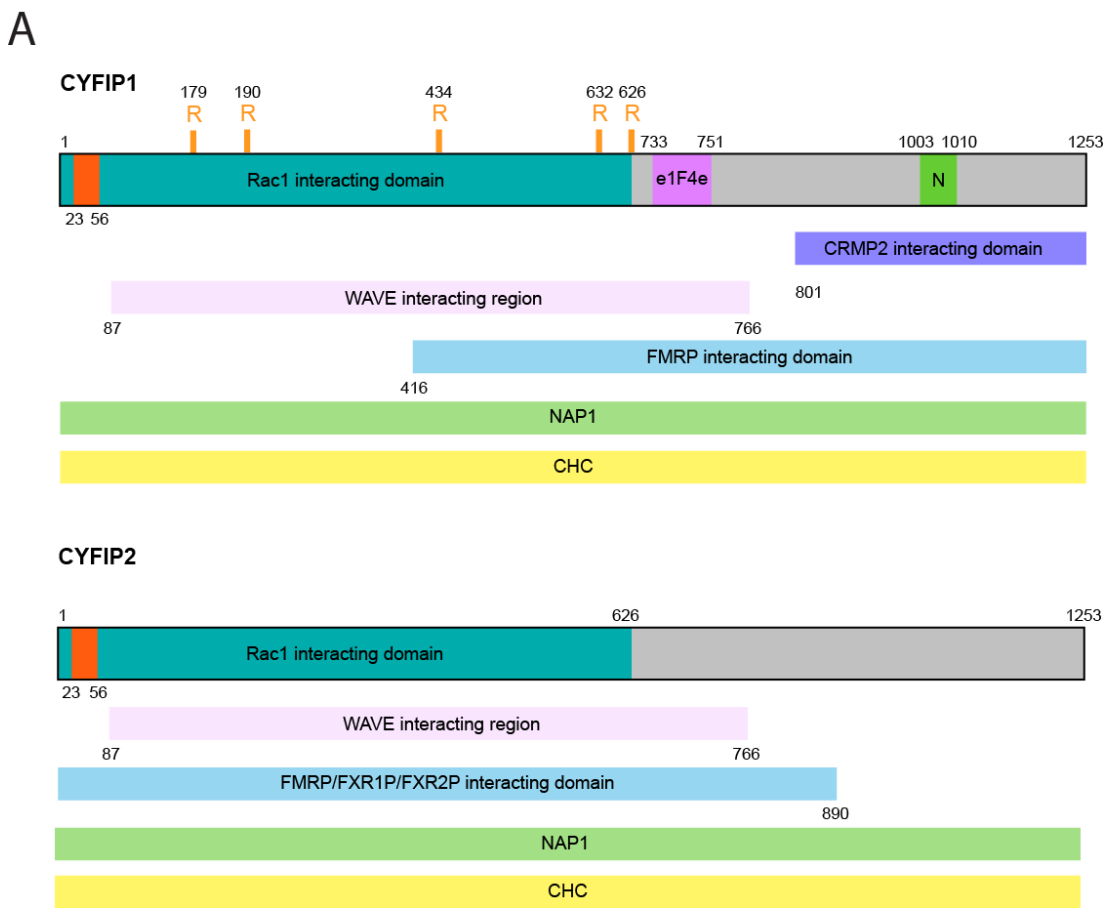

Figure 3.1: A schematic of human CYFIP1 and CYFIP2

A summary of the protein interacting domains described in the literature for human CYFIP1 and CYFIP2. Both proteins are equal length and share 88% sequence homology. Proteins contain: an N-terminal Rac1 interacting domain (GST) (Kobayashi et al., 1998); a small linker region within the N-terminus required for binding to Abi and HSPC300 of the WRC (Struc) (Chen et al., 2010b); NAP1 (Struc) and clathrin heavy chain (CHC) (Y2H, IP) binding domains although the sites are not defined (Anitei et al., 2010; Chen et al., 2010b); a WAVE interacting domain between amino acids 87 and 766 (Struc) (Chen et al., 2010b). CYFIP1 alone has been shown to contain a C-terminal CRMP-2 binding domain (GST) (Kawano et al., 2005), a region critical for NAP1 binding (N) (IP) (De Rubeis et al., 2013), a conserved 4E-BP binding site where e1F4e interacts (GST) (Napoli et al., 2008) and an FMRP interacting domain (416-1253aa) (GST, Y2H) (Schenck et al., 2001). CYFIP2 alone contains a FMRP/FXR1P/FXR2P interacting domain (1-890aa) (Y2H) (Schenck et al., 2001). Putative Rac1 interacting residues are labelled (R) (Struc) (Chen et al., 2010b). Interactions identified by: GST=GST fusion protein pull down; IP=immunoprecipitation; Struc=structural analysis; Y2H=yeast two-hybrid screen.

3.2 Results

In order to investigate the effects of manipulating CYFIP1 and CYFIP2 gene expression on synaptic maintenance and neuronal morphology it was critical to develop and characterise the necessary biological tools. Using the Gateway Cloning System, human CYFIP1 and CYFIP2 cDNA were cloned into the pDEST47 or the pDESTmCherry-N1 mammalian expression vectors containing a C-terminal GFP tag and an N-terminal mCherry tag respectively. To confirm the expression of the tagged proteins in a mammalian system, the generated constructs were transfected into COS7 cells and the cytosolic localisation of CYFIP1 and CYFIP2 GFP or mCherry-tagged proteins were observed (Fig. 1A,G). Samples of COS-7 cells transfected with $CYFIP1^{GFP}$ or $CYFIP2^{GFP}$ were also subjected to SDS-PAGE and western blotting. When the membrane was probed with a GFP antibody, both transfected cell lysates showed a clear band between 130 and 250kDa corresponding to the expected molecular weight of $CYFIP1^{GFP}$ and $CYFIP2^{GFP}$ ~175kDa. This confirmed that these constructs were readily expressed and not subjected to protein cleavage (Figure 3.2B,E). The 175kDa band was not present in the untransfected control lysate and was therefore, considered to be the exogenously expressed $CYFIP1^{GFP}$ or $CYFIP2^{GFP}$.

Two commercially available CYFIP1 antibodies were characterised for their specificity against the human CYFIP constructs. An Upstate antibody (UPST) against CYFIP1 specifically detected the human CYFIP1 construct by immunofluorescence and western blotting (Figure 3.2A,B), whereas a Synaptic Systems antibody (SySy) produced against mouse CYFIP1 specifically detected human $CYFIP1^{GFP}$ by immunofluorescence but detected both $CYFIP1^{GFP}$ and $CYFIP2^{GFP}$ by western blot among other nonspecific bands (Figure 3.2D,E). Both antibodies detected mouse CYFIP1 at the expected weight for endogenous rodent CYFIP1 of ~145kDa. However, only the UPST antibody detected rat CYFIP1 at ~145kDa (Figure 3.2C,F). Due to the CYFIP1 specificity of the Upstate antibody and its ability to detect rat CYFIP1, the Upstate antibody was used in all following studies.

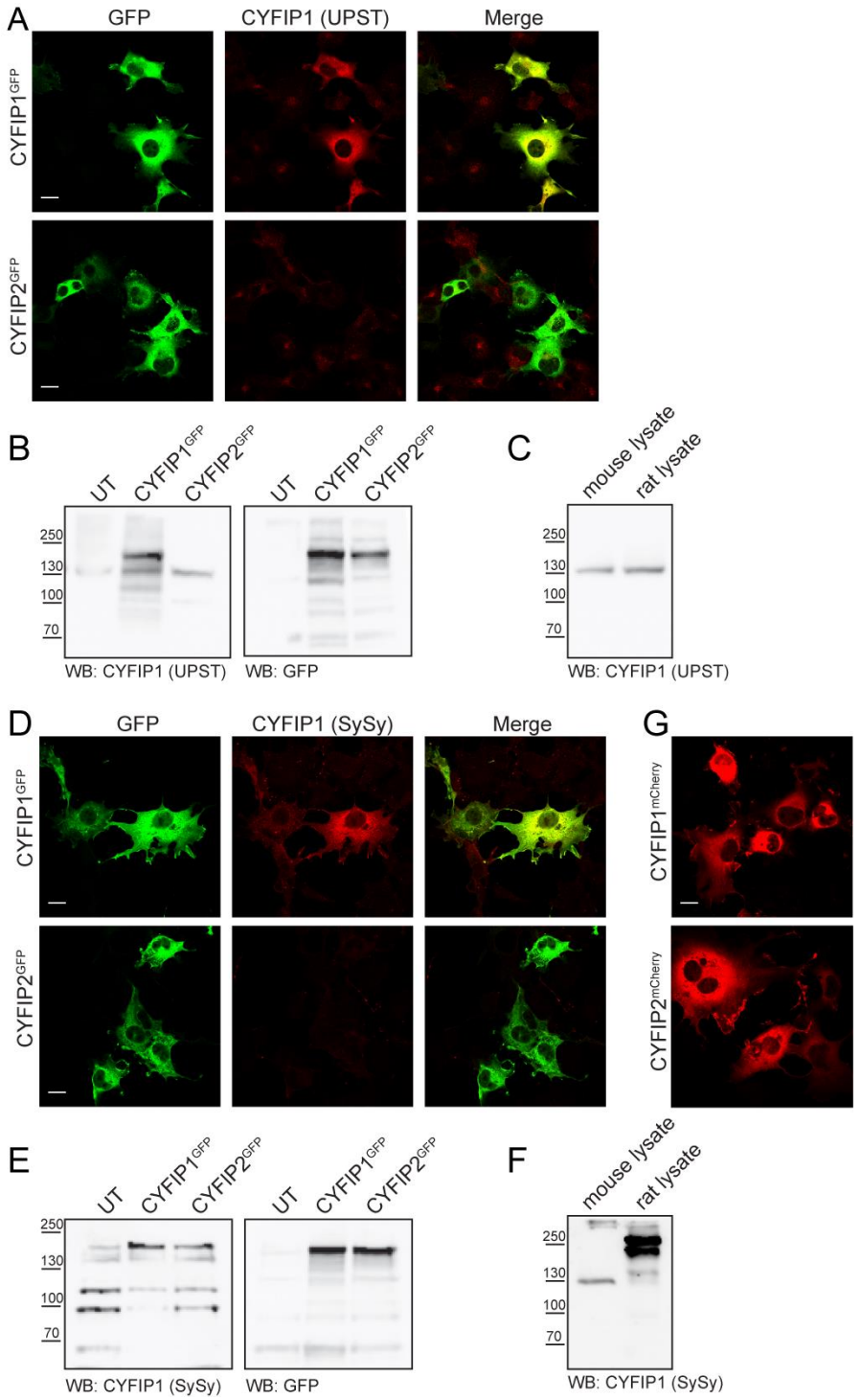

Figure 3.2: Cloning of GFP and mCherry tagged CYFIP1 and CYFIP2 constructs and characterisation of a CYFIP1 specific antibody

(A and D) Transfection of COS-7 cells with human CYFIP1^{GFP} or CYFIP2^{GFP} constructs. Strong GFP signal confirms that these fusion proteins are readily expressed. Immunostaining of CYFIP1^{GFP} or CYFIP2^{GFP} transfected cells with either **(A)** an Upsate (UPST) or **(D)** a Synaptic Systems (SySy) commercial anti-CYFIP1 antibody shows that both antibodies for

immunocytochemistry are specific to human CYFIP1 alone. Scale bar, 20μm. **(B and E)** Western blotting of untransfected (UT), CYFIP1^{GFP} or CYFIP2^{GFP} transfected COS-7 cell lysates and probing for GFP (right panels) confirms that these constructs generate fusion proteins of the expected molecular weight ~175 kDa. Probing for CYFIP1 with **(B)** UPST and **(E)** SySy antibodies (left panels) confirms the specificity of UPST producing a specific band for CYFIP1^{GFP} alone at ~175 kDa while SySy recognises both proteins. Probing mouse and rat brain lysate on a western blot with **(C)** UPST or **(F)** SySy antibodies confirms that the UPST antibody reacts to both rat and mouse endogenous CYFIP1 whereas the SySy antibody is mouse specific both producing a band at the expected molecular weight ~145 kDa. **(G)** Transfection of COS-7 cells with human CYFIP1^{mCherry} or CYFIP2^{mCherry} constructs. Strong mCherry signal confirms that these fusion proteins are readily expressed. Scale bar, 20μm.

3.2.1 Neuronal subcellular localisation of CYFIP1 and its homologue CYFIP2

Prior to this work the subcellular localisation of CYFIP1 and its homologue CYFIP2 in mammalian neurons had been poorly described (Kawano et al., 2005; Pilpel and Segal, 2005). A clear description of the spatial localisation of a protein can shed light on how that protein may function within a particular cell type. Therefore, to explore in detail the localisation of CYFIP1 and CYFIP2 in neurons CYFIP1^{GFP} or CYFIP2^{GFP} were co-expressed in mature hippocampal neurons with DsRed to provide a fluorescent cell fill and act as a marker of neuronal morphology. Following three days expression neurons were fixed and stained with anti-GFP to enhance the GFP signal and analysed using confocal microscopy. CYFIP1^{GFP} and CYFIP2^{GFP} were detected throughout the whole neuronal architecture. Their localisation was diffuse within the soma. However, both proteins had a more distinct localisation along the dendrites (Figure 3.3A). CYFIP1^{GFP} and CYFIP2^{GFP} could also be detected within the axons.

Upon closer inspection using high-resolution zoom images, CYFIP1^{GFP} and CYFIP2^{GFP} exhibited a non-uniform distribution along dendrites compared to the localisation of DsRed, which uniformly filled both dendritic processes and spines. Indeed, both GFP-tagged proteins appeared to be selectively targeted to punctate clusters within the dendritic shaft and interestingly, localised to dendritic spines (Figure 3.3B,C). A similar enrichment at spines was observed for endogenous CYFIP1 using the characterised CYFIP1-specific antibody. In neurons transfected with actin^{GFP} to label spine and neuronal morphology, endogenous CYFIP1 displayed marked colocalisation with actin^{GFP} in spines (Figure 3.3D). The consistency between the dendritic localisation of endogenous and GFP-tagged CYFIP1 confirms that the overexpression system used does not result in the mislocalisation of CYFIP1 or CYFIP2. To graphically represent the colocalisation of CYFIP1^{GFP}, CYFIP2^{GFP} and endogenous CYFIP1 at dendritic spines, a line was drawn though a zoom image of the dendritic shaft and a single spine head and pixel intensity of the different channels were plotted against line length. CYFIP1^{GFP}, CYFIP2^{GFP} and endogenous CYFIP1 all showed greater fluorescence intensity in the spine head compared to the dendrite (Figure 3.3B-D).

Dendritic spines are small membrane protrusions that extend out from the dendritic

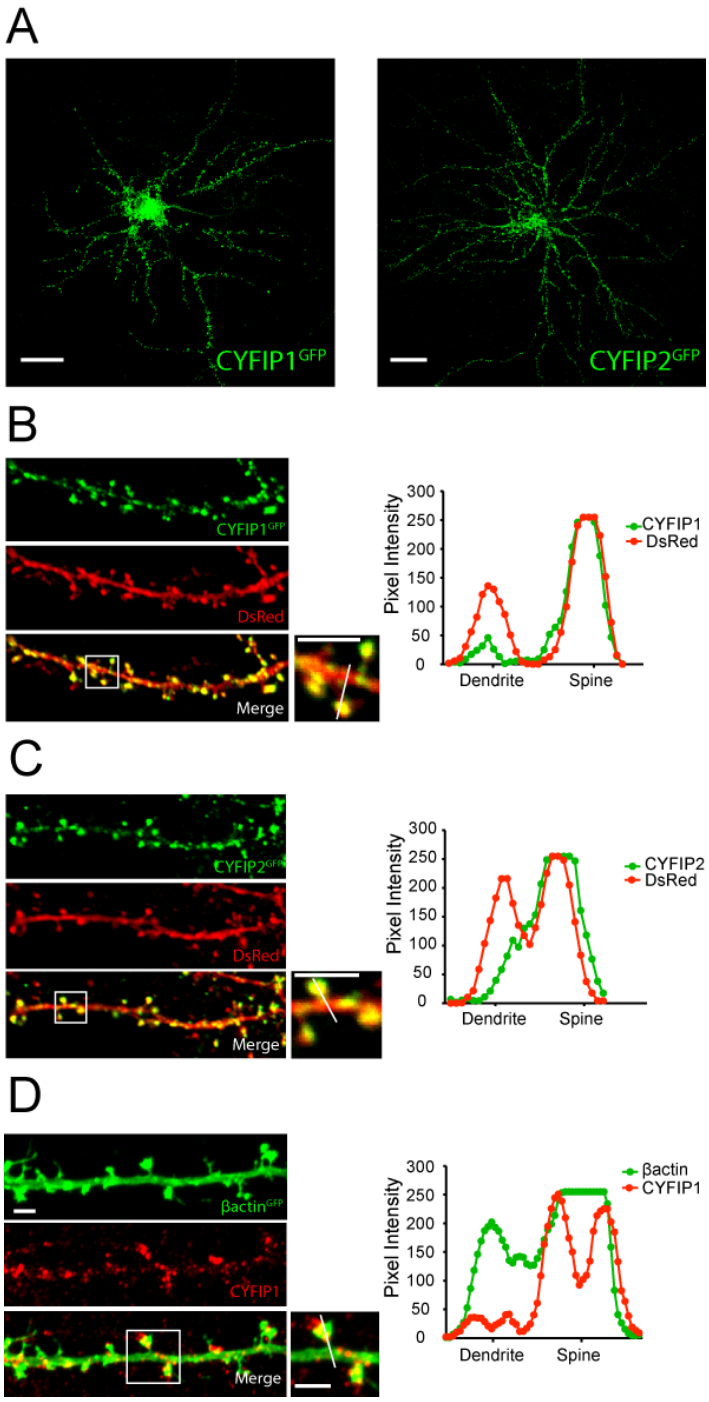

Figure 3.3: CYFIP1 and CYFIP2 are localised at dendritic spines.

(A) CYFIP1^{GFP} and CYFIP2^{GFP} were transfected into mature rat hippocampal neurons. Both transgenes were readily expressed with a diffuse staining in the soma and a punctate staining along dendrites. Scale bars, 20µm. CYFIP1^{GFP} **(B),** CYFIP2^{GFP} **(C)** or endogenous CYFIP1 **(D)** localise to dendritic spines. DsRed **(B, C)** or actin^{GFP} **(D)** were used to label processes. A line-scan through the dendritic shaft and spine head (right graphs) shows the fluorescence intensity of the green and red channels depicting the enrichment of CYFIP1^{GFP}, CYFIP2^{GFP} or endogenous CYFIP1 in the spine compared to the dendrite. Scale bars, 2µm.

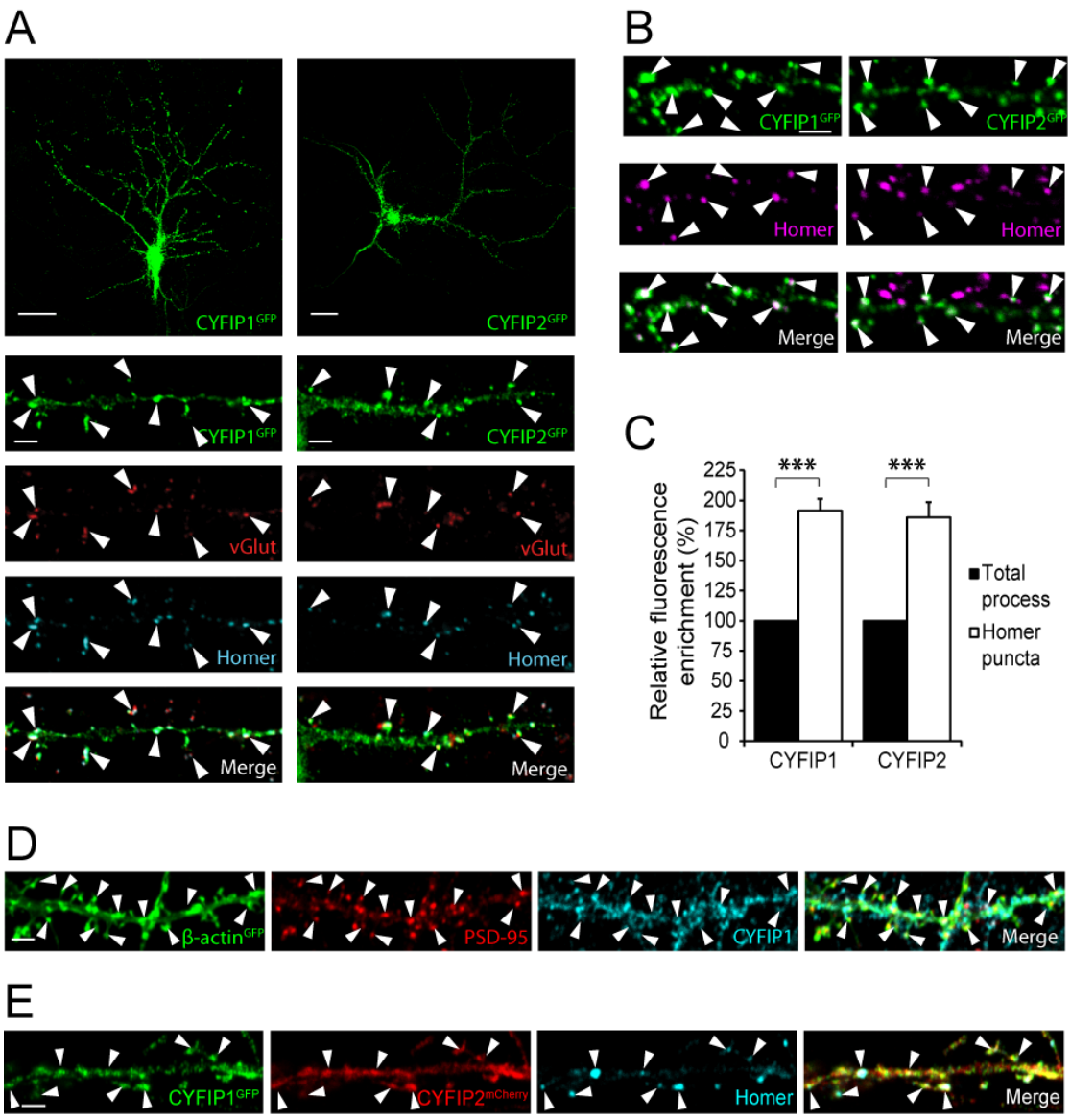

Figure 3.4: CYFIP1 and CYFIP2 are enriched at excitatory synapses.

CYFIP1^{GFP} and CYFIP2^{GFP} were transfected into mature rat hippocampal neurons and stained with antibodies against the pre and postsynaptic excitatory markers vGlut and homer respectively. CYFIP1^{GFP} and CYFIP2^{GFP} clusters colocalised with the excitatory synaptic markers (arrowheads). **(B,C)** Quantification of CYFIP1^{GFP} and CYFIP2^{GFP} fluorescence intensity at excitatory homer puncta shows there is an enrichment of CYFIP1^{GFP} and CYFIP2^{GFP} at excitatory synapses compared to the total process (CYFIP1 n=61, CYFIP2 n=54; Wilcoxon signed rank test; ***p<0.001). **(D)** Endogenous CYFIP1 co-localises with the excitatory postsynaptic marker PSD95 (arrowheads) in actin^{GFP} expressing cells. **(E)** CYFIP1^{GFP} and CYFIP2^{mCherry} colocalise along dendritic processes at excitatory synapses labeled by homer immunostaining. Scale bars, 20µm, 2µm.

shaft. They function to spatially compartmentalise the excitatory synapse and are critical for normal synaptic function (Bourne and Harris, 2008). Having determined that CYFIP1 and CYFIP2 are found at spines, experiments were conducted to further investigate their excitatory synaptic localisation using immunofluorescence and confocal microscopy. CYFIP1^{GFP} and CYFIP2^{GFP} were transfected into mature hippocampal neurons and expressed for 3 days. These neurons were then subjected to immunofluorescence labelling with antibodies against the vesicular glutamate transporter vGLUT and the PSD structural protein homer, used to label the excitatory pre and postsynapse respectively. Both CYFIP constructs colocalised with homer puncta at dendritic spines opposed to presynaptic vGLUT clusters (Figure 3.4A).

Quantification of CYFIP1^{GFP} and CYFIP2^{GFP} in dendrites revealed that the fluorescence intensity of both proteins was ~90% increased at synaptic homer puncta when normalised to the non-synaptic total dendritic process (Figure 3.4B,C) (homer puncta: CYFIP1, 191.44 ± 9.77%; CYFIP2, 185.88 ± 12.63%; ***$p<0.001$). Moreover, immunostaining with a CYFIP1 specific antibody demonstrated endogenous CYFIP1 was also highly enriched at excitatory synapses and colocalised with the postsynaptic marker PSD95. Dendritic and spine morphology were labelled with actin^{GFP} (Figure 3.4D). Finally, to address whether CYFIP1 and CYFIP2 were present together at the same locations within dendrites coexpression experiments were performed with CYFIP1^{GFP} and CYFIP2^{mCherry}. The majority of CYFIP1^{GFP} colocalised with CYFIP2^{mCherry} and overlapping puncta were found both in dendritic processes and spines colocalised with the excitatory postsynaptic marker homer (Figure 3.4E). Thus, endogenous CYFIP1, along with CYFIP1^{GFP} and CYFIP2^{GFP} are enriched at excitatory synapses and exhibit high levels of expression at sites of F-actin accumulation, like dendritic spines.

3.2.2 Modelling the effects of CYFIP1 and CYFIP2 genetic duplication on neuronal morphology

CNV at the CYFIP1-encoding 15q11.2 region of the human genome is associated with increased susceptibility to neuropsychiatric diseases. In particular, microduplications within this region, which increase the expression levels of CYFIP1, have been specifically linked to ASD and SCZ (Tam et al., 2010; van der Zwaag et al., 2010). One cellular mechanism thought to contribute to the pathogenesis of these

neuropsychiatric disorders is connectivity defects between brain regions. Impaired long-range circuits and excessive local connections particularly within the cortex are thought to be important contributing factors to ASD, while loss of cortical mass and connectivity is more prevalent SCZ (Belmonte et al., 2004; Harvey et al., 1993; Karlsgodt et al., 2008). Indeed, advancements in neuronal imaging has provided increasing experimental evidence in support of this hypothesis (Minshew and Keller, 2010; Ruiz et al., 2013). These observations therefore, imply that increased CYFIP1 expression may impact on CNS connectivity and function.

To investigate whether CYFIP1 and CYFIP2 regulate neuronal morphology and connectivity, changes in dendritic complexity were analysed in rat hippocampal neurons overexpressing $CYFIP1^{GFP}$ or $CYFIP2^{GFP}$ to model microduplication of the genes. Cells were transfected at DIV 10 and transgene expression was allowed for 3-4 days before cells were fixed for imaging (Figure 3.5A). Neurons were co-transfected with DsRed to label morphology. A method known as Sholl analysis was applied to quantify dendritic complexity. This method first described in the 1950s requires the dendritic arbour of the imaged neuron to be traced. Concentric rings are then plotted equal distance apart, beginning at the cell soma and expanding out until all the dendrites have been encircled (Sholl, 1953). The dendritic length, number of times a dendrite intersects a ring and the number of branch points can then be quantified between each ring as indicators of morphological complexity. These values are then either plotted as a function of distance from the soma to give a visual representation of where the neuron is most complex or can be summed to present the total dendritic length, intersections and branch points per cells.

Overexpression of CYFIP1 or CYFIP2 resulted in a significant increase in both the number of intersections and the number of branch points as a function of distance from the soma compared to control neurons expressing GFP alone (*$p<0.05$, **$p<0.01$, ***$p<0.001$) (Figure 3.5B,C). In addition, total dendritic length and the total number of branch points per cell were also increased in cells overexpressing CYFIP1 or CYFIP2 (Figure 3.5D,E) (dendritic length: GFP, 2098.88 ± 162.99µm; CYFIP1, 2875.85 ± 174.46µm; CYFIP2, 2787.38 ± 151.80µm, *$p<0.05$, **$p<0.01$; branch points: GFP 44.85 ± 4.71; CYFIP1, 66.54 ± 6.98; CYFIP2, 90.08 ± 5.59; *$p<0.05$, ***$p<0.001$).

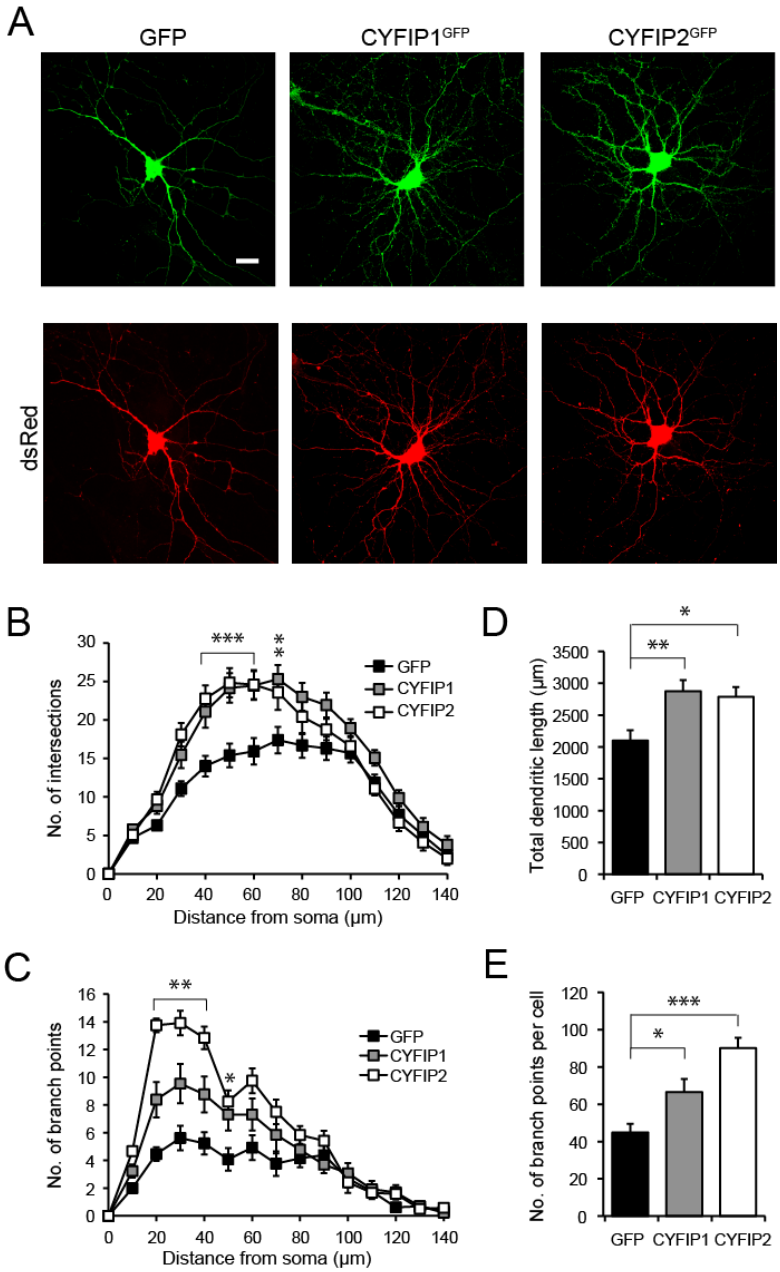

Figure 3.5: Overexpression of CYFIP1 and CYFIP2 promote increased dendritic complexity.

(A) Overexpression of CYFIP1^{GFP} or CYFIP2^{GFP} for 4 days results in increased dendritic complexity compared to expression of control GFP in 14DIV rat hippocampal neurons cotransfected with DsRed. Scale bar, 20μm. Quantification by Sholl analysis shows that number of intersections **(B)** and number of branch points **(C)** are significantly increased with distance from the soma in CYFIP1^{GFP} or CYFIP2^{GFP} overexpressing neurons compared to GFP control (data points represent an average of 12-13 cells; stars represent points where both CYFIP1 and CYFIP2 are significantly different from control; 2-way ANOVA; *p<0.05; **p<0.01, ***p<0.001). Expression of CYFIP1^{GFP} or CYFIP2^{GFP} increases total dendritic length **(D)** and number of branch points per cell **(E)** (n=12-13; ANOVA; *p<0.05, **p<0.01, ***p<0.001).

Many neuropsychiatric disorders have been coined spineothapies as often these disorders present with defects in dendritic spine structure and function as observed in post-mortem studies and animal models (Fiala et al., 2002; Hutsler and Zhang, 2010; Penzes et al., 2011; Purpura, 1974). Furthermore, dendritic spines are actin-rich synaptic compartments that undergo many structural changes during neuronal transmission and synaptic plasticity. Therefore, it seemed appropriate to investigate the effects of CYFIP1 and CYFIP2 on spine morphology due to the key role these proteins play in actin regulation and their association with neuropsychiatric disorders.

To study the impact of CYFIP1 and CYFIP2 overexpression on dendritic spine morphology mature neurons were transfected with either CYFIP1^{mCherry} or CYFIP2^{mCherry} and actin^{GFP} to label spine structure (Figure 3.6A). Neurons were fixed and high-resolution confocal stacks were taken of cotransfected cells. Images were analysed using Imaris software (Bitplane AG). Lengths of dendrite and spines were traced and accurate 3D reconstructions of the traced neuronal fragments were generated. From this reconstruction, spines were then classified into subtypes based on their length, width and volume. The four subtypes were the common spine classifications: stubby, mushroom, long thin and filipodia. The former two classes are considered more mature and the latter two more immature spine morphologies. There was no overall difference in spine density upon overexpression of either CYFIP1^{mCherry} or CYFIP2^{mCherry} compared to control neurons expressing DsRed (Figure 3.6B) (spine density (spines/μm): DsRed, 0.60 ± 0.02; CYFIP1, 0.65 ± 0.02; CYFIP2, 0.63 ± 0.02; NS). However, when spines were classified into subtypes, neurons overexpressing CYFIP1^{mCherry} or CYFIP2^{mCherry} showed altered spine subtype distribution (Figure 3.6C). Overexpression of both CYFIP proteins resulted in significantly more long, thin spines and a trend towards more filipodia. CYFIP2 overexpression also resulted in a decrease in stubby spines while increased CYFIP1 levels produced a slight but significant increase in mushroom spines (Spines/μm, stubby: DsRed, 0.23 ± 0.01; CYFIP1, 0.21 ± 0.01; CYFIP2, 0.20 ± 0.01; *$p<0.05$; mushroom: DsRed, 0.25 ± 0.01; CYFIP1, 0.28 ± 0.01; CYFIP2, 0.27 ± 0.01; *$p<0.05$; long,thin: DsRed, 0.12 ± 0.01; CYFIP1, 0.15 ± 0.01; CYFIP2, 0.16 ± 0.01; *$p<0.05$, **$p<0.01$; filopodia: DsRed, 0.002 ± 0.001; CYFIP1, 0.007 ± 0.002; CYFIP2, 0.006 ± 0.001). Additionally, the cumulative frequency curve of spine length was shifted to the right for cells overexpressing CYFIP1^{mCherry} or CYFIP2^{mCherry} compared to control,

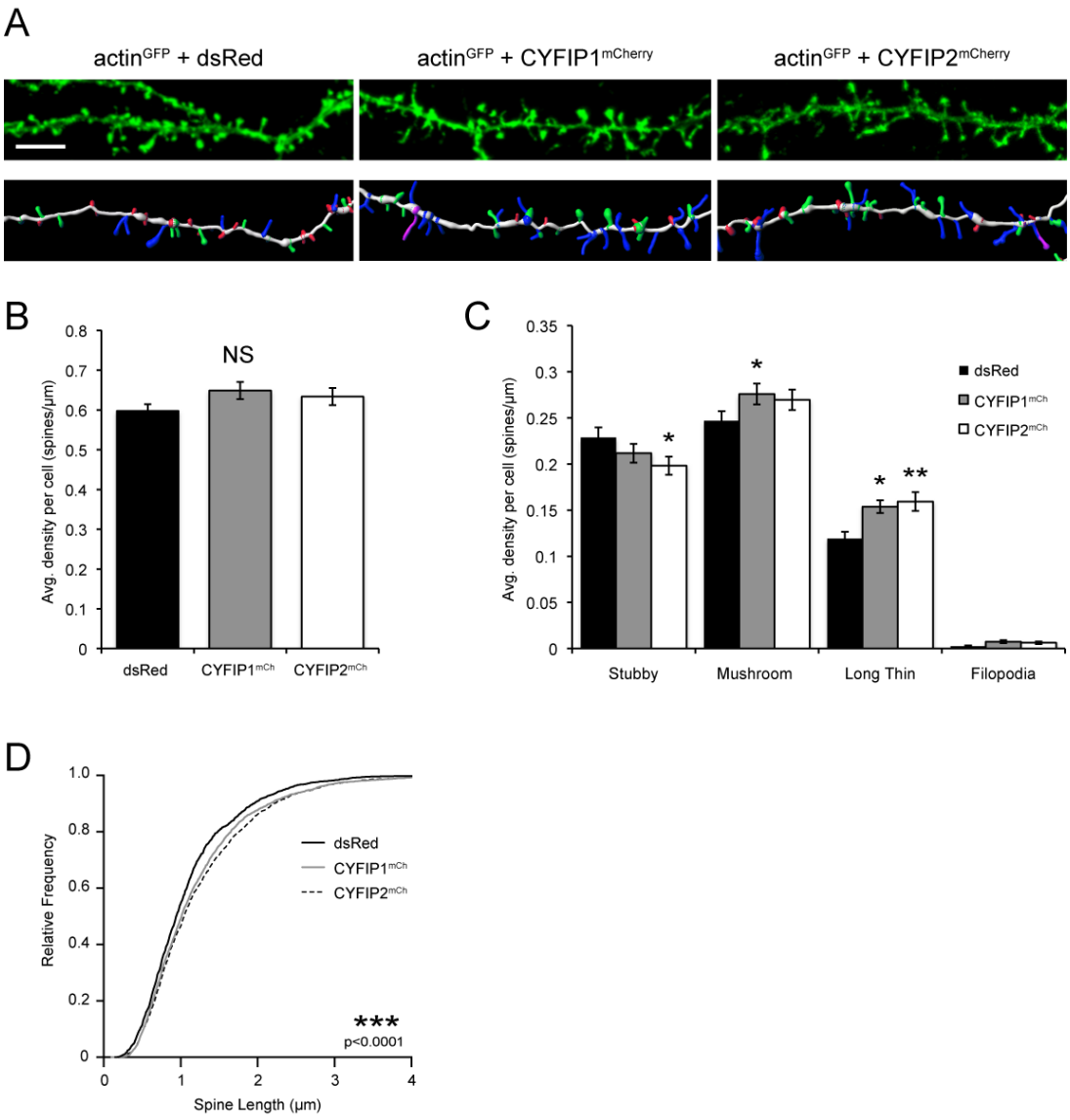

Figure 3.6: Overexpression of CYFIP1 and CYFIP2 alter dendritic spine structure.

Spine morphology was analysed at 21DIV in CYFIP1^{mCherry} or CYFIP2^{mCherry}+actin^{GFP} expressing rat hippocampal neurons and compared to DsRed+actin^{GFP} expressing cells **(A)** (upper panel: representative image; lower panel: 3D reconstruction). Scale bar, 5µm. Colour key for spine type in 3D reconstruction: green = mushroom, red = stubby, blue = long thin, pink = filipodia. **(B)** Quantification of total spine density in DsRed control, CYFIP1^{mCherry} or CYFIP2^{mCherry} over expressing cells (n=49-66 filaments per condition; ANOVA; NS). **(C)** Quantification of spine subtype density. CYFIP1^{mCherry} and CYFIP2^{mCherry} overexpression resulted in increased long, thin spines and filopodia (n=49-66 filaments per condition; 2-way ANOVA; *p<0.05, **p<0.01). **(D)** Cumulative frequency curve of spine length. CYFIP1 and CYFIP2 overexpressing neurons have significantly more, longer spines compared to control neurons (n=1500-1900 spines per condition; Krustal Wallis test; ***p<0.001).

indicating an overall significant shift towards longer more immature spines when CYFIP proteins were overexpressed (***p<0.001) (Figure 3.6D). These experiments demonstrate that modelling microduplication of CYFIP1 or CYFIP2 effects dendritic and spine morphology. This suggests CYFIP1 and CYFIP2 are important regulators of neuronal complexity and spine remodelling, mechanisms thought to be important in the pathogenesis of neuropsychiatric disorders such as ASD and SCZ.

3.2.3 CYFIP1 haploinsufficiency provides a model for studying 15q11.2 microdeletion

The previous experiments have studied the effect of CYFIP overexpression on neuronal morphology and synaptic maintenance to model a form of CNV that enhances the expression of a gene, microduplication. However, genetic variation can also result in the loss of genetic material, known as microdeletion, leading to a decrease in the copy number and expression of a gene. Microdeletion in the 15q11.2 region of the genome, where CYFIP1 is expressed, is associated with intellectual disability, epilepsy as well as ASD and SCZ (Doornbos et al., 2009; Kirov et al., 2012; Stefansson et al., 2008; Zhao et al., 2013b). Therefore, in addition to investigating the neuronal effects of CYFIP1 overexpression, a CYFIP1 knockout (KO) mouse system was characterised. This model was used to explore the effect of reduced CYFIP1 expression on neuronal architecture, actin dynamics, synaptic content and morphology.

The CYFIP1 KO mouse was generated by the Wellcome Trust Sanger Insitute. Briefly, a reporter tagged insertion allele was constructed into a targeting vector containing a drug resistance selection marker and homologous regions specific to *Cyfip1* between exons 3 and 4. The insertion allele uses the KO first technique disrupting the transcription of *Cyfip1* with the inclusion of a LacZ cassette resulting in a non-functional truncated *Cyfip1* mRNA product and the expression of the reporter enzyme β-galactosidase (Skarnes et al., 2011; White et al., 2013). The LacZ cassette is flanked by FRT sites to allow for the removal of the cassette in the presence of Flip recombinase and rescue of the wild-type (WT) gene. The remaining LoxP sites flanking exons 4-6 can then be used to conditionally KO *Cyfip1* in a cre recombinase dependent manner (Figure 3.7A). The vector was electroporated into mouse embryonic stem (ES) cells and cells that had undergone correct recombination were

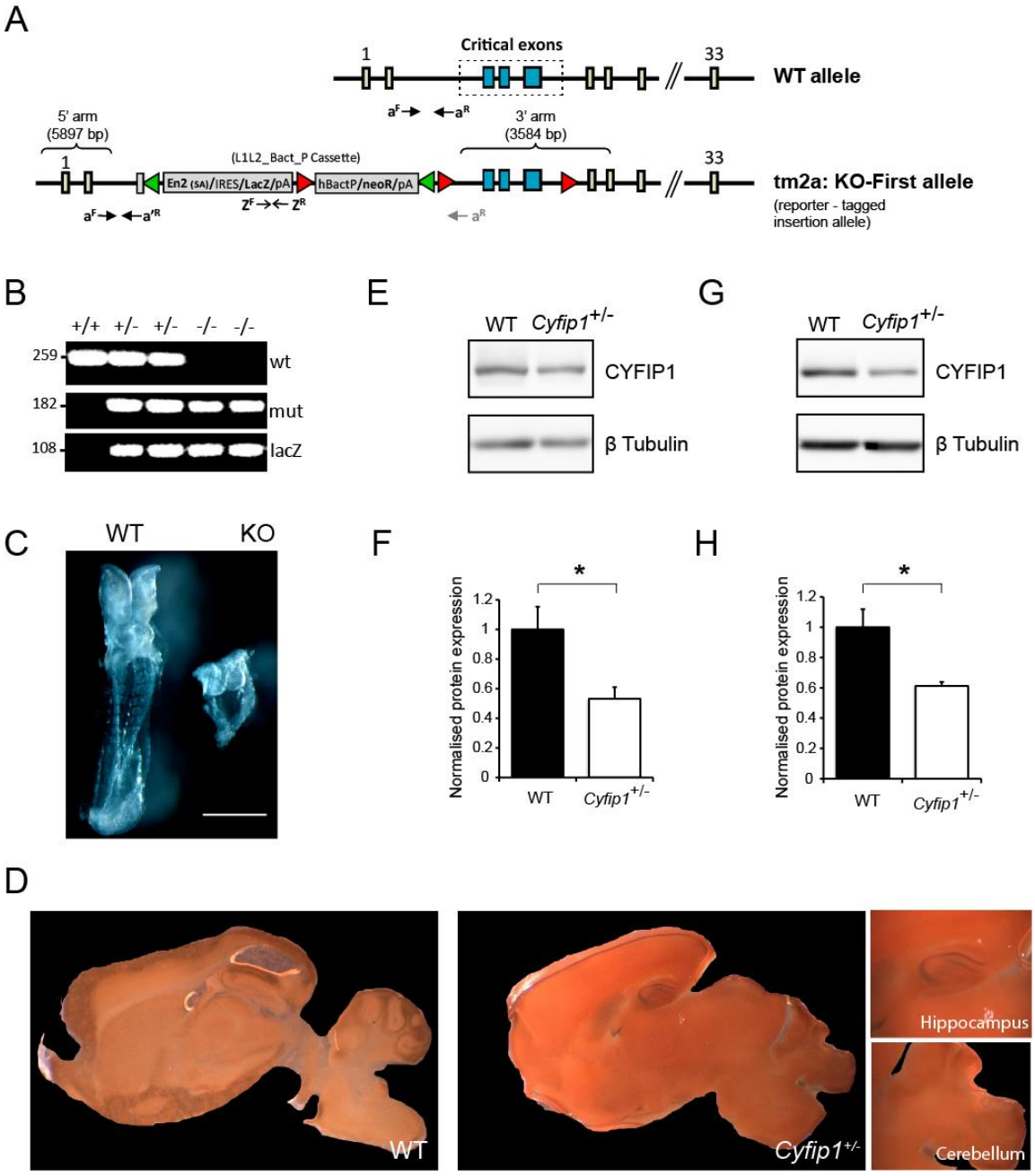

Figure 3.7: Generation of *Cyfip1* knockout and *Cyfip1* haploinsufficient mice.

(A) Design of the knockout (KO)-first allele system showing the wild-type (WT) allele; the KO-first *Cyfip1* allele (tm2a allele) containing an IRES:*lacZ* trapping cassette and a floxed promoter-driven *neo* cassette inserted between exons 3 and 4 of *Cyfip1*, disrupting gene function. Both cassettes are bound by frt sites (green triangles). The neo cassette and 3' frt site are flanked by loxP sites with an additional distal loxP site present 3' of exon 6 (red triangles). *Cyfip1* KO animals had two KO-first alleles while haploinsufficient animals were heterozygous for the KO-first allele (Skarnes et al., 2011; White et al., 2013). **(B)** PCR analysis of F1 progeny from parental mice heterozygous for the KO-first allele. Animals were

genotyped with the primers a^F and a^R to produce a PCR product of 259 base pairs (bp) from the WT allele, these primers were too distant from each other to produce a product from the KO-first allele. Primers a^F and a'^R produced a 182 bp product from the KO-first allele with a'^R annealing at the very 5' region of the *lacZ* cassette. Primers Z^F and Z^R produced a 108 bp product from the KO-first allele within the introduced *lacZ* gene. Lane 1 is a WT mouse (+/+) positive for just the WT product, lanes 2 and 3 are heterozygous animals (+/-) positive for both the WT allele and the KO-first allele PCR products, lanes 4 and 5 are KO animals with no WT PCR product present (-/-). **(C)** Representative images of *Cyfip1* WT and KO embryos at E8.5 highlighting the developmental defects seen in KO animals. Scale bar, 0.5mm. *Dissection and image acquired by Guillermo López-Doménech.* **(D)** Adult WT and *Cyfip1*$^{+/-}$ sagittal brain sections subjected to X-gal staining. Western blot analysis and quantification displaying fold change of CYFIP1 protein levels from control (WT) and *Cyfip1*$^{+/-}$ P55 hippocampal brain lysates **(E,F)** or DIV16 cultured cortical lysates **(G,H)**. Both hippocampal brain lysates and cortical neurons from *Cyfip1*$^{+/-}$ animals had ~40% less CYFIP1 protein compared to WT controls (n=3-4; student's t-test; *p<0.05).

selected for and expanded. ES cells were injected into an early mouse embryo and implanted into a pseudopregnant mouse. The result of this pregnancy was chimeric mice, which were then crossed with WT mice to obtain mice that were exclusively derived from the modified ES cells. These mice were heterozygous for the *Cyfip1* KO first allele and could then be crossed with each other to generate homozygous mutant mice.

To study the *Cyfip1* KO mouse, heterozygous animals for the KO first allele were crossed and the progeny genotyped (Figure 3.7B). CYFIP1 KO mice (*Cyfip1*$^{-/-}$) were found to be embryonically lethal, as they were never detected at birth. Following this observation, pregnancy was disrupted at earlier time points to determine when during development *Cyfip1*$^{-/-}$ embryos were dying. The latest a KO embryo could be detected and confirmed by genotyping was embryonic day (E) 8.5 post-coitum. However, it was evident even at this early embryonic stage that the KO embryo was reduced in size and seriously developmentally delayed, being about a quarter of the length of a WT littermate control (Figure 3.7C). *Cyfip1* heterozygous animals (*Cyfip1*$^{+/-}$) on the other hand, were viable until adulthood and fertile. These observations suggest that adequate levels of CYFIP1 are critical for proper development through early stages of embryogenesis.

Genetic microdeletions often occur on just one allele and the other remains intact and fully functioning resulting in reduced gene expression rather than total loss of expression. *Cyfip1* haploinsufficient mice therefore, provide the ideal model to study the effects of decreased *Cyfip1* gene dosage. To indicate which brain regions displayed reduced *Cyfip1* expression the β-galactosidase reporter gene was used. This reporter also demonstrates the expression pattern of *Cyfip1* in the brain. Adult brains were sagittally sliced into 300μm sections, fixed and incubated with X-Gal staining solution, which is catalysed into a blue product by β-galactosidase (Figure 3.7D).

Blue product was observed in the dense cell layers of the hippocampus and the cerebellum and could also be detected using a microscope more diffusely in the cortex of the *Cyfip1*$^{+/-}$ brain slice. The WT control showed no blue staining as expected. Under the conditions used here this assay was not particularly sensitive and the blue signal appeared weak. However, the blue product from the X-Gal reaction was still detectable, demonstrating β-galactosidase was being expressed in the hippocampus,

cortex and cerebellum of *Cyfip1*$^{+/-}$ brains. This highlights the expression pattern of *Cyfip1* and that genetic disruption of the allele has occurred in these brain regions. To confirm the genetic loss of *Cyfip1* expression resulted in a reduction of CYFIP1 protein, adult hippocampal brain lysate or cultured cortical cells were analysed by western blotting for CYFIP1 protein levels. Samples from *Cyfip1*$^{+/-}$ animals showed a ~40% reduction in CYFIP1 compared to control samples (Figure 3.7E-H) (brain lysate: WT control, 100 ± 15.4%; *Cyfip1*$^{+/-}$, 53.2 ± 7.8%; cortical neurons: WT control 100 ± 11.8%; *Cyfip1*$^{+/-}$, 61.1 ± 2.6%; *p<0.05). Taken together these data confirm that CYFIP1 is expressed in both the hippocampus and the cortex and that in *Cyfip1* haploinsufficient animals this expression is reduced by ~40%. Therefore, the *Cyfip1*$^{+/-}$ animals provide an ideal model for studying the effect of reduced CYFIP1 expression on neuronal function and morphology.

3.2.4 The impact of CYFIP1 haploinsufficiency on neuronal morphology and dendritic spines

Microdeletion at the 15q11.2 region of the human genome, resulting in CYFIP1 haploinsufficiency, has been associated with neuropsychiatric disorders (Table 3.1). Therefore, investigating the morphological effects of reduced CYFIP1 expression may provide insights into how microdeletion at the 15q11.2 region results in disease. With this in mind the effects of CYFIP1 haploinsufficiency on dendritic complexity and spine morphology were analysed (*the work contributing to Figure 3.8 was carried out by Dr. Manav Pathania*). Cultured hippocampal neurons from *Cyfip1*$^{+/-}$ and WT control animals were transfected with actin^{GFP} to label cell morphology, fixed at DIV14 and imaged (Figure 3.8A,B). As described previously, imaged neurons were traced and subjected to Sholl analysis. *Cyfip1*$^{+/-}$ neurons showed a decrease in dendritic complexity, measured by plotting the number of intersections as a function of distance from the soma, compared to WT control neurons (Figure 3.8C) (**p<0.01, ***p<0.001). In agreement with this, the total dendritic length and total number of branch points were also significantly decreased in the *Cyfip1*$^{+/-}$ neurons compared to control (Figure 3.8D,E) (dendritic length: WT, 2704 ± 96.8μm; *Cyfip1*$^{+/-}$, 2298 ± 80.2μm; branchpoints: WT, 76.7 ± 4.1; *Cyfip1*$^{+/-}$, 61.4 ± 3.6; **p<0.01). Interestingly, these results illustrate the opposite effect to the enhanced dendritic complexity observed in CYFIP1 overexpressing cells.

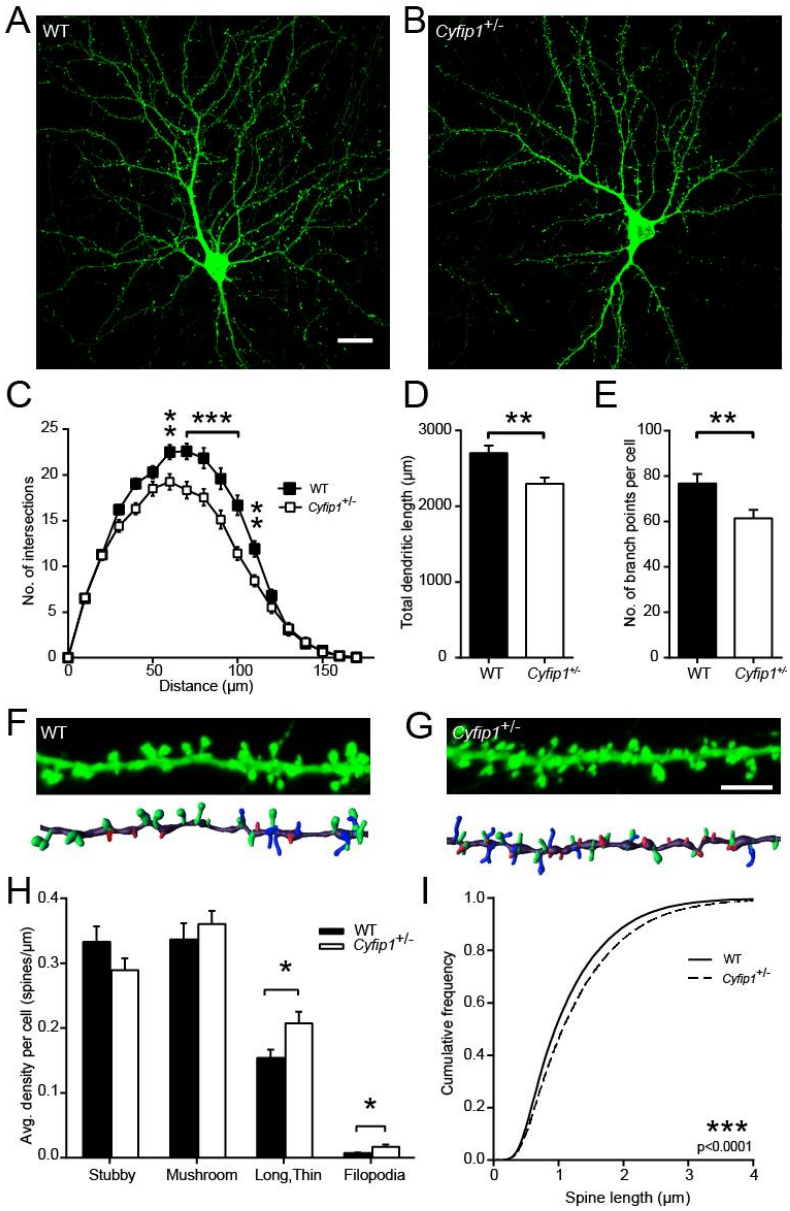

Figure 3.8: *Cyfip1*$^{+/-}$ effects neuronal morphology and dendritic spines.

Cyfip1$^{+/-}$ hippocampal neurons had reduced dendritic complexity compared to WT controls at 14DIV **(A,B)**. Scale bar, 20 µm. Dendritic morphology was examined using Sholl analysis. *Cyfip1*$^{+/-}$ neurons show significantly less complex morphology when compared to WT neurons (n=18; 2-way ANOVA; **p<0.01, ***p<0.001) **(C).** Total dendritic length **(D)** and total number of branch points **(E)** were also reduced in *Cyfip1*$^{+/-}$ neurons compared to WT (n=18, student's t-test; **p<0.01). Spine morphology was analysed at 21DIV in *Cyfip1*$^{+/-}$ neurons and compared to WT cells **(F,G)** (upper panel: representative image; lower panel: 3D reconstruction). Scale bar, 5µm. Colour key for spine type in 3D reconstruction: green = mushroom, red = stubby, blue = long thin, pink = filipodia. **(H)** Quantification of spine subtype density. *Cyfip1*$^{+/-}$ neurons possessed increased long, thin spines and filopodia (n=27-31; student's t-test; *p<0.05). **(I)** Cumulative frequency curve of spine length (n=approx. 39000 spines per condition, Mann-Whitney test, ***p<0.001). *Experiments performed and analysed by Dr. Manav Pathania.*

Dendritic spine morphology analysis revealed that although there was no difference in the spine density of *Cyfip1*$^{+/-}$ neurons there was a change in spine morphology compared to WT control neurons. As previously described, when spines were classified into subtypes based on structural measurements *Cyfip1*$^{+/-}$ neurons showed more long, thin spines and filopodia compared to control neurons (Figure 3.8H) (Spines/μm, long,thin: WT: 0.15 ± 0.01, *Cyfip1*$^{+/-}$: 0.20 ± 0.01; filopodia: WT, 0.007 ± 0.001, *Cyfip1*$^{+/-}$, 0.016 ± 0.003; *p<0.05). Moreover, the cumulative frequency curve for spine length was shifted to the right for *Cyfip1*$^{+/-}$ neurons indicating a significant shift towards more long immature spines compared to control (Figure 3.8I) (***p<0.001).

3.2.5 CYFIP1 haploinsufficiency dysregulates spine actin dynamics

Actin rich dendritic spines undergo many structural changes in response to neuronal transmission; these structural changes are brought about by tightly controlled local modifications to the actin cytoskeleton (Hotulainen and Hoogenraad, 2010; Kasai et al., 2010). As both an increase and a decrease of CYFIP1 levels result in a change in spine morphology and CYFIP1 is a critical actin regulator, coupling Rac1 signalling to WRC regulation (Chen et al., 2010b), it was of interest to investigate whether altered CYFIP1 expression levels impacted on actin dynamics at dendritic spines. This may help explain the spine morphological phenotypes observed when CYFIP1 expression is manipulated.

To study the impact of altered CYFIP1 expression on actin dynamics live fluorescence recovery after photobleaching (FRAP) was carried out on the spines of mature *Cyfip1*$^{+/-}$ hippocampal neurons transfected with actin^{GFP} (Figure 3.9A,B). Analysing the recorded movies revealed a significant difference in the fluorescence recovery of *Cyfip1*$^{+/-}$ neurons compared to WT controls (Figure 3.9C; *p<0.05, **p<0.01). Moreover, the fluorescence recovery of *Cyfip1*$^{+/-}$ neurons plateaued at a greater intensity than WT neurons, which was confirmed by a significant increase in the total mobile fraction (Figure 3.9D) (*i.e.* the amount of final recovered fluorescence as a proportion of the total bleached fluorescence; WT, 68.54 ± 5.51%; *Cyfip1*$^{+/-}$, 86.45 ± 4.20%; *p<0.05). However, there was no change in the recovery rate constant, time constant or half-life between *Cyfip1*$^{+/-}$ and WT neurons (Figure 3.9E-G).

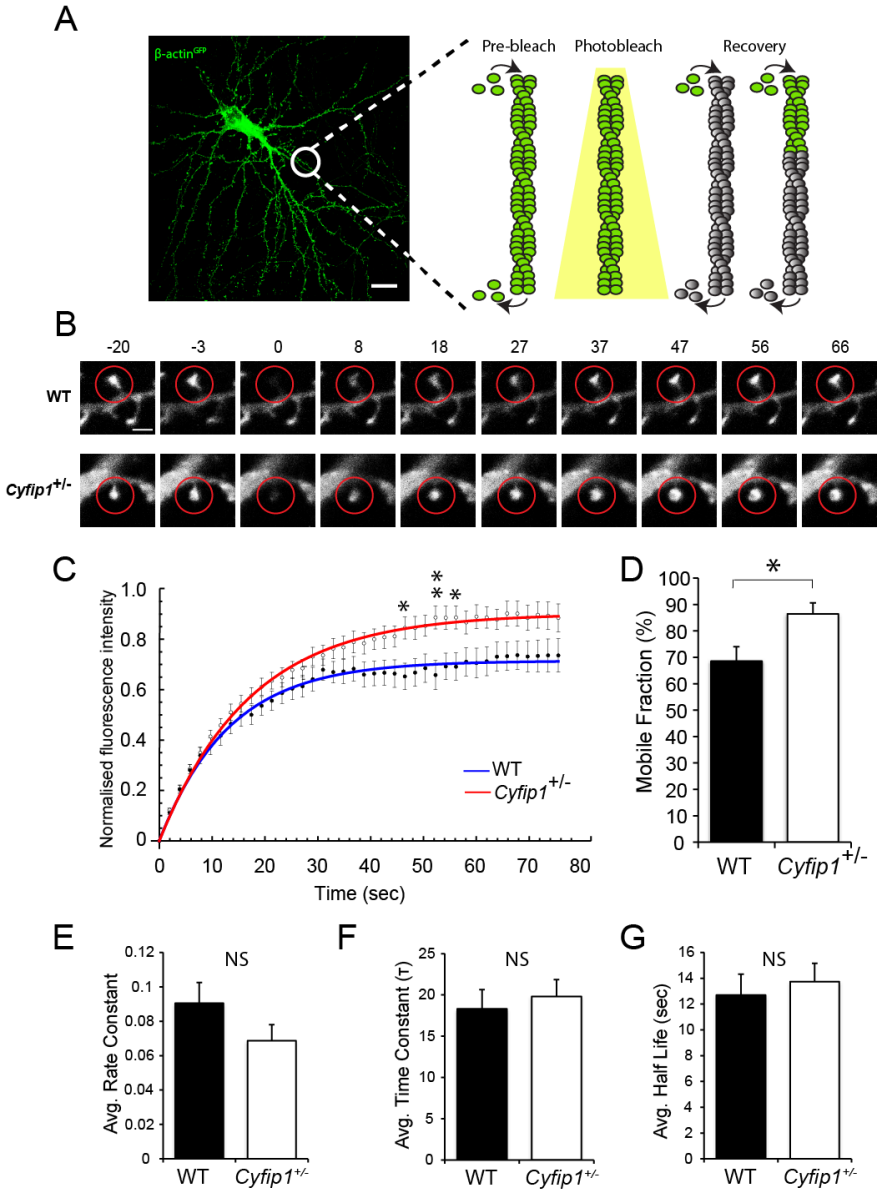

Figure 3.9: *Cyfip1* deficiency dysregulates spine actin^{GFP} dynamics.

Cyfip1$^{+/-}$ and WT hippocampal neurons were transfected with actin^{GFP} at 17-20DIV and subjected to FRAP live-imaging 2 days later. Spines were imaged for 100 seconds and bleaching occurred after the first 20 seconds. **(A)** A schematic of the actin bleaching and fluorescence recovery. Scale bar, 20µm. **(B)** Representative images over time of actin^{GFP} fluorescence recovery in WT and *Cyfip1*$^{+/-}$ spines (sec). The red circles highlight the bleached spine. Scale bar, 2µm. **(C)** Quantification of fluorescence intensity within the spine head region of WT or *Cyfip1*$^{+/-}$ neurons transfected with actin^{GFP} (n=29-33; 2-way ANOVA; *p<0.05, **p<0.01). Data are fitted with single exponentials (coloured lines). **(D)** Mobile fraction is significantly increased in *Cyfip1*$^{+/-}$ neurons expressing actin^{GFP} (n=29-33; student's t-test; *p<0.05). **(E)** The rate constant, **(F)** time constant and **(G)** recovery half life generated from fitting a single exponential curve to each data set, revealed no significant difference between WT and *Cyfip1*$^{+/-}$ neurons (n=25-33; Mann-Whitney test; NS).

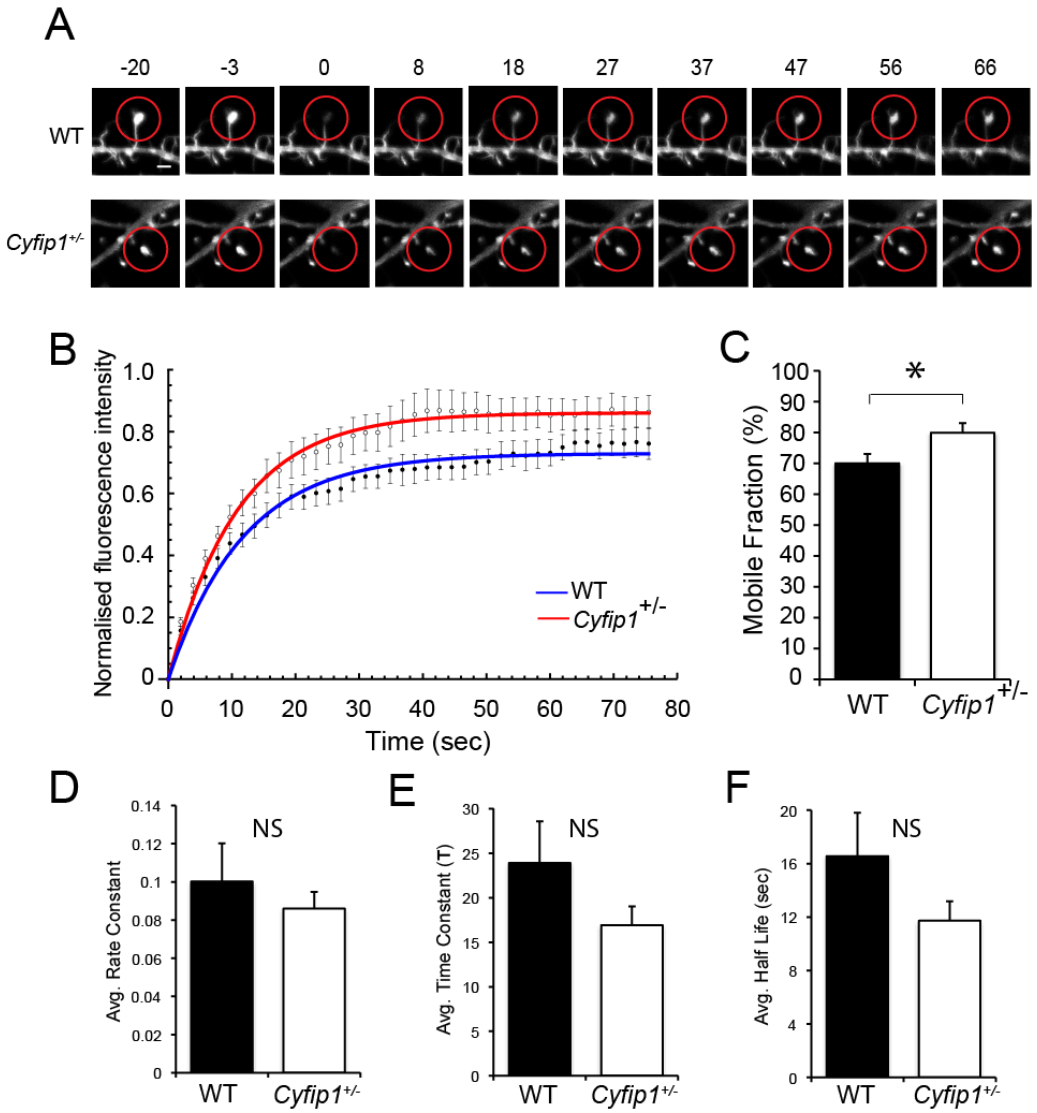

Figure 3.10: *Cyfip1* deficiency dysregulates spine Lifeact dynamics.

Cyfip1$^{+/-}$ and WT hippocampal neurons were transfected with Lifeact^{GFP} at 17-20DIV and subjected to FRAP live-imaging 2 days later. Spines were imaged for 100 seconds and bleaching occurred after the first 20 seconds. **(A)** Representative images over time of Lifeact^{GFP} fluorescence recovery in WT and *Cyfip1*$^{+/-}$ spines (sec). The red circles highlight the bleached spine. Scale bar, 2µm. **(B)** Quantification of fluorescence intensity within the spine head region of WT or *Cyfip1*$^{+/-}$ neurons transfected with Lifeact^{GFP} (n=24-29; 2-way ANOVA; NS). Data are fitted with single exponentials (coloured lines). **(C)** Mobile fraction is significantly increased in *Cyfip1*$^{+/-}$ neurons expressing Lifeact^{GFP} (n=24-29; student's t-test; *p<0.05). **(D)** The rate constant, **(E)** time constant and **(F)** recovery half-life generated from fitting a single exponential curve to each data set, revealed no significant difference between the WT and *Cyfip1*$^{+/-}$ neurons (n=24-29; Mann-Whitney test; NS).

To further demonstrate that altered CYFIP1 expression affects actin dynamics within dendritic spines, the FRAP experiments were repeated using Lifeact^{GFP}, an F-actin specific fluorescent probe suitable for FRAP experiments (Rocca et al., 2013), and similar results were obtained. Again, a difference in the fluorescence recovery was observed between WT and *Cyfip1*$^{+/-}$ neurons resulting in a significant increase in the total mobile fraction (Figure 3.10A-C; WT, 70.01 ± 3.03%, *Cyfip1*$^{+/-}$, 79.91 ± 3.12%; *p< 0.05). There was no change in the recovery rate constant, time constant or half-life between *Cyfip1*$^{+/-}$ and WT neurons (Figure 3.10D-F). Taken together, the increased fluorescence recovery of actin^{GFP} and Lifeact^{GFP} suggests altered actin dynamics in the dendritic spines of CYFIP1 haploinsufficient neurons compared to control neurons.

3.2.6 The effect of reduced CYFIP1 expression *in vivo*

The CYFIP1 haploinsufficient mouse provides an *in vivo* model to study microdeletion of CYFIP1. Having determined reduced CYFIP1 levels effect dendritic spines and neuronal morphology *in vitro*, it seemed appropriate to determine whether loss of CYFIP1 altered the excitatory synaptic content of dendritic spines or gross brain morphology *in vivo*. To address the effect of reduced CYFIP1 expression on the excitatory synaptic content of dendritic spines, brain regions lysates were generated from the hippocampus and cortex of *Cyfip1*$^{+/-}$ and WT brains aged P16 (juvenile) or P55 (adult). These samples were then analysed by western blotting and protein levels of excitatory structural molecules and CYFIP1 interactors were analysed (Figure 3.11).

To confirm the specificity of the haploinsufficient model the lysates were probed for CYFIP1. In the adult cortex and hippocampus a ~40% reduction in CYFIP1 protein was observed in *Cyfip1*$^{+/-}$ animals compared to WT (Figure 3.11D; hippocampus: WT, 100 ± 10.66%; *Cyfip1*$^{+/-}$, 57.27 ± 8.45%; *p<0.05; cortex: WT, 100 ± 21.37%; *Cyfip1*$^{+/-}$, 59.55 ± 6.44%; p=0.09). Unusually, the *Cyfip1*$^{+/-}$ P16 cortex showed little reduction in CYFIP1, most likely due to sample variability however, the *Cyfip1*$^{+/-}$ P16 hippocampus showed as expected a ~40% reduction in CYFIP1 although due to large error this was not significant (Figure 3.11C; cortex: WT, 100 ± 13.03%; *Cyfip1*$^{+/-}$, 86.41 ± 17.63%; NS; hippocampus: WT, 100 ± 25.21%; *Cyfip1*$^{+/-}$, 58.17 ± 8.81%; NS). The samples were analysed for the expression levels of PSD structural proteins Shank1-3, PSD95, chapsyn110 and homer. Only Shank family proteins showed a change in

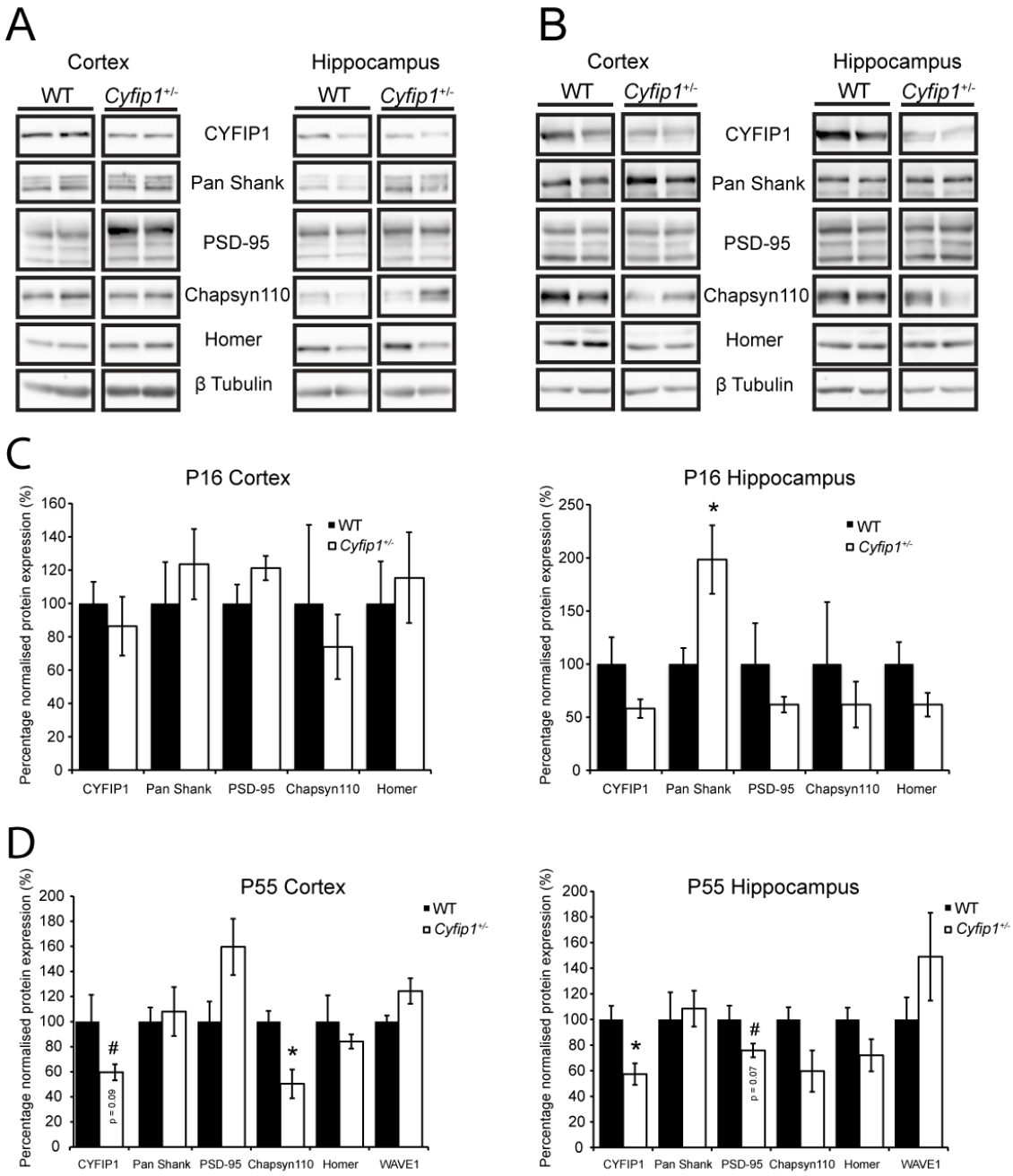

Figure 3.11: The impact of CYFIP1 haploinsufficiency on excitatory synaptic protein levels.

Brain lysates were prepared from the cortex and hippocampus of juvenile (P16) and adult (P55) *Cyfip1*$^{+/-}$ and wild-type (WT) mice. **(A)** P16 and **(B)** P55 cortical (left) and hippocampal (right) samples were subjected to western blotting and probed for key synaptic proteins. Quantification of percentage protein expression from **(C)** P16 and **(D)** P55 *Cyfip1*$^{+/-}$ brain lysates normalised to WT control, cortical lysates (left) and hippocampal lysates (right) (n=3-5; student's t-test; *p<0.05; #close to significance).

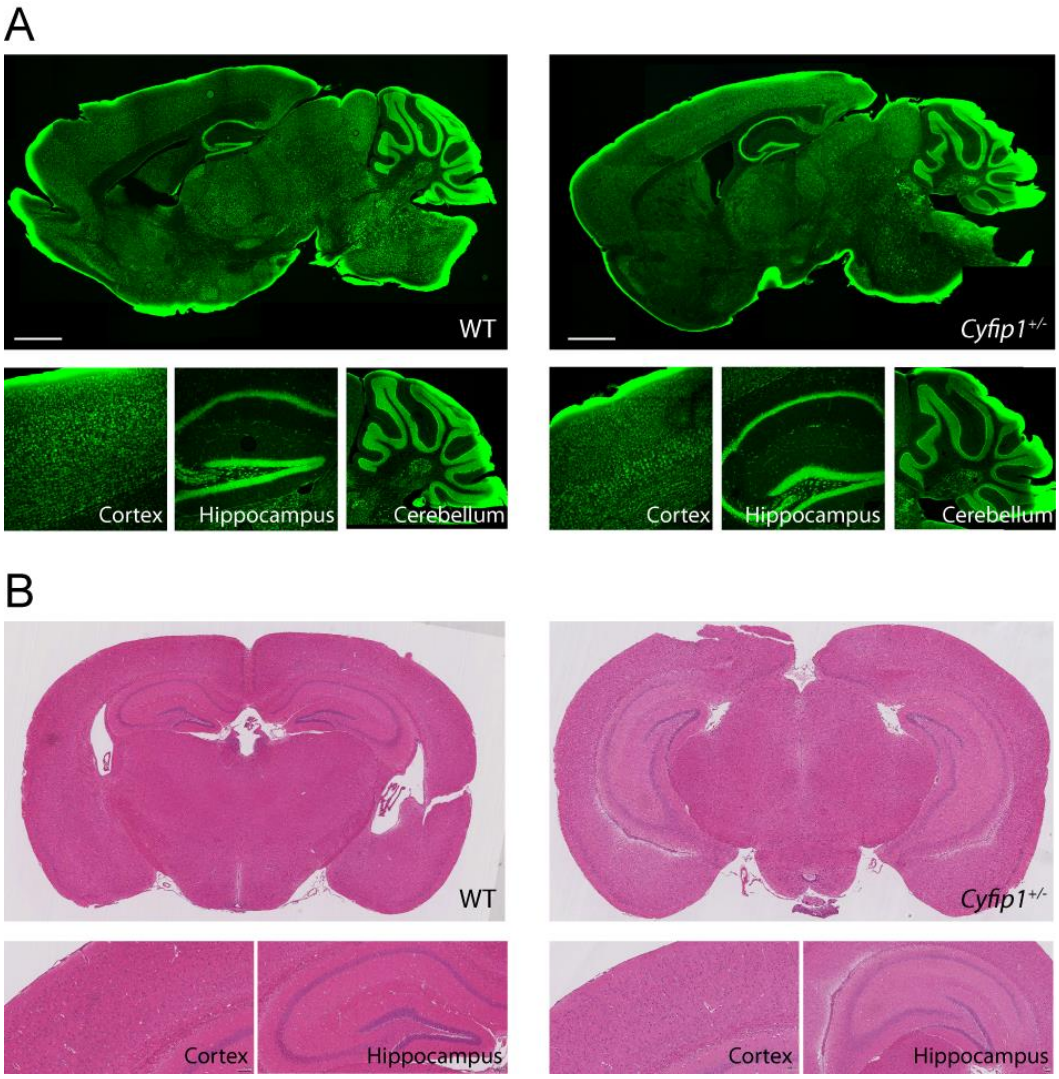

Figure 3.12: CYFIP1 haploinsufficiency results in no gross changes in brain morphology.

(A) Nissl staining of WT and *Cyfip1*$^{+/-}$ adult mouse sagittal brain sections shows no major change in gross brain morphology between the two genotypes. Scale bar, 1mm. **(B)** Hematoxylin and eosin staining of WT and *Cyfip1*$^{+/-}$ adult mouse coronal brain sections shows no major change in gross brain morphology between the two genotypes. Hematoxylin is a basic, positively charged dye that stains negatively charged structures, such as DNA, blue and therefore labels the cell nucleus. Eosin is an acidic, negatively charged dye which stains positively charged eosinophilic structures red. The cytoplasm, cell membranes and proteins are stained in this way. *Staining carried out by the UCL histology service, Institute of Neurology.*

expression level between *Cyfip1*$^{+/-}$ and WT animals in the juvenile brain samples, this two-fold increase was restricted to the hippocampus (Figure 3.11B) (hippocampus: WT, 100 ± 15.06%; *Cyfip1*$^{+/-}$, 198.32 ± 32.22%; *p<0.05). In the adult brain samples, cortical chapsyn110 was significantly reduced by 50% in *Cyfip1*$^{+/-}$ animals compared to WT, with a similar trend being observed in the hippocampus (cortex: WT, 100 ± 8.47%; *Cyfip1*$^{+/-}$, 50.31 ± 11.53%; *p<0.05; hippocampus: WT, 100 ± 9.48%; *Cyfip1*$^{+/-}$, 59.69 ± 16.11%; NS). PSD95 expression was almost significantly reduced in the adult hippocampus tissue, a trend that was also seen in the juvenile hippocampal tissue (Figure 3.11C,D; P55 hippocampus: WT, 100 ± 10.84%; *Cyfip1*$^{+/-}$, 75.80 ± 5.32%; p=0.07; P16 hippocampus: WT, 100 ± 38.52%; *Cyfip1*$^{+/-}$, 61.98 ± 7.30%; NS). It was interesting to note that in all the brain regions where CYFIP1 was clearly reduced homer also appeared to be slightly reduced however, this result was not significant (Figure 3.11C,D). Taken together, loss of CYFIP1 could be impacting on PSD protein levels as CYFIP1 haploinsufficiency results in disrupted levels of chapsyn110, Shank family proteins and PSD95 however, further experiments and repeats will be required to confirm this.

To determine whether gross brain morphology was disrupted in *Cyfip1*$^{+/-}$ animals preliminary experiments were carried out to simply compare visually whether there were any obvious alterations in brain anatomy between sagittal sections of CYFIP1 haploinsufficient brains compared to WT. Sections were stained with fluro-Nissl to label neuronal cell bodies and brain region architecture. In this experiment, only a limited number of sections were stained, small structures such as the olfactory bulb were missing and finding equivalent depth sections in the two samples was difficult. However, at first glance brains appeared to be of a similar size and no gross structural changes were observed between *Cyfip1*$^{+/-}$ and WT samples (Figure 3.12A). Coronal sections of CYFIP1 haploinsufficient and WT brains were also subjected to hematoxylin and eosin (H&E) staining to label cellular structures and brain anatomy. Due to the difference in anatomical sections presented it was difficult to compare the two samples although brain size appeared unchanged between *Cyfip1*$^{+/-}$ and WT animals (Figure 3.12B). This analysis would benefit from further quantification of individual brain regions. Taken together this data shows loss of CYFIP1 does not appear to alter gross brain morphology, however, it has been suggested to disrupt synaptic protein levels. Importantly, additional work carried out in the lab by Dr. Manav Pathania showed, by analysing fixed Golgi-stained slices, that CA1

hippocampal neurons displayed reduced dendritic complexity (Appendix A). It is potentially these more subtle changes in individual neuronal complexity within the hippocampus combined with changes in synaptic protein levels that may account for the effects on behaviour and neurotransmission observed in CYFIP1 haploinsufficient mice (Bozdagi et al., 2012).

3.2.7 CYFIP1 and CYFIP2 are enriched at inhibitory synapses

The role of actin at excitatory synapses has been extensively studied over recent years. The actin-rich dendritic spine is critical for remodelling the excitatory synapse during neuronal transmission and synaptic plasticity (Bourne and Harris, 2008; Hotulainen and Hoogenraad, 2010; Matsuzaki, 2007). Furthermore, there is increasing evidence to suggest that actin is required for tethering and stabilising synaptic receptors within nanostructures at the PSD (Allison et al., 1998; Blanpied et al., 2008; Burette et al., 2012; Frost et al., 2010a, 2010b). Finally, the role for actin in the rapid trafficking, endocytosis and insertion of receptors into the membrane at excitatory synapses has been well described (Bellot et al., 2014; Frost et al., 2010b; Hanley, 2014). However, how actin functions at the inhibitory synapse, an equally dynamic structure undergoing remodelling and receptor trafficking, is only just emerging (Smith et al., 2014). As CYFIP1 and CYFIP2 are critically involved in regulating actin polymerisation and due to the findings presented here suggesting their importance in the maintenance of excitatory synaptic structure and morphology it seemed important to explore the function of CYFIP proteins at the inhibitory synapse.

Initially, experiments were carried out to determine if CYFIP1 and CYFIP2 were localised at inhibitory synapses. Mature hippocampal neurons were transfected with $CYFIP1^{GFP}$ or $CYFIP2^{GFP}$, fixed and stained with antibodies against vGAT and gephyrin to label the inhibitory pre and postsynapse respectively. The vesicular GABA transporter (vGAT) is frequently used as a marker for the inhibitory presynapse while the multifunctional scaffold molecule gephyrin is a common marker of the inhibitory postsynapse (Tyagarajan and Fritschy, 2014). Clustered regions of $CYFIP1^{GFP}$ and $CYFIP2^{GFP}$ were found to robustly colocalise with gephyrin puncta opposed to presynaptic vGAT puncta along the dendritic shafts of transfected neurons (Figure 3.13A). In addition, when average intensity of $CYFIP1^{GFP}$ or $CYFIP2^{GFP}$ fluorescence was analysed, both $CYFIP1^{GFP}$ and $CYFIP2^{GFP}$ were found significantly enriched by

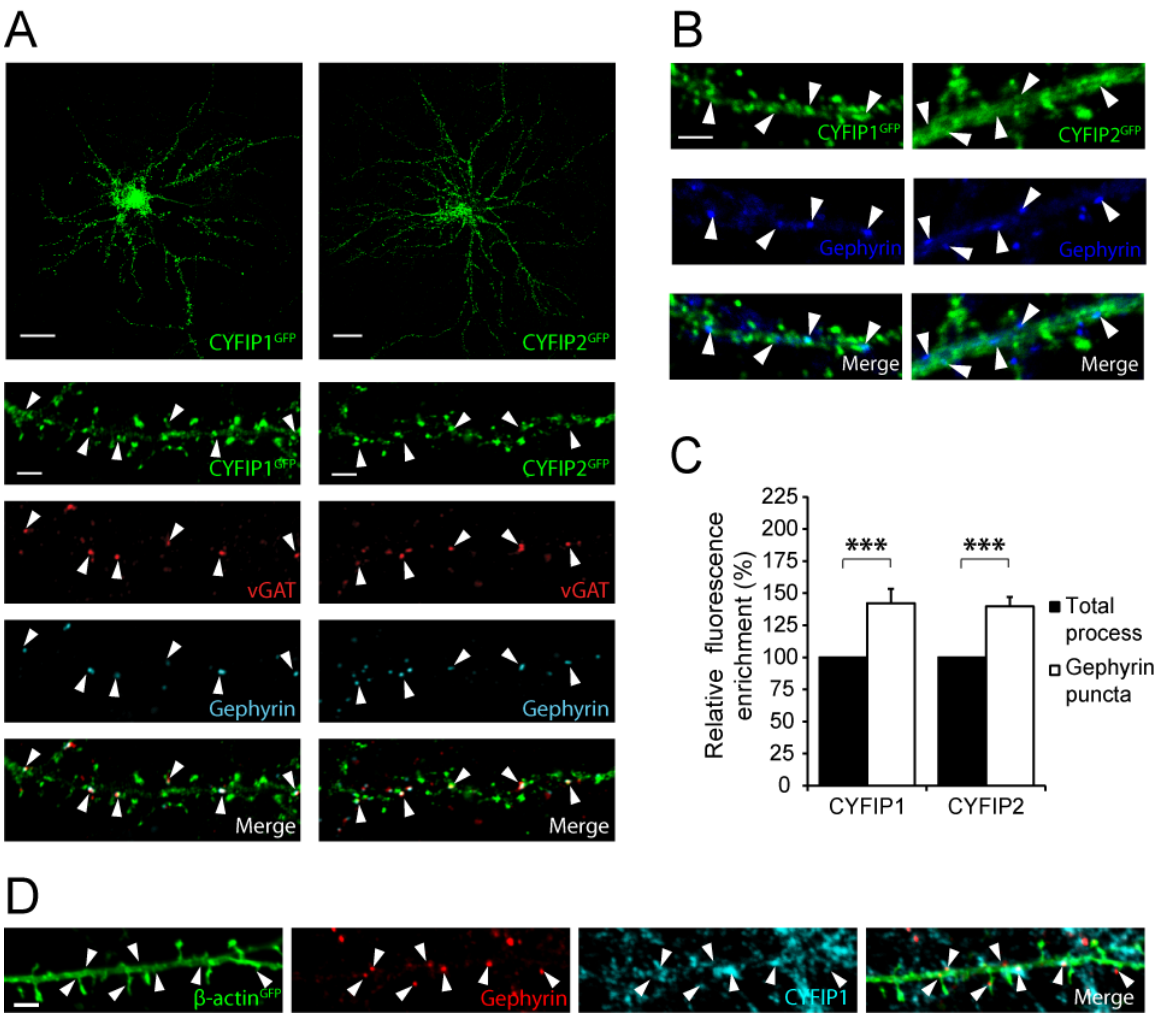

Figure 3.13: CYFIP1 and CYFIP2 are enriched at inhibitory synapses.

(A) CYFIP1^{GFP} and CYFIP2^{GFP} were transfected into mature rat hippocampal neurons and stained with antibodies against the inhibitory pre and postsynaptic markers vGAT and gephyrin respectively. CYFIP1^{GFP} and CYFIP2^{GFP} clusters colocalised with the inhibitory synaptic markers (arrowheads). **(B)** CYFIP1^{GFP} and CYFIP2^{GFP} transfected neurons stained with gephyrin for quantitative analysis. **(C)** Quantification of CYFIP1^{GFP} and CYFIP2^{GFP} fluorescence intensity at inhibitory gephyrin puncta compared to the total process. CYFIP1^{GFP} and CYFIP2^{GFP} are significantly enriched at inhibitory synapses (n=33-42; Wilcoxon signed rank test; ***p<0.001). **(D)** Endogenous CYFIP1 co-localises with the inhibitory postsynaptic marker gephyrin (arrowheads) in actin^{GFP} expressing cells. Scale bars, 20µm, 2µm.

~40% at inhibitory synapses, labelled with gephyrin, compared to the surrounding total dendritic process (Figure 3.13B,C; gephyrin puncta: CYFIP1, 142.42 ± 11.16%; CYFIP2, 139.67 ± 7.29%; ***p<0.001). By staining neurons, transfected with actin^{GFP} to label cell morphology, with an antibody to CYFIP1 it was also observed that endogenous CYFIP1 was present at inhibitory synapses and colocalised with gephyrin clusters (Figure 3.13D). These data provide evidence that CYFIP1 and CYFIP2 localise to inhibitory synapses and are therefore, spatially positioned to have a role in inhibitory synaptic maintenance or transmission.

3.2.8 The effect of CYFIP1 and CYFIP2 overexpression on inhibitory synapse stability

These findings are the first to describe an inhibitory synaptic localisation for CYFIP proteins and therefore the role of CYFIP proteins at these synapses is entirely unknown. In an attempt to study CYFIP1 and CYFIP2 at the inhibitory synapse an overexpression system was used. Observing the effects of altered CYFIP gene expression not only allows conclusions to be draw about the functions of CYFIP proteins at inhibitory synapses but also provides a good model for studying the effects of CYFIP CNV.

Rat hippocampal neurons were transfected with CYFIP1^{GFP} or CYFIP2^{GFP} and allowed to express the transgene for 4 days. Neurons were then fixed at DIV14 and subjected to immunocytochemistry with a gephyrin antibody before being imaged using confocal microscopy. Analysis of the inhibitory synaptic gephyrin clusters along dendrites revealed a significant decrease in both total number of gephyrin clusters and total gephyrin cluster area upon overexpression of either CYFIP1^{GFP} or CYFIP2^{GFP} compared to control GFP expressing cells (Figure 3.14; gephyrin cluster number: GFP, 9.87 ± 0.61; CYFIP1, 6.30 ± 0.88; CYFIP2, 6.60 ± 0.57; **p<0.01; gephyrin cluster area: GFP, 3.05 ± 0.20μm^2; CYFIP1, 2.06 ± 0.31μm^2; CYFIP2, 1.94 ± 0.20μm^2; *p<0.05, **p<0.01).

This study has shown that actin dynamics are disrupted following CYFIP1 haploinsufficiency at excitatory synapses in dendritic spines. It was therefore interesting to determine whether actin dynamics were being altered at inhibitory synapses following CYFIP1^{GFP} or CYFIP2^{GFP} overexpression. Disrupted actin

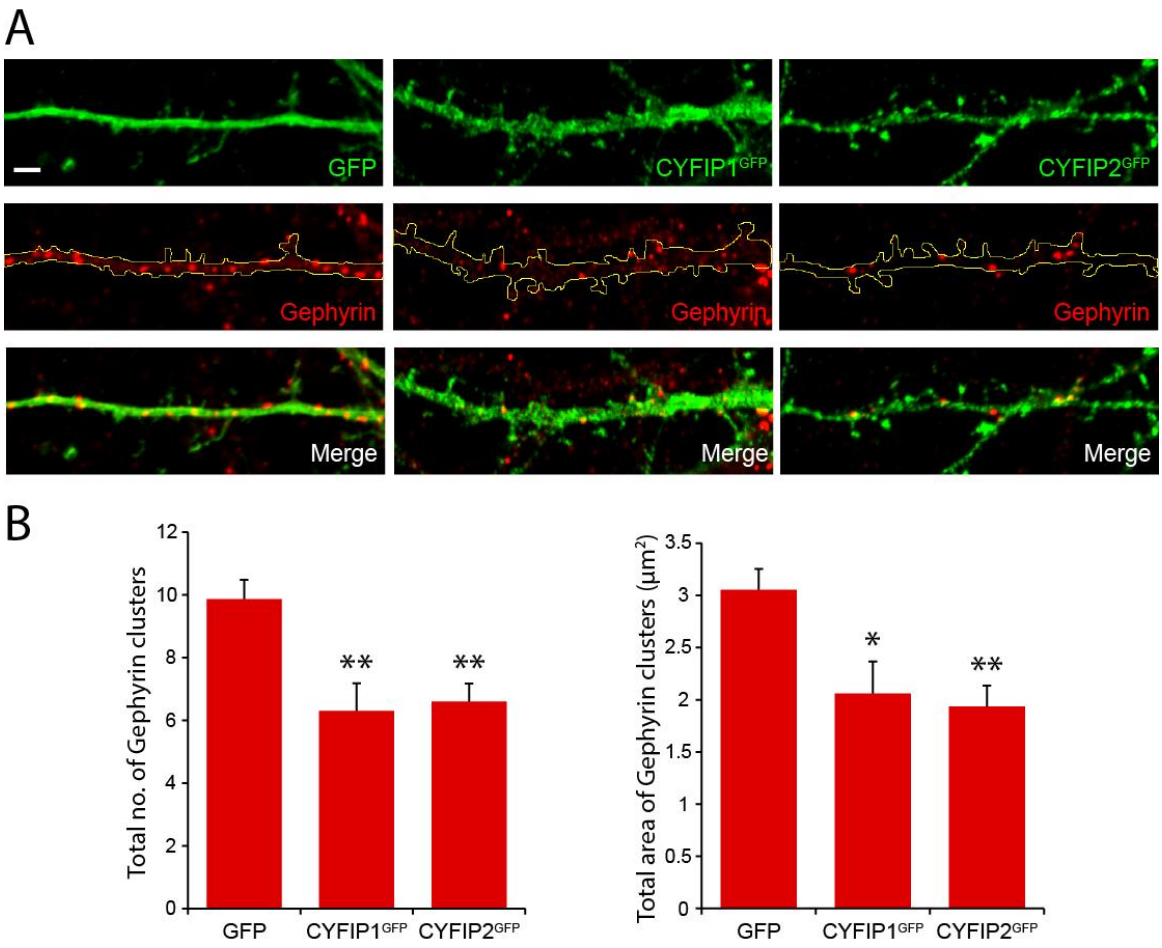

Figure 3.14: Overexpression of CYFIP1 or CYFIP2 reduces gephyrin clusters at inhibitory synapses.

(A) Hippocampal neurons were transfected with CYFIP1^{GFP}, CYFIP2^{GFP} or GFP control at DIV10 and allowed to express the transgene for 4 days before fixing and staining with an antibody to the scaffold molecule gephyrin, a marker of inhibitory synapses. **(B)** Analysis of clusters revealed a decrease in gephyrin cluster number and cluster area upon CYFIP1^{GFP} or CYFIP2^{GFP} overexpression compared to control cells. (n=20; ANOVA; *p<0.05, **p<0.01). Scale bars, 2µm.

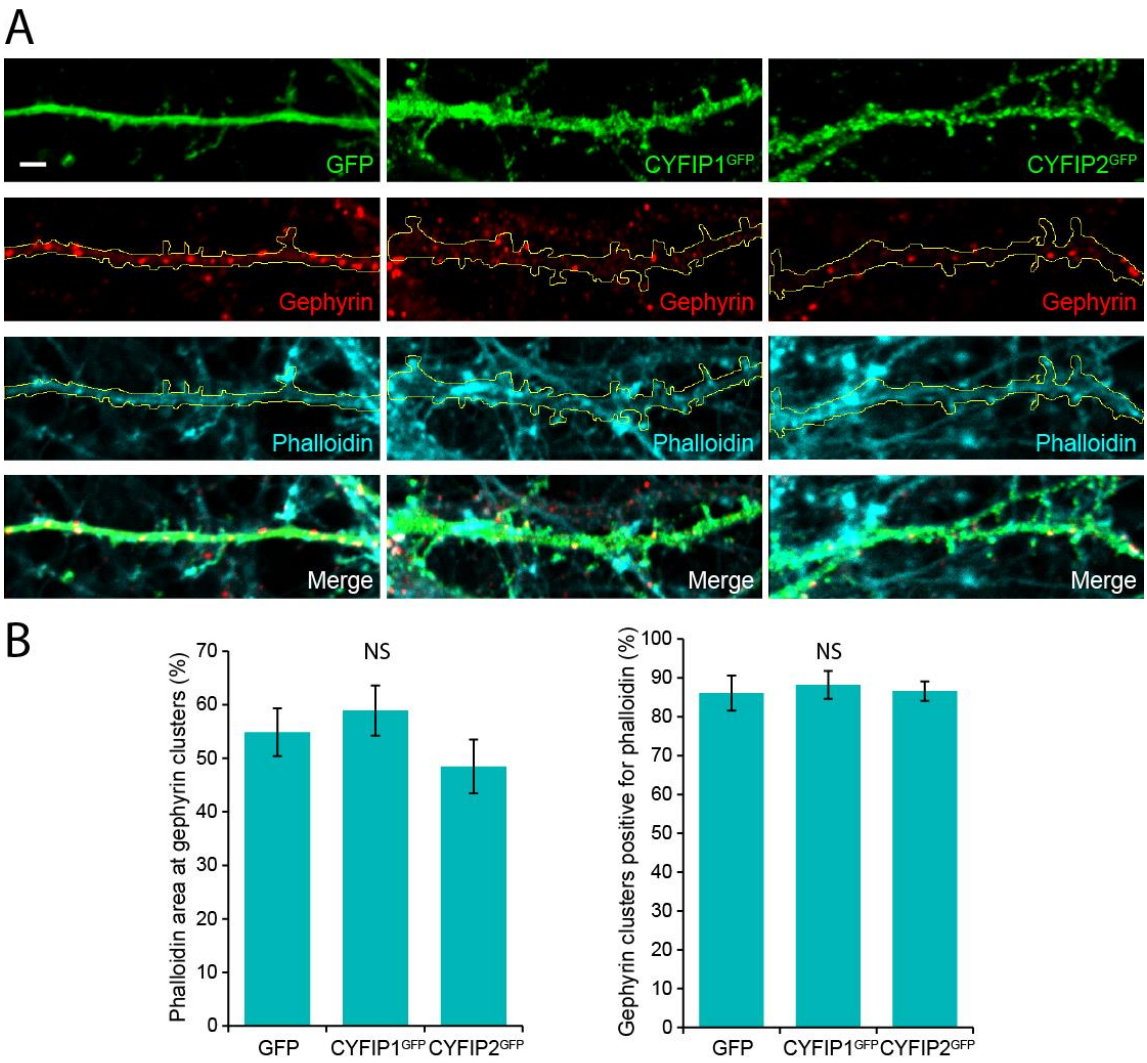

Figure 3.15: Overexpression of CYFIP1 and CYFIP2 does not affect inhibitory synapse F-actin content.

(A) Hippocampal neurons were transfected with CYFIP1^{GFP}, CYFIP2^{GFP} or GFP control at DIV10 and allowed to express the transgene for 4 days before fixing and staining with an antibody to the scaffold molecule gephyrin, a marker of inhibitory synapses, and phalloidin conjugated to alexa fluro-647 to label F-actin. **(B)** Analysis of phalloidin area at inhibitory synapses and number of inhibitory synapses positive for phalloidin revealed no difference between cells overexpressing CYFIP1^{GFP} and CYFIP2^{GFP} compared to control GFP expressing neurons. Gephyrin was used to label inhibitory synapses for the analysis. (n=19-20; ANOVA; NS). Scale bars, 2µm.

dynamics may have caused the loss of gephyrin clustering observed. Levels of F-actin were imaged and analysed using the F-actin binding toxin phalloidin conjugated to alexa-647. Neurons were costained with an antibody against gephyrin to label inhibitory synapses. Intriguingly, there was no change in the area of phalloidin at gephyrin clusters or the percentage of gephyrin clusters positive for phalloidin (Figure 3.15; phalloidin area: GFP, 54.86 ± 4.48μm²; CYFIP1, 58.90 ± 4.70μm², CYFIP2 48.46 ± 5.03μm²; NS; phalloidin positive gephyrin clusters: GFP, 86.11 ± 4.52%; CYFIP1 88.20 ± 3.57%; 86.61 ± 2.51%; NS). This suggests that overexpression of $CYFIP1^{GFP}$ or $CYFIP2^{GFP}$ does not dramatically change the amount of F-actin at inhibitory synapses. Indeed, unlike at excitatory synapses altered CYFIP expression does not appear to impact on inhibitory synapse F-actin content. However, live imaging will be required to reveal if there are more subtle spatial and temporal effects of CYFIP overexpression on actin regulation at inhibitory synapses.

3.2.9 CYFIP1 and CYFIP2 and the excitatory/inhibitory balance

Gephyrin is the major postsynaptic scaffolding protein of GABAergic synapses and is critically linked to inhibitory synapse integrity via its role in clustering $GABA_AR$s to synapses (Kneussel et al., 1999; Tyagarajan and Fritschy, 2014). Therefore, to determine whether the observed decrease in gephyrin cluster number and area was having an effect on $GABA_AR$ synaptic targeting, $CYFIP1^{GFP}$ or $CYFIP2^{GFP}$ overexpressing neurons were subjected to a surface stain with an antibody to an extracellular epitope of the $GABA_AR$ γ2 subunit. This assay identifies synaptic $GABA_AR$ clusters as the γ2 subunit is only a component of synaptic $GABA_AR$s not extrasynaptic receptors. In agreement with the initial findings for gephyrin, compared to control GFP expressing cells, overexpression of $CYFIP1^{GFP}$ or $CYFIP2^{GFP}$ resulted in a significant reduction in number and area of surface $GABA_AR$ γ2 subunit clusters (**Error! Reference source not found.**A,B; $GABA_AR$ cluster number: GFP, 8.11 ± .86; CYFIP1, 5.44 ± 0.77; CYFIP2 5.20 ± 0.73; $^{**}p<0.01$; $GABA_AR$ cluster area: GFP, 2.83 ± 0.60μm²; CYFIP1, 1.12 ± 0.18μm²; CYFIP2 1.31 ± 0.22μm²; $^{*}p<0.05$, $^{**}p<0.01$).

Interestingly, when the excitatory synapse was studied under the same conditions the opposite effect on synaptic stability was observed. Neurons were stained with an antibody to homer, the excitatory PSD structural molecule, to label the excitatory

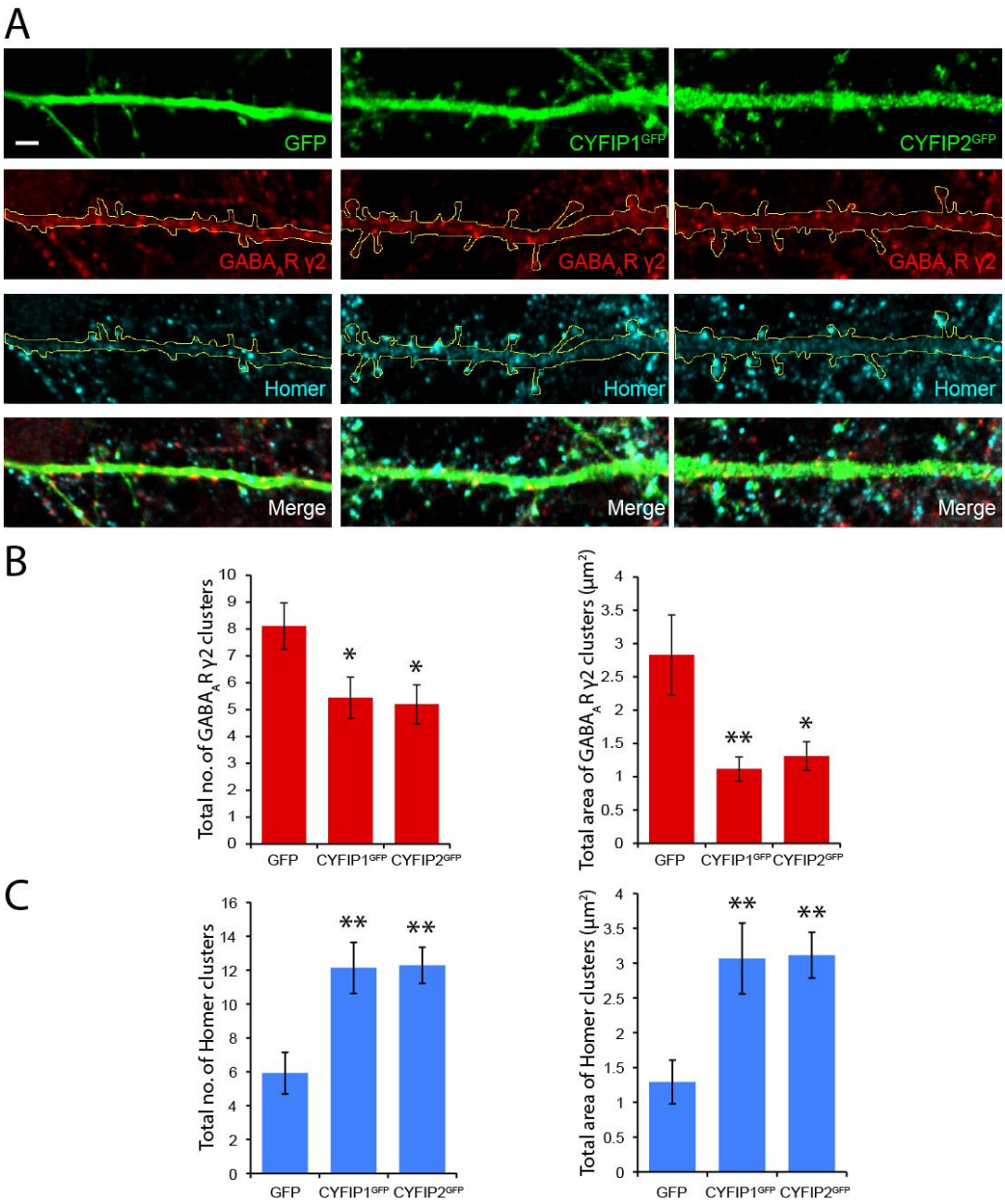

Figure 3.16: The effect of CYFIP1 and CYFIP2 overexpression on $GABA_AR$ γ2 and homer clusters.

(A) Hippocampal neurons were transfected with $CYFIP1^{GFP}$, $CYFIP2^{GFP}$ or GFP control at DIV10 and allowed to express the transgene for 4 days before fixing and staining for surface $GABA_AR$ γ2 inhibitory synaptic clusters and excitatory synaptic homer clusters. **(B)** Analysis of surface $GABA_AR$ γ2 clusters revealed a decrease in cluster number and cluster area upon $CYFIP1^{GFP}$ or $CYFIP2^{GFP}$ overexpression compared to control cells. (n=21-25; ANOVA; *p<0.05, **P<0.01). **(C)** Analysis of homer clusters revealed an increase in cluster number and cluster area upon $CYFIP1^{GFP}$ or $CYFIP2^{GFP}$ overexpression compared to control cells. (n=15-17; ANOVA; **p<0.01). Scale bars, 2μm.

postsynapses. Upon overexpression of CYFIP1^{GFP} or CYFIP2^{GFP} both total number and area of homer clusters were significantly increased about 2 fold compared with control cells (**Error! Reference source not found.**A,C; homer cluster number: FP, 5.92 ± 1.23; CYFIP1, 12.14 ± 1.51; CYFIP2 12.29 ± 1.06; **p<0.01; homer cluster area: GFP, 1.29 ± 0.31µm²; CYFIP1, 3.07 ± 0.51µm²; CYFIP2 3.11 ± 0.33µm²; **p<0.01).

Taken together, overexpression of CYFIP1^{GFP} or CYFIP2^{GFP} is negatively impacting on inhibitory synaptic structure and receptor content. However, overexpression equally appears to be enriching excitatory synaptic number and area. From these results, it can be hypothesised that CYFIP overexpression at synapses could somehow be disrupting the balance between inhibitory and excitatory transmission. This hypothesis highlights another potential contributing factor in the pathogenesis of neuropsychiatric disorders associated with CYFIP CNV. However, how mechanistically overexpression of CYFIP proteins are causing these effects at synapses still remains to be elucidated.

3.3 Discussion

The work presented in this chapter describes the effects of CYFIP1 and CYFIP2 CNVs on neuronal morphology and synaptic maintenance in an attempt to understand more about how altered CYFIP1 expression might be contributing to neuropsychiatric disease. Initially, CYFIP1 and CYFIP2 were shown to be enriched at excitatory synapses within dendritic spines. Overexpression techniques were used to model genetic microduplication and increased expression of both CYFIP1 and CYFIP2 were shown to increase dendritic complexity and alter spine morphology. The effects of CYFIP1 microdeletion were studied using a CYFIP1 haploinsufficient mouse model. Haploinsufficient neurons developed less complex dendritic arborisation, the opposite effect to the increased dendritic complexity observed in CYFIP1 overexpressing cells. Interestingly, both haploinsufficiency and overexpression altered spine morphology in the same way resulting in more long, thin immature spines. Live imaging of actin in spines showed that actin dynamics were disrupted in *Cyfip1*$^{+/-}$ neurons (Figure 3.17). CYFIP1 KO mice were found to be embryonically lethal illustrating the critical function CYFIP1 must play in development, probably through its actin regulatory role. However, reduced CYFIP1 levels must be sufficient for development as *Cyfip1*$^{+/-}$ mice developed normally and presented with no gross changes in brain morphology. Finally, CYFIP1 and CYFIP2 were also found to be enriched at inhibitory synapses and overexpression of either protein impacted on inhibitory synapse integrity. Inhibitory gephyrin and $GABA_AR$ clusters were reduced while excitatory homer clusters were increased suggesting that CYFIP protein overexpression may in some way affect the E/I balance, highlighting another potential mechanism of disease pathogenesis for CYFIP CNVs.

3.3.1 CYFIP proteins, dendritic complexity and development

Rho GTPases are global actin regulators critical for normal dendritic branch dynamics, extension and development (Auer et al., 2011; Jan and Jan, 2010; Newey et al., 2004). One downstream effector of the GTPase Rac1 is the WRC, which once stimulated by GTP-bound Rac1, brings about Arp2/3 activation resulting in actin nucleation and polymerisation. CYFIP proteins form one component of the WRC and provide the binding site for active GTP-bound Rac1 making them too, critical actin modulators. Indeed, in steady-state conditions CYFIP1 represses the activity of the

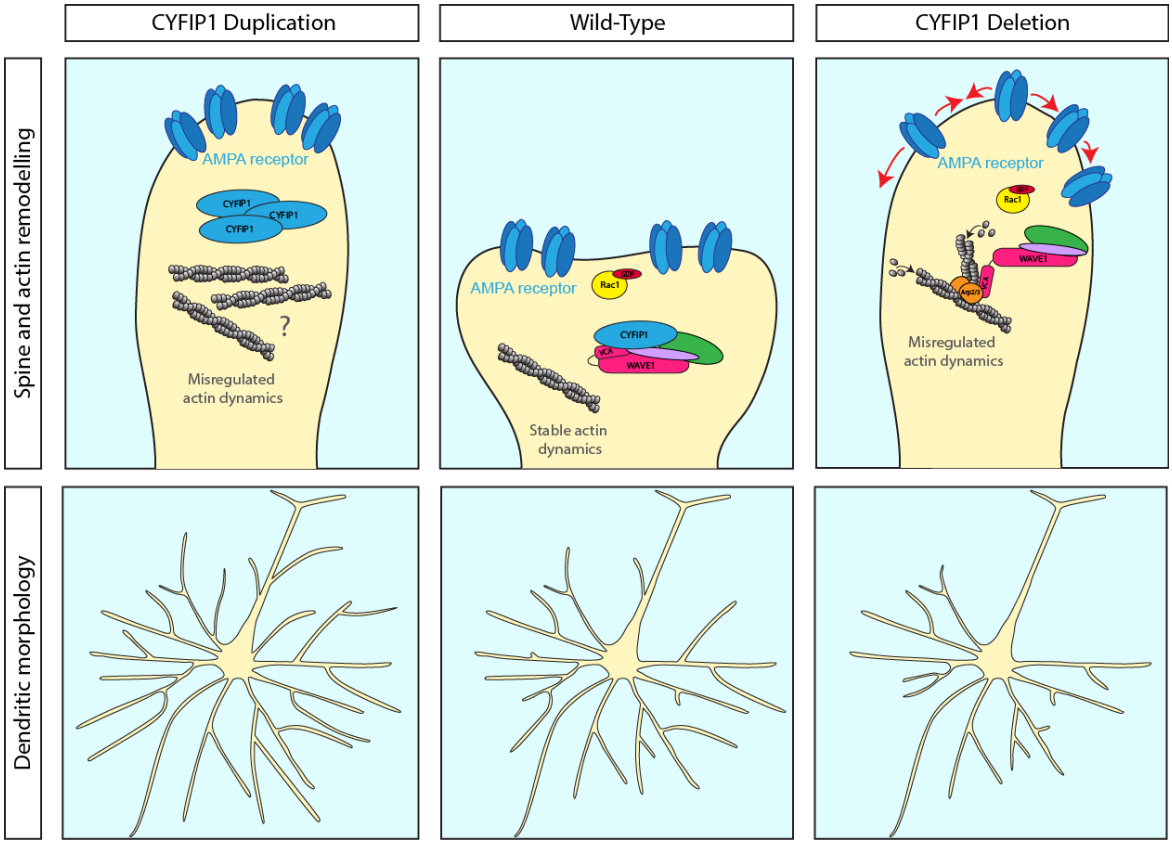

Figure 3.17: A summary of the morphological effects caused by CYFIP1 CNV on dendritic complexity and spine structure.

Compared to wild-type conditions where dendritic complexity and spine morphology are normal, when CYFIP1 is overexpressed in neurons to model CYFIP1 microduplication (left panels) dendritic complexity is enhanced and there is a shift towards more long, thin immature spines. Conversely, when CYFIP1 haploinsufficient neurons are studied to model CYFIP1 microdeletion dendritic complexity is reduced however, there is still a shift towards more long, thin spines. These spines display altered actin dynamics caused by loss of CYFIP1 which may contribute to this structural phenotype.

WRC by inhibiting the active VCA domain of WAVE. Following Rac1 activation, Rac1 binds to CYFIP1 causing a conformation change in the molecule that leads to removal of the WAVE inhibition and consequently actin polymerisation (Chen et al., 2010b; Ismail et al., 2009). Disrupted CYFIP protein levels may therefore, effect Rac1 downstream signalling events to the WRC and impact on dendritic branching. Indeed, here it is demonstrated that appropriate CYFIP1 and CYFIP2 levels are important for normal dendritic arborisation and neuronal complexity. Increased CYFIP1 or CYFIP2 dosage led to enhanced dendritic length and branching, while loss of CYFIP1 expression reduced dendritic complexity.

Active Rac1 often occurs at the membrane where it is spatially localised to bring about cytoskeletal rearrangement and membrane extension during cell growth and development. CYFIP proteins contain a WIRS motif that has been shown to interact with membrane proteins (Chen et al., 2014a). Therefore, one explanation for the effects of altered CYFIP dosage on dendritic development could be that CYFIP proteins are required to recruit the WRC to the cell membrane where Rac1 can subsequently activate it. Greater levels of CYFIP could result in more WRC targeted to the membrane where it can be activated to bring about actin polymerisation, membrane extension and dendritic development. On the other hand, in conditions where CYFIP is decreased, this recruitment is lost and dendritic complexity is reduced. Alternatively, microtubule (MT) dynamics are highly important in dendritic growth and maintenance (Jan and Jan, 2010); therefore perhaps CYFIP proteins have an as yet unidentified role in MT regulation.

Interestingly, a recent study observed similar morphological results to those presented here when CYFIP1 was either overexpressed in differentiated neuroblastoma cells or in a transgenic mouse. Consistent with the data here, they reported a significant increase in total branch number, and also reported an increase in cell size and a reduction in neurite length (Oguro-Ando et al., 2014). Furthermore, as well as having effects on dendritic morphogenesis, CYFIP1, in an actin regulatory complex with WAVE1, has been shown to be necessary for CRMP-2-induced axonal outgrowth and axon-dendrite specification (Kawano et al., 2005) while CYFIP2 has been identified to be critical in retinal axonal outgrowth (Pittman et al., 2010). Taken together, the evidence points towards CYFIP playing a key role in neuron development and maintenance particularly impacting on dendritic complexity.

Defects in dendritic complexity and hence connectivity have long been considered features of ASD and SCZ with impaired long-range connectivity and enhanced local connections thought to be contributing factors (Belmonte et al., 2004; Hutsler and Zhang, 2010; Karlsgodt et al., 2008). CYFIP proteins, via their regulation of actin dynamics, could be impacting on dendritic arborisation and hence cortical connectivity, providing one explanation for their neuropsychiatric disease association. This suggestion could also explain why there appears to be no change in gross brain organisation in CYFIP1 haploinsufficient mice. It is more likely that pathogenic changes would occur at the level of neuronal cell architecture. Further detailed morphological analysis studying cell number, cortical column density and layer thickness may identify local structural changes in *Cyfip1*$^{+/-}$ animals similar to structural defects seen in ASD and SCZ brains (Harvey et al., 1993; Kulkarni and Firestein, 2012; Raymond et al., 1996). Interestingly, a recent study investigated induced pluripotent stem cell (iPSC)-derived neural progenitors generated from SCZ patients carrying the 15q11.2 microdeletion. These reprogrammed neurons displayed adherens junction and apical polarity defects and to this date are the only human model of CYFIP1 mutations described. The authors demonstrated that CYFIP1 was necessary to maintain adherens junctions and apical polarity. In addition, reduced CYFIP1 expression in the developing mouse cortex resulted in defects in radial glia migration which led to the ectopic localisation of RGCs outside of the ventricular zone. This describes another mechanism by which CYFIP1 could impact on cortical development and connectivity (Yoon et al., 2014).

CYFIP1 appears not only important in dendritic development but also vital for embryonic development. Recent work has highlighted that rare complete gene knockouts in humans have a significant role in ASD and major mental illness (Lim et al., 2013). Although both deletions and duplication in CYFIP1 have been described in humans, it seems unlikely that patients with total loss of CYFIP1 will be described as data presented here shows that CYFIP1 KO mice are embryonically lethal. This is consistent with previous studies of mice lacking critical actin regulatory genes which have been described to display characteristic abnormalities resulting in death during developmental progression between E7.5 and E12.5 (Dubielecka et al., 2011). For example, inactivation of murine *Rac1* and *Nap1* are lethal during gastrulation at E7.5 and 9.5 respectively while *n-WASP* and *WAVE2* are lethal during organogenesis at E11 and mid-gestation at E12.5 respectively (Migeotte et al., 2010; Rakeman and

Anderson, 2006; Snapper et al., 2001; Yan et al., 2003). *Cyfip1*$^{-/-}$ embryos do not survive beyond E8.5. Thus, CYFIP1 signalling events are likely crucial for gastrulation and normal patterning of embryonic structure during developmental progression (Liu et al., 2000). *CYFIP1* KO embryos were too small to detect specific morphogenic defects but one explanation for the severe developmental delay seen in these embryos is due to dysregulated cell movement and cell fate during gastrulation as a result of disrupted CYFIP1/WAVE-mediated actin regulation similar to what is observed in *Nap1* KO animals (Rakeman and Anderson, 2006).

3.3.2 CYFIP proteins regulate spine morphology and actin dynamics

Tight actin regulation, mediated by Rho GTPases, is critical for normal excitatory synaptic functions such as receptor trafficking, endocytosis and spine development and maintenance (Bourne and Harris, 2008; Hanley, 2014; Hotulainen and Hoogenraad, 2010). The localisation studies shown here strongly reveal the presence of CYFIP1 and CYFIP2 at dendritic spines and demonstrate both proteins are enriched at excitatory synapses. The restricted localisation of these proteins suggests they function within the excitatory postsynaptic compartment. Indeed, as key Rac1 effectors and regulators of the WRC, both CYFIP1 and CYFIP2 are correctly positioned at excitatory synapses to regulate actin dynamics. Thus, altered CYFIP levels may lead to changes in actin turnover that could impact on spine morphology and excitatory synapse stability. In agreement with this, it is shown here that overexpression of CYFIP1, CYFIP2 or CYFIP1 haploinsufficency effect dendritic spine structure, resulting in more immature long thin spines and filopodia. Furthermore, recent studies from others have also shown reducing CYFIP1 levels using RNAi in cultured hippocampal neurons and over expression of CYFIP1 *in vivo* alter spine morphology (Han et al., 2014; Oguro-Ando et al., 2014; De Rubeis et al., 2013). These results are consistent with the dysregulated expression of other key actin regulatory molecules impacting on spine structure and morphology including WAVE, Arf1 and Arp2/3 (Kim et al., 2013, 2006; Rocca et al., 2013).

FRAP experiments carried out here were used to study the recovery of fluorescently labelled actin in dendritic spines of hippocampal neurons. The greater recovery and increased mobile fraction observed in the *Cyfip1*$^{+/-}$ neurons showed that normal actin dynamics within spines were disrupted. These altered actin dynamics could explain

the spine morphology defects observed in CYFIP1 haploinsufficient neurons. This finding, within a mammalian neuronal system, is consistent with previously published *in vitro* experiments, which show CYFIP1 acts as a negative regulator of actin polymerisation due to its inhibitory function over the WRC (Chen et al., 2010b). Furthermore, results in line with the findings presented here were observed in dCYFIP mutant *Drosophila*. The neuromuscular junction (NMJ) in mutant flies showed dysregulated morphology resulting in shorter NMJs with more satellite boutons. In addition, FRAP experiments at the NMJ revealed an increase in actin^{GFP} recovery in dCYFIP mutants compared to WT. Interestingly, the actin effect was rescued by decreased SCAR expression (the *Drosophila* homologue of WAVE) (Zhao et al., 2013a). This provides evidence that the NMJ defects are caused by an overactive WRC due to the lack of inhibition by dCYFIP. It would be interesting to determine if knockdown of WAVE, within the CYFIP1 haploinsufficient neurons here, could rescue the enhanced fluorescence recovery and the spine phenotype observed in a similar way. The NMJ morphology and actin phenotypes observed in mutant *Drosophila* are consistent with the altered spine morphology and actin dynamics illustrated here in *Cyfip*$^{+/-}$ neurons, adding strength to these results. Others have also reported changes in phalloidin staining at dendritic spines subjected to CYFIP1 RNAi, again demonstrating the critical role of CYFIP1 in F-actin regulation at spines (De Rubeis et al., 2013).

It is intriguing that both CYFIP1 overexpression and haploinsufficiency result in more immature spines. Mechanistically, reduced CYFIP1 could lead to less WAVE inhibition and therefore more Arp2/3 activation and actin polymerisation. While CYFIP1 overexpression could be sequestering active Rac1 away from activating PAK resulting in less cofilin activity. Active cofilin causes actin depolymerisation (Bellot et al., 2014). Interfering with both pathways in this way would result in increased actin assembly whether CYFIP1 was up or down regulated possibly leading to the same downstream morphological effects. It is furthermore interesting to note, that a number of other actin regulatory proteins have been reported to have the same effect on spine morphology whether they are up- or down-regulated, including VCP/neurofibromin, Abi3 and cofilin (Bae et al., 2012; Hotulainen et al., 2009; Meng et al., 2002; Wang et al., 2011). It appears that a critical level of CYFIP1 is required for normal spine morphology and shifting its levels either above or below a threshold may force spines into an unstable immature state.

Long thin, immature spines are a hallmark of many neuropsychiatric disorders. Post-mortem brains from patients with ID, FXS and ASD present with long thin spines while SCZ patients show a reduction in spine density (Fiala et al., 2002; Glantz and Lewis, 2000; Hutsler and Zhang, 2010; Purpura, 1974). Both overexpression and reduction of CYFIP1 result in an enrichment of immature thin spines demonstrating the appropriateness of CYFIP1 CNV as a model for neuropsychiatric disease. Indeed, the fact CYFIP1 CNV generates such a strong morphological hallmark of neuropsychiatric disorders may help explain why altered CYFIP expression has been associated with ASD and SCZ (Doornbos et al., 2009; Leblond et al., 2012; Nishimura et al., 2007; Zhao et al., 2013b). Moreover, thin, immature spines are known to form weaker synaptic connections and can have a negative impact on network connectivity, particularly within the cortex, making this phenotype an important factor in the pathogenesis of ASD and SCZ (Penzes et al., 2011).

3.3.3 CYFIP1, CYFIP2 and protein translation

It must not be overlooked that CYFIP proteins, together with FMRP and eIF4e, have also been described to be involved in a protein translation regulatory complex capable of repressing mRNA translation locally at synapses (Napoli et al., 2008). In fact recently, the use of CYFIP1 mutants that uncouple its protein translation and actin regulation roles demonstrated that both functions were required to rescue the immature spine phenotype seen in CYFIP1 knockdown neurons (De Rubeis et al., 2013). This highlights the importance of both CYFIP functions in dendritic spine maintenance and suggests its role in translational regulation may be influencing the morphological results observed here too. It would be interesting to use these CYFIP1 mutants that disrupt its interaction with either eIF4e or the WRC in the CYFIP overexpression system to unpick which pathways are required for the increase in dendritic complexity observed.

Fmr-1 knockout mice have been intensively studied as a model for FXS and among other phenotypes, defects in protein expression due to FMRP's translational repressive role have been characterised (Zalfa et al., 2003). As this repression is mediated, at least in part by CYFIP1 (Napoli et al., 2008), CYFIP1-deficient animals may also show defects in protein expression. Indeed, here it has been described that juvenile *Cyfip1*$^{+/-}$ mice have increased hippocampal Shank family protein expression

compared to WT control. Furthermore, adult *Cyfip1*$^{+/-}$ mice show decreased levels of chapsyn110 and PSD95 in the cortex and hippocampus respectively. Altered expression of key synaptic structural molecules have been shown to effect dendritic branching and spine dynamics and have been implicated in neuropsychiatric disorders (Penzes et al., 2011; Vessey and Karra, 2007). In particular, proteins of the PSD, such as PSD95, Shank2 and 3 have been shown to increase spine density and size (Roussignol et al., 2005; Steiner et al., 2008). Furthermore, altered expression of all three Shank proteins have been implicated in ASD (Arons et al., 2012; Leblond et al., 2012; Peça et al., 2011; Sato et al., 2012). Therefore, the defects in expression of postsynaptic scaffold proteins seen in CYFIP1 haploinsufficient mice not only mirror the phenotypes seen in FXS mice but may also help explain the neuropsychiatric defects observed in patients with 15q11.2 microdeletions. Further experiments such as quantitative PCR from mRNA samples of the brain regions would add strength to these initial findings.

CYFIP1 and CYFIP2 share 98% sequence similarity, have been described in the same functional pathways and interact with many of the same proteins. Therefore, due to their functional and structural similarities at the protein level it was interesting to further explore whether *Cyfip2* could be a candidate susceptibility gene for major mental illness like *Cyfip1*. Indeed, with this in mind experiments carried out in this chapter were extended to include CYFIP2 in an attempt to shed light on its role in neuronal morphology and synaptic maintenance.

The *Cyfip2* gene has not been directly associated with any neuropsychiatric disorders, however, has been described as a susceptibility locus for SCZ and attention-deficit/hyperactive disorder (ADHD) (Arcos-Burgos et al., 2004; Gurling et al., 2001). Furthermore, increased CYFIP2 protein levels have been identified in brain tissue samples of patients with SCZ and FXS (Föcking et al., 2014; Hoeffer et al., 2012). It is unclear whether the increased CYFIP2 levels observed in these patients are to compensate for reduced CYFIP1 levels or whether CYFIP2 has its own pathogenic mechanisms. Intriguingly, the high levels of CYFIP2 in FXS patients did not correlate with increased CYFIP2 mRNA and CYFIP2 mRNA is a target of FMRP translational regulation (Darnell et al., 2011). Therefore, in FXS patients increased CYFIP2 could be a direct result of loss of FMRP and points towards enhanced dosage of CYFIP2 having its own pathogenic mechanisms. The data in this chapter illustrates that raised

CYFIP2 levels cause an increase in dendritic arborisation and defects in spine morphology implying that CYFIP2 alone could contribute to neuropsychiatric disease pathogenesis. These effects could also be due to the interchangeable role of CYFIP2 and CYFIP1 in the regulation of the WRC (Takenawa and Suetsugu, 2007). It is yet to be revealed whether CNV at the 5q33.3 locus will be found to be associated with neuropsychiatric disease.

Few attempts have been made to determine whether CYFIP2 has independent functions from CYFIP1. Due to their high sequence similarity often reports assume CYFIP2 behaves like CYFIP1 and suggest it may even provide some functional compensation should CYFIP1 expression be disrupted. However, CYFIP2 alone has been shown to bind the whole FMRP family of proteins including FXR1 and FXR2 while CYFIP1 is only FMRP specific (Schenck et al., 2001) suggesting CYFIP2 could have its own independent function in regulating translation. On the other hand, *Drosophila* only express one FMRP family protein dFMRP and one CYFIP protein (dCYFIP) indicating that perhaps CYFIP2 and FXR1/2 contribute to a more complex level of translational regulation required for higher order organisms still to be elucidated. The shared effects observed with overexpression of both CYFIP1 and CYFIP2 seen in this chapter indicate that both proteins are implicated in the regulation of dendritic morphology and synapse stability. It would be interesting to try and rescue the effects of CYFIP1 haploinsufficient neurons with CYFIP2 overexpression to determine more about any redundancy between these proteins.

3.3.4 CYFIP proteins and the excitatory/inhibitory balance

The final experiments in this chapter place CYFIP1 and CYFIP2 at the inhibitory GABAergic synapse and show both proteins are enriched at gephyrin clusters, the major scaffolding protein of GABAergic and glycinergic synapses. This is the first time CYFIP proteins have been shown to localise to inhibitory synapses and suggests that they may be spatially targeted here to carry out specific functions. Indeed, when either CYFIP1 or CYFIP2 were overexpressed in neurons, gephyrin cluster number and area was reduced as well as $GABA_AR$ γ2-subunit cluster number and area. Loss of gephyrin clusters have previously been shown to reduced $GABA_AR$ clustering (Marchionni et al., 2009; Yu et al., 2007) while losing γ2 clusters has reduced presynaptic innervation (Li et al., 2005) both resulting in disrupted inhibitory transmission. Interestingly,

actin is required for GABAergic synapse integrity, maintenance and postsynaptic mobility (Charrier et al., 2006). Moreover, recently Rac1 was described in a novel actin signalling pathway critical for inhibitory synaptic stability and function (Smith et al., 2014). It could be tempting to suggest that CYFIP1 and CYFIP2, potentially via their ability to interact with active Rac1, may be involved in an inhibitory synapse specific actin regulatory mechanism that is important for maintaining the stability of inhibitory synaptic clusters. However, there was no difference in F-actin levels at inhibitory synapses when phalloidin was used to label F-actin in fixed CYFIP overexpressing cells. A more sensitive experiment such as actin live-cell imaging will be required to determine whether there are effects on actin turnover at inhibitory synapses when CYFIP proteins are overexpressed.

Decreased inhibition due to a reduction of surface $GABA_ARs$, such as the reduced γ2 clustering shown here, can upset the E/I balance of neuronal circuits, causing disrupted information processing which may result in altered animal behaviour (Blundell et al., 2009; Crestani et al., 1999; Tretter et al., 2009; Yizhar et al., 2011). Furthermore, defects in inhibitory neurotransmission leading to an altered E/I balance have also been implicated in multiple neuropsychiatric disorders including ASD (Paluszkiewicz et al., 2011), depression (Luscher et al., 2011b), bipolar disorder (Craddock et al., 2010) and SCZ (Charych et al., 2009). Overexpression of CYFIP proteins not only reduced inhibitory synaptic clusters but also increased homer clusters, a marker of the excitatory postsynapse. This result is an anti-homeostatic effect and could point towards disrupted CYFIP1 or CYFIP2 expression impacting on the E/I balance. This provides another potential mechanism for why CNV of CYFIP1 and the CYFIP2 locus have been implicated in neurological dysfunction. These intriguing opposite effects of CYFIP overexpression at inhibitory and excitatory synapses could be due to the proteins being involved in very different synapse specific pathways. Alternatively, perhaps overexpression of CYFIP1 or CYFIP2 enhances the translational repression of proteins required for increasing inhibitory synapse size and stability and for limiting excitatory synaptic number simultaneously. Further investigation is required to understand the mechanism of these synaptic effects.

In summary, this chapter has demonstrated that CYFIP1 and CYFIP2 are enriched within dendritic spines, altered CYFIP1 and CYFIP2 expression results in spine and dendritic morphology defects, and that CYFIP1 deficiency affects F-actin assembly at

spines. Taken together with the previously published findings reporting CYFIP1 and CYFIP2 as actin regulators (Chen et al., 2010b; Schenck et al., 2003) it can be proposed that CYFIP proteins function to regulate local actin dynamics within spines to maintain spine structure and potentially control dendritic morphology through an actin regulatory mechanism. Changes in spine size and shape are intimately linked to synaptic plasticity and neuronal function (Hotulainen and Hoogenraad, 2010). Therefore, disruption of CYFIP1 and CYFIP2 expression, such as in CNV, may result in neuropsychiatric phenotypes due to defects in spine and dendritic morphology, a form of pathogenesis already associated with neuropsychiatric disorders (Kulkarni and Firestein, 2012; Penzes et al., 2011). Additionally, CYFIP1 and CYFIP2 overexpression has a negative effect on inhibitory synapse stability and increases excitatory synaptic sites. This could alter the E/I balance and suggests a new mechanism for CYFIP1 and CYFIP2 associated neuropsychiatric disorder pathogenesis.

Chapter 4

Identification and characterisation of rare *Cyfip1* variants in SCZ

4.1 Introduction

Our ability to sequence the human genome has led to the identification of many disease causing allelic variants and genes. In the last decade, next-generation sequencing has revolutionised this field providing fast and efficient genetic sequencing technologies with a large fall in costs compared to traditional Sanger methods. These new technologies have allowed genome-wide association studies (GWAS), CNV analysis and whole exome or genome sequencing of large patient cohorts to take place to discern rare mutations associated with disease. In particular, the contribution of rare variants to diseases with complex inheritance has been given a large amount of attention in an effort to improve our understanding of the disease mechanisms and provide new targets for therapeutics. Indeed, there is great interest in determining which genomic loci infer risk for SCZ, a highly heritable disorder.

Currently, CNV at the 15q11.2 genomic region, where *Cyfip1* is situated, has been associated with SCZ. Large genomic screens have implicated both microduplications and microdeletions of the 15q11.2 region in SCZ (Consortium, 2008; Kirov et al., 2012; Stefansson et al., 2008). However, this genomic region comprises four genes and although the neuronal functions of CYFIP1 point towards it being the disease-causing gene there is less support for a direct association between *Cyfip1* and SCZ (Purcell et al., 2014; Tam et al., 2010; Zhao et al., 2013b). Consequently, identification of undescribed SCZ-associated variants in *Cyfip1* will provide further evidence for the gene being a risk factor for SCZ. To address this a genetic analysis approach can be used.

The UK10K consortium (The UK10K consortium 2014, a full list of investigators who contributed to the generation of this data is available online: http://www.uk10k.org/) was developed to sequence 10000 patients between 2010 and 2013 in an attempt to

identify rare genetic variants associated with disease. A combination of whole-exome analysis and genome-wide sequencing was carried out on different patient groups including neurodevelopmental, SCZ, obese and rare disease sample sets. The published data is available for scientists to analyse; comparing DNA sequencing from case and control groups to identify disease-associated genetic variations. The vast scale and depth of the UK10K sequencing records increases the power of the analysis and allows for the identification rare SNPs which occur at low frequencies (<0.05%) in the population. In this way, uncommon variants associated with SCZ can be identified within a gene of interest which would otherwise go undetected in normal GWAS. Indeed, it is possible to seek rare variants in *Cyfip1* that are linked with SCZ. Moreover, functional characterisation of any variants identified is also critical to increase our understanding of the molecular mechanisms of SCZ pathogenesis and how CYFIP1 might be implicated.

In parallel to unravelling how mutations in CYFIP1 impact its function, there is still much to be learned about CYFIP1 from loss of function studies using KO models. It is only by combining the findings from all these experimental systems that a bigger, clearer picture of CYFIP1 function and how it might be implicated in neuropsychiatric disorders will be elucidated. A previous report and data generated here in Chapter 3 describe constitutive KO CYFIP1 mice to be embryonically lethal. Bozdagi and colleagues state CYFIP1 KO embryos generated from heterozygous crosses can be detected until embryonic day 3-5 (Bozdagi et al., 2012) whereas it is shown here that KO embryos can be identified until day 8.5 *in utero*. Additionally, loss of CYFIP1 in flies was reported to induced lethality during pupal life (Schenck et al., 2003). This lethality makes loss of function studies extremely challenging. As an alternative approach, RNAi has been used to observe the effects of depleted CYFIP1 levels. In human fibroblasts reduced CYFIP1 expression impaired lamellipodia formation, decreased membrane ruffling upon growth factor treatment, and abolished the establishment of Rac1 induced lamellipodia (Steffen et al., 2004). Furthermore, RNAi induced knockdown of CYFIP1 in neurons has been shown to impair dendritic spine morphology consistent with data from Chapter 3 and disrupt the regulation of adherens junctions and apical polarity (De Rubeis et al., 2013; Yoon et al., 2014). To this end however, there have been no loss of function studies carried out with CYFIP1 KO cells and indeed, the effect of total loss of CYFIP1 on cell function remains an interesting question.

On the other hand, CYFIP1 haploinsufficient mice are viable and, similarly to RNAi approaches, have been used to study the functional effects of reduced CYFIP1 levels. In the previous chapter, these mice have been studied as a model for CYFIP1 microdeletion. CYFIP1 haploinsufficient neurons showed defects in spine and dendritic morphology thought to be a result of deregulated actin dynamics. Additionally, a recent electrophysiological study revealed CYFIP1 haploinsufficiency produced FXS-like characteristics. Hippocampal mGluR induced LTD was enhanced in *Cyfip1*$^{+/-}$ animals compared to WT and was insensitive to protein synthesis inhibitors. Furthermore, these mice had a mild behavioural phenotype of enhanced extinction in inhibitory avoidance compared to control mice; similar to behaviours exhibited by FXS model mice (Bozdagi et al., 2012). Intriguingly, CYFIP2 haploinsufficient mice showed no morphological or electrophysiological differences to WT animals in the hippocampus. However, dendritic spines were altered in the cortex of these mice and mGluR induced spine regulation was impaired in cortical neurons (Han et al., 2015). The disparate effects of CYFIP1 and CYFIP2 haploinsufficiency in the hippocampus and cortex suggest that the patterns of redundancy and compensatory mechanisms between these two homologues differ depending on the brain region in question.

Conditional KO (cKO) mice allow time and region specific deletion of a protein and provide a powerful tool for carrying out loss of function studies on a protein that is normally essential for viability. Indeed, using this system, KO can be induced postnatally which allows the uncoupling of a protein's function in development from its role in maintenance. This idea is specifically relevant for CYFIP1 due to the embryonic lethality of constitutive CYFIP1 KO mice. Hence, the generation of CYFIP cKO mice would provide the first example of complete CYFIP1 loss of function studies and would shed more light on many as yet unanswered aspects of CYFIP1 function.

In this chapter, firstly, genetic analysis of a large cohort of SCZ patient DNA sequencing has revealed *Cyfip1* as a SCZ-associated gene due to an excess of potentially damaging rare variants identified within the gene. Of these variants SNP 22963816 was found to be significantly associated with SCZ. Furthermore, five of the variants, selected based on their potential to disrupt functional CYFIP1 protein interactions, were genotyped in an independent SCZ cohort. Again SNP4 (22963816) occurred more frequently in cases than controls, however, this association was not

significant. Functional characterisation of all five candidate SCZ-associated CYFIP1 variants revealed they retained their localisation to excitatory and inhibitory synapses. Furthermore, the different variants showed no alterations in their interaction with a member of the WRC. Secondly, the first example of CYFIP1 knockout MEFs was characterised. KO cells appeared to show reduced survival rates and disrupted actin structure appearing smaller and more rounded. Moreover, postnatal deletion of CYFIP1 in the forebrain resulted in a 50% loss of CYFIP1 in the hippocampus and an alteration in CA1 pyramidal basal dendrite morphology in six month old mice. In summary, this data provides evidence that *Cyfip1* is a SCZ-associated gene. Initial studies show individual variants do not appear to be functionally damaging suggesting that an accumulation of variants may have more harmful effects. Finally, loss of function studies using novel CYFIP1 cKO models revealed CYFIP1 function appears to be critical for viability in fast dividing cells while postnatal deletion of CYFIP1 in neurons results in defects in dendritic morphology and points towards a role for CYFIP1 in dendritic maintenance as well as development.

4.2 Results

4.2.1 Identification of novel CYFIP1 schizophrenia-associated variants

In order to investigate the functional effects of CYFIP1 SCZ-associated variants, it was first important to determine if *Cyfip1* was associated with SCZ and if any novel variants could be identified within the gene. In collaboration with Dr. Dave Curtis from Queen Mary University of London the weighted burden test was applied to data produced from the UK10K project to determine if *Cyfip1* or *Cyfip2* were associated with SCZ. The SCZ cohort consisted of 1392 subjects recruited from five British centres. These subjects were considered cases and were compared to an unaffected control cohort, which in this case was the UK10K obese cohort consisting of 982 subjects. The weighted burden test provides a rapid method for combined analysis of common and rare variants within a gene of interest. Considering all the variants of a gene when looking for association with disease can be deemed more appropriate as it models the biological reality that a number of different variants may separately impact on the function of a gene (Curtis, 2012).

Briefly, the raw data was processed by a custom-built programme developed by Dr. Dave Curtis (geneVarAssoc, unpublished). Variants from all SCZ transcripts found in either *Cyfip1* or *Cyfip2* were extracted and the programme generated a prediction about the effect of each variant on the protein product. The programme used the reference sequence and the coordinates of all the exons, along with transcription start and end points of the gene of interest as provided by the online resource RefSeq (Pruitt et al., 2014). With this information the programme was then simply able to resolve whether each variant was a nonsense, nonsynonymous or synonymous variant and was capable of predicting the consequence of each variant on the protein product based on the effect the variant had on the amino acid code. Where there were multiple transcripts, and hence multiple possible effects, the most severe effect is described.

The weighted burden test was then ran on the input files produced from the geneVaAssoc programme using another custom-built software (SCOREASSOC (Curtis, 2012)). A narrow category of variants restricted to non-synonymous (NS), splice-site or nonsense variants having a minor allele frequency (MAF)<0.1 in either cases or control were selected for further analysis. Narrow category variants for *Cyfip1*

are listed in Appendix B. Each variant was given a weight so that variants deemed more likely to have an effect on gene expression or protein function were allocated higher weights. Nonsense variants were given a higher weight than NS variants, which were given a higher weight than splice-site variants. Likewise, rarer variants were given a higher weight than common variants. An overall weight for each variant was calculated by multiplying these values together. Each subject was then assigned a score consisting of the sum of the weights of all the variants within the gene of interest possessed by that subject (Curtis, 2012). The average scores were compared between SCZ cases and unaffected controls. This analysis revealed that the average score for *Cyfip1* was significantly higher in cases compared to controls demonstrating that cases had an excess of rare, potentially damaging variants in *Cyfip1* (mean score: control, 1.904; cases, 2.415; $t(2372\ df) = 1.658$; $p<0.05$). There was no significant difference in the scores for *Cyfip2*.

To identify if individual *Cyfip1* variants were associated with SCZ a compiled list of all the NS variants, that had a higher MAF in cases compared to control, were analysed. NS variants were studied as any interesting variants could be cloned into expression vectors and used for downstream functional analysis in biological systems. Variants with a higher occurrence in cases than control had more potential of being pathogenic. The genotypes of these variants were studied and compared to the unaffected control group. Chi squared tests were carried out to determine if the observed genotyping for each variant was significantly different between cases and control. Interestingly, of these variants some stood out. A variant at position 15:22963816 occurred in seven cases and was not seen in the unaffected subjects. This variant yielded a significant association with SCZ ($p<0.05$). Variants 15:22963869, 15:22990087 and 15:22993121 were somewhat commoner among cases but did not individually show significant association with SCZ. That said, variant 15:22990087 showed a trend towards significance ($p=0.078$). There was a general excess of singleton variants among SCZ cases, which contributed to the overall p value produced by SCOREASSOC (Table 4.1).

To add further strength to these initial findings, the *Cyfip1* variants were genotyped in an independent SCZ case-control cohort to determine if the results from the UK10K analysis could be replicated. SCZ patient DNA and control samples were available within the Division of Psychiatry at UCL and genotyped in collaboration with Dr. Andrew McQuillin. Screening the UCL cohort for all the identified CYFIP1 variants

Table 4.1: Non-synonymous *Cyfip1* variants identified from the UK10K whole exome sequencing data analysis.

Variant ID	Unaffected Genotypes				Case Genotypes				Allele Change	Residue Change	Residue Number	Functional prediction	p value
	AA	AB	BB	MAF	AA	AB	BB	MAF					
22928169	982	0	0	0	1391	1	0	0.0004	cTg/cCg	L/P	83	probably damaging	NS
22933848	982	0	0	0	1391	1	0	0.0004	aCg/aTg	T/M	256	possibly damaging	NS
22940807	982	0	0	0	1390	2	0	0.0007	Cgc/Tgc	R/C	358	possibly damaging	NS
22947019	982	0	0	0	1390	2	0	0.0007	aGc/aAc	S/N	431	benign	NS
22947045	982	0	0	0	1391	1	0	0.0004	Cgc/Tgc	R/C	440	probably damaging	NS
22954273	982	0	0	0	1391	1	0	0.0004	Gcc/Acc	A/T	475	benign	NS
22954276	982	0	0	0	1391	1	0	0.0004	Atc/Gtc	I/V	476	possibly damaging	NS
22956358	982	0	0	0	1391	1	0	0.0004	tCt/tTt	S/F	-	unknown	NS
22963782	982	0	0	0	1391	1	0	0.0004	Cgt/Agt	R/S	766	benign	NS
22963816	982	0	0	0	1385	7	0	0.0025	tAt/tGt	Y/C	777	benign	0.026
22963869	976	6	0	0.0031	1377	15	0	0.0054	Ata/Gta	I/V	795	probably damaging	0.234
22969215	982	0	0	0	1391	1	0	0.0004	cGg/cAg	R/Q	814	benign	NS
22969251	982	0	0	0	1391	1	0	0.0004	cGg/cAg	R/Q	826	possibly damaging	NS
22969353	982	0	0	0	1391	1	0	0.0004	tCt/tGt	S/C	860	probably damaging	NS
22990087	975	7	0	0.0036	1371	21	0	0.0075	Ggc/Agc	G/S	903	benign	0.078
22993121	954	27	1	0.0148	1340	51	1	0.019	gCc/gTc	A/V	1003	possibly damaging	0.266
22999403	980	2	0	0.001	1391	1	0	0.0004	aTg/aCg	M/T	1092	benign	NS
22999457	982	0	0	0	1391	1	0	0.0004	cGc/cAc	R/H	1110	benign	NS
23002888	982	0	0	0	1391	1	0	0.0004	Atg/Gtg	M/V	1204	benign	NS

Non-synonymous variants taken from the SCOREASSOC output for the analysis of *Cyfip1* treating SCZ subjects from the UK10K project as cases and obese subjects as unaffected. The table shows genotype counts, MAF, allelic and residue changes and predicted functional effects. Significant association for each variant with SCZ was tested using the chi squared test, *p<0.05.

listed in Table 1 was unfeasible due to time constraints therefore, a shortlist of five was created based on their likelihood of being functionally damaging. Certain criteria were considered when making the shortlist. Firstly, variants which fell within functionally interesting domains of the protein were considered. Indeed, Chapter 3 of this thesis has suggested that the actin regulatory role of CYFIP1 may be critical for its effect on dendritic morphology and synaptic maintenance, both processes which when disrupted have been implicated in SCZ pathogenesis (Broadbelt et al., 2002; Garey et al., 1998; Glantz and Lewis, 2000). Therefore, using the previously published structure of CYFIP1 in the WRC and information about essential residues for binding (Figure 4.1A,B) (Chen et al., 2010b), variants which caused an amino acid change in a region of CYFIP1 critical for its interaction with other WRC proteins were identified. Secondly, the type of amino acid change which was incurred by the genetic variation was considered.

Five variants were shortlisted (Figure 4.1C) and from here in are named SNP1-5. Two of the variants caused amino acid changes within the Rac1 binding domain of CYFIP1. SNP1 results in a serine at residue 431 being mutated to an asparagine (S431N). Although this variant does not cause a change in the charge of the residue and was predicted to be benign it is in close proximity to a published Rac1 interacting residue 434 and therefore still of interest. SNP2 was predicted to be probably damaging and results in a positively-charged arginine at residue 440 being mutated to a cysteine which contains a sulphide group capable of forming disulphide bonds (R440C). Again this residue is close to a residue critical for Rac1 binding and could therefore impact on active Rac1-dependent CYFIP1 conformational changes. Three of the SNPs caused amino acid changes in the WAVE binding domain. SNP3 and SNP5 result in positively charged arginine residues being mutated to uncharged serine and glutamine residues respectively (R766S, R826Q). SNP4 mutates a tyrosine, capable of undergoing phosphorylation, to a cysteine which instead can form disulphide bonds (Y777C). SNP3 and SNP4 were predicted to be benign whereas SNP5 was predicted to be possibly damaging. By studying the WRC structure all three variants occur at residues that fall within close proximity to either a CYFIP1 WAVE interacting residue, or they appear to be important in the WAVE binding pocket formed by CYFIP1 (Figure 4.1B).

These five SNPs were then genotyped in the UCL SCZ case-control samples consisting of ~1300 control and ~900 case samples. To do this, specific primers to detect both

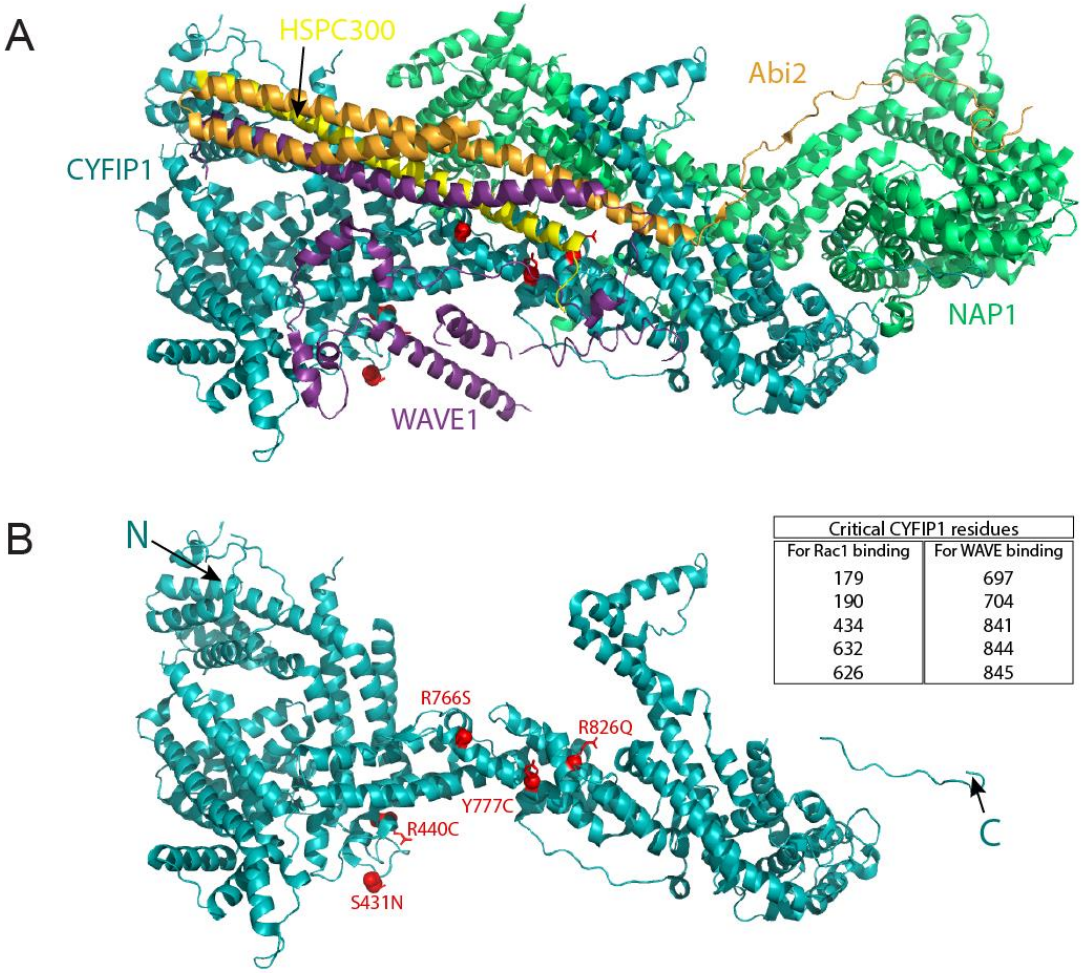

C

Name	Variant ID	MAF in unaffected	Case Genotypes			MAF in cases	Allele Change	Residue Change	Residue	Protein domain
			AA	AB	BB					
SNP1	22947019	0	1390	2	0	0.000718	aGc/aAc	S/N	431	Rac1 binding domain
SNP2	22947045	0	1391	1	0	0.000359	Cgc/Tgc	R/C	440	Rac1 binding domain
SNP3	22963782	0	1391	1	0	0.000359	Cgt/Agt	R/S	766	WAVE binding domain
SNP4	22963816	0	1385	7	0	0.002514	tAt/tGt	Y/C	777	WAVE binding domain
SNP5	22969251	0	1391	1	0	0.000359	cGg/cAg	R/Q	826	WAVE binding domain

Figure 4.1: Description of the 5 shortlisted SCZ-associated CYFIP1 SNPs.

(A) The crystal structure of CYFIP1 in the WRC generated in Pymol (The PyMOL Molecular Graphics System, Version 1.7.4 Schrödinger, LLC) using the published 2.3 ångstrom structure of the WRC (Chen et al., 2010b). The proteins of the complex are coloured as follows: CYFIP1, cyan; NAP1, green; WAVE1, purple; Abi1, orange; HSPC300, yellow. **(B)** The crystal structure of CYFIP1 in the WRC alone with the 5 shortlisted SCZ-associated SNPs highlighted in red, selected based on their proximity to previously described predicted Rac1 interacting residues and residues critical for WAVE1 binding (inset). **(C)** A summary of the 5 shortlisted SNPs highlighting whether they are predicted to interfere with the Rac1 or WAVE binding capability of CYFIP1.

the WT allele and the mutant allele were designed and the KASPar endpoint genotyping method was carried out (see page 83). Unfortunately, the primers for SNP1 could not be suitably optimised for genotyping in the time available and therefore only SNP2-5 were genotyped (Table 4.2). Of the four SNPs genotyped, SNP3 occurred in one case and in no control samples. Genotyping SNP4 revealed there were two heterozygous cases and one homozygous case but also two heterozygous controls. Although both these SNPs occurred more frequently in cases, these numbers were too small to be statistically significant. Interestingly, these genotyping results show consistencies with the UK10K data. The MAFs for SNP3 and SNP5 are similar in both screens and SNP4 which was the variant closest to being significantly associated with SCZ showed a significant association in the UK10K data. SNP2 and SNP5 did not occur in the UCL cohort.

Taken together, although incredibly rare, all five candidate variants have been identified in a patient with SCZ either in the UCL or the UK10K cohort. Moreover, the MAFs of the variants genotyped in the UCL cohort were consistent with the UK10K data, thus, validating the UK10K results. Importantly, SNP4 shows a significant association with SCZ when a large dataset such as the UK10K is analysed and also shows a consistently greater number of affected cases than controls in the UCL cohort although this result does not yield a significant association.

Table 4.2: Genotyping of candidate *Cyfip1* variants in the UCL SCZ cohort.

Name	Control Genotypes				Case Genotypes				Odds Ratio	p value
	AA	AB	BB	MAF	AA	AB	BB	MAF		
SNP2	1290	0	0	0	909	0	0	0	-	-
SNP3	1287	0	0	0	910	1	0	0.00055	-	0.444
SNP4	1312	2	0	0.00076	893	2	1	0.00223	2.937	0.192
SNP5	1291	0	0	0	923	0	0	0	-	-

4.2.2 Generation and neuronal localisation of candidate SCZ-associated CYFIP1 variants

Amino acid mutations at critical residues in a protein can lead to conformational changes in the protein structure that have the potential to result in altered protein function or inhibit protein-protein interactions. To determine whether the five candidate SCZ-associated variants studied in this chapter resulted in any functional

consequences the CYFIP1 mutants were generated on the human wild-type CYFIP1 cDNA backbone.

Site-directed mutagenesis was carried out on the pENTR_CYFIP1 vector to introduce the mutations into the cDNA which were then confirmed with sequencing. The Gateway Cloning System was then used to clone the wild-type and the CYFIP1 mutants into the pDESTeGFP-N1 mammalian expression vector which contained a C-terminal GFP tag. The CYFIP1 constructs were then transfected into COS-7 cells to confirm expression of the tagged proteins in a mammalian system. Confocal microscopy revealed the GFP tagged proteins were readily expressed and that the CYIFP1^{GFP} SNP constructs displayed a cytosolic localisation similar to WT CYFIP1^{GFP} (Figure 4.2A). Samples of COS-7 cells transfected with the CYFIP1^{GFP} SNP constructs were also subjected to SDS-PAGE and western blotting. When the membrane was probed for GFP a band was detected for WT CYFIP1^{GFP} and all five SNPs at ~175kDa corresponding to the expected weight of CYFIP1 plus GFP. No band was detected in the untransfected control lane indicating that this band was specific to the transfected cells. To confirm the band was indeed exogenously expressed CYFIP1 the same samples were probed with a CYFIP1 specific antibody. This antibody revealed an identical band at ~175kDa for each sample that was not present in the untransfected control lane demonstrating that these bands were CYFIP1^{GFP} constructs. Endogenous CYFIP1 could also be detected with the CYFIP1 specific antibody in all lanes at ~145kDa (Figure 4.2B). Interestingly, CYFIP1^{GFP} SNP1 expression was reduced compared to the other variants suggesting this point mutation may impact on protein expression or stability.

The subcellular localisation of a protein can provide insights into how that protein functions. Furthermore, if the normal localisation of a protein is disrupted it is likely to indicate that the function of the protein has been altered or the protein can no longer be targeted correctly perhaps due to disrupted protein-protein interactions. In Chapter 3 the excitatory and inhibitory synaptic enrichment of CYFIP1 was demonstrated and CYFIP1 was shown to be important in both excitatory and inhibitory synaptic maintenance. Having determined all five CYFIP1 variants are readily expressed in mammalian cells it was therefore, interesting to investigate if the neuronal subcellular localisation of these CYFIP1 variants was altered.

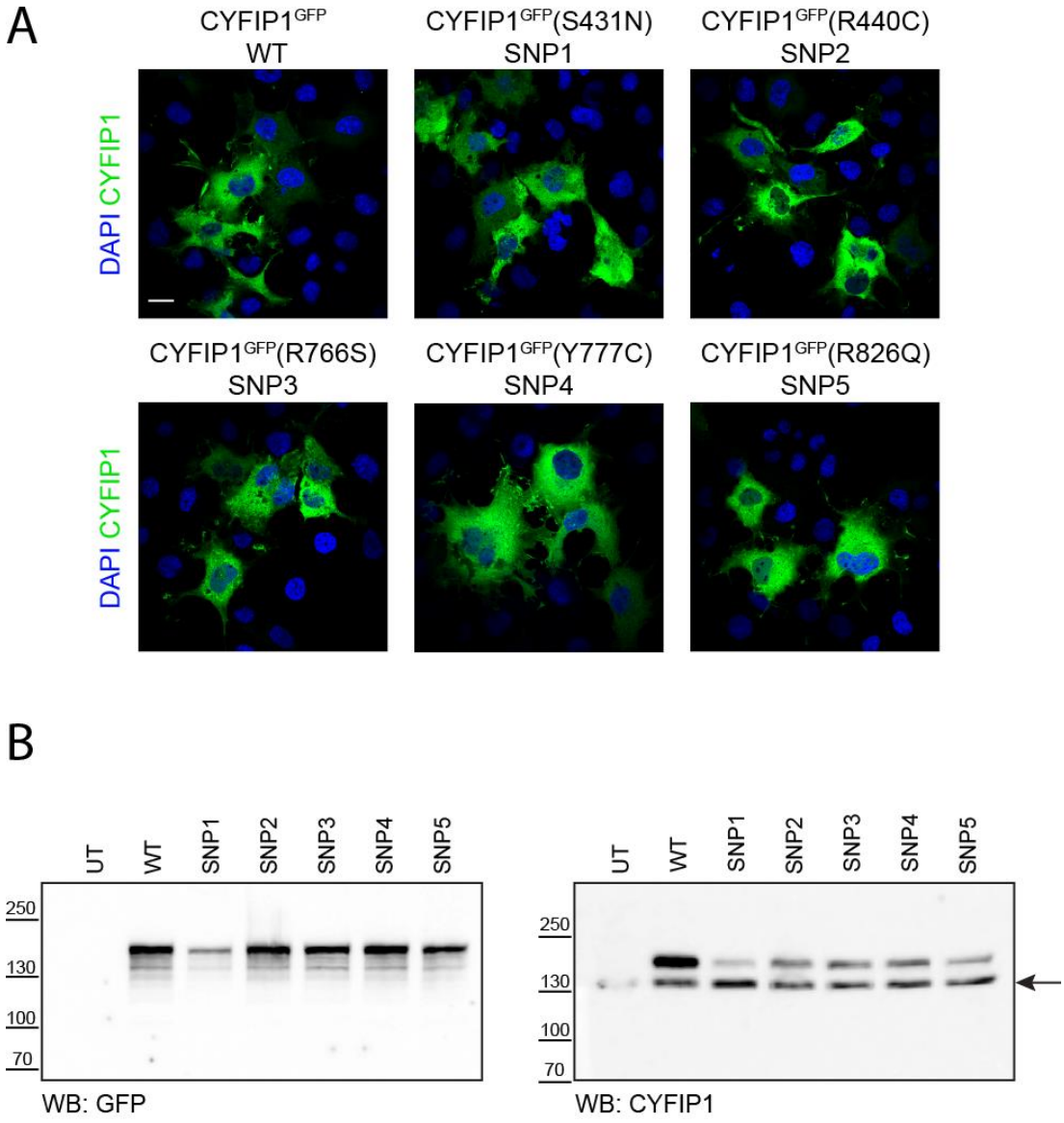

Figure 4.2: Cloning and characterisation of GFP-tagged CYFIP1 SCZ-associated variants.

(A) Transfection of COS-7 cells with human WT CYFIP1^{GFP} or CYFIP1^{GFP} SCZ-associated variants S431N (SNP1), R440C (SNP2), R766S (SNP3), Y777C (SNP4) and R826Q (SNP5). Strong GFP signal confirms that these fusion proteins are readily expressed. Scale bar, 20µm. **(B)** Western blotting of untransfected (UT), WT CYFIP1^{GFP} or CYFIP1^{GFP} SNPs 1-5 transfected COS-7 cell lysates and probing for GFP (left panel) confirms that these constructs generate fusion proteins of the expected molecular weight ~175 kDa. Probing for CYFIP1 (right panel) confirmed the five variants of CYFIP1 could still be detected with a specific anti-CYFIP1 antibody producing a band for CYFIP1^{GFP} alone at ~175 kDa and a band for endogenous CYFIP1 at ~145 kDa (arrow).

CYFIP1^{GFP} SNPs were individually transfected into mature hippocampal rat neurons. Neurons were fixed after three days transfection and stained with a GFP antibody to amplify the GFP signal and either excitatory or inhibitory synaptic markers. All five CYFIP1^{GFP} SNP constructs were present in the dendrites, soma and axon of hippocampal neurons similarly to WT CYFIP1 (Figure 4.3A; Figure 3.4; Figure 3.13). Interestingly, compared to the pDEST47_CYFIP1^{GFP} vector used throughout Chapter 3 the expression pattern for all the pDESTeGFP-N1_CYFIP1 constructs was more diffuse along the dendrites probably due to the increased expression efficiency of this vector. Nevertheless, using high-resolution confocal zoom images to look in more detail at the dendrites and their synapses all the CYFIP1 variants appeared partially clustered with an uneven distribution along the dendritic shaft. Strikingly, all the CYFIP1^{GFP} SNPs appeared to be present in dendritic spines and colocalised with the post excitatory synaptic marker Homer opposed to the presynaptic marker vGlut in the same way as has been described for WT CYFIP1^{GFP} (Figure 4.3B; Figure 3.4). The zoom confocal images also revealed that the distribution of CYFIP1 variants overlapped with inhibitory synapses. In Chapter 3, a clear enrichment of WT CYFIP1 was visible at inhibitory synapses (Figure 3.13). However, due to the different vector backbone and the more diffuse expression pattern of the CYFIP1^{GFP} SNPs, further quantification would be required to conclude an inhibitory synaptic enrichment of these variants. Even so, the CYFIP1^{GFP} SNPs were detected at gephyrin positive inhibitory postsynaptic sites opposed to the presynaptic marker, vGAT (Figure 4.4). Therefore, if not enriched, these variants are at least present at inhibitory synapses. Taken together, the CYFIP1 SCZ-associated variants do not appear to modify the subcellular localisation of CYFIP1^{GFP} in neurons. This suggests that if the mutations are impacting on CYFIP1 function they are most likely having more subtle effects on protein function and not disrupting its localisation.

4.2.3 The effect of candidate SCZ-associated CYFIP1 variants on protein interactions

The candidate SCZ-associated CYFIP1 variants were selected partly because the mutation caused an amino acid change within a region of CYFIP1 predicted to be important for its interaction with either Rac1 or WAVE in the WRC (Figure 4.5A). To directly test whether the CYFIP1 variants altered these protein interactions coimmunoprecipitation experiments were carried out in HEK293 cells overexpressing the CYFIP1^{GFP} SNP constructs. HEK293 cells are a human embryonic

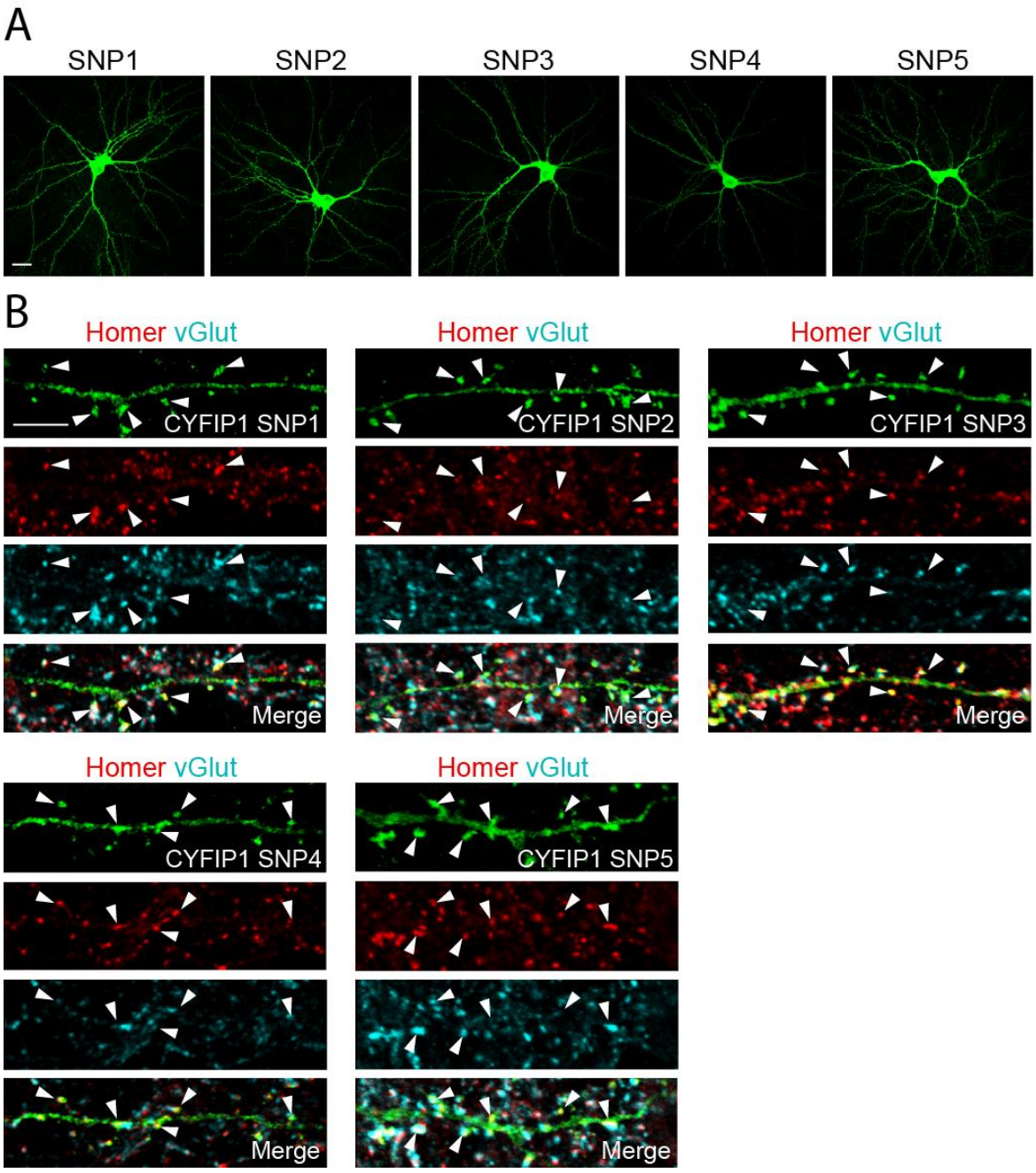

Figure 4.3: CYFIP1 SCZ-associated variants are located at excitatory synapses.

(A) Five SCZ-associated GFP-tagged variants of CYFIP1 (SNP1-5) were transfected into mature rat hippocampal neurons. CYFIP1 variants are detected in the soma, dendrites and axon. **(B)** Neurons were stained with antibodies against the pre and postsynaptic excitatory markers vGlut and Homer respectively. CYFIP1 SNP variants show a punctate distribution along dendrites and an enrichment in dendritic spines. Each variant colocalised with the excitatory synaptic markers within dendritic spines (arrowheads). Scale bars, 20µm, 2µm.

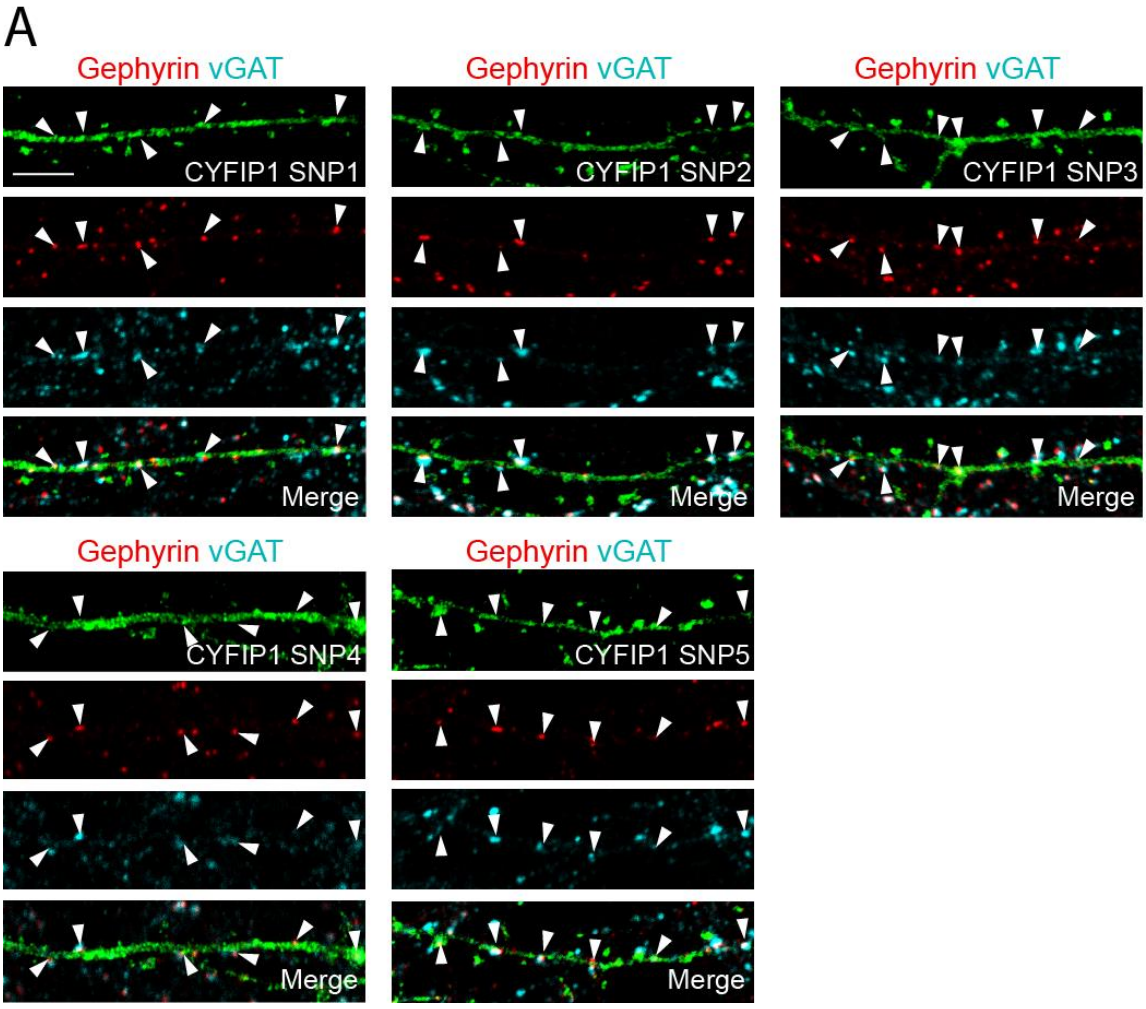

Figure 4.4: CYFIP1 SCZ-associated variants are localised at inhibitory synapses.

(A) Five SCZ-associated GFP-tagged variants of CYFIP1 (SNP1-5) were transfected into mature rat hippocampal neurons. Neurons were stained with antibodies against the inhibitory pre and postsynaptic markers vGAT and gephyrin respectively. CYFIP1 SNP variants showed a punctate distribution along dendrites. The variant clusters colocalised with the inhibitory synaptic markers along the dendritic shafts (arrowheads). Scale bar, 2µm.

kidney cell line. These cells were chosen so interactions between the human CYFIP1^{GFP} variants and the endogenous human WRC proteins could be analysed. Furthermore, a human cell line system is more physiologically relevant when studying SCZ-associated mutations identified from patient DNA. WT and all the CYFIP1^{GFP} SNPs could be immunoprecipitated from HEK293 cells via their GFP tag using GFP TRAP beads. Endogenous NAP1 a large protein within the WRC that forms a pseudo-symmetric dimer with CYFIP1 could be coimmunoprecipitated with all the CYFIP1^{GFP} SNP constructs. Endogenous WAVE2, a ubiquitously expressed form of WAVE, was also coimmunoprecipitated with all the CYFIP1 constructs (Figure 4.5B). Quantification over repeated experiments revealed that none of the GFP-tagged SNPs appear to interact differently with WAVE2 when compared with WT CYFIP1^{GFP} (Figure 4.5C). This suggests that the candidate SCZ-associated CYFIP1 variants do not interfere with the WAVE interaction. Rac1 could not be coimmunoprecipitated with any of the CYFIP1 constructs therefore the effects of the CYFIP1 variants on this interaction could not be tested. CYFIP1 interacts specifically with activated GTP-bound Rac1 (Kobayashi et al., 1998) therefore using drugs to stimulate Rac1 activation may push the system enough to observe this interaction by coimmunoprecipitation.

In summary, the five candidate SCZ-associated CYFIP1 variants can still be detected in the same synaptic subcellular compartments as WT CYFIP1. However, it cannot be concluded that the variants maintain the same enrichment at excitatory and inhibitory synaptic puncta without further quantification. Furthermore, the different CYFIP1 variants did not affect the interaction between CYFIP1 and WAVE. If the mutations are having an effect on CYFIP1 function then, judging by the data presented here, they are likely to be quite subtle and will only be unpicked with more sensitive assays which will require further investigation.

4.2.4 Characterisation of a CYFIP1 KO MEF cell line

The previous experiments in this chapter and those carried out in Chapter 3 have modelled CYFIP1 disease-associated genetic alterations to investigated CYFIP1 function and how it is implicated in neuropsychiatric disorders. However, in addition to modelling CYFIP1 disease-associated genetic alterations there is much to be learned about a protein by carrying out loss of function experiments using KO model systems. Constitutive CYFIP1 KO animals are embryonically lethal therefore, CYFIP1 loss of function on postnatal or adult animals cannot be studied with this mouse line.

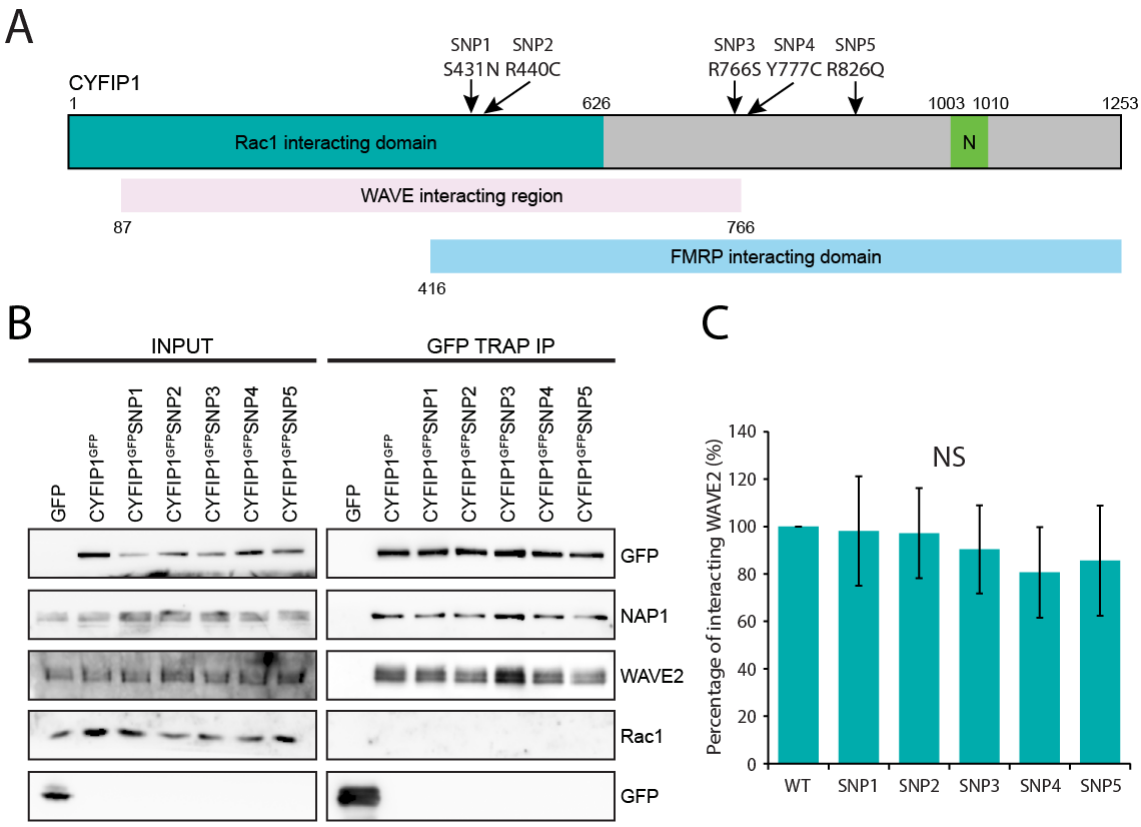

Figure 4.5: CYFIP1 SCZ-associated variants interact with WAVE.

(A) A schematic of CYFIP1 showing important protein interacting domains (N = critical NAP1 binding region) and depicting the five SCZ-associated CYFIP1 variants identified in this study. **(B)** Western blots of protein complexes coimmunoprecipitated using anti-GFP TRAP beads from HEK cells transfected with WT, SNP1, SNP2, SNP3, SNP4 or SNP5 CYFIP1^{GFP}. Input samples (Input) represent 5% of the cell lysate included in the immunoprecipitation samples (IP). Anti-GFP TRAP beads efficiently coimmunoprecipitated endogenous NAP1 and WAVE2 from CYFIP1^{GFP} transfected cell lysates but not from GFP only transfected cells. CYFIP1^{GFP} constructs were revealed with an anti-GFP antibody while anti-NAP1, anti-WAVE2 and anti-Rac1 antibodies were used to visualise endogenous NAP1, WAVE2 and Rac1 respectively. **(C)** Quantification of the amount of coimmunoprecipitated WAVE2 protein normalised to the amount of CYFIP1^{GFP} pulled down (n=7; ANOVA; NS).

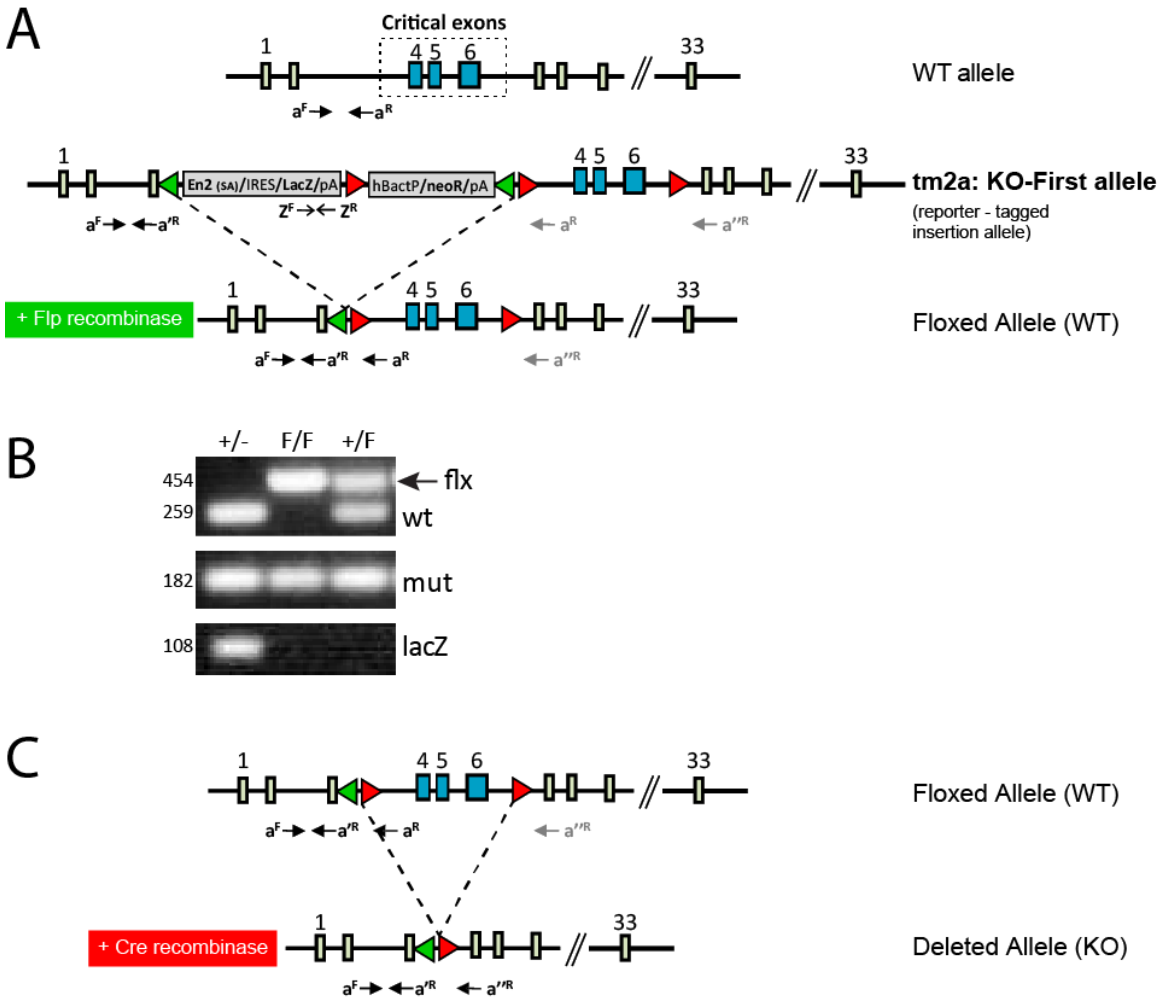

Figure 4.6: Generation of CYFIP1 floxed mice.

(A) A schematic of the knockout (KO)-first allele system, demonstrating the generation of the *Cyfip1* floxed allele following Flp recombination of the KO-first *Cyfip1* allele (tm2a allele). The KO-first allele cassettes are described in Figure 3.7. Both cassettes are bound by frt sites (green triangles). The neo cassette and 3' frt site are flanked by loxP sites with an additional distal loxP site present 3' of exon 6 (red triangles). The presence of Flp recombinase extrudes the mutant cassettes from the KO-first allele, by recombining the frt sites, reconstituting a floxed allele capable of expressing functional CYFIP1 mRNA. **(B)** Genotyping to distinguish between WT, KO-first mutant and floxed alleles (primers: a^F a^R, a^F a'^R, Z^F Z^R). From the left a heterozygous WT mutant animal (+/-) produced a wild-type (wt), mutant (mut) and lacZ PCR product. A homozygous floxed animal (F/F) produced a shifted floxed (flx) (arrow) and mut product but no lacZ as flp recombination had occurred. A heterozygous WT floxed animal (F/+) produced a WT and a floxed band from the same primers and a mutant band. **(C)** A schematic of the conditional *Cyfip1* KO strategy, depicting the deleted allele following Cre recombination of the floxed allele. The presence of Cre recombinase with the floxed allele results in the recombination of the LoxP sites (red triangles), the removal of three critical *Cyfip1* exons (blue boxes) and abolishes gene expression.

Indeed, primary neurons cannot even be cultured from constitutive CYFIP1 KO embryos as they die too early in development at E8.5. To overcome these problems, CYFIP1 can be genetic deleted in a conditional manner either dependent on the administration of a drug or the expression of a recombinase enzyme. This approach allows the study of CYFIP1 loss of function in a region and temporal specific manner thus, avoiding the need of global CYFIP1 KO which results in lethality.

The CYFIP1 transgenic mouse studied in Chapter 3 was generated using the KO-first system (Skarnes et al., 2011; White et al., 2013). As previously discussed, a LacZ cassette was inserted into the CYFIP1 gene between exons 3 and 4. This cassette disrupted the expression of CYFIP1 resulting in non-functional *Cyfip1* mRNA and expression of the reporter gene. The cassette is flanked by FRT sites which will undergo recombination and extrude the flanked mutant cassette, in the presence of Flp recombinase, reconstituting a floxed allele (Figure 4.6A). This floxed allele allows the expression of function *Cyfip1* mRNA but still contains LoxP sites flanking exons 4-6 of the CYFIP1 gene. Floxed animals were healthy and indistinguishable from WT animals. When genotyped floxed animals (F/F) generated a larger floxed product (454 bp) from the a^F and a^R primers due to the inclusion of the LoxP site. The mutant band was present and the LacZ band was lost confirming Flp recombinase deletion of the KO-first cassette had taken place (Figure 4.6B). The presence of the LoxP sites around exons 4-6 of *Cyfip1* make these floxed CYFIP1 animals KO-ready. With the expression of a different enzyme Cre recombinase (Cre) another recombination event can occur between the LoxP sites extruding the DNA encoding these three critical exons. The result is a deleted allele and loss of functional *Cyfip1* mRNA expression in a conditional manner dependent on the presence of Cre (Figure 4.6C).

Mouse embryonic fibroblasts (MEFs) are simple to generate from transgenic tissue and easy to culture. They can be transformed and passaged many times. Furthermore, unlike primary neurons, MEFs divide and undergo migration therefore, they provide an ideal system for studying CYFIP1 loss of function effects on cell motility and actin dynamics. With this in mind, attempts were made to develop CYFIP1 KO MEFs.

Crossing CYFIP1 floxed mice with Cre expressing mice will result in recombination and CYFIP1 conditional KO (cKO) cells. By regulating the expression pattern of Cre

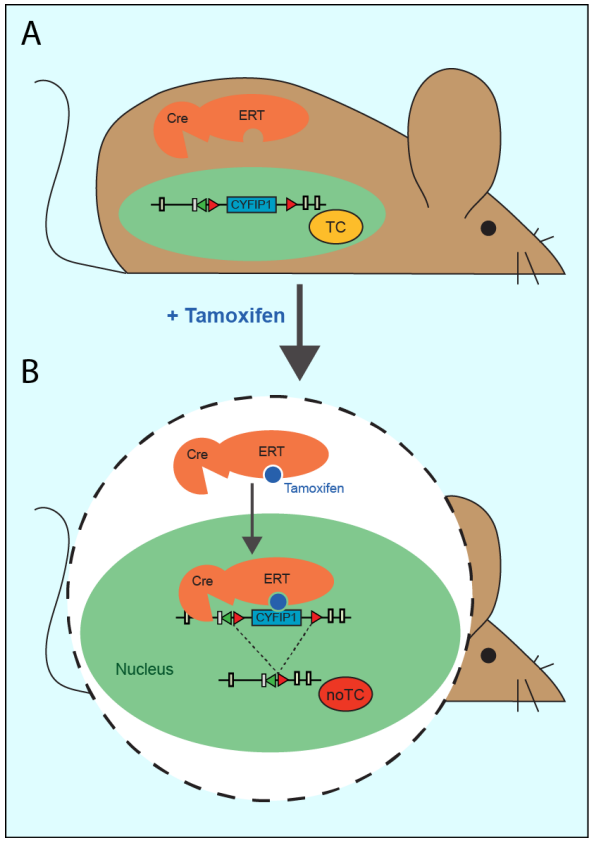

Figure 4.7: A schematic of Cre^{ERT} recombinase function.

Inducible gene inactivation using CreERT recombinase (Cre^{ERT}) is based on tamoxifen (TAM)-inducible excision of a loxP flanked gene in cells expressing TAM-dependent Cre^{ERT}. Cre^{ERT} consists of Cre fused to a mutated ligand-binding domain (LBD) of the oestrogen receptor. **(A)** Under control conditions, in the absence of TAM, Cre^{ERT} is retained in the cytoplasm. The gene of interest (CYFIP1) is transcribed and expressed as normal (TC). **(B)** Binding of TAM to the LBD induces translocation of Cre^{ERT} to the nucleus (green oval) where it can recombine its loxP flanked (red triangles) DNA substrate (CYFIP1). This results in loss of the gene of interest and no transcription or protein expression (no TC). TAM binding regulates the localisation of the Cre rather than its enzymatic activity. Spatiotemporal control of DNA removal and hence genetic knockout can be achieved by tissue specific expression of Cre^{ERT}. Adapted from (Feil et al., 2009).

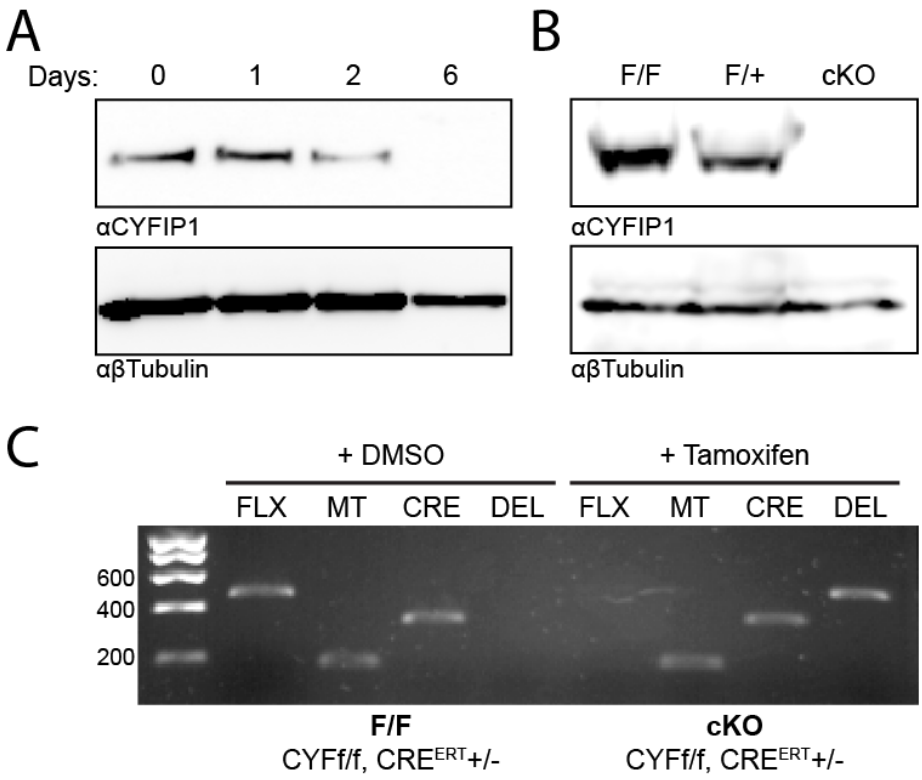

Figure 4.8: Generation of *Cyfip1* conditional knockout MEFs.

(A) Western blot showing CYFf/f Cre^{ERT}+/- MEF cell lysates either untreated (UT) or treated with 1μM TAM for 1, 2 or 6 days prior to lysis and probed with a CYFIP1-specific antibody. **(B)** Western blot showing CYFf/f Cre^{ERT}+/- (F/F), CYFf/+ Cre^{ERT}+/- (F/+) and CYFf/f Cre^{ERT}+/- (cKO) MEF cell lysates after DMSO (F/F) or TAM (F/+ and cKO) treatment. Cells were seeded sparsely and treated with 1μM TAM or DMSO following three passages before lysis. All CYFIP1 protein is lost from the cKO cell line. **(C)** PCR analysis of F/F (CYFf/f, Cre^{ERT}+/-, +DMSO) and cKO (CYFf/f, Cre^{ERT}+/-, +TAM) MEF cell DNA. Cells were genotyped with the primers a^F and a^R to produce the shifted floxed (FLX) PCR product and a^F and a'^R to produce the mutant (MT) product. Detection of these bands confirmed the presence of the floxed allele originating from the mutant KO-first allele. Primers against Cre produced a product if the Cre gene was present (CRE). Primers A^F and A''^R produced a product from the deleted allele (DEL). F/F control cells were positive for the floxed allele and Cre but lacked the deletion allele product due to no TAM induced recombination. cKO cells were positive for the deleted allele and Cre but lacked the floxed allele product confirming complete recombination had occurred with TAM treatment.

the population of cells within which CYFIP1 is removed can be controlled. Alternatively, CYFIP1 floxed mice can be crossed with mice expressing Cre under a germline promoter to induce CYFIP1 loss in all cell types. However, it is known from Chapter 3 that constitutive KO of CYFIP1 in mice is embryonically lethal and thereforethis cross would not result in any viable KO embryos for the generation of MEFs. For that reason, an inducible Cre approach was used (Feil et al., 2009). CYFIP1 floxed mice were crossed with CreER(T2) recombinase (Cre^{ERT}) mice. This form of Cre is ligand dependent and is only activated in the presence of the drug tamoxifen (TAM) (Figure 4.7) (Feil et al., 1997). MEFs were generated from Cre^{ERT} positive, CYFIP1 floxed embryos (CYFf/f, CRE^{ERT}+/-) and transformed by Prof. Josef Kittler. To characterise CYFIP1 protein turnover and determine how long after TAM treatment was required for total loss of CYFIP1 protein a time course was carried out. Seeded CYFf/f, CRE^{ERT}+/- MEFs were cultured in 1μM TAM for 1, 2 or 6 days and the amount of CYFIP1 present in the cell lysates was assayed by SDS-PAGE and western blotting. The time course revealed that after 2 days treatment with TAM almost all CYFIP1 had been lost from the cells and by day 6 CYFIP1 could not be detected by western blotting. However, treatment for 6 days appeared to cause some cell death which can be deduced from the reduction in the β-tubulin band (Figure 4.8A).

CYFIP1 cKO cells may have disrupted actin dynamics and cell division therefore, attempts were made to totally eradicated floxed MEFs from the TAM treated cultures. Any remaining CYFIP1 expressing floxed cells could be more viable and out compete the cKO cells resulting in a mixed population of floxed and cKO cells. To be sure all cells underwent recombination in the production of cKO MEFs a different treatment approach was tested. CYFf/f, CRE^{ERT}+/- MEFs were plated at a very low density and treated with 1μM TAM or vehicle DMSO control to generate cKO CYFIP1 and floxed CYFIP1 expressing MEFs respectively. Plated CYFf/+, CRE^{ERT}+/- MEFs were treated with 1μM TAM to generate CYFIP1 haploinsufficient cells. Cells were passaged three times, each time the cells were plated at a low density and retreated. The low density plating was used to ensure all cells originated from recombined cells. Following this, cells from each of the 3 conditions were lysed in sample buffer, subjected to SDS-PAGE and western blotting. Western blotting revealed that treatment of CYFf/f, CRE^{ERT}+/- MEFs with TAM in this way resulted in complete eradication of CYFIP1 levels as expected (cKO). TAM treatment of CYFf/+, CRE^{ERT}+/- cells (F/+) resulted in reduced CYFIP1 levels compared to DMSO-treated floxed cells (F/F) as would be

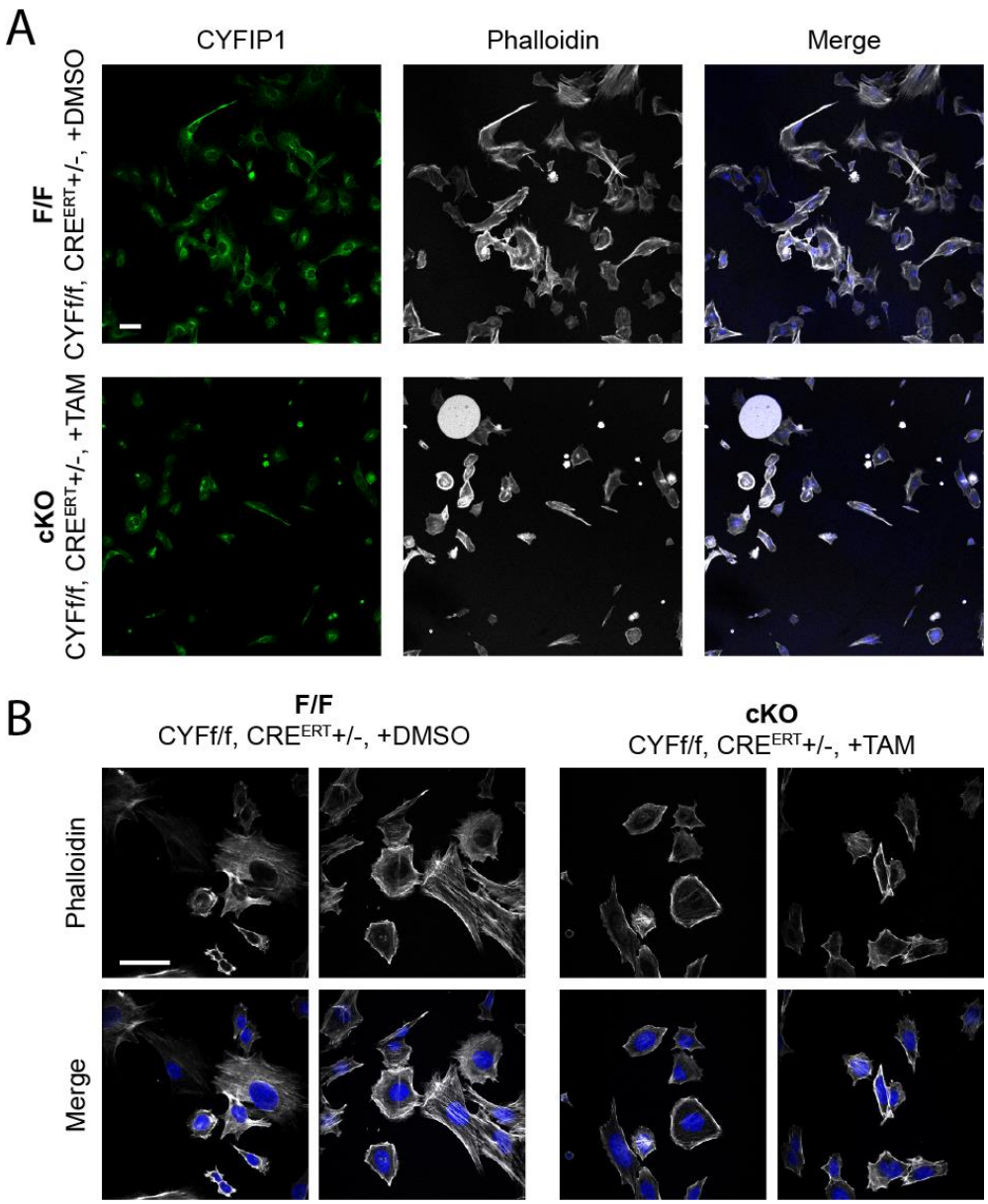

Figure 4.9: F-actin levels and morphology of CYFIP1 cKO MEFs.

(A) Confocal images of CYFIP1 F/F control (CYFf/f, Cre^{ERT}+/-, +DMSO) and cKO (CYFf/f, Cre^{ERT}+/-, +TAM) MEFs immunostained with a CYFIP1 specific antibody (green), the F-actin binding toxin phalloidin (grey) and DAPI (blue). KO cells appeared sparser, smaller and more rounded. **(B)** Zoom confocal images of the same cells highlighting the reduced phalloidin staining in the KO cells. Scale bars, 50µm.

expected for cells haploinsufficient for CYFIP1 (Figure 4.8B). For further confirmation that cKO cells had been produced DNA was extracted and genotyped by PCR. Genotyping the DMSO and TAM treated CYFf/f, CRE^{ERT}+/- cells confirmed that recombination had occurred in all the TAM treated cells. There was total loss of the floxed band, demonstrating all floxed alleles had undergone recombination. Additionally, a deletion band was present. A PCR product from the deletion primers would only be produced if LoxP recombination had occurred (Figure 4.8C).

Following production of CYFIP1 cKO MEFs, cells were plated onto glass coverslips, fixed and subjected to confocal microscopy. Cells were stained with a CYFIP1-specific antibody (Upstate) with an appropriate fluorescent secondary antibody and the F-actin binding toxin, phalloidin, conjugated to alexa-647. DAPI was used to label the cell nucleus. CYFIP1 cKO cells showed less CYFIP1 antibody staining as expected, however, the residual staining observed was unexpected and could be the result of nonspecific background staining. Both F/F and cKO cells displayed phalloidin labelling. An interesting observation noted was that the density of cKO cells was always considerably less than F/F cells suggesting that more cell death may be occurring in CYFIP1 cKO cells. cKO cells also appeared smaller and more rounded when compared to F/F CYFIP1 expressing cells (Figure 4.9A). Zoom images were acquired to analyse the distribution of F-actin more closely. Again cKO cells appeared rounder. Furthermore, the phalloidin staining seemed weaker and fewer stress fibres were present in cKO cells (Figure 4.9B). These results demonstrate that a novel CYFIP1 cKO MEF line has been generated. Initial observations suggest that cell morphology and cell viability are effected by loss of CYFIP1 perhaps due to the altered F-actin network detected.

4.2.5 Conditional deletion of CYFIP1 from mouse hippocampus and cortex

In parallel to the generation of CYFIP1 cKO MEFs, floxed mice allowed the study of CYFIP1 loss of function in neurons. As constitutive CYFIP1 KO mice died during embryogenesis, CYFIP1 must be essential for development. By knocking out CYFIP1 postnatally and specifically in neurons the function of CYFIP1 can be uncoupled from its role in development as it was predicted to overcome the embryonic lethality of constitutive CYFIP1 KO mice. In this way, CYFIP1 loss of function in adult neurons can be studies to further unpick the neuronal role of CYFIP1 and determine if CYFIP1

is important in neuronal maintenance.

To determine the consequences of CYFIP1 loss in postnatal neurons floxed CYFIP1 mice were crossed with transgenic Camkcre4 (Cre^{CAMKII}) mice (Mantamadiotis et al., 2002). These animals expressed Cre recombinase postnatally under the control of the 8.5-kb promoter fragment of the calcium/calmodulin-dependent protein kinase II- α gene (CAMKIIα). Under this promoter Cre expression has been described to be high in the forebrain including the cortex, hippocampus, striatum, thalamus and amygdala. Cre-mediated recombination has been shown to be extensive in all areas of the brain where the recombinase is expressed (Mantamadiotis et al., 2002).

Cre positive CYFIP1 floxed mice were viable, progressed to adulthood and were indistinguishable from control littermates. Observations revealed there was no gross difference in brain size between adult floxed (CYFf/f, CRE^{CAMKII}-/-), heterozygous (CYFf/+, CRE^{CAMKII}+/-) and cKO (CYFf/f, CRE^{CAMKII}+/-) CYFIP1 animals (Figure 4.10A). The hemispheres, cerebellum and olfactory bulbs were all of an equivalent size when genotypes were compared. Adult floxed and cKO brains were dissected and tissue from the cortex and hippocampus was prepared into cell lysates for SDS-PAGE and western blotting. DNA was also extracted from floxed and cKO hippocampal tissue and genotyped using PCR (Figure 4.10B). As expected the floxed DNA samples produced a floxed band and mutant band demonstrating the presence of the floxed CYFIP1 alleles containing the LoxP sites. A band for Cre was not detected and therefore no deletion band was detected. The cKO sample on the other hand, produced a Cre band indicating the presence of Cre in the hippocampal tissue and a deletion band demonstrating that recombination and KO of the CYFIP1 gene had occurred. However, the floxed band was still present highlighting that the hippocampal DNA sample contained a mixed population of cells, some with the critical exons deleted and others remaining floxed. This was to be expected due to the neuronal specific expression pattern of CAMKIIα promoter which is not expressed in non-neuronal cell types.

When western blots of hippocampal and cortical lysates were probed for CYFIP1 a reduction in the amount of protein was observed in cKO tissue (Figure 4.10C). Quantification revealed a significant 25% reduction in CYFIP1 protein levels in the cortex and a 50% reduction of CYFIP1 levels in the hippocampus compared to floxed

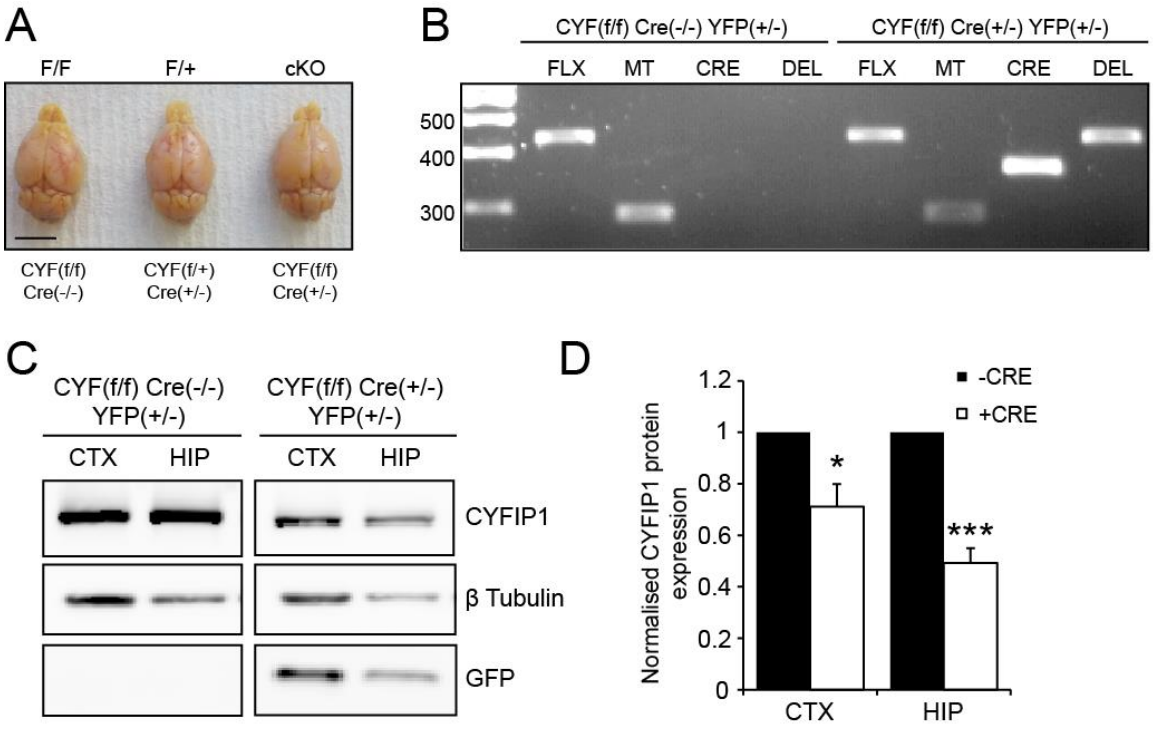

Figure 4.10: Characterisation of CYFIP1 Cre^{CAMKII} cKO mice.

(A) Example brains from CYFIP1 floxed control (F/F; CYFf/f, Cre^{CAMKII}-/-), conditional haploinsufficient (F/+; CYFf/+, Cre^{CAMKII}+/-) and conditional KO (cKO; CYFf/f, Cre^{CAMKII}+/-) adult mice. Scale bar, 5mm. **(B)** Genotyping of hippocampal tissue from control floxed (CYFf/f, Cre^{CAMKII}-/-, YFP+/-) and cKO (CYFf/f, Cre^{CAMKII}+/-, YFP+/-) animals by PCR. DNA was genotyped with the primers a^F and a^R to produce the shifted floxed (FLX) PRC product and a^F and a'^R to produce the mutant (MT) product. Detection of these bands confirmed the presence of the floxed allele originating from the mutant KO-first allele. Primers against Cre produced a product if the Cre gene was present (CRE). Primers A^F and A''^R produced a product from the deleted allele (DEL). Floxed control DNA (CYFf/f, Cre^{CAMKII}-/-, YFP+/-) was positive for the floxed allele but lacked the deletion allele due to the lack of Cre induced recombination. cKO DNA (CYFf/f, Cre^{CAMKII}+/-, YFP+/-) was positive for Cre and the floxed allele therefore was also positive for the deletion allele. **(C)** Western blot analysis and **(D)** quantification of CYFf/f Cre^{CAMKII}-/- YFP+/- (-CRE) and CYFf/f Cre^{CAMKII}+/- YFP+/- (+CRE) adult brain region lysates probed with antibodies against CYFIP1, the loading control β-tubulin and GFP to detect YFP expression as a reporter for Cre recombinase activity. cKO brains had ~30% less CYFIP1 in the cortex (CTX) and ~50% less CYFIP1 in the hippocampus (HIP) (n=3; student's unpaired t-test; *p<0.05, ***p<0.001).

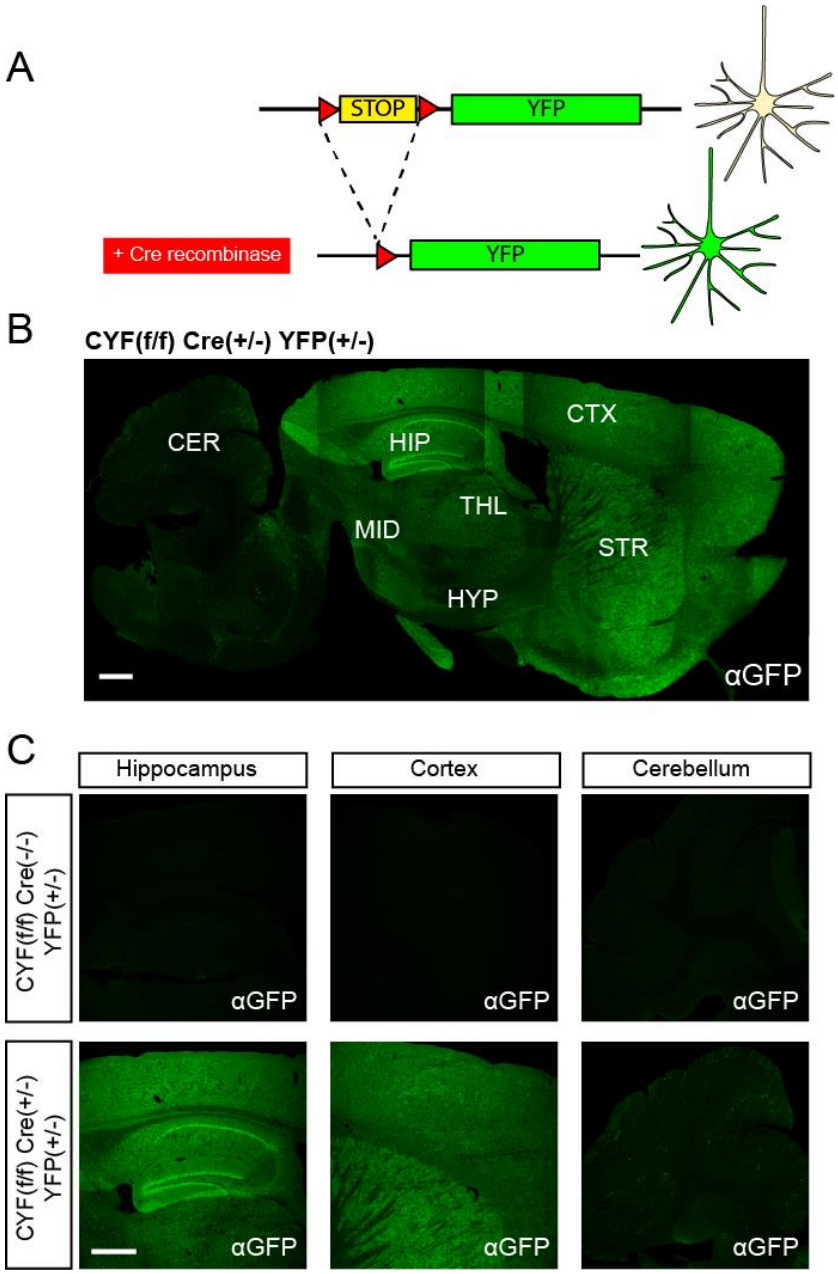

Figure 4.11: Cre^{CAMKII} expression in CYFIP1 floxed mice.

(A) Schematic of the floxed STOP YFP gene in the Rosa26 locus depicting Cre induced expression of YFP and the production of labelled cells. **(B)** Immunohistochemistry of CYFf/f Cre^{CAMKII}+/- YFP+/- (cKO) adult mouse sagittal 30µm brain section. Slices were stained with a GFP antibody to detect YFP expression as a reporter for Cre recombinase expression and activity. YFP expression was detected in the prefrontal brain demonstrating Cre activity in the hippocampus (HIP), cortex (CTX), striatum (STR), thalamus (THL), hypothalamus (HYP) and midbrain (MID) with less activity in the cerebeluum (CER). **(C)** Zoomed images of floxed control (CYFf/f Cre^{CAMKII}-/- YFP+/-) and cKO (CYFf/f Cre^{CAMKII}+/- YFP+/-) adult mouse sagittal brains sections stained with anti-GFP. YFP could not be detected in floxed control brains. YFP was detected in cKO brains in the hippocampus and cortex with little detection in the cerebellum. Scale bars, 500µm.

control samples (Figure 4.10D) (cortex: WT, 100%; cKO, 71.18 ± 8.69%; hippocampus: WT, 100%; cKO, 49.93 ± 5.69%; *p<0.05, ***p<0.001). These mice were also crossed with a YFP Rosa26 reporter mouse line to incorporate a reporter allele for Cre expression into their genome (Ribeiro et al., 2013). YFP Rosa26 reporter mice contain the gene encoding YFP (yellow fluorescent protein) within the Rosa26 locus following a LoxP flanked STOP site. Therefore, Cre expression would extrude the STOP site and YFP would be expressed (Figure 4.11A). Expression of YFP was confirmed by probing the hippocampal and cortical lysate western blots with an antibody to GFP (Figure 4.10C). As expected no YFP was detected in the Cre negative floxed samples while in the cKO tissue YFP was detected in the cortex and hippocampus.

Consistent with this finding, immunohistochemistry on 30µm sagittal sections from CYFIP1 cKO brain (CYFf/f, Cre^{CAMKII}+/-, YFP+/-) using a GFP antibody revealed the expression pattern and recombination efficiency of Cre driven by the CAMKIIα promoter. YFP could be detected throughout the hippocampus and cortex as well as in the striatum, thalamus and midbrain regions. However, little YFP expression was found in the cerebellum (Figure 4.11B,C). Control animals showed no YFP illustrating the specificity of the Cre induced YFP expression (Figure 4.11C). This pattern of Cre expression is consistent with previous publications using this camkcre4 transgenic mouse strain (Mantamadiotis et al., 2002).

4.2.6 Conditional deletion of CYFIP1 alters hippocampal dendritic morphology *in vivo*

Here a postnatal neuronal specific CYFIP1 cKO mouse model has been generated and characterised. As an extension of the experiments carried out in Chapter 3, it was interesting to study the effect complete loss of CYFIP1 in neurons had on hippocampal dendritic morphology. Comparisons could then be made between the CYFIP1 haploinsufficient and cKO models. Analysis of dendritic morphology was carried out in Golgi stained 150µm coronal brain slices. Pyramidal CA1 neurons were traced from 6 month old floxed and CYFIP1 cKO brains using Neurolucida software and traces were subjected to Sholl analysis (Sholl, 1953) (Figure 4.12A). Briefly, concentric rings were drawn out equal distance apart from the cell soma and the number of dendrites that intersect each ring were plotted as a function of distance from the soma. This analysis generates a readout for dendritic complexity. The dendritic trace also allowed

other parameters such as total dendritic length and total number of branch points to be measured. In the CYFIP1 cKO neurons a small effect on morphology was observed in basal dendrites, however, when corrections were made for multiple comparisons this effect was not significant (Figure 4.12B). That said, when considered alone, cKO neurons were significantly more complex 60μm away from the soma (Figure 4.12C) (intersections: floxed, 10.78 ± 0.36; cKO, 12.82 ± 0.64; *$p<0.05$). This effect did not translate into an overall change in the total number of branch points or total dendritic length per cell (Figure 4.12D,E) (branch points: WT, 32.11 ± 3.32; cKO, 30.64 ± 2.34; length: WT, 2921.52 ± 164.84μm; cKO, 3035.95 ± 131.28μm; NS). This experiment would benefit from increasing the sample size to more convincingly demonstrate an effect on morphology. Intriguingly, CYFIP1 haploinsufficiency resulted in the opposite effect and caused a decrease in dendritic complexity, both in cultured neurons and in CA1 pyramidal neurons from Golgi-stained adult brains (Figure 3.8; Appendix A; work carried out by Dr. Manav Pathania). The contrasting effects on dendritic morphology between CYFIP1 postnatal cKO and constitutive haploinsufficient neurons suggest a role for CYFIP1 in non-neuronal cells when considering the regulation of dendritic morphology or perhaps CYFIP1 plays different roles in dendritic development and maintenance.

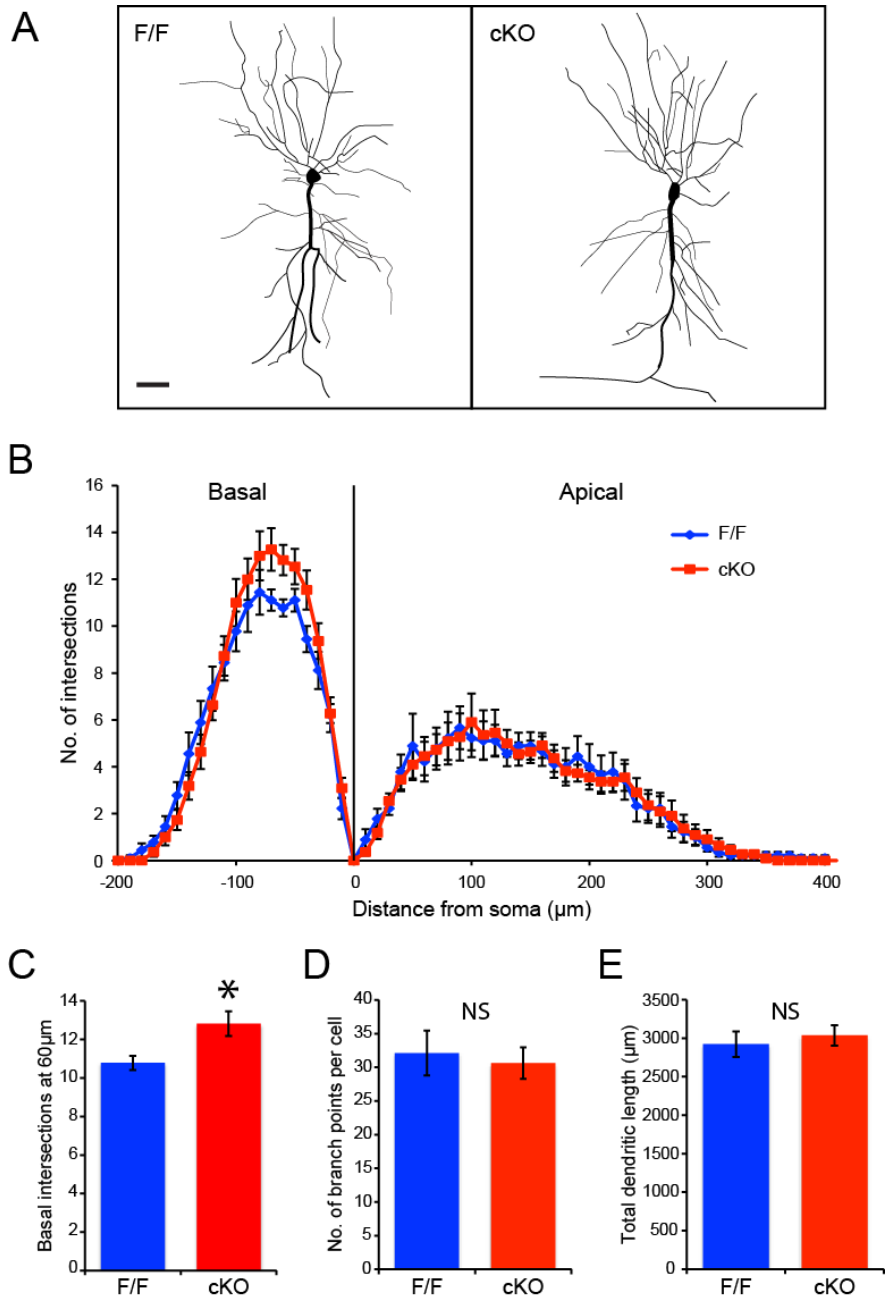

Figure 4.12: cKO of CYFIP1 alters basal dendritic morphology of CA1 pyramidal neurons.

Golgi stained CA1 neurons from 6 month old cKO (CYFf/f Cre^{CAMKII}+/-) and floxed (CYFf/f Cre^{CAMKII}-/-) littermate controls were traced to analyse dendritic morphology. **(A)** Example traces of cKO and floxed (F/F) neurons. Scale bar, 35µm. **(B)** Quantification of dendritic complexity using Sholl analysis indicates that there is no significant difference between cKO and floxed neurons when data is corrected for multiple comparisons (n=9-11; 2-way ANOVA; NS). However, when considered alone the cKO basal dendrites appear more complex at 60µm compared with floxed neurons **(C)** (n=9-11; student's unpaired t-test; *p<0.05). **(D)** Total number of branch points and **(E)** total dendritic length per cell was unchanged between cKO and floxed (F/F) CA1 neurons (n=9-11; student's unpaired t-test; NS).

4.3 Discussion

In this chapter, application of the weighted burden test to the UK10K whole-exome sequencing database of SCZ patients revealed *Cyfip1* as a SCZ-associated gene due to an excess of potentially damaging rare variants identified within the gene. Furthermore, one individual CYFIP1 variant at position 15:22963816 was shown to be significantly associated with SCZ. A shortlist of five candidate CYFIP1 SCZ-associated variants were generated for functional characterisation based on the amino acid change and the position within the protein of the altered residue brought about by the non-synonymous mutation. Four of these five SNPs were genotyped in an independent UCL SCZ patient cohort to confirm their association with the disease. Although no variants yielded significance SNP4 appeared promising mirroring the significant association of this SNP with SCZ observed in the UK10K database. The five CYFIP1 rare variants chosen for functional characterisation included potentially two Rac1 and three WAVE interacting mutants. However, none of these variants appeared to alter CYFIP1's synaptic localisation or interaction with WAVE.

Finally, two CYFIP1 cKO systems were characterised to further understand the neuronal role of CYFIP1 by studying loss of function. Initial observations revealed CYFIP1 cKO MEFs showed a decreased cell density compared to floxed control cells suggesting altered survival rates. Furthermore, actin subcellular structure appeared disrupted in cKO cells resulting in a smaller more rounded cell morphology. CYFIP1 cKO in forebrain neurons resulted in a 50% reduction in hippocampal CYFIP1 protein levels and when dendritic morphology was analysed basal dendritic complexity appeared slightly increased in cKO CA1 pyramidal neurons compared to floxed animals. Taken together, this data provides more support for *Cyfip1* as a neuropsychiatric disease-associated gene. Individual CYFIP1 variants did not alter CYFIP1 function therefore, speculation can be made that an accumulation of rare variations within the gene may be required to render CYFIP1 functionally damaging. Lastly, in the first description of cKO CYFIP1 models, loss of CYFIP1 appears to impact on viability of fast dividing cells and alters dendritic morphology of CA1 hippocampal cell when postnatally deleted from forebrain neurons.

4.3.1 *Cyfip1*, a SCZ-associated gene

Improved sequencing techniques and more cost effective methods have increased the

number of patient genome sequencing projects over recent years. This in turn has led to an increase in the analysis of such databases to highlight novel genetic risk factors for neuropsychiatric disorders. Prior to the work carried out in this chapter *Cyfip1*, has mainly been associated with SCZ through CNV of the 15q11.2 region. Both microduplications and microdeletions of 15q11.2 have been implicated in SCZ (Consortium, 2008; Kirov et al., 2012; Stefansson et al., 2008; Tam et al., 2010; Zhao et al., 2013b). Four genes are located within this genomic region *Tubgcp5, Cyfip1, Nipa1* and *Nipa2*. Of these four genes, *Tubgcp5* encodes a gamma tubulin complex component, NIPA1/2 encode magnesium transporters and *Cyfip1* encodes a protein enriched in brain tissue known to regulate actin dynamics and control local translation of proteins. Due to the important functions of CYFIP1 and their relevance to synaptic mechanisms much interest has surrounded this protein (Bozdagi et al., 2012; Napoli et al., 2008; Oguro-Ando et al., 2014; De Rubeis et al., 2013). It is thought *Cyfip1* is likely to be the dosage-sensitive gene that results in CNV at the 15q11.2 locus being associated with SCZ.

That said, compared to the available evidence supporting a role for *Cyfip1* in ASD pathogenesis (Leblond et al., 2012; Nishimura et al., 2007; van der Zwaag et al., 2010), there is little evidence of a direct association of *Cyfip1* with SCZ (Tam et al., 2010; Zhao et al., 2013b). Chapter 3 of this thesis and others have shown the importance of CYFIP1 in regulating neuronal and synapse morphology both critical mechanisms in the etiology of neuropsychiatric disorders, but this finding is not specific to SCZ (Oguro-Ando et al., 2014; De Rubeis et al., 2013). In fact, only one very recent report addresses whether *Cyfip1* is the dosage sensitive gene in 15q11.2 SCZ-associated CNV. By studying iPSC derived neural progenitors from SCZ patients with 15q11.2 microdeletions, Yoon and colleagues showed these cells were haploinsufficient for CYFIP1, had reduced levels of WAVE and had deficits in adherens junctions and apical polarity. They rescued the effects with CYFIP1 overexpression demonstrating that the 15q11.2 microdeletion cell effects were CYFIP1 specific (Yoon et al., 2014). The significant association of *Cyfip1* with SCZ reported in this chapter does not consider CNV and instead shows an association due to an excess of rare *Cyfip1* variants that occur to a greater extent in cases compared to controls. Taken together with previously published work, this finding provides more direct evidence for *Cyfip1* as a risk factor for SCZ.

In the chapter, it is shown that running a weighted burden test on a large cohort of exome sequencing from British SCZ patients returned *Cyfip1* as a significant SCZ-associated gene. However, when carrying out automated database analysis such as this the results often show weak significance. Furthermore, if other genes are investigated during the analysis significant results rarely withstand correction for multiple testing. This is in line with previous exome studies and highlights the necessity to study very large datasets to produce conclusive results that implicate rare variants and genes (Purcell et al., 2014). It is becoming clear that next-generation sequencing studies applied to small cohorts, in the low thousands, are hypothesis generating and are less likely to produce results which conclusively implicate variants or genes. Indeed, this is an issue that is beginning to be addressed. Recently, the SCZ consortium compiled the largest set of GWAS data through collaborations and pooling smaller databases, the results of the analysis yielded 108 convincing novel SCZ-associated loci that withstood corrections for multiple comparisons (Ripke et al., 2014).

Nevertheless, for smaller-scale studies, such as the analysis carried out here, interesting variants can still be identified however, carrying out follow up analysis is important to seek conclusive evidence of an association before embarking on time intensive functional studies. This often involves carrying out genotyping in an additional case-control cohort. However, for some genes, the weighted burden analysis highlights an association based on an excess of many different variants, each occurring in only one or two subjects rather than few variants occurring frequently enough in cases over controls to yield significance. In this case it becomes very difficult to pinpoint which of the variants are potentially pathogenic. Indeed, genotyping the variants in a new cohort is challenging as it is difficult to identify, from the excess of variants initially identified, which are the 'disease causing' variants that should be genotyped again. Furthermore, the variants are extremely rare and to validate them would require a very large number of subjects. It has been suggested that an alternative approach to follow up identified rare variants is to carry out family studies on the individuals possessing the variant (Curtis, 2011). Thus, if there are affected relatives who also have the variant one gains confidence that it has an effect whereas an affected relative not sharing the variant casts doubt on its relevance.

In this chapter, a shortlist of potentially functionally damaging variants was generated

based on biological interest and frequency of appearance in the UK10K dataset for confirmation sequencing in an independent SCZ case-control cohort. Unfortunately, due to their extremely rare occurrence (MAF ranging from 0.0004-0.0025) genotyping the shortlisted variants did not result in a significant association with SCZ. Repeating this genotyping in a much larger case-control cohort would generate more reliable data. Alternatively as discussed above, access to family DNA of affected patients carrying the *Cyfip1* variants would be another way of validating the importance of these identified rare variants however, these samples were not available in this study. To strengthen the data generated here validating the genotyping results against the original sample genomic DNA using PCR and sequencing would also be appropriate.

One final point to mention is the suitability of the unaffected control group from the UK10K project. The obese group was selected as they represented a phenotypically homogenous group from similar geographical origins to the SCZ group. However, the obese group has been compiled on another trait and this may confound the results from the burden analysis. It would have been more appropriate to compare the SCZ cohort to a true unaffected group of controls however, this data was not available within the UK10K project. This supports the requirement for follow up studies to confirm initial findings generated from next-generation sequencing analysis.

4.3.2 The functional effects of CYFIP1 SCZ-associated variants

In this chapter experiments were carried out to assay the effects of individual CYFIP1 variants on CYFIP1 function. None of the five candidate SNPs appeared altered the neuronal subcellular localisation of CYFIP1 or its ability to interact with members of the WRC. These findings suggest that the variants alone are not particularly functionally damaging. They perhaps only result in small, subtle changes to CYFIP1 function or indeed, possibly one SNP alone does not disrupt CYFIP1 function and that an accumulation of CYFIP1 mutations are required for pathogenic effects. Interestingly, two of the variants identified in the initial analysis of the UK10K database were shown to be in linkage disequilibrium (finding from Dr. D. Curtis) suggesting that there is the possibility these SNPs may occur together.

The five candidate SNPs were predicted to interfere with the ability for CYFIP1 to interact with Rac1 or WAVE. However, coimmunoprecipitation experiments carried

out here under steady-state conditions revealed there was no significant change in WAVE binding and a Rac1 interaction could not be detected. CYFIP1 only interacts with active GTP-bound Rac1 (Kobayashi et al., 1998), this causes a conformational change in CYFIP1, relieving its repression of WAVE allowing active WAVE to activate Arp2/3 and bring about branched actin polymerisation (Chen et al., 2010b; Ismail et al., 2009). Therefore, the lack of Rac1 interaction detected in these experiments could be due to low levels of active Rac1 in the experimental conditions. To generate conditions where the Rac1 CYFIP1 interaction could be assayed, Rac1 activators such as EGF (Ridley et al., 1992) could be used to stimulate Rac1 activation to generate a detectable pool of Rac1-bound CYFIP1. In line with this, another explanation for the lack of SNP-dependent functional effects observed here could be because the effects are activity dependent. The SNP mutations may interfere with the Rac1-dependent regulation of CYFIP1's repressive function over WAVE or its ability to hold WAVE in an inactive state rather than disrupting the interactions completely. To test this, coimmunoprecipitation assays could be carried out in the presence of Rac1 activating and inhibiting drugs. Furthermore, a read out for downstream actin polymerisation activity would be interesting. F-actin/G-actin ratios could be measured by biochemistry using appropriate sample fractions and antibodies or *in vitro* pyrene-actin assembly assays could be performed using the CYFIP1 mutants (Chen et al., 2010b; Rocca et al., 2013).

4.3.3 Total loss of CYFIP1 affects cell survival and dendritic branching

Findings from Chapter 3 have already revealed that constitutive CYFIP1 KO animals are embryonically lethal (undetectable from E8.5). This is probably due to defects in embryonic patterning and cell migration during gastrulation, consistent with similar effects caused by other WRC KO animals (Dubielecka et al., 2011; Migeotte et al., 2010; Rakeman and Anderson, 2006). Therefore, generating KO CYFIP1 cells posed a biological problem. To conquer this problem CYFIP1 floxed animals were generated and crossed with a CreERT(T2) mouse strain. These animals were viable to adulthood and the cKO of CYFIP1 was dependent on treatment of the cells with tamoxifen (TAM) (see Figure 4.7). MEFs generated from these mice were repeatedly subjected to TAM to induce the removal of *Cyfip1*. Loss of *Cyfip1* was confirmed by genotyping and western blotting. General observations from the culturing of these cells revealed a consistent decreased cell density in the cKO cells when compared to control floxed cells. This loss of cell density could be due to a decrease in cell survival or a decrease

in cell division. Tight actin regulation is critically required for both these cellular functions (Lee and Dominguez, 2010; Pollard and Cooper, 2009). Considering CYFIP1 has been previously shown, and demonstrated here, to regulate actin dynamics (Chen et al., 2010b; Galy et al., 2011; Ismail et al., 2009; Steffen et al., 2004; Zhao et al., 2013a), quite possibly, total loss of CYFIP1 is critically impacting on actin dynamics leading to cell death. These suggestions require further investigation. Cell survival experiments could be carried out using propidium iodide. Furthermore, time lapse live cell imaging and analysis of cell division events could be performed.

Interestingly, preliminary evidence here shows that these cKO cells appear to have reduced F-actin labelling by phalloidin. They also appear smaller and more rounded. These observation are consistent with an actin polymerisation defect. Indeed, KO cells of other actin regulatory molecules show similar cell effects (Dubielecka et al., 2011; Steffen et al., 2004). To further explore the precise actin defects taking place in these MEFs live FRAP imaging techniques similar to those carried out in Chapter 3 (Figure 3.9; Figure 3.10) could be implemented to understand more about the dynamics of actin turnover following total loss of CYFIP1. Alternatively, actin comet formation could be studied in cells infected with *Listeria monocytogenes* (Lambrechts et al., 2008). Culturing MEFs on fibronectin patterned dishes will restrict the growth of cells to regular shapes so the morphology and F-actin distribution can be quantified in fixed cells using a scoring or Sholl analysis type approach (Caesar et al., 2015). Lastly, scratch/migration assays could also be used to give a more functional readout for the actin defects (Dubielecka et al., 2011). If these experiments were to show loss of CYFIP1 alters actin dynamics and cell motility it would provide evidence towards the hypothesis that developmental patterning defects due to loss of cell motility cause the embryonic lethality of constitutive CYFIP1 KO mice. These assays could be repeated with overexpression of the CYFIP1 variants in the KO MEFs to determine how the point mutations impact on actin regulation compared to rescuing with WT CYFIP1. Indeed, overexpression on a KO background would remove any confounding effects of the endogenous protein and allow for a more accurate study of functional effects of the mutant constructs. However, if loss of CYFIP1 does indeed effect cell survival as predicted from observations here then carrying out these experiments could prove challenging especially if drug treatments, transfections or high cell densities are necessary for the protocols. Furthermore, in the event that recombination is not 100% efficient following TAM treatment cells still expressing CYFIP1 would out compete KO

cells leading to a mixed population diluting the effects of any downstream experiments.

To generate CYFIP1 cKO neurons floxed animals were crossed with animals expressing Cre driven by the CAMKIIα promoter. This resulted in CYFIP1 cKO cells predominantly in the hippocampus and prefrontal cortex with little expression in the cerebellum (Figure 4.11). This expression pattern was consistent with others who have experimented with this mouse strain (Mantamadiotis et al., 2002). Unlike the constitutive CYFIP1 KO animals, these animals were viable until adulthood and indistinguishable from floxed control littermates, similarly to the inducible cKO CYFIP1 mice. Intriguingly, even though Cre recombination efficiency was high in adult hippocampal neurons, determined by the YFP reporter expression, western blotting revealed here that the reduction in CYFIP1 was only 50%. This discovery was surprising and led to the consideration that perhaps non-neuronal cells (that do not express CAMKIIα and therefore retain their CYFIP1) express high levels of CYFIP1. Indeed, a recent screen studying mRNA levels across the eight major cell classes of the brain revealed that CYFIP1 levels were three fold higher in astrocytes than neurons and dramatically six fold higher in microglia (Zhang et al., 2014). As the brain region lysates generated for the characterisation of this CYFIP1 cKO model contained a mixed cell population and not just pure neurons this may explain the incomplete knockdown observed. Perhaps the high levels of *Cyfip1* expression in these non-neuronal cells, especially the microglia, is due to their high migratory activity as migration is heavily dependent on actin turnover. However, it must be noted a very recent publication claims CYFIP1 cannot be detected in astrocytes at the protein level (Huang and Chen, 2015), demonstrating that these theories require further validation.

The morphology of CYFIP1 cKO neurons was analysed to investigate the impact of total loss of CYFIP1 on dendritic complexity compared to CYFIP1 haploinsufficiency reported in Chapter 3. Furthermore, the postnatal conditional deletion of CYFIP1 was predicted to uncouple its critical role in development from any potential roles in neuronal maintenance so they could be studied. cKO CA1 pyramidal neurons showed a slight increase in dendritic complexity proximally to the soma in basal dendrites but no changes in apical dendrites. Interestingly, this result was opposite to the effects observed in constitutive CYFIP1 haploinsufficient mice. One potential explanation for these contrasting effects could be that CYFIP1 has a role in non-neuronal cells that

influences dendrite morphology. Indeed, glial cells are emerging as important players in orchestrating neuronal development. In particular, defects in astrocyte development and function, the most abundant glial cells in the brain, are now considered to contribute to the pathogenesis of neurodevelopmental disorders (Molofsky et al., 2012; Sloan and Barres, 2014; Yang et al., 2013). Astrocytes derived from a mouse model of FXS have been shown to induce developmental delays in dendritic maturation of hippocampal neurons in coculture (Jacobs and Doering, 2010). Perhaps CYFIP1 haploinsufficiency in non-neuronal cells plays a dominant role in the reduced dendritic complexity observed in CYFIP1 haploinsufficient neurons. For example, disrupted actin dynamics may be altering astrocyte process motility. Alternatively, perhaps the postnatal loss of CYFIP1 in cKO neurons highlights a specific role for CYFIP1 in dendritic maintenance which is masked in the haploinsufficient model due to reduced CYFIP1 levels during development. The CA1 basal dendrites receive inputs from the CA3 Schaffler collaterals closest to the CA1 within the hippocampus. This connection forms part of the major hippocampal circuitry which is vital for learning and memory (Spruston, 2008). Therefore, it is not surprising these dendrites are tightly regulated during neuronal development and maintenance.

In conclusion, the work presented in this chapter has provided further evidence that *Cyfip1* is a SCZ-associated gene and has highlighted a novel variant within CYFIP1 at position 15:22963816 (SNP4) which is significantly associated with the disorder. This variant did not yield significance when attempts to validate the association in an independent cohort were carried out due to the low sample numbers however, did show a similar MAF. Functional characterisation of five candidate SCZ-associated CYFIP1 variants, including SNP4, did not alter the synaptic localisation or WRC interactions of CYFIP1. This suggests an accumulation of variants might be required to render CYFIP1 functionally damaging or that the individual variants may be having more subtle activity dependent effects on CYFIP1 function. Finally, the generation of CYFIP1 cKO systems revealed that cKO MEFs appear smaller, rounder and less dense, possibly due to altered F-actin distribution while, CYFIP1 cKO CA1 neurons show more proximal neuronal complexity in basal dendrites. These novel cKO systems could be used in future rescue experiments to resolve the functional effects of CYFIP1 SCZ-associated variants. Additionally, they provide the ideal platform to further elucidate the spatial and temporal roles of CYFIP1 in neurons.

Chapter 5
The role of Ahi1 in neuronal trafficking and morphology

5.1 Introduction

Monogenic disorders of the nervous system such as Rett's syndrome, tuberous sclerosis and Fragile X syndrome often present with neuropsychiatric phenotypes (Bateup et al., 2013; Moretti and Zoghbi, 2006; Rubeis and Bagni, 2011). Studying the cellular function of the individual genes mutated in these diseases provides information not only about the mechanisms of disease pathogenesis but also sheds light on new pathways implicated in mental illness. One such disorder is the ciliopathy Joubert's syndrome (JS), an autosomal recessive developmental disorder where patients often present with depressive and autistic behaviours (see page 65 for a detailed description of JS). Loss of function mutations in the gene Abelson helper integration site 1 (*Ahi1*) were the first identified genetic cause of JS (Dixon-Salazar et al., 2004; Ferland et al., 2004).

The gene *Ahi1* has been genetically linked to various neuropsychiatric disorders. Association and linkage studies have identified *Ahi1* as a susceptibility gene for SCZ (Amann-Zalcenstein et al., 2006; Ingason et al., 2007, 2011; Rivero et al., 2010; Torri et al., 2010). Various reports state linkage signals for SCZ map to human chromosome 6q23.3, the genomic region where *Ahi1* is located. More detailed analysis mapped the association to single-nucleotide polymorphisms (SNPs) within *Ahi1*, providing evidence for *Ahi1* being a SCZ susceptibility gene (Amann-Zalcenstein et al., 2006; Rivero et al., 2010; Torri et al., 2010). A study in an Icelandic sample based on original findings from a family sample of Israeli-Arabs confirmed two strongly associated SCZ markers in a genomic region upstream of *Ahi1*. A replication study of these findings was later carried out in a large European sample (Ingason et al., 2007, 2010). More recently, Ahi1 mRNA levels were analysed in immortalised lymphoblasts from patients in the Israeli-Arab sample. Patients with early age onset of SCZ had higher Ahi1 expression than controls and late-onset patients (Slonimsky et al., 2010).

Linkage studies have also associated *Ahi1* with ASD (Retuerto et al., 2008). A three-stage family-based association study demonstrated evidence of an associated haplotype in *Ahi1* with ASD in a region of the gene known to be a SCZ risk locus (Retuerto et al., 2008). More recently, massively parallel sequencing (MPS) has been used to investigate the genetic etiology of 8 patients with developmental delay, intellectual disability and ASD. Variants in *Ahi1* were detected in patients 5 and 7 (Brett et al., 2014). Interestingly, the *Ahi1* variant found in patient 7 (E1086G) is a known pathological mutation in a case of JS (Kroes et al., 2008). Indeed, many features of ASD have also been described in up to 40% of JS patients (Holroyd et al., 1991; Ozonoff et al., 1999). Equally, Ahi1 KO animals models of JS show anxiolytic and depressed phenotypes (Lotan et al., 2013; Ren et al., 2014; Xu et al., 2010). From this perspective *Ahi1* is emerging as a promising candidate neuropsychiatric disease-associated gene. However, despite the strong genetic evidence linking *Ahi1* with susceptibility to mental illness the role of Ahi1 in normal brain development and disease pathogenesis remains poorly understood.

The gene *Ahi1* was initially identified as a common helper provirus integration site for Abelson leukaemias and lymphomas (Poirier et al., 1988). The encoded protein is conserved among mammals and enriched within the brain (Doering et al., 2008; Jiang et al., 2002). Protein expression is developmentally regulated peaking in mouse during the first postnatal week from E17 through to P7 with lower levels of expression persisting into adulthood (Doering et al., 2008; Ferland et al., 2004). Areas of the mid and hind mouse brain show the largest amount of Ahi1 expression with the highest protein levels detected in the amygdala, hypothalamus and ventral hippocampus (Doering et al., 2008; Sheng et al., 2008). Furthermore, in human foetal tissue *Ahi1* mRNA is highly expressed in the brain and kidney and in adult brain tissue expression is highest in the cerebellum and cerebral cortex (Ferland et al., 2004). This conserved enrichment in brain tissue points towards Ahi1 functioning in neurons. *Ahi1* encodes a unique 1047 amino acid protein containing 7 WD40 repeats, an SH3 domain, potential SH3 binding motifs and, in the human protein, an N-terminal coiled-coil domain, all known mediators of protein-protein interactions (Esmailzadeh and Jiang, 2011; Jiang et al., 2002). The large number of functional domains and signalling motifs present in Ahi1 point towards the protein having a critical role in signalling and regulation (Figure 5.1).

5.1.1 Ahi1 in signalling

Ahi1 has been localised to the basal body and transition zone (TZ) of the primary cilium, a highly conserved organelle central to the regulation of developmental signalling pathways, such as the Wnt-β-catenin and sonic hedgehog pathways (turn to page 65 for a description of cilia) (D'Angelo and Franco, 2009; Hsiao et al., 2009; Lancaster et al., 2011b; Lee et al., 2014). Overexpressed myc-tagged Ahi1 also localises to the basal body but this localisation is lost when a JS associated Ahi1 V433D mutation is overexpressed (Tuz et al., 2013). More recently, super-resolution microscopy has revealed that within the TZ Ahi1 colocalises with CYB1 and OFD1 in a ring like structure at the distal end of the centriole. The amount of centriole recruited via Ahi1 is reduced in $CYB1^{-/-}$ cells suggesting Ahi1 may contribute to the ciliogenesis defects observed in these cells (Lee et al., 2014). Indeed, i*n vitro* experiments in IMCD3 cells have shown that Ahi1 knockdown results in a decrease in cells expressing cilia, defects in cilia formation and cell polarity (Hsiao et al., 2009; Simms et al., 2011). Disrupted formation of primary cilia has also been observed *in vivo*. Zebrafish injected with an Ahi1 morpholino show loss of primary cilia on pronephric ducts while Ahi1 knockout mice ($Ahi1^{-/-}$) show dysregulated photoreceptor cilia formation (Simms et al., 2011; Westfall et al., 2010). Furthermore, primary cilia formation and localisation of ciliary proteins is defective in fibroblasts from JS syndrome patients with *Ahi1* mutations (Tuz et al., 2013). Ahi1 is thought to act as a gatekeeper protein regulating the trafficking of vesicles and membrane proteins into the cilia (Reiter et al., 2012). Taken together, loss of Ahi1 expression or Ahi1 mutations impair cilia formation resulting in altered downstream signalling.

In addition to a role in cilia formation, emerging data from Lancaster and colleagues has identified Ahi1 as a potential regulator of the canonical Wnt signalling pathway and imply defects in this pathway may contribute to JS pathogenesis (Lancaster et al., 2009, 2011a, 2011b). In their initial study, *Ahi1* null mice were shown to have cystic kidneys, a common symptom of JS in human subjects. Interestingly, the kidney defects in *Ahi1* null mice were shown to be owing to decreased Wnt activity (Lancaster et al., 2009). Ahi1 was described to interact with β-catenin, a downstream effector of Wnt signalling. Wnt activity stimulates the translocation of β-catenin to the nucleus where it regulates gene transcription (Willert and Nusse, 1998). More recently, the authors investigate the role of Wnt signalling in the neurodevelopmental phenotypes of JS (Lancaster et al., 2011a). They demonstrated that both developing Ahi1 KO mice

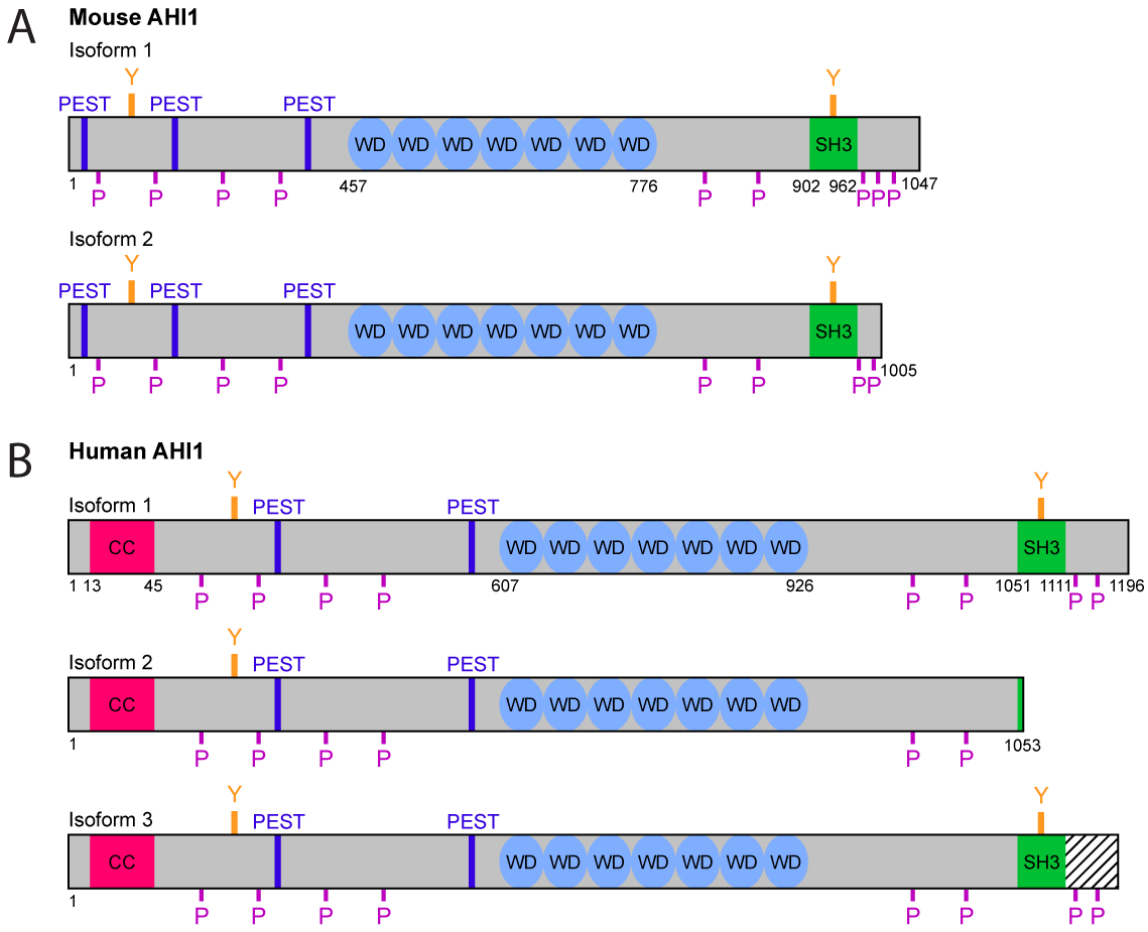

Figure 5.1: A schematic of mouse and human Ahi1 protein isoforms.

A summary of the structural motifs identified in **(A)** mouse and **(B)** human Ahi1 protein isoforms. Isoforms contain: seven WD40 repeats (blue circles), an SH3 domain (green square), proline rich motifs (P), PEST sequences (dark blue line) and tyrosine phosphorylation sites (Y). Human Ahi1 contains an additional coiled-coil domain at the N-terminus (pink square) that is entirely absent from rodent isoforms. Human isoform 2 is shorter and lacks the SH3 domains while isoform 3 still has the SH3 domain but a variable C-terminus (lined box). SH3 domains are known to bind proline-rich regions and mediate specific protein interactions (Shi et al., 2009). Tandem copies of WD40 repeats (repeating tryptophan and aspartate residues) often fold together to form a circular protein-protein interacting domain called a WD40 domain important in membrane signalling, gene transcription and cell cycle regulation (Neer et al., 1994). PEST sites are thought to mediate protein degradation. Adapted from (Esmailzadeh and Jiang, 2011).

and foetal MRI imaging of human subjects with JS showed the same defects in cerebellar midline fusion. By crossing the *Ahi1*$^{-/-}$ mice with Wnt reporter BATgal transgenic mice, Wnt activity at the defective midline fusion site was found to be decreased in *Ahi1* null mice and could be partially rescued by the Wnt pathway agonist lithium (Lancaster et al., 2011a).

5.1.2 Ahi1 and trafficking

Importantly, Ahi1 has also been implicated in a number of trafficking functions. Ahi1 is known to interact with Rab8a and be essential for the correct targeting of Rab8a to the cilia basal body (Hsiao et al., 2009, 2012). Knockdown of Ahi1 in IMCD3 cells impaired ciliogenesis and resulted in loss of Rab8a from the basal body. These effects could not be rescued by overexpression of CA Rab8a showing that Ahi1 is necessary for the targeting of Rab8a to cilia (Hsiao et al., 2009). Rab8 is a small GTPase critical for polarised membrane trafficking and the formation and function of cilia (Leroux, 2007). Expression of a dominant negative (DN) or a constitutively active (CA) form of Rab8 in *Xenopus laevis* disrupted trafficking in photoreceptor cells and inhibited and promoted ciliogenesis respectively in IMCD3 cells (Follit et al., 2010; Moritz et al., 2001; Nachury et al., 2007). Additionally, Ahi1 is involved in Rab8a-mediated transport in retinal photoreceptor cells (Louie et al., 2010; Westfall et al., 2010). Indeed, patients with JS and other ciliopathies often present with retinal degeneration (Doherty, 2009; Waters and Beales, 2011). Photoreceptors have modified cilia with a basal body, axoneme and outer segment. The outer segment contains stacked membrane discs containing opsin and the signalling machinery required for phototransduction. This segment is continually replaced and therefore transport of opsin to these membrane structures is vital. Ahi1 KO retinal cells resulted in abnormal distribution of opsin and cilia specific vesicle targeting was lost due to failed transport (Louie et al., 2010; Westfall et al., 2010). The authors observed a loss of Rab8a expression in Ahi1 KO retinal cells and concluded that Ahi1 is critical for the trafficking of outer segment proteins and Rab8a-mediated transport in retinal photoreceptors (Westfall et al., 2010).

Ahi1 also plays a role in the stabilisation and trafficking of neuronal receptors such as the serotonin 2C receptor ($5HT_{2C}R$) and the neurotrophic receptor tyrosine kinase B (TrkB) (Wang et al., 2012; Xu et al., 2010). Ahi1 deficiency has been demonstrated to alter TrkB trafficking resulting in depressive phenotypes in mice (Sheng et al., 2008;

Xu et al., 2010). Trks are responsible for binding neurotrophins and eliciting effects on the cell. TrkB binds to BDNF, and upon activation causes numerous downstream signalling events implicated in cell survival, axonal outgrowth, synaptic activity and differentiation (Gupta et al., 2013). Often when activated, TrkBs are internalised to enhance their interaction with downstream adaptor proteins and facilitate signalling. Internalised TrkBs are then either recycled or degraded, but their proper trafficking is critical for correct signalling (Patapoutian and Reichardt, 2001). Ahi1 neuronal-specific cKO mice show impaired endocytic sorting and increased lysosomal degradation of internalised TrkB following BDNF stimulation (Xu et al., 2010). Additionally, Ahi1 has been proposed to mediate feeding behaviour through an interaction with the $5HT_{2C}R$ (Niu et al., 2011, 2012; Wang et al., 2012). Ahi1 was shown to promote the degradation of the $5HT_{2C}R$ through the lysosomal pathway. In neuroblastoma cells overexpressing Ahi1 and $5HT_{2C}R$, more $5HT_{2C}R$ was localised to lysosomes compared to control cells. Furthermore, in cells transfected with Ahi1, levels of $5HT_{2C}R$ decreased over time, compared to a C-terminal mutant of Ahi1 that could not interact with the receptor (Wang et al., 2012). Indeed, Ahi1 levels were shown to be upregulated in the hypothalamus of fasted mice while $5HT_{2C}R$ levels were reduced (Niu et al., 2011, 2012; Wang et al., 2012).

Of interest, Ahi1 has been reported to strongly interact with the trafficking adaptor huntingtin-associated protein-1 (HAP1), and both proteins are detected in the same rodent brain regions (Sheng et al., 2008; Tuz et al., 2013; Xu et al., 2010). Moreover, the two proteins have been shown to stabilise each other; levels of HAP1 are dramatically decrease in Ahi1 KO brain tissue and in HAP1 KO tissue Ahi1 levels are reduced (Sheng et al., 2008; Tuz et al., 2013; Xu et al., 2010). HAP1 is an adaptor molecule that has been described to have a myriad of trafficking functions and can interact with numerous microtubule motors and non-motor trafficking proteins (Li and Li, 2005; Rong et al., 2007a; Wu and Zhou, 2009). In a collection of reports from the same group, HAP1 was shown to be involved in the trafficking and stabilisation of neurotropic receptors: TrkA, TrkB and EGF receptor (Li et al., 2002; Rong et al., 2006, 2007b; Sheng et al., 2008). Altered HAP1 expression, disrupted the trafficking of these receptors leading to loss of neurite outgrowth. HAP1 has also been linked to microtubule-based trafficking. Shortly after HAP1 was first identified, the anterograde and retrograde trafficking of HAP1 positive organelles was observed (Engelender et al., 1997; Li et al., 1998). Since then HAP1 has been shown to have many protein binding domains and interact with multiple components of microtubule

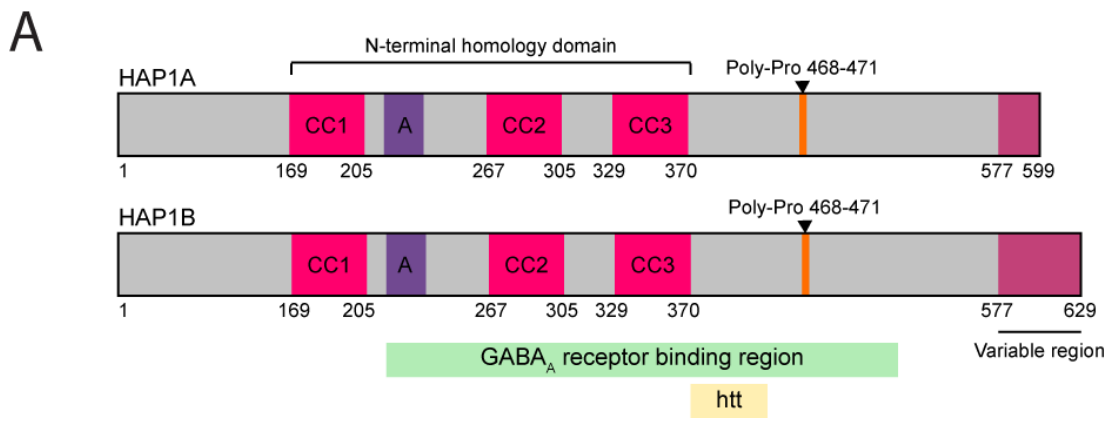

Figure 5.2: A schematic of rodent Huntingtin-associated proteins 1 (HAP1) isoforms.

A summary of the structural motifs and binding domains of rodent HAP1A and HAP1B. Both proteins are identical over the first 577 residues and then each have a variable C-terminus (maroon box) with HAP1B forming a longer protein. The proteins possess three coiled-coil (CC) domains (pink box), which together make up the HAP1 N-terminal Homology Domain, important for protein-protein interactions. There is an acidic rich amino acid region between CC1 and CC2 (purple box) and a C-terminal poly-proline region (orange line). A Y2H screen revealed $GABA_AR$ β subunits bind to HAP1 at residues 220-520 (Kittler et al., 2004). Huntingtin (htt) interacts with HAP1 over residues 371-420 (Li et al., 1995).

motors and other trafficking proteins (Figure 5.2). A Y2H screen identified p150^{Glued} as a HAP1 interactor, a vital subunit of the dynactin complex important for dynein mediated retrograde transport of vesicles. The same screen revealed that HAP1 also interacts with KIF5C, a homologue of human kinesin heavy chain (Engelender et al., 1997). More recently, HAP1 has been show to bind to kinesin light chain (KLC), a part of the conventional anterograde kinesin motor. This study showed anterograde trafficking was impaired in HAP1 KO neurons (McGuire et al., 2006).

Other non-motor protein-protein interactions have been described for HAP1 implicating it in trafficking and cytoskeletal regulation. One study demonstrated that HAP1 interacts with the endocytic trafficking protein Hrs (hepatocyte growth factor-regulated tyrosine kinase substrate) (Li et al., 2002). Hrs is a key substrate of Trks and is central for their signal transduction. HAP1 and Hrs together have been shown to be important in the stability of internalised neurotrophic receptors (Li et al., 2002; Xu et al., 2010). HAP1 also binds 14-3-3. The 14-3-3 family are well conserved regulatory proteins that bind a large number of cytoskeletal and trafficking proteins and are key to the regulation of many cellular processes (Rong et al., 2007b). Other functions of HAP1 include: its ability to interact with the Rac1 GEF Kalirin-7 (Colomer, 1997); its ability to traffic BDNF containing vesicles and proBDNF (Gauthier et al., 2004; Wu et al., 2010); its capacity of binding to other PolyQ proteins and its role in regulating transcription (Wu and Zhou, 2009).

Notably, HAP1 has been identified as an adaptor protein necessary for the trafficking of $GABA_AR$s at inhibitory synapses (Kittler et al., 2004). By linking $GABA_AR$ containing transport vesicles to the kinesin KIF5, HAP1 was shown to mediate the rapid recycling of $GABA_AR$s to the synapses. Furthermore, in a model of Huntington's disease (HD) this $GABA_AR$ trafficking was disrupted by the strong interaction between mutant htt and HAP1 (Li et al., 1995). The result was reduced delivery of $GABA_AR$s to synapses and reduced inhibitory synaptic transmission (Twelvetrees et al., 2010). Altered GABAergic signalling in this way may disrupt the balance between neuronal excitation and inhibition. Such an imbalance is thought to be a contributing factor in the pathogenesis of neuropsychiatric disorders (Smith and Kittler, 2010).
The finding that Ahi1 can interact with HAP1 (Sheng et al., 2008) coupled with the fact Ahi1 is implicated in numerous trafficking functions make the protein a potential candidate $GABA_AR$ trafficking molecule. It can be hypothesised that Ahi1, due to its

many signalling and protein interacting domains, may provide a level of regulation to the $GABA_AR$ trafficking function of HAP1. Altered expression or disease mutations in Ahi1 may disrupt $GABA_AR$ recycling and the number of $GABA_ARs$ at synapses leading to pathological effects on the E/I balance that may explain the prevalence of neuropsychiatric phenotypes seen in patients with JS. However, currently the role of Ahi1 in $GABA_AR$ trafficking is unknown and warrants investigation.

5.1.3 Ahi and neurite outgrowth

Lastly, the accurate formation of neuronal networks and synaptic connections is vital for normal brain function. Indeed, disrupted neuronal connectivity is one of the key prevailing theories in the development of neuropsychiatric dysfunction (Kulkarni and Firestein, 2012). The structure and function of primary cilia are known to be crucial for the proper development of neurons (D'Angelo and Franco, 2009; Waters and Beales, 2011). In fact, malformations of brain anatomy are a feature of many ciliopathies, including JS (Ferland et al., 2004; Lee and Gleeson, 2010). Ahi1 has been implicated in the mechanisms of neuronal development not only via its roles in cilia formation and function but also via its interaction with HAP1 (Sheng et al., 2008). HAP1 has been shown to promote neurite outgrowth in PC12 cells through preventing degradation of internalised TrkA (Li et al., 2000; Rong et al., 2006). Loss of HAP1 expression using RNAi led to reduced HAP1 in neurite tips, reduced neurite outgrowth and decreased levels of internalised TrkA (Rong et al., 2006). The role of Ahi1 in stabilising TrkB also implicates Ahi1 in neuronal development as activation of TrkB signalling is known to promote neurogenesis and has also been implicated in the maintenance of dendritic complexity and branching (Cohen-Cory et al., 2010). Furthermore, a small mass spectrometry screen has revealed Ahi1 can interact and stabilise Cend1, a neuronal protein that mediates nerve cell differentiation (Weng et al., 2013). Taken together these results illustrate a role for Ahi1 in neurite outgrowth however, the impact Ahi1 has on dendritic morphology and synaptic connections has not been investigated.

In this chapter, the previously described interaction between Ahi1 and HAP1 was confirmed both in an overexpression system and in rodent brain. Furthermore, a novel Ahi1/HAP1/KIF5 trafficking complex was identified that could be detected *in vivo* from rodent brain lysate. Ahi1 was shown to be trafficking in this complex by KIF5 in a HAP1 dependent manner. The subcellular neuronal localisation of

endogenous Ahi1 was investigated and Ahi1 was shown to be localised to excitatory and inhibitory synapses pointing towards a synaptic function for Ahi1. The impact of both Ahi1 overexpression and knockdown on the surface levels of $GABA_A$Rs and the integrity of inhibitory postsynaptic scaffold molecules were investigated. To further explore the role of Ahi1 in the pathogenesis of neuropsychiatric disorders, Ahi1 autism-associated mutants were generated. These mutants could still interact with HAP1 and be trafficked by KIF5 in a HAP1 dependent manner suggesting these mutants are likely to be having more subtle effects on Ahi1 signalling and function. Finally, knockdown of Ahi1 was shown to significantly impact on dendritic morphology a result consistent with the neuronal developmental defects observed in JS.

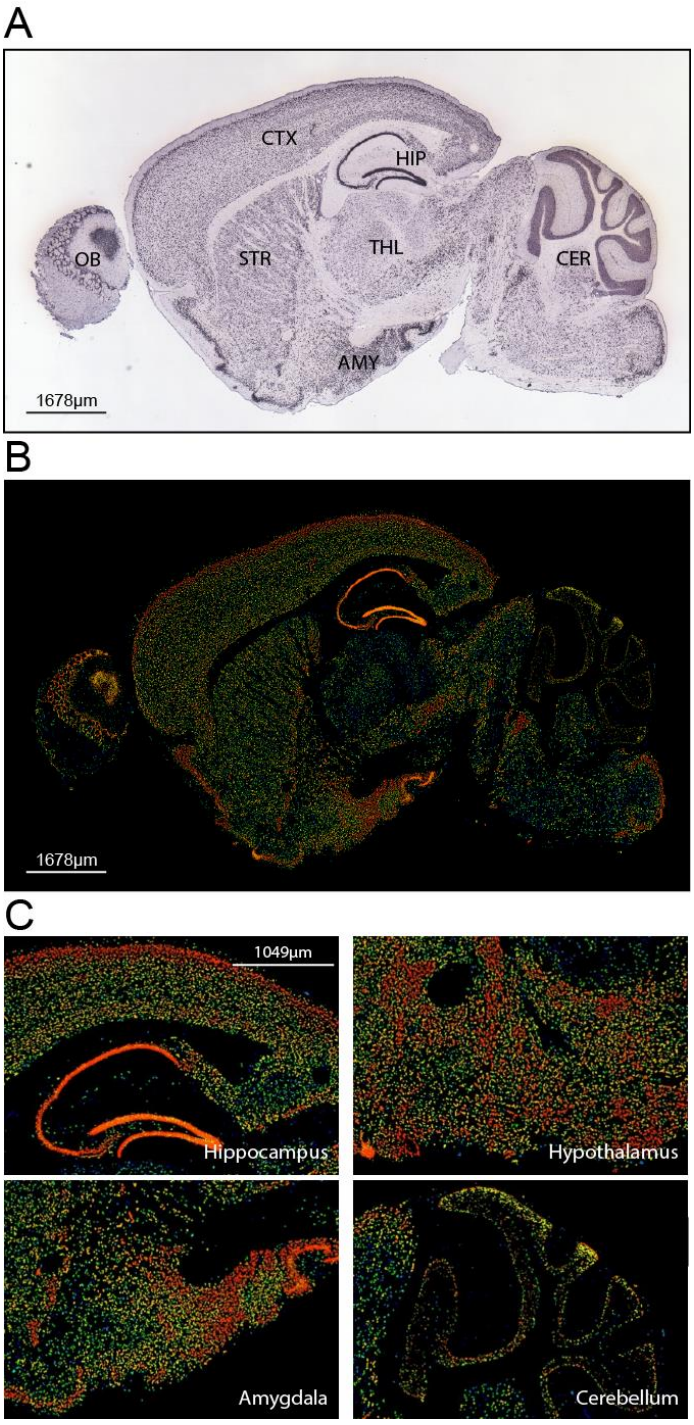

Figure 5.3: Ahi1 mRNA expression in adult sagittal mouse brain sections.

Taken from the Allan Brain Atlas (©2014 Allen Institute for Brain Science. Allen Mouse Brain Atlas [Internet]. Available from: http://mouse.brain-map.org/). P56 male WT mouse (strain C57BL/6J) sagittal brain sections were generated and subjected to **(A)** *in situ* hybridisation (ISH) using an Ahi1 mRNA antisense probe to demonstrate where Ahi1 mRNA is expressed. Results of ISH were overlaid with hematoxylin and eosin staining to identify brain regions. **(B and C)** A heat map representation of Ahi1 mRNA expression levels in different brain regions (hot colours=high expression, cold colours=low expression) (Lein et al., 2007).

5.2 Results

5.2.1 A HAP1 interacting protein Ahi1 and its expression in brain

In order to investigate the role of Ahi1 in neuronal trafficking and morphology it was important to determine the neuronal expression pattern of Ahi1. Previous reports have described Ahi1 to be enriched within the brain (Doering et al., 2008; Jiang et al., 2002) and the often severe neuronal defects seen in JS suggests the function of Ahi1 in the brain is critical. Indeed, *in situ* hybridisation data taken from the Allan Mouse Brain Atlas (©2014 Allen Institute for Brain Science. Allen Mouse Brain Atlas [Internet]. Available from: http://mouse.brain-map.org/ (Lein et al., 2007)) demonstrates that Ahi1 mRNA can be detected in specific mouse brain regions, principally the hippocampus (Figure 5.3A,B). In fact, the levels of Ahi1 mRNA expression are highest in the hippocampus, layers I-III of the cortex, the hypothalamus and the amygdala. This can be seen by the red rendering on the heat maps of mRNA expression and is consistent with previous findings (Figure 5.3B,C) (Doering et al., 2008; Sheng et al., 2008). Ahi1 protein levels could also be detected from rodent brain with two commercial antibodies (Figure 5.4A). The Santa Cruz antibody detected two protein bands at the expected molecular weight of Ahi1 ~130 kDa. These bands correspond to the two isoforms of Ahi1 known to be expressed in rodent brain with a non-specific band appearing in all lanes at 100 kDa. Interestingly, the expression of the smaller isoform is much less pronounced within the rat cortex compared to total rat brain lysate. The commercial Abcam Ahi1 monoclonal antibody appears to be species and isoform specific, detecting only one isoform of Ahi1 at the expected molecular weight in mouse brain lysate alone.

Mouse Ahi1 cDNA was cloned into myc and GFP vectors which tagged the protein at the N-terminus. The constructs were readily expressed when transfected into COS-7 cells and western blotting against the protein tags revealed bands at the expected molecular weights, 130 kDa and 160kDa for msAhi1^{myc} and msAhi1^{GFP} respectively. Neither fusion protein could be detected with the mouse specific Abcam antibody (Figure 5.4B,C). The cellular localisation of both mouse constructs and an N-terminally tagged human Ahi1^{GFP} (hAhi1^{GFP}) construct obtained from Addgene could be detected via GFP fluorescence or immunostaining with an anti-myc antibody (Figure 5.4D). The expression of all three constructs appeared to be cytosolic similar to the GFP only control however, there was little Ahi1 present within the nucleus. High

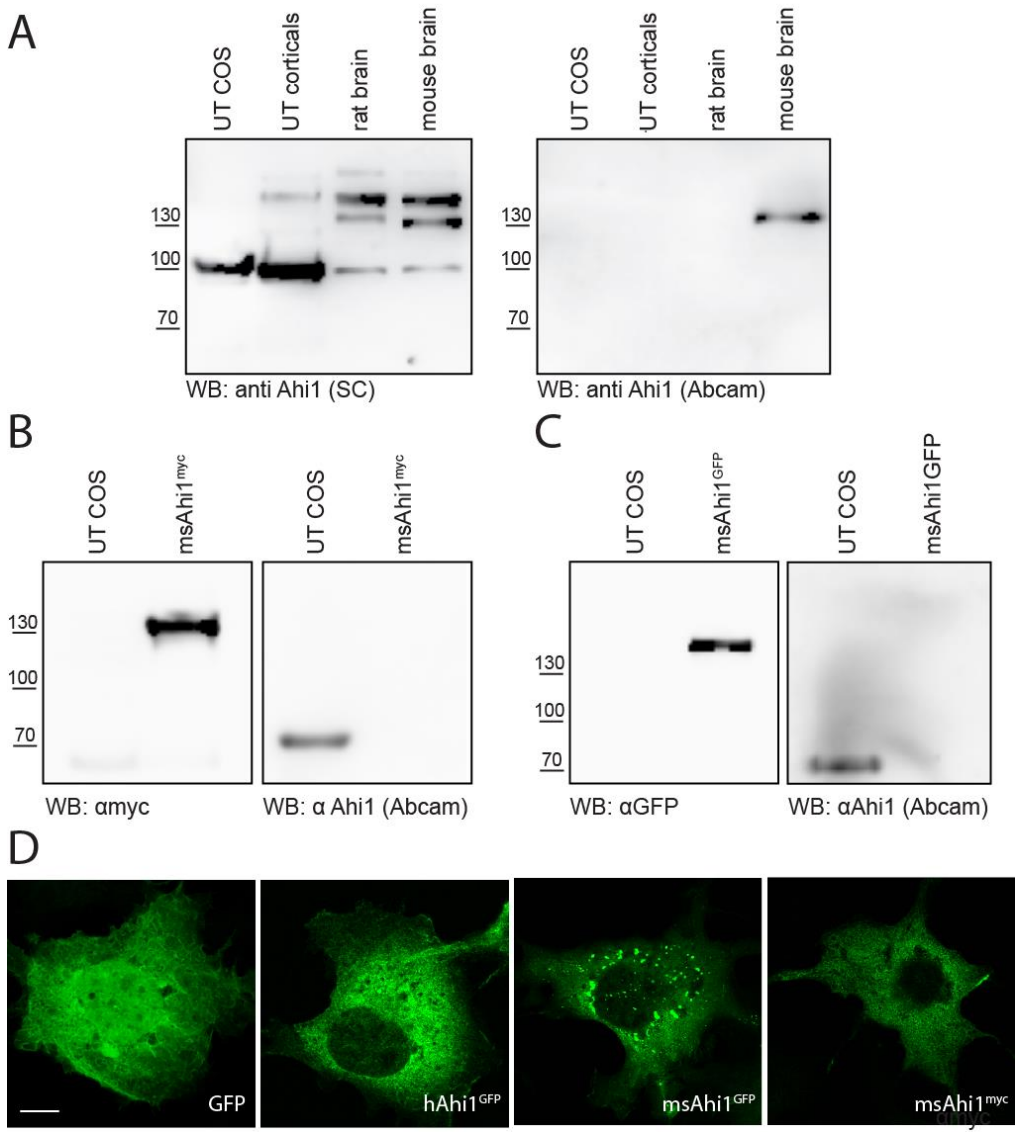

Figure 5.4: Ahi1 antibody characterisation and detection in rodent brain lysate.

(A) Characterisation of Ahi1 antibodies. Western blotting of untransfected COS-7 cell lysate, rat cultured cortical lysate, rat and mouse brain lysate and probing with a Santa Cruz Ahi1 antibody (left panel) shows two specific Ahi1 bands at ~130kDa and ~140kDa in rodent lysate of which only the larger isoform is present in rat cortical neurons. Probing with a monoclonal Abcam antibody (right panel) shows specificity to the smaller mouse isoform of Ahi1 at ~130kDa only. Neither antibody detects Ahi1 in COS-7 cell lysate. The Santa Cruz antibody (left panel) detected a non-specific band at 100kDa in all samples. Western blots of **(B)** msAhi1^{myc} or **(C)** msAhi1^{GFP} transfected COS-7 cell lysates and untransfected (UT) control lysates were probed for myc and GFP (left panels) to confirm the constructs generated fusion proteins of the expected molecular weight ~130kDa and ~160kDa respectively. The Ahi1 specific Abcam monoclonal antibody did not detect the mouse constructs (right panels). **(D)** Confocal images of COS-7 cells transfected with GFP control, hAhi1^{GFP}, msAhi1^{GFP} or msAhi1^{myc}. Immunofluorescence with a myc antibody was used against the msAhi1^{myc} construct. Scale bar, 20μm.

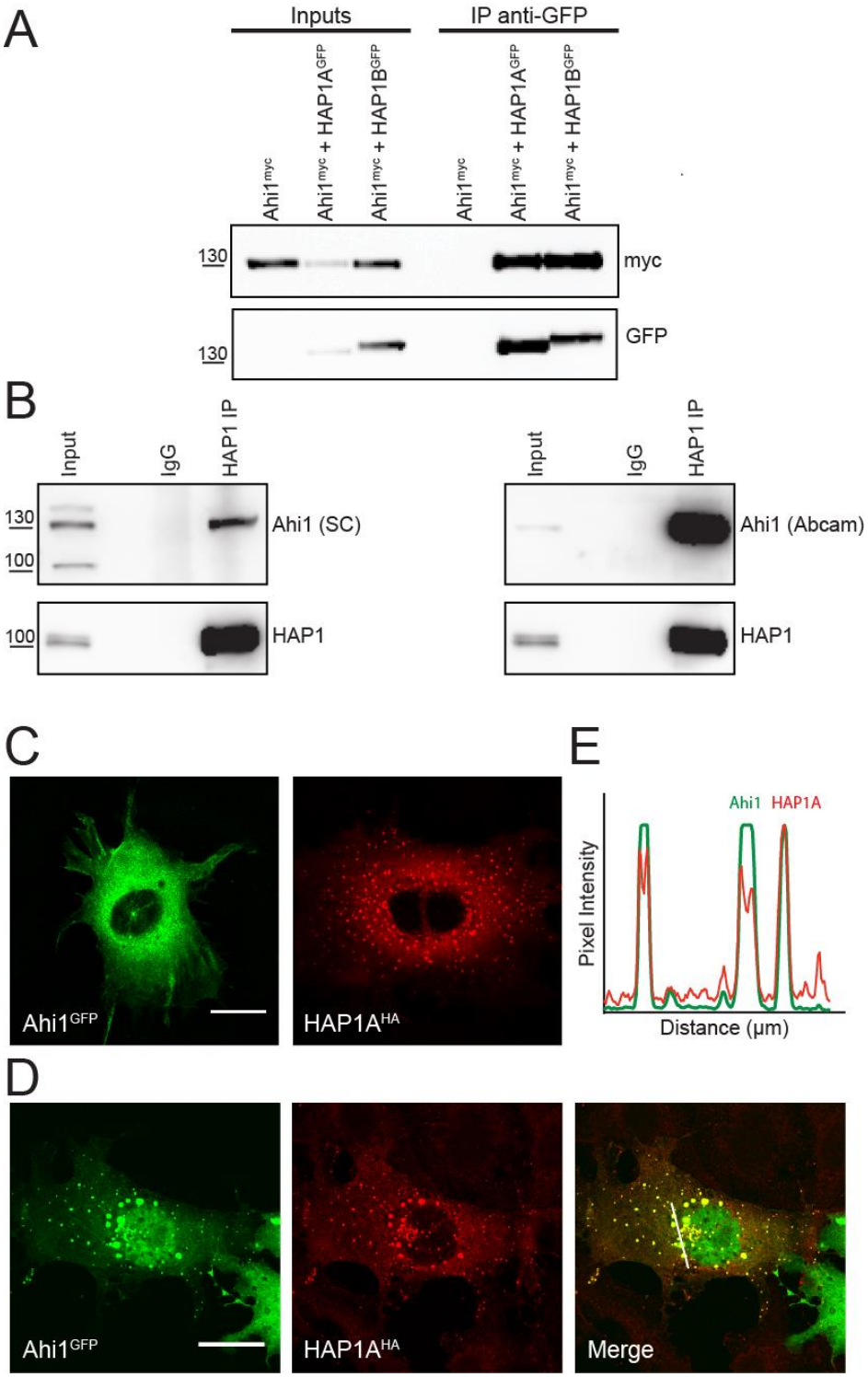

Figure 5.5: Ahi1 interacts and colocalises with the trafficking molecule HAP1.

Coimmunoprecipitation and colocalisation experiments demonstrating an interaction between Ahi1 and HAP1A or HAP1B. **(A)** Western blots of protein complexes coimmunoprecipitated using anti-GFP TRAP beads from COS-7 cells transfected with $Ahi1^{myc}$ and either $HAP1A^{GFP}$ or $HAP1B^{GFP}$. Input samples (Inputs) represent 5% of the cell lysate

included in the immunoprecipitation (IP). Anti-GFP TRAP beads efficiently immunoprecipitated Ahi1^{myc} from cotransfected cell lysates but not from Ahi1^{myc} only transfected cells. **(B)** Western blots of endogenous protein complexes coimmunoprecipitated from mouse brain lysate with anti-HAP1 antibody. Input represent 5% of the brain lysate included in the IP (HAP1 IP). IgG is the non-immune control antibody experiment for non-specific protein binding. Mouse anti-HAP1 antibody efficiently immunoprecipitated Ahi1 (left panel Santa Cruz Ahi1 antibody, right panel Abcam antibody) from mouse brain lysate. Confocal images of COS-7 cells **(C)** singularly transfected or **(D)** cotransfected with Ahi1^{GFP} and HAP1A^{HA} and subjected to immunofluorescence with anti-GFP and anti-HA antibodies respectively. Colocalisation appears yellow in the merged image. **(E)** Graph (above) shows a line scan through the merge image of HAP1^{HA} and Ahi1^{GFP} fluorescence, demonstrating the cellular distribution and colocalisation of the proteins with the peaks corresponding to protein clusters. Scale bar, 20μm.

expression of Ahi1 appeared to form aggregates as can be seen with msAhi1^{GFP}, which could be due to the ability of Ahi1 to dimerise (Tuz et al., 2013).

To explore the hypothesis that Ahi1 may play a trafficking role with HAP1 at the inhibitory synapse, first an interaction between the two proteins needed to be confirmed. Immunoprecipitation experiments from COS-7 cell lysates demonstrated that mouse Ahi1^{myc} could be coimmunoprecipitated with both isoforms of HAP1, HAP1A^{GFP} and HAP1B^{GFP}, when they were pulled down via their GFP tags (Figure 5.5A). Furthermore, immunoprecipitation experiments from mouse brain lysate confirmed that endogenous Ahi1 and HAP1 interact in brain. The interaction is via the smaller Ahi1 isoform, as the immunoprecipitated band is detected by the isoform specific Abcam antibody and appears as the lower band using the Santa Cruz antibody (Figure 5.5B). To study whether Ahi1 and HAP1 colocalise in cells immunofluorescence was carried out on COS-7 cells cotransfected with msAhi1^{GFP} and HAP1A^{HA}. This experiment revealed a striking recruitment phenotype when the two proteins were coexpressed. Alone Ahi1^{GFP} appeared diffuse within the cytosol while HAP1A^{HA} was also cytosolic but formed protein clusters that have been previously described (Figure 5.5C) (Li et al., 1998). However, when the two proteins are coexpressed msAhi1^{GFP} was dramatically recruited to HAP1A^{HA} clusters and the two proteins strongly colocalise. This can be seen by the overlapping line scan profile of pixel intensity for the two proteins (Figure 5.5D,E).

To further characterise the Ahi1 HAP1 interaction, constructs expressing N-terminal truncated versions of HAP1A were used to map the Ahi1 binding site on HAP1. Mouse Ahi1^{GFP} was transfected alone as a control into COS-7 cells or cotransfected with HAP1A$^{myc153-599}$, HAP1A$^{myc215-599}$, HAP1A$^{myc329-599}$ or HAP1A$^{myc371-599}$. The 153-599 mutant lacked the very N-terminal region of HAP1A, the 215-599 mutant lacked the N-terminus plus the first coiled-coil (CC) domain, the 329-599 mutant lacked the N-terminus and both CC domains 1 and 2, while the 371-599 mutant contained none of the CC domains and just expresses the C-terminus of HAP1A (Figure 5.6A). The mutants were immunoprecipitated from the transfected cell lysates via their myc tags using anti-myc beads and western blotting revealed any coimmunoprecipitation of Ahi1^{GFP}. Mouse Ahi1^{GFP} was robustly pulled down by the longest HAP1A truncation containing all the CC domains and was partially pulled down with the 215-599 mutant lacking only CC domain 1. Mouse Ahi1^{GFP} did not interact with the HAP1A mutants

containing only the third CC domain or none of the CC domains (Figure 5.6B). When these experiments were repeated with hAhi1^{GFP} a similar result was observed (Figure 5.6C). hAhi1^{GFP} strongly coimmunoprecipitated with the 152-599 mutant however, there was no partial interaction with the 215-599 mutant. These data confirm that both rodent and human Ahi1 either directly interact with the first CC domain of HAP1A or at least require the presence of this domain for HAP1 to be in the correct protein orientation to allow Ahi1 to interact.

5.2.2 Ahi1 forms a trafficking complex with HAP1

Previous work has described Ahi1 as a trafficking adaptor molecule involved in the transport of cargo along the primary cilia (Hsiao et al., 2009). HAP1 on the other hand, is an adaptor protein that couples $GABA_A$Rs to the KIF5C kinesin motor and is required for the recycling of $GABA_A$Rs within the inhibitory synapse (Twelvetrees et al., 2010). Confirming an interaction exists between Ahi1 and HAP1 suggests that these two proteins may form a trafficking complex together. Indeed, when HAP1 was immunoprecipitated from either rat or mouse brain lysate, using a HAP1 specific antibody, both Ahi1 and KIF5 coprecipitated with it, indicating that these three proteins can form an endogenous complex in the brain (Figure 5.7A,B). The doublet observed for HAP1 in the immunoprecipitation lane corresponds to both isoforms of HAP1, which can be enriched for with the HAP1 antibody. Of note, the stoichiometry of the HAP1/Ahi1/KIF5 complex appears to be different between rat and mouse with a larger proportion of Ahi1, compared to KIF5, binding HAP1 in mouse verses equal proportions of Ahi1 and KIF5 binding HAP1 in rat. These differences could potentially be explained by the different Ahi1 isoforms present in rat and mouse and could suggest subtle differences in the function of the complex between the two species.

Following the observation that HAP1, KIF5 and Ahi1 can form a protein complex together it was interesting to investigate whether this complex was functional and whether Ahi1 as well as HAP1 could be trafficked by KIF5. When KIF5C^{myc} alone was transfected into COS-7 cells and immunofluorescence was used to reveal its subcellular localisation, the staining showed a distinct filamentous pattern typical of KIF5C decorating the microtubules (Figure 5.8A). When GFP was cotransfected with KIF5C^{myc} the even distribution of KIF5C^{myc} along the microtubules was not disrupted (Figure 5.8B). However, when HAP1A^{HA} was cotransfected with KIF5C^{myc} both the typical distribution of HAP1A^{HA} and KIF5C^{myc} was altered. Instead of HAP1A^{HA}

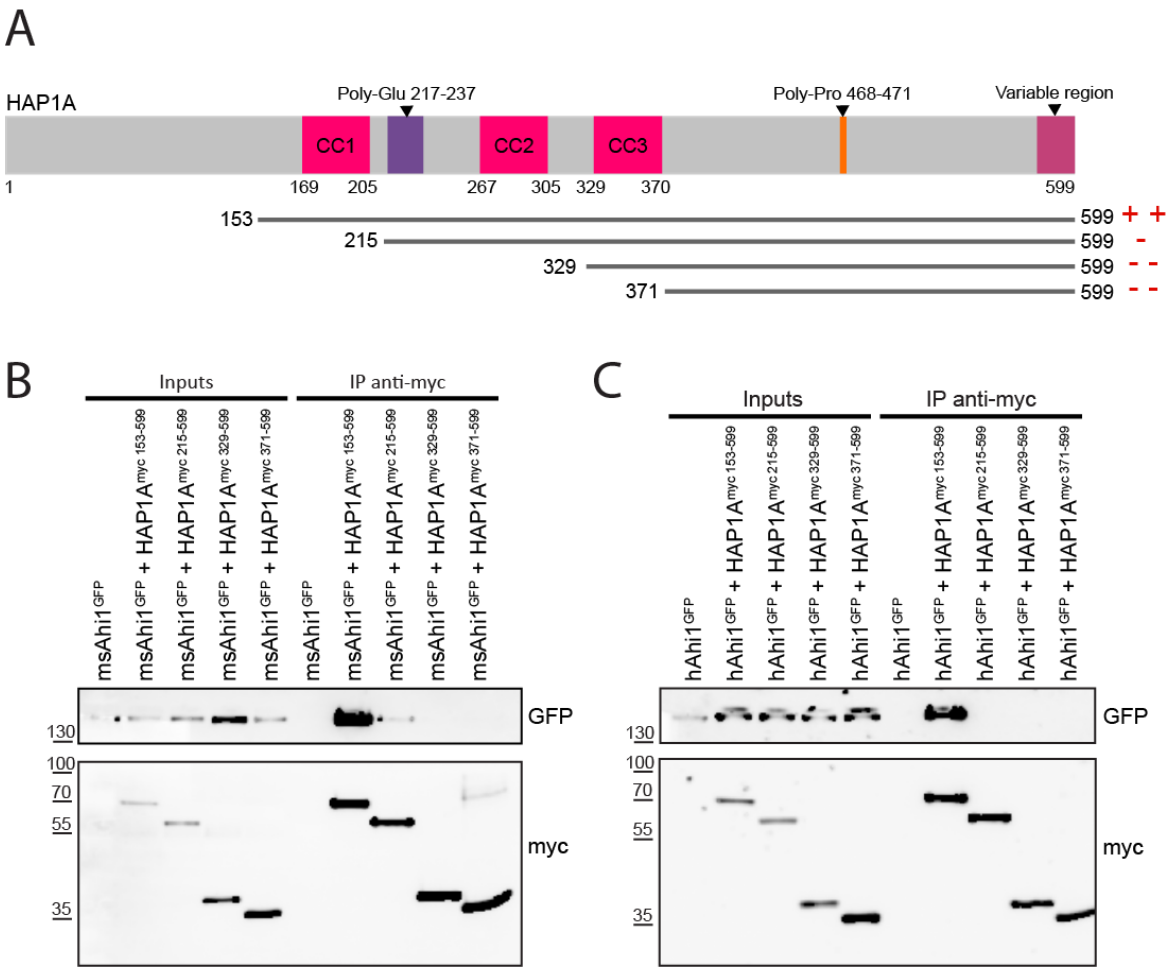

Figure 5.6: Mapping the Ahi1 binding site of HAP1.

Coimmunoprecipitation experiments reveal the first coiled-coil domain of HAP1 is necessary for Ahi1 binding. **(A)** A schematic of HAP1A depicting the 3 coiled-coil domains (CC) the glutamine rich region (poly-glu), the proline rich region (poly-pro) and the variable C-terminus. Grey bars below represent the 4 truncated versions of the protein and red plus and minus symbols summerise which trucations can interact with Ahi1 (+: interaction; -: no interaction). Western blots of protein complexes coimmunoprecipitated using anti-myc beads from COS-7 cells cotransfected with mouse **(B)** or human **(C)** Ahi1^{GFP} and either 153-599, 215-599, 329-599 or 371-599 HAP1A^{myc} trucations. Input samples (Inputs) represent 5% of the cell lysate included in the immunoprecipitation samples (IP). Anti-myc beads efficiently immunoprecipitated both mouse and human Ahi1^{GFP} from cells coexpressing 153-599 HAP1A^{myc} but not from cells coexpressing 215-599, 329-599 or 371-599 HAP1A^{myc} or from Ahi1^{GFP} only expressing cells.

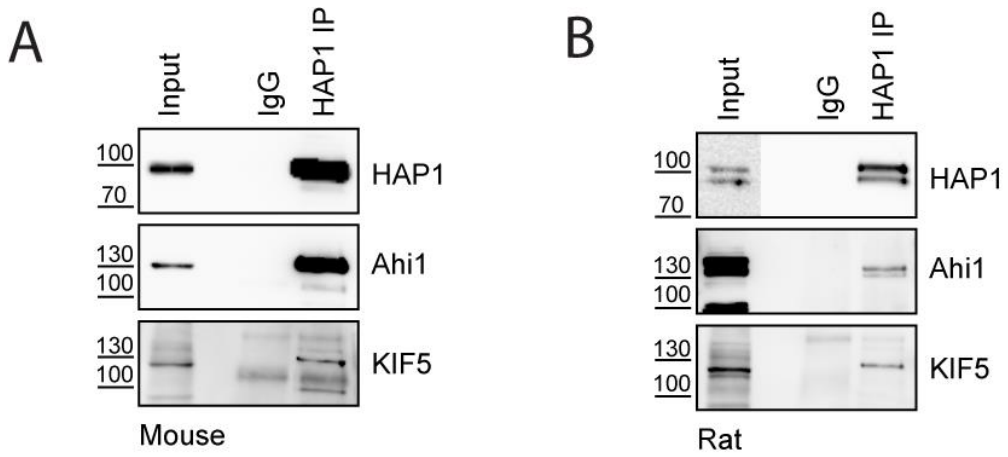

Figure 5.7: Ahi1 forms a trafficking complex with HAP1 and KIF5 in rodent brain.

Western blots of endogenous protein complexes coimmunoprecipitated from mouse **(A)** or rat **(B)** brain lysates with anti-HAP1 antibody. Input samples (Input) represent 5% of the brain lysate included in the immunoprecipitation samples (HAP1 IP). IgG is the non-immune control antibody experiment for non-specific protein binding. Mouse anti-HAP1 antibody efficiently immunoprecipitated both Ahi1 and KIF5 from mouse and rat brain lysates.

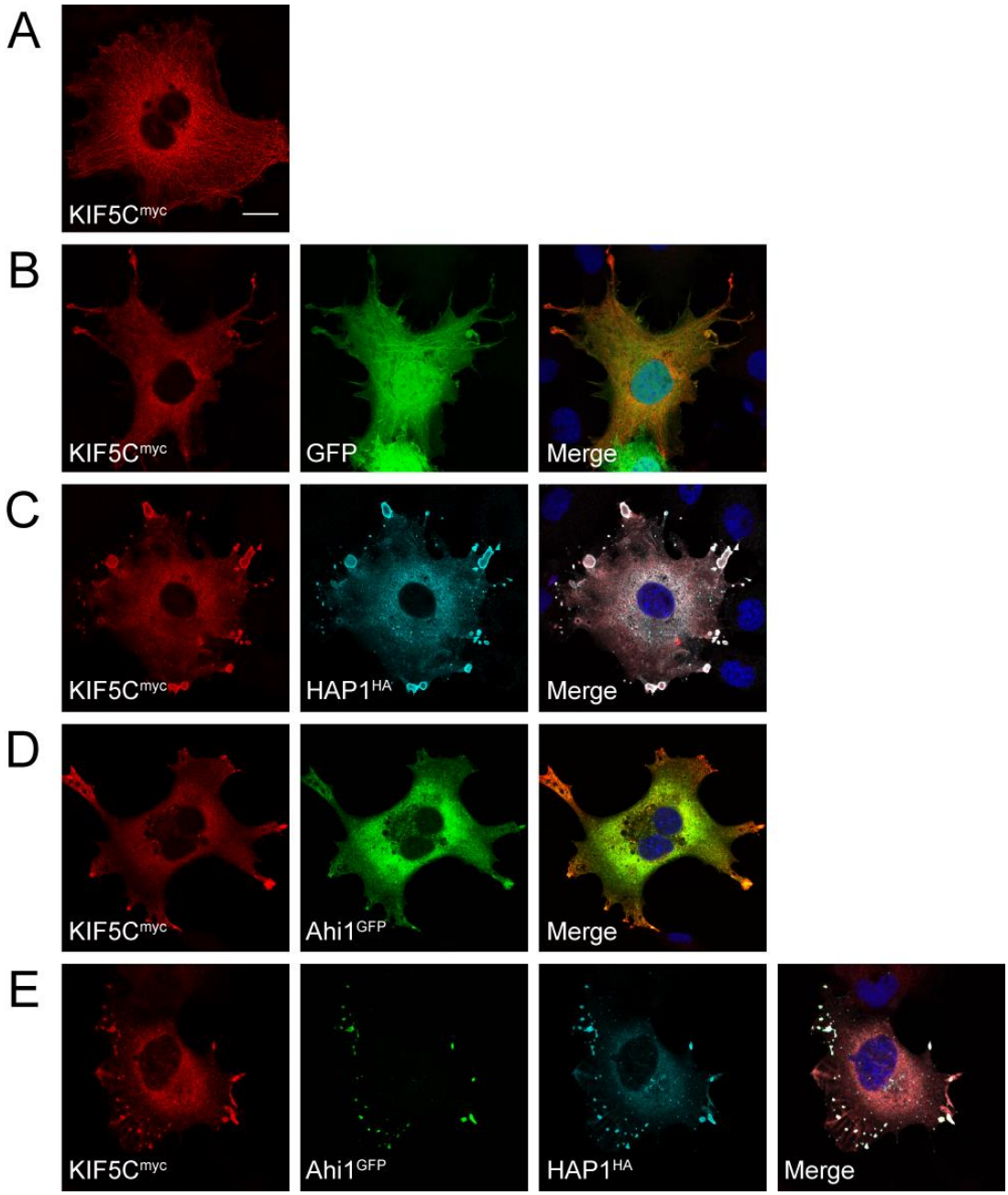

Figure 5.8: Ahi1 is trafficked by KIF5C in a HAP1 dependent manner.

Transfected COS-7 cells were fixed and immunolabelled against the expressed fusion protein tags before being imaged using confocal microscopy. **(A)** Localisation of KIF5C^{myc} on microtubules in single transfected cells. **(B)** Coexpression of KIF5C^{myc} and GFP does not affect the microtubule localisation of KIF5C^{myc}. **(C)** Coexpression of KIF5C^{myc} with HAP1A^{HA} results in KIF5C^{myc} colocalising with HAP1A^{HA} and HAP1A^{HA} clusters being trafficked to the outer-membrane. **(D)** Coexpression of KIF5C^{myc} with Ahi1^{GFP} does not interfere with KIF5C^{myc} microtubule staining. Ahi1^{GFP} is not redistributed with KIF5C^{myc}. **(E)** A triple transfection of KIF5C^{myc}, HAP1A^{HA} and Ahi1^{GFP} results in all three proteins colocalising and HAP1A^{HA} and Ahi1^{GFP} positive clusters being trafficking to the cell membrane. Scale bar, 20µm.

forming protein clusters evenly throughout the cytoplasm, as previously shown (Figure 5.5C), these clusters were trafficked out to the cell periphery. Furthermore, KIF5C^{myc}, although maintaining some microtubule staining, also showed colocalisation with the HAP1A^{HA} clusters (Figure 5.8C). This data demonstrates that HAP1A^{HA} clusters can be trafficked along microtubules by KIF5C^{myc} in an anterograde direction typical of a kinesin motor. Intriguingly, upon cotransfection of Ahi1^{GFP} and KIF5C^{myc} there was no redistribution of Ahi1^{GFP} to the cell periphery, instead the subcellular localisation of Ahi1^{GFP} remained cytosolic (Figure 5.8D). However, when all three proteins were transfected into COS-7 cells together both Ahi1^{GFP} and HAP1^{HA} could be redistributed to the edge of the cell. In addition, Ahi1^{GFP}, HAP1A^{HA} and KIF5C^{myc} all colocalised, confirming by immunofluorescence that these three proteins interact and form a trafficking complex (Figure 5.8E). Taken together this data shows that the Ahi1/HAP1/KIF5C complex identified from brain lysate immunoprecipitation experiments can occur within a cell system. Moreover, it shows that Ahi1 can be functionally trafficked by KIF5C in a HAP1-dependent manner.

5.2.3 Subcellular distribution of Ahi1 in neurons

The identification of an Ahi1/HAP1/KIF5C complex that exists in brain and the evidence that Ahi1, in the presence of HAP1, can be trafficked by KIF5C raised the question as to what function Ahi1 may play with respect to HAP1 in $GABA_AR$ trafficking at the inhibitory synapse. In order to determine whether Ahi1 could impact on HAP1 function at the inhibitory synapse it was first necessary to determine whether Ahi1 could be detected at synapses in neurons. To study the subcellular localisation of Ahi1, mature cortical neurons transfected with Ahi1^{GFP} for 3 days, were fixed and stained for inhibitory synaptic markers. The presynaptic markers vGAT, or GAD6 were used. The same neurons were costained for the inhibitory postsynaptic markers, gephyrin or the $GABA_AR$ synaptic specific subunit γ2. Ahi1^{GFP} displayed an even distribution throughout the neuron showing expression in the soma, axon and dendrites. Interestingly, Ahi1^{GFP} appeared punctate along the dendrites and Ahi1^{GFP} puncta colocalised with inhibitory pre and postsynaptic markers (Figure 5.9A, white arrowheads). It was noted that Ahi1^{GFP} appeared to be present in dendritic spine heads and therefore the localisation of Ahi1^{GFP} with respect to excitatory synaptic markers was also studied. Ahi1^{GFP} colocalised with the PSD scaffold protein homer, an excitatory postsynaptic marker, opposed to vGlut, an excitatory presynaptic marker (Figure 5.9A).

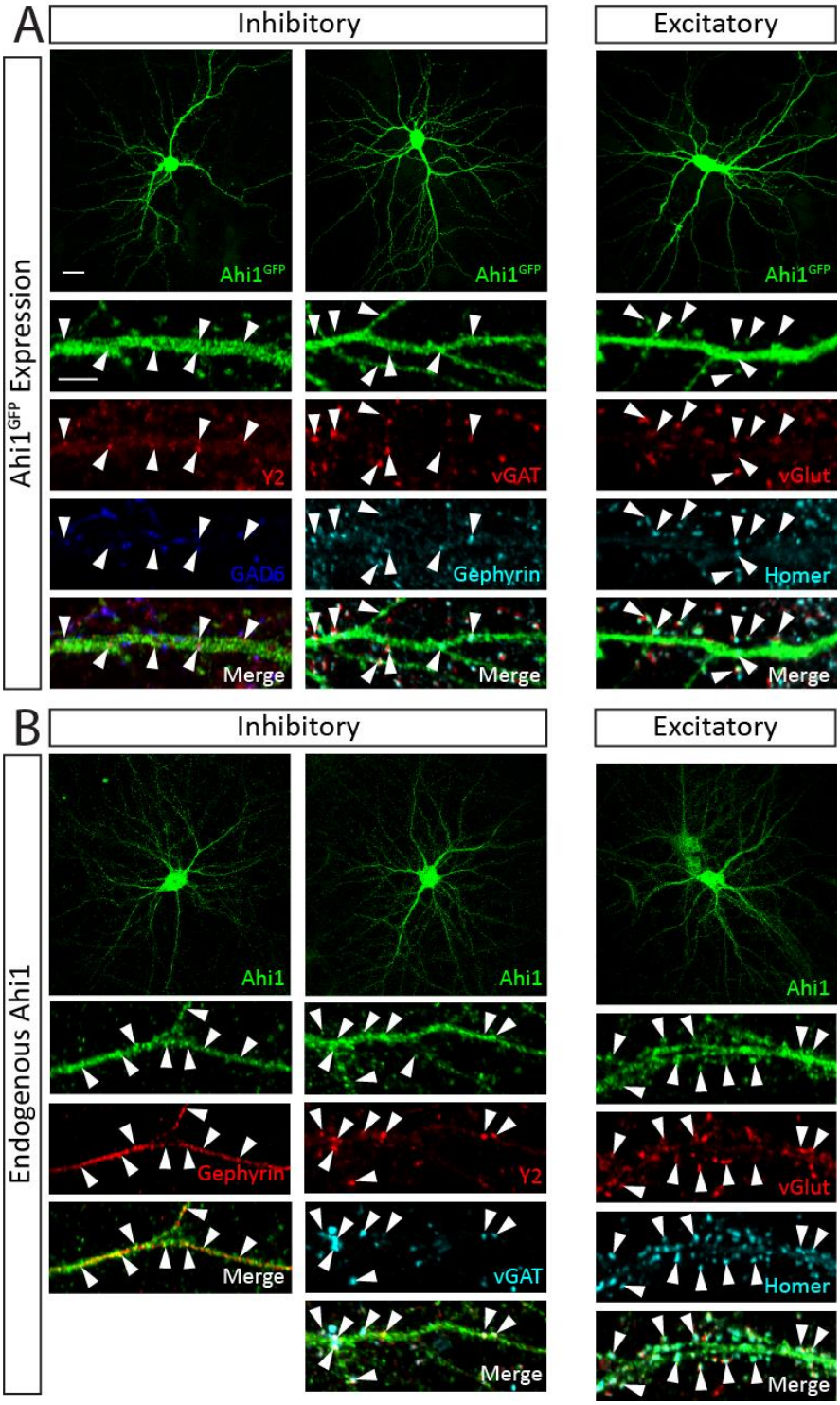

Figure 5.9: Ahi1 is present at inhibitory and excitatory synapses.

(A) Ahi1^{GFP} was transfected into mature mouse cortical neurons and stained with antibodies against the pre and postsynaptic inhibitory markers vGAT or GAD6 and gephyrin or $GABA_AR$-γ2 respectively (left panel). Ahi1^{GFP} colocalised with the postsynaptic inhibitory markers opposed to presynaptic markers (arrowheads). Transfected neurons were also stained for

the excitatory synaptic pre and postsynaptic markers vGlut and homer respectively (right panel). Ahi1^{GFP} was present in dendritic spines colocalised with homer and vGlut (arrowheads). **(B)** Endogenous Ahi1 was labelled in neurons using an Ahi1-specific antibody and produced clustered staining along dendrites. Endogenous Ahi1 colocalised with the inhibitory postsynaptic markers gephyrin and $GABA_AR$-γ2 opposite presynaptic vGAT clusters (left panel, arrowheads). Endogenous Ahi1 colocalised with the excitatory pre and postsynaptic markers vGlut and homer respectively (right panel, arrowheads). Scale bars, whole cell 20μm, zoom 2μm.

Interestingly, carrying out the same experiments with a specific Ahi1 antibody, to observe the localisation of endogenous Ahi1, enhanced the punctate distribution of Ahi1 along dendrites. Endogenous Ahi1 also colocalised with the inhibitory presynaptic markers vGAT and GAD6 and the postsynaptic markers gephyrin and $GABA_AR$-γ2. In addition, endogenous Ahi1 could be detected in dendritic spines and localised with the excitatory pre and postsynaptic markers, vGlut and homer respectively (Figure 5.9B). Taken together these data highlight that Ahi1 is detected at both inhibitory and excitatory synapses along dendrites. However, due to the presence of $Ahi1^{GFP}$ and endogenous Ahi1 throughout the dendrites Ahi1 is not enriched at synapses. Nevertheless, Ahi1 could potentially function as a trafficking adaptor protein that may play a role at these sites and contribute to the maintenance of normal synaptic transmission.

5.2.4 Ahi1 does not play a role in the $GABA_AR$ trafficking function of HAP1

This study has identified Ahi1 as a novel member of the HAP1/KIF5 trafficking complex and has furthermore, illustrated that Ahi1 can be detected at inhibitory synapses. Previous work has demonstrated that HAP1 functions as an adaptor protein coupling $GABA_ARs$ via the β3 subunit to the KIF5C motor within the inhibitory synapse. This interaction promotes the recycling of $GABA_AR$ containing vesicles back to the membrane to allow insertion of the receptors. Knockdown of HAP1 by RNAi results in a decrease in the number of surface $GABA_ARs$ (Twelvetrees et al., 2010). It therefore seemed appropriate to study whether Ahi1 could impact on the $GABA_AR$ trafficking function of HAP1. To investigate this, DIV10 hippocampal neurons were transfected with $HAP1^{GFP}$, $Ahi1^{GFP}$ or GFP control (Figure 5.10A). The neurons were left to overexpress the exogenous proteins for 3-4 days before being fixed and subjected to immunofluorescence. A surface stain protocol was used with an antibody specific to an extracellular epitope of the synaptic $GABA_AR$-γ2 subunit. This staining only labelled surface $GABA_ARs$ inserted into the membrane; typically the staining appeared clustered along the dendrites characteristic of $GABA_ARs$ tethered within synapses. By analysing the number and area of surface clusters information about the amount of postsynapses and strength of synapses can be revealed. Following surface staining neurons were then permeablised and stained with antibodies against GAD6 the presynaptic marker and GFP to amplify the fluorescent protein signal. Neurons overexpressing HAP1 showed significantly more $GABA_AR$ clusters and a significantly

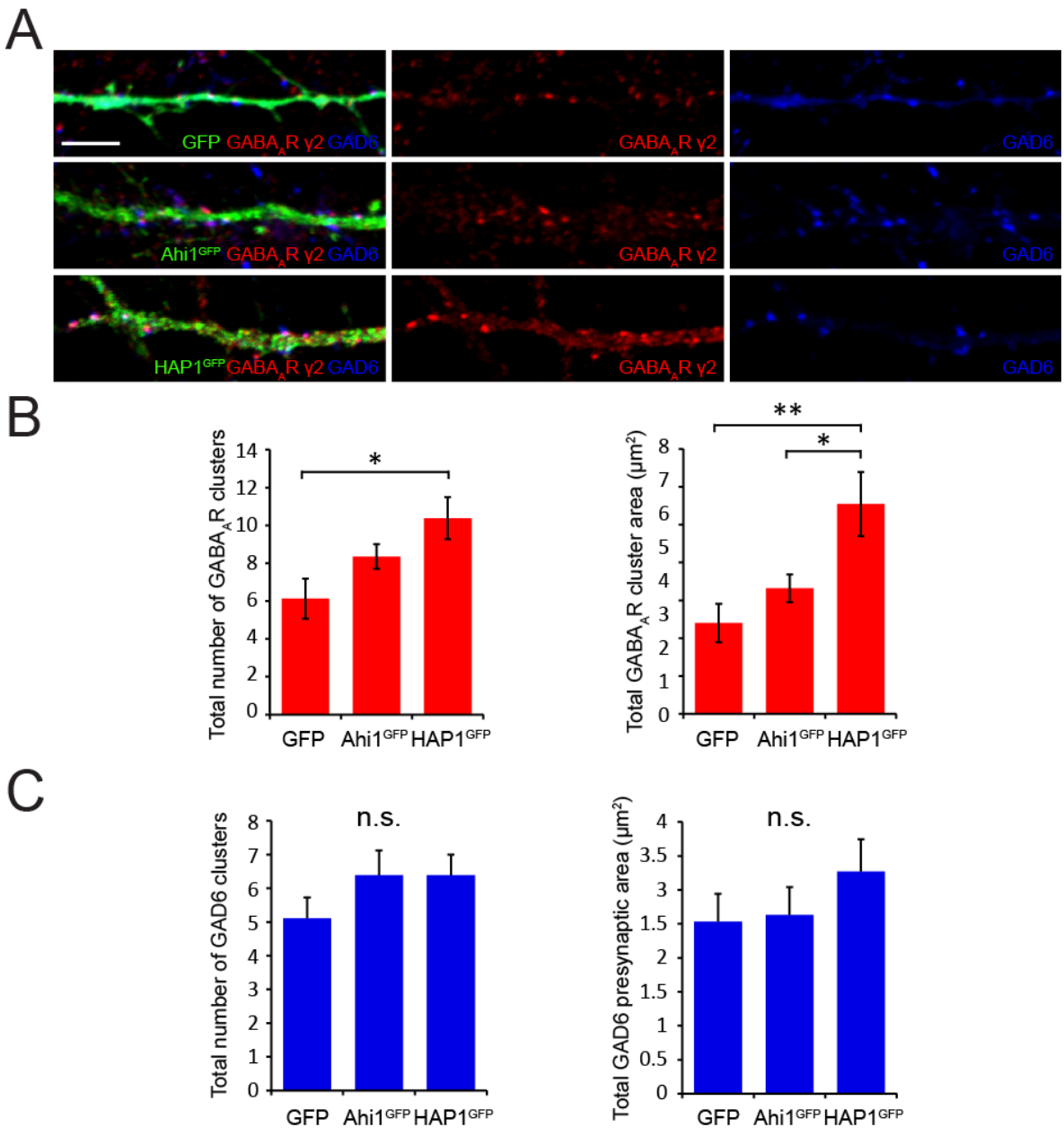

Figure 5.10: Overexpression of HAP1 but not Ahi1 effects surface GABA$_A$R clusters.

(A) Rat hippocampal neurons were transfected with Ahi1^{GFP}, HAP1^{GFP} or GFP control at DIV10 and allowed to express the transgene for 4 days before fixing and staining for surface GABA$_A$R-γ2 inhibitory synaptic clusters. Neurons were then permeablised and stained for GAD6 inhibitory presynaptic clusters. **(B)** Analysis of surface GABA$_A$R-γ2 clusters revealed both number of clusters and total cluster area increased upon HAP1^{GFP} but not upon Ahi1^{GFP} overexpression compared to control cells (n=20-23 cells; one-way ANOVA; *p<0.05, **p<0.01). **(C)** Analysis of GAD6 presynaptic clusters revealed no significant difference in cluster number and cluster area upon Ahi1^{GFP} or HAP1^{GFP} overexpression compared to control cells (n =18-20 cells; one-way ANOVA; NS). Scale bars, 2μm.

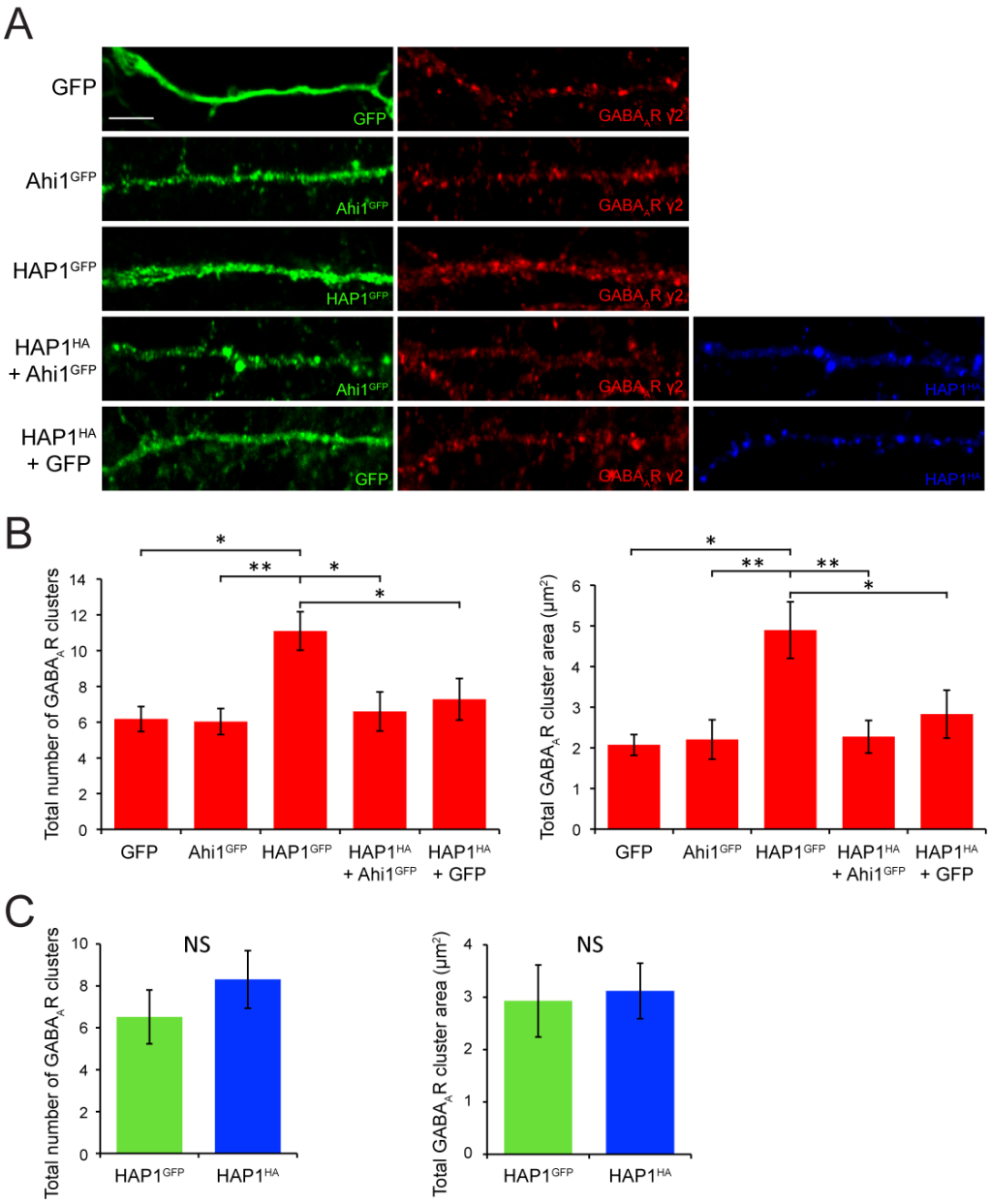

Figure 5.11: The effect of Ahi1 and HAP1 coexpression on GABA$_A$R surface clusters.

(A) Rat hippocampal neurons were transfected with either GFP, Ahi1^{GFP}, HAP1^{GFP}, Ahi1^{GFP} + HAP1^{HA} or GFP + HAP1^{HA} at DIV10 and allowed to express the transgenes for 4 days before fixing and staining for surface GABA$_A$R-γ2 inhibitory synaptic clusters. Neurons were then permeablised and expression of the transfected proteins was confirmed by staining with anti-GFP and/or anti-HA antibodies. **(B)** Analysis of surface GABA$_A$R-γ2 clusters revealed both number and total cluster area increased upon HAP1^{GFP} but not Ahi1^{GFP} overexpression compared to control cells. Following coexpression of Ahi1^{GFP} + HAP1^{HA} the HAP1-mediated increase in surface clusters could not be observed. Coexpresison of GFP + HAP1^{HA} also blocked the HAP1 alone effect (n=19-24 cells; Kruskal-Wallis ANOVA; *p<0.05, **p<0.01). Scale bars, 2μm. **(C)** Analysis of HAP1^{GFP} and HAP1^{HA} overexpressing cells showed no significant difference in the effect on surface GABA$_A$R-γ2 cluster number or area.

greater total area of $GABA_AR$ clusters compared to control GFP expressing neurons (Figure 5.10B). However, upon overexpression of $Ahi1^{GFP}$, the number and total area of $GABA_AR$ clusters did not differ from control ($GABA_AR$ cluster number: GFP, 6.13 ± 1.06; $Ahi1^{GFP}$, 8.35 ± 0.65; $HAP1^{GFP}$, 10.38 ± 1.11; *p<0.05; cluster area: GFP, 2.40 ± 0.51μm², $Ahi1^{GFP}$, 3.32 ± 0.37μm², $HAP1^{GFP}$, 5.55 ± 0.85μm²; *p<0.05, **p<0.01). Interesting, the postsynaptic effects observed with overexpression of $HAP1^{GFP}$ had no impact on the presynapse as the number and total area of GAD6 clusters was not significantly different from control cells when either $HAP1^{GFP}$ or $Ahi1^{GFP}$ were expressed (Figure 5.10C; cluster number: GFP, 5.11 ± 0.62; $Ahi1^{GFP}$, 6.38 ± 0.74; $HAP1^{GFP}$, 6.39 ± 0.61; cluster area: GFP, 2.53 ± 0.41μm², $Ahi1^{GFP}$, 2.63 ± 0.41μm², $HAP1^{GFP}$, 3.27 ± 0.48μm²; NS).

Although Ahi1 alone does not appear to influence the number of surface $GABA_ARs$ it was interesting to determine whether Ahi1 as a protein interactor of HAP1 could either promote of antagonise HAP1's $GABA_AR$ trafficking function. In a second set of experiments, the surface levels of the $GABA_AR$-γ2 subunit were analysed upon coexpression of both HAP1 and Ahi1. Neurons expressing $HAP1^{HA}$ and $Ahi1^{GFP}$ were compared to single transfected cells, or $HAP1^{HA}$ and GFP expressing cells (Figure 5.11A). As in the previous set of experiments, overexpression of $HAP1^{GFP}$ alone resulted in a significant increase in total number and total area of $GABA_AR$ clusters compared to GFP control cells (Figure 5.11B). These increases were not seen when $Ahi1^{GFP}$ was overexpressed. Initially, it appeared very intriguing that when $HAP1^{HA}$ and $Ahi1^{GFP}$ were coexpressed the HAP1-mediated increase in total $GABA_AR$ cluster number and area could not be observed. This suggested that Ahi1 could have been negatively regulating HAP1 function. However, with the addition of a further condition, to control for expression changes brought about by plasmid competition in cotransfected cells, it was shown that coexpression of $HAP1^{HA}$ and GFP could also non-specifically block the HAP1-mediated increase in $GABA_AR$ clusters. Taken together, this implies the occlusion of a HAP1-mediated increase in surface $GABA_AR$ clusters upon coexpression of $HAP1^{HA}$ and $Ahi1^{GFP}$ could be non-specific (Figure 5.11B; $GABA_AR$ cluster number: GFP, 6.18 ± 0.69; $Ahi1^{GFP}$, 6.03 ± 0.73; $HAP1^{GFP}$, 11.1 ± 1.07; $HAP1^{HA}$ + $Ahi1^{GFP}$, 6.8 ± 1.09; $HAP1^{HA}$ + GFP, 7.28 ± 1.16; cluster area: GFP, 2.07 ± 0.26μm²; $Ahi1^{GFP}$, 2.21 ± 0.48μm²; $HAP1^{GFP}$, 4.89 ± 0.7μm²; $HAP1^{HA}$ + $Ahi1^{GFP}$, 2.27 ± 0.4μm²; $HAP1^{HA}$ + GFP, 2.83 ± 0.59μm²; *p<0.05, **p<0.01). In summary, overexpression of HAP1 can induce changes in surface $GABA_AR$ levels that result in

more and larger $GABA_AR$ clusters. In contrast, overexpression of Ahi1 does not influence the surface levels of $GABA_ARs$. Lastly, it can be concluded that Ahi1 does not positively modulate HAP1's $GABA_AR$ trafficking function.

5.2.5 Characterisation of Ahi1 knockdown and its effect on $GABA_AR$ trafficking

It is possible that Ahi1 is expressed at high levels within neurons under steady-state conditions. Therefore, the overexpression experiments described above may not alter the system to a great extent, resulting in there being little or no effect on the experimental readout. With that in mind, an RNA interference (RNAi) approach was developed to look at the effects of reduced Ahi1 expression on $GABA_AR$ trafficking. Short hairpin RNA constructs (shRNA) were developed to target Ahi1 mRNA for degradation resulting in knockdown of the protein levels within the transfected cell. A previously published shRNA sequence against Ahi1 (Hsiao et al., 2009) was cloned into the pSuper vector (Oligoengine), which contained a GFP reporter gene under a different promoter to the shRNA to allow for identification of transfected cells. To characterise the Ahi1 shRNA in the experimental systems used in this study, mouse hippocampal neurons were transfected with Ahi1 shRNA or a scrambled control shRNA at DIV10. Neurons were then fixed and stained with the Ahi1 specific Abcam antibody at DIV14 allowing 4 days of Ahi1 shRNA expression (Figure 5.12A). Quantification revealed that average fluorescence intensity of Ahi1 immunolabelling was significantly reduced by 55% in neurons expressing Ahi1 shRNA compared to control shRNA expressing neurons (Figure 5.12B; control shRNA: 100 ± 12.75%; Ahi1 shRNA: 45.45 ± 2.65%; ***$p<0.001$). This demonstrates the effectiveness of the Ahi1 specific shRNA at decreasing endogenous levels of Ahi1 protein.

Ahi1 RNAi was then used to explore the effect of Ahi1 knockdown on $GABA_AR$ trafficking. Mouse hippocampal neurons were transfected with Ahi1 shRNA or control shRNA, and fixed after 4 days of expression. The neurons were then surface stained using an extracellular $GABA_AR$-γ2 subunit specific antibody to label surface $GABA_AR$ clusters. Cluster analysis showed that there was no change in total $GABA_AR$ cluster number or area in Ahi1 knockdown cells compared to control cells (Figure 5.13; $GABA_AR$ cluster number: control shRNA, 6.98 ± 0.9; Ahi1 shRNA, 6.89 ± 0.7; cluster area: control shRNA, 2.13 ± 0.29μm²; Ahi1 shRNA, 2.02 ± 0.21μm²; NS). This result demonstrates that reduced levels of Ahi1 have no impact on the levels of $GABA_ARs$

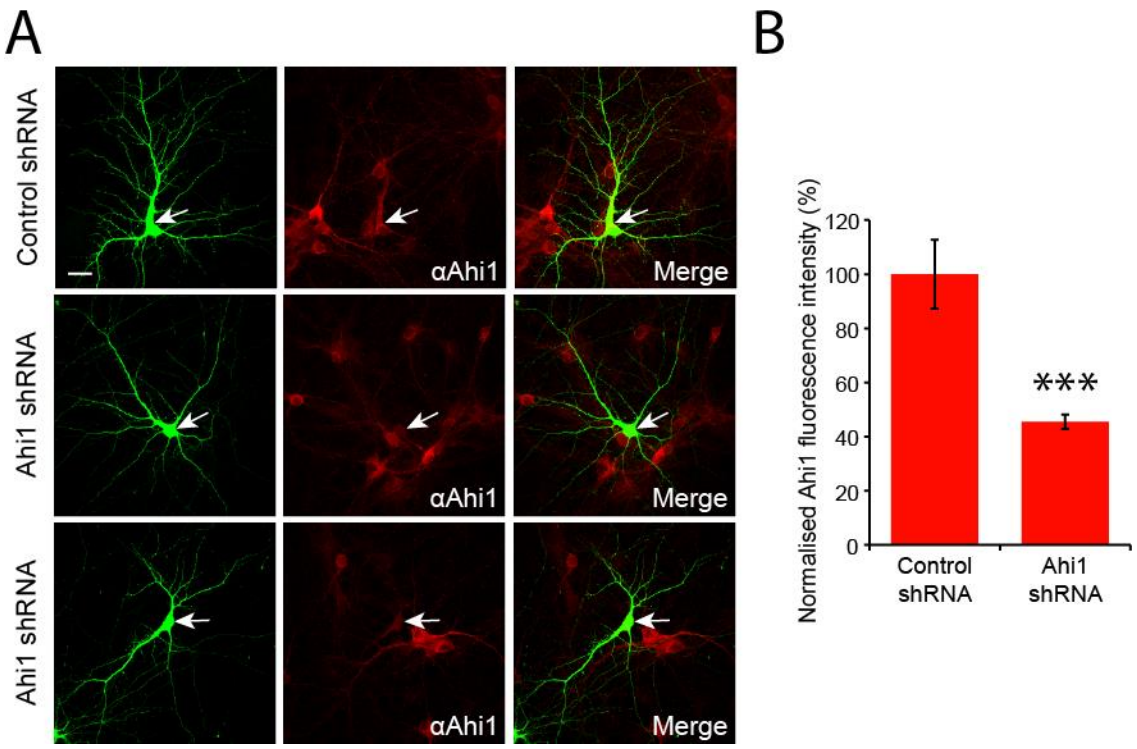

Figure 5.12: Characterisation of Ahi1 RNAi.

(A) Mouse hippocampal neurons were transfected with either control or Ahi1 specific short hairpin RNA (shRNA) at DIV10 and allowed to express the shRNA for 4 days before fixing and staining for endogenous Ahi1 with an Ahi1 specific antibody. Transfected neurons were detected by their GFP fluorescence due to a GFP-reporter gene present on the shRNA vector. **(B)** Analysis of endogenous Ahi1 average fluorescence intensity in Ahi shRNA compared to control shRNA transfected cells. Expression of Ahi1 specific shRNA produced a significant ~50% reduction in the endogenous levels of Ahi1 compared to control shRNA expressing cells confirming the efficiency of the Ahi1 shRNA (n=24-25; Mann-Whitney U test; ***p<0.001). Scale bar, 20µm.

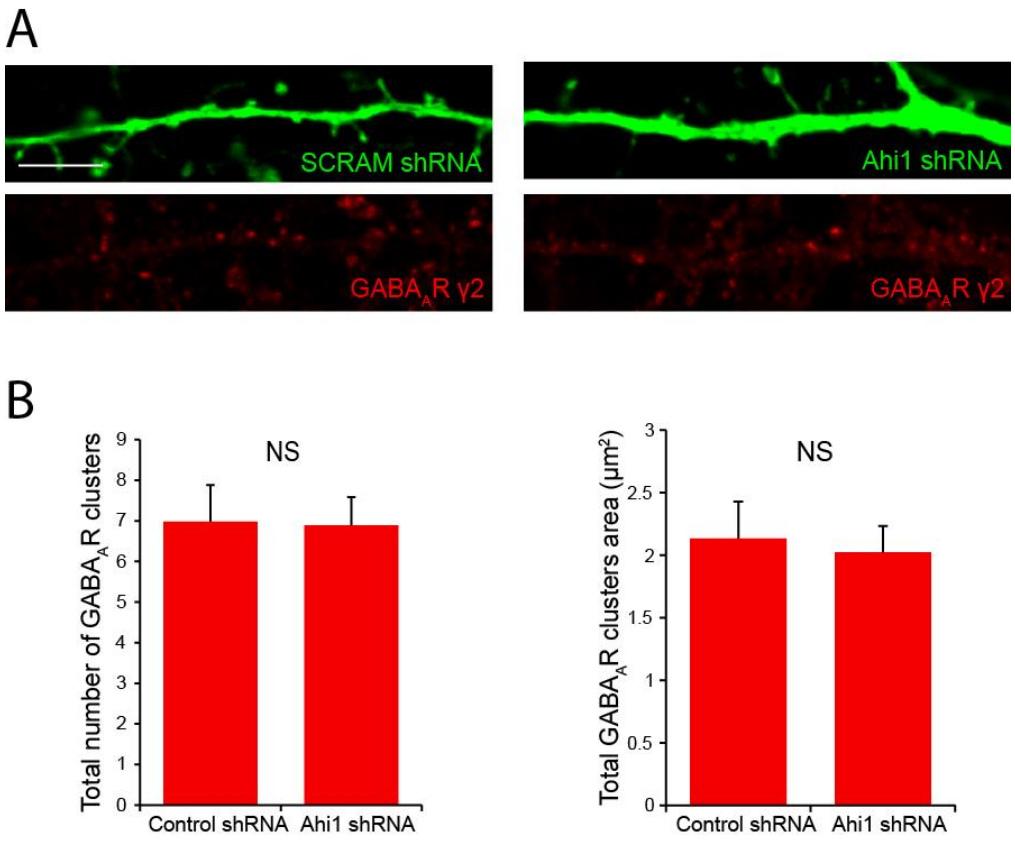

Figure 5.13: Ahi1 knockdown does not affect surface GABA$_A$R clusters.

(A) Mouse hippocampal neurons were transfected with control shRNA or Ahi1 shRNA at DIV10 and allowed to express the shRNA for 4 days before fixing and staining for surface GABA$_A$R-γ2 inhibitory synaptic clusters. **(B)** Analysis of surface GABA$_A$R-γ2 clusters revealed no significant difference in both number of clusters and total cluster area upon expression of Ahi1 shRNA compared to control (n=18; Mann-Whitney U test; NS). Scale bars, 2μm.

within the membrane. This suggests that although Ahi1 can interact with HAP1, a protein known to be important in $GABA_AR$ trafficking, Ahi1 itself does not appear to be playing a role in this pathway. Hence, these findings suggest that disrupted $GABA_AR$ trafficking is unlikely to be a pathogenic mechanism of Ahi1 loss of function mutations in humans.

5.2.6 The effect of Ahi1 knockdown on dendritic morphology

Dysregulated neuronal development and connectivity, particularly within the cortex and hippocampus, are long standing hallmarks of brain disorders such as ASD and SCZ. Disrupted neuronal morphology has also been associated with other psychiatric disorders such as bipolar, anxiety and mental retardation (Kulkarni and Firestein, 2012). Patients with CNVs or mutations in *Ahi1* present with neuropsychiatric disorders such as ASD and SCZ (Amann-Zalcenstein et al., 2006; Retuerto et al., 2008). Therefore, it was interesting to assay whether dendritic development and connectivity was affected in cells with reduced Ahi1 expression. To study this, dendritic complexity was analysed, using Sholl analysis (Sholl, 1953), in DIV14 mouse hippocampal neurons transfected with Ahi1 shRNA or control shRNA for 4 days (Figure 5.14A). In brief, the neuronal morphology was traced and concentric rings equally spaced apart were created expanding out from the cell soma. The number of times a dendrite intersects each ring was plotted as a function of distance from the soma and generated an output for dendritic complexity. Ahi1 knockdown resulted in a significant increase in both the number of intersections and the number of branch points as a function of distance from the soma compared to control shRNA expressing neurons (Figure 5.14B; $*p<0.05$, $**p<0.01$). In addition, total dendritic length and the total number of branch points per cell were also significantly increased, by 28 and 41% respectively, in Ahi1 knockdown cells compared to control (Figure 5.14C; dendritic length: control shRNA, 2175.58 ± 197.87µm; Ahi1 shRNA, 2795.76 ± 187.53µm; branch points: control shRNA, 47.83 ± 5.21; Ahi1 shRNA, 67.58 ± 5.49; $*p<0.05$). In summary knockdown of Ahi1 impacts on neuronal morphology resulting in cells displaying increased dendritic complexity.

5.2.7 The impact of Ahi1 ASD-associated mutations on Ahi1 function

Recent genetic studies have associated the gene *Ahi1* with ASD (Brett et al., 2014; Retuerto et al., 2008). One particular investigation has highlighted that those patients with JS, the neurodevelopmental disease brought about by mutations in *Ahi1*, present

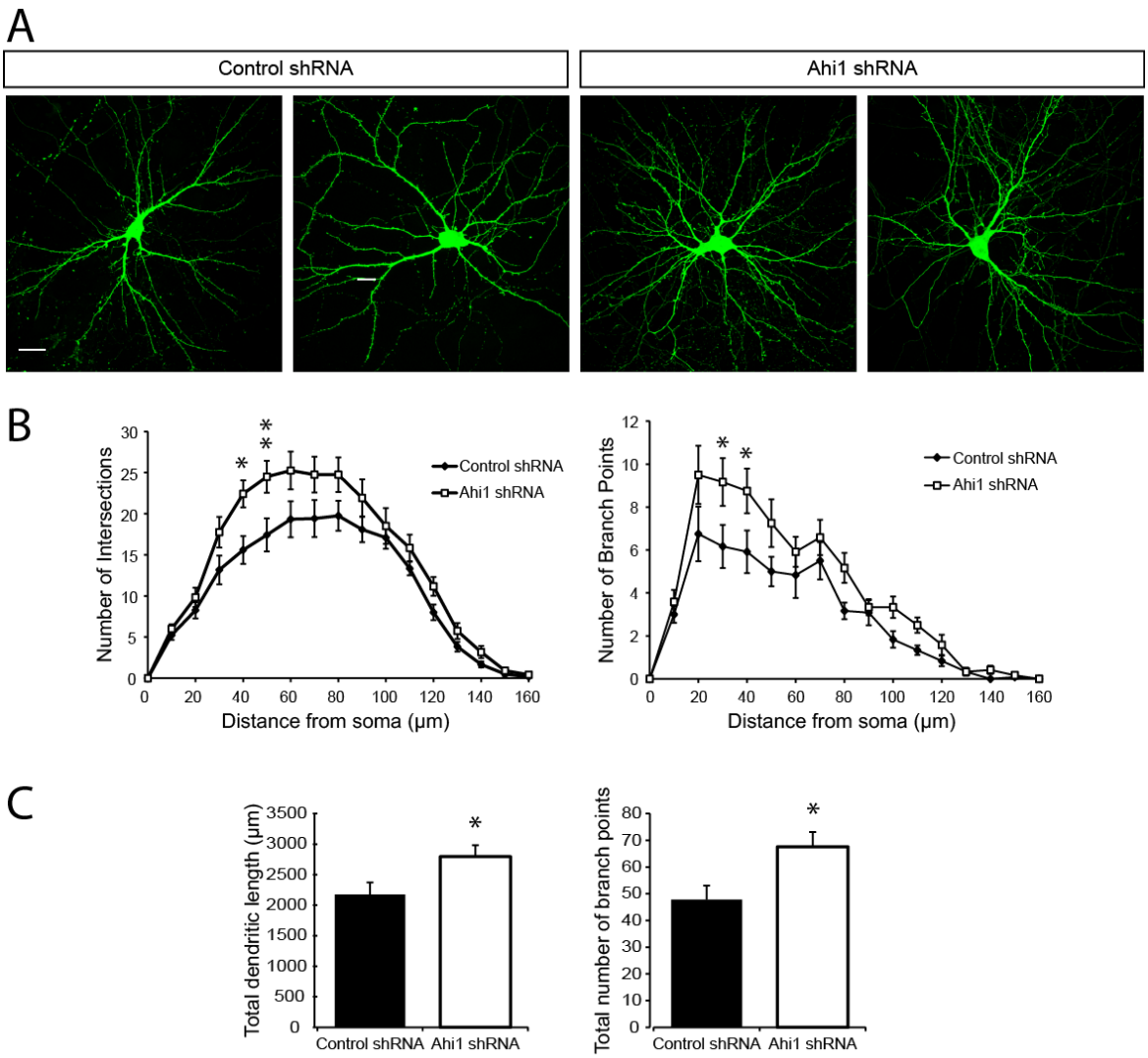

Figure 5.14: Ahi1 knockdown affects dendritic morphology.

(A) Mouse hippocampal neurons were transfected with control shRNA or Ahi1 shRNA at DIV10 and allowed to express the shRNA for 4 days before fixing and staining with an anti-GFP antibody to amplify the shRNA GFP reporter fluorescence for efficient dendritic tracing. **(B)** Quantification by Sholl analysis shows that number of intersections (left panel) and number of branch points (right panel) are significantly increased with distance from the soma in Ahi1 shRNA expressing neurons compared to control shRNA expressing cells (data points represent an average of 12 cells; 2-way ANOVA; *p<0.05, **p<0.01). **(C)** Expression of Ahi1 shRNA increases total dendritic length and total number of branch points per cell compared to neurons expressing control shRNA (n=12; student's t-test; *p<0.05). Scale bar 20μm.

Table 5.1: Summary of Ahi1 ASD-associated mutations

Residue Change	Allele Change	Variant Type	Disease Association	Reference
R351X	C1051T	Nonsense	JB, ASD	(Ferland et al., 2004)
R435X	C1303T	Nonsense	JS, ASD	(Ferland et al., 2004)
V433D	T1328A	Missense	JS, ASD	(Dixon-Salazar et al., 2004; Ferland et al., 2004)
Y933C	A2798G	Missense	ASD	(Retuerto et al., 2008; Yu et al., 2013)

with ASD characteristics (Retuerto et al., 2008). A number of pathogenic point mutations in *Ahi1* have been described to cause JS (Table 4.2). Therefore, exploring how these mutations impact on Ahi1 function may provide some insights not only into the mechanisms of JS but why patients display neuropsychiatric behaviours.

Point mutations in the human Ahi1 coding sequence were introduced into hAhi1^{GFP} using PCR. All four hAhi1 mutants were confirmed by sequencing and readily expressed in COS-7 cells (Figure 5.15A,B). Interestingly, the two C-terminal truncated mutants of hAhi1^{GFP}, R351X and R435X, were highly expressed in the nucleus. hAhi1$^{GFP(R435X)}$ also showed diffuse cytosolic staining similar to WT hAhi1^{GFP} however, hAhi1$^{GFP(R351X)}$ only showed some small puncta within the cytosol with the majority of protein retained within the nucleus. It appears the C-terminal truncations may have altered the protein folding of Ahi1 and exposed a nuclear localisation signal (NLS) targeting these mutants to the nucleus. The distribution of hAhi1$^{GFP(V433D)}$ and hAhi1$^{GFP(Y933C)}$ appeared unchanged from WT. Coimmunoprecipitation experiments from COS-7 cells transfected with hAhi1^{GFP} mutants and HAP1B^{HA} revealed that all the hAhi1^{GFP} mutants could still interact with HAP1B^{HA} despite the disrupted cellular localisation of the C-terminal truncated mutants R351X and R435X (Figure 5.15C). Quantification of these interactions revealed the hAhi1$^{GFP(R351X)}$ and hAhi1$^{GFP(R435X)}$ showed a trend towards less binding with HAP1B^{HA} compared to WT hAhi1^{GFP}. Indeed, this could be due to more of the truncated Ahi1 mutants being targeted to the nucleus and therefore less able to interact with HAP1 (Figure 5.15D; normalised amount of Ahi1^{GFP} binding: WT, 1 ± 0; R351X, 0.59 ± 0.28; R435X, 0.49 ± 0.18; V433D, 1.5 ± 0.5; Y933C, 1.39 ± 0.66; NS). In agreement with the biochemical coimmunoprecipitation experiment, when hAhi1^{GFP} mutants and HAP1A^{HA} were

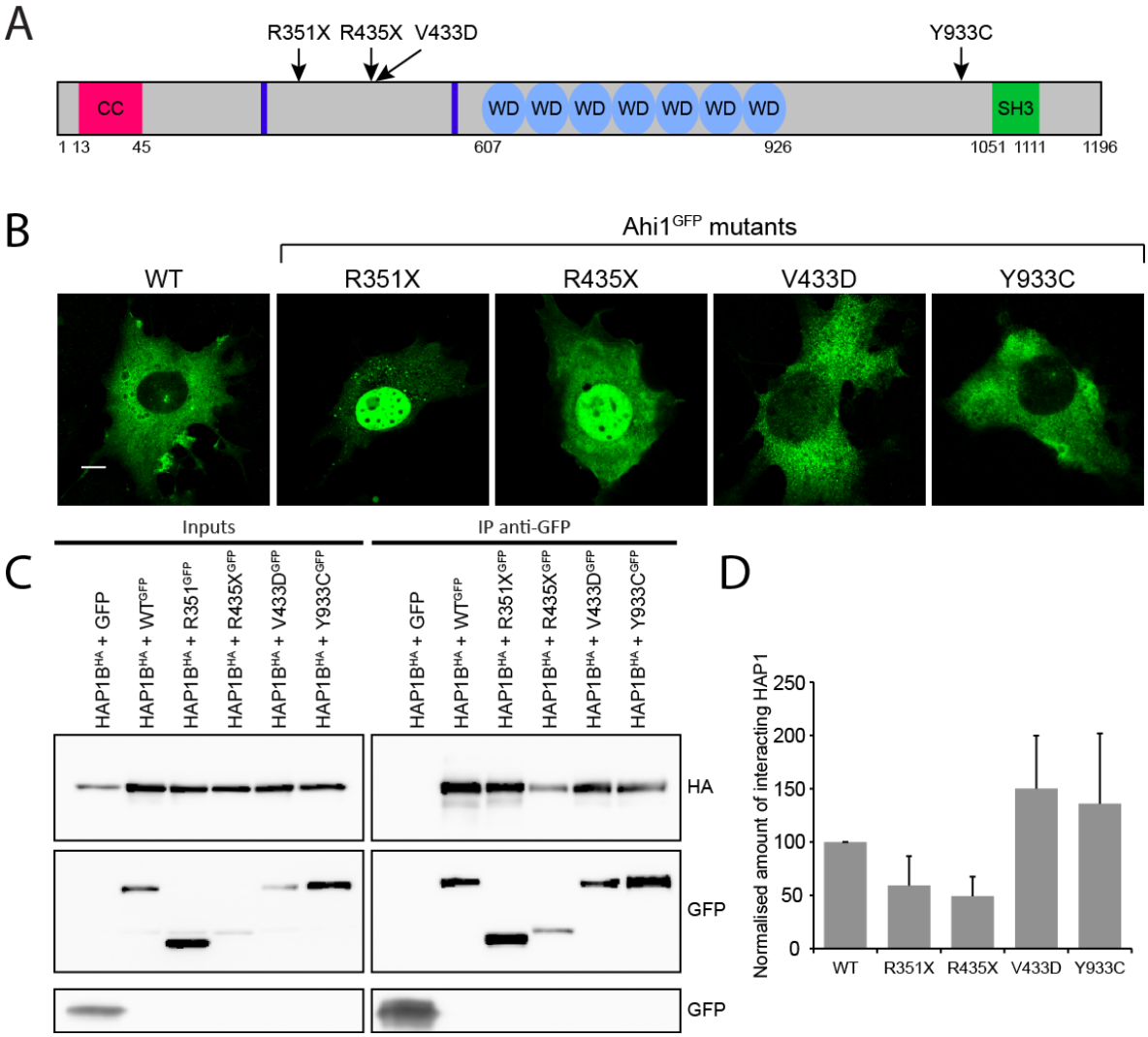

Figure 5.15: Ahi1 ASD mutants interact with full-length HAP1.

(A) A schematic depicting four point mutants in hAhi1 that have been found in patients with JS and associated with ASD. **(B)** Confocal images of COS-7 cells transfected with WT human Ahi1^{GFP}, or the four mutants R351X, R435X, V433D, Y933C resulting in 2 N-terminal truncated proteins, 1 with a mutation in the regions upstream of the WD40 domain and one with a mutation in the C-terminal SH3 domain. All proteins were readily expressed. **(C)** Western blots of protein complexes coimmunoprecipitated using anti-GFP TRAP beads from COS-7 cells transfected with HAP1B and either WT human Ahi1^{GFP} or R351X, R435X, V433D, Y933C human Ahi1^{GFP}. Input samples (Inputs) represent 5% of the cell lysate included in the immunoprecipitation (IP). Anti-GFP TRAP beads efficiently coimmunoprecipitated HAP1B^{HA} from cotransfected cell lysates but not from HAP1B^{HA} only transfected cells. Ahi1^{GFP} constructs were revealed with an anti-GFP antibody while an anti-HAP1 antibody was used to visualise HAP1B. **(D)** Quantification of amount of HAP1 coimmunoprecipitation normalised to the amount of Ahi1 pulled down (n=4; Kruskal-Wallis ANOVA; NS).

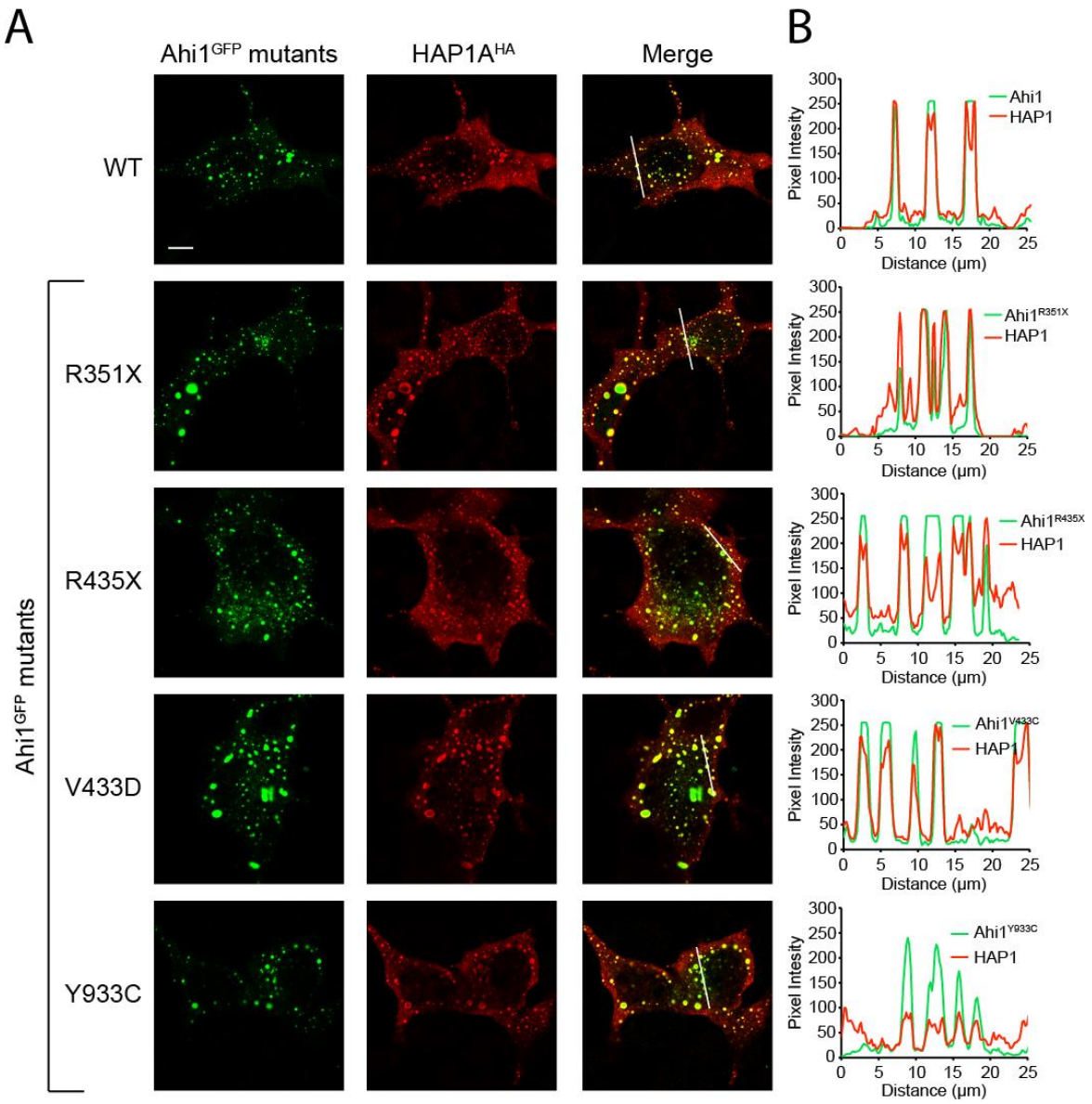

Figure 5.16: Ahi1 ASD mutants are recruited to HAP1-positive clusters in cells.

(A) Confocal images of COS-7 cells cotransfected with WT or mutant forms of human Ahi1^{GFP} and HAP1A^{HA} and subjected to immunofluorescence with anti-GFP and anti-HA antibodies. Colocalisation of Ahi1^{GFP} constructs and HAP1A^{HA} appears yellow in the merged image. **(B)** Line scans through the merged images show the fluorescence intensity of the green (Ahi1 mutants) and red (HAP1) channels, with overlapping peaks representing colocalisation. All four of the ASD associated Ahi1 mutants, like WT Ahi1, are redistributed from their cytosolic/nuclear localisation to large HAP1A positive clusters when coexpressed with HAP1A. Scale bar, 20µm.

cotransfected in COS-7 cells and subjected to immunofluorescence and confocalimaging all Ahi1 mutant proteins, in a similar way to WT Ahi1^{GFP}, were recruited into HAP1A^{HA} clusters. This can been seen by the yellow puncta in the merged image and the overlapping pixel intensity of the green and red channels in the line scans. Of note the truncated Ahi1 mutants R351X and R435X are no longer targeted to the nucleus in the presence of HAP1 suggesting the interaction with HAP1 may occlude any uncovered NLS (Figure 5.16).

This chapter has identified a novel Ahi1/HAP1/KIF5 trafficking complex that can be detected in brain tissue and demonstrates that Ahi1 can be trafficked by KIF5C in a HAP1 dependent manner. To explore the functional effects of the Ahi1 ASD mutants further, experiments were carried out to determine whether they too could be trafficked in a complex with HAP1 and KIF5C. WT hAhi1^{GFP} is not redistributed when coexpressed in COS-7 cells with KIF5C^{myc}. However, when HAP1A^{HA} is also expressed with WT Ahi1^{GFP} and KIF5C^{myc}, Ahi1^{GFP} is recruited to HAP1A^{HA} clusters and these clusters are trafficked in an anterograde direction to the cell membrane (Figure 5.17A). The Ahi1 ASD mutants follow the same pattern of redistribution. When all four mutants were coexpressed with KIF5C^{myc} alone their cellular localisation was unaffected. However, when the mutants were coexpressed with HAP1A^{HA} and KIF5C^{myc} the mutant Ahi1 proteins colocalised to HAP1A^{HA} clusters and were trafficked to the edge of the cell by KIF5C^{myc} (Figure 5.17B-E). Taken together this data demonstrates that Ahi1 ASD mutant proteins can still interact with HAP1 and be recruited to HAP1 clusters within the cell. Furthermore, the Ahi1 mutants can still be trafficked by KIF5C in a HAP1 dependent manner suggesting that these mutants must have more subtle effects on Ahi1 function and do not interfere with its HAP1 protein interactions.

-

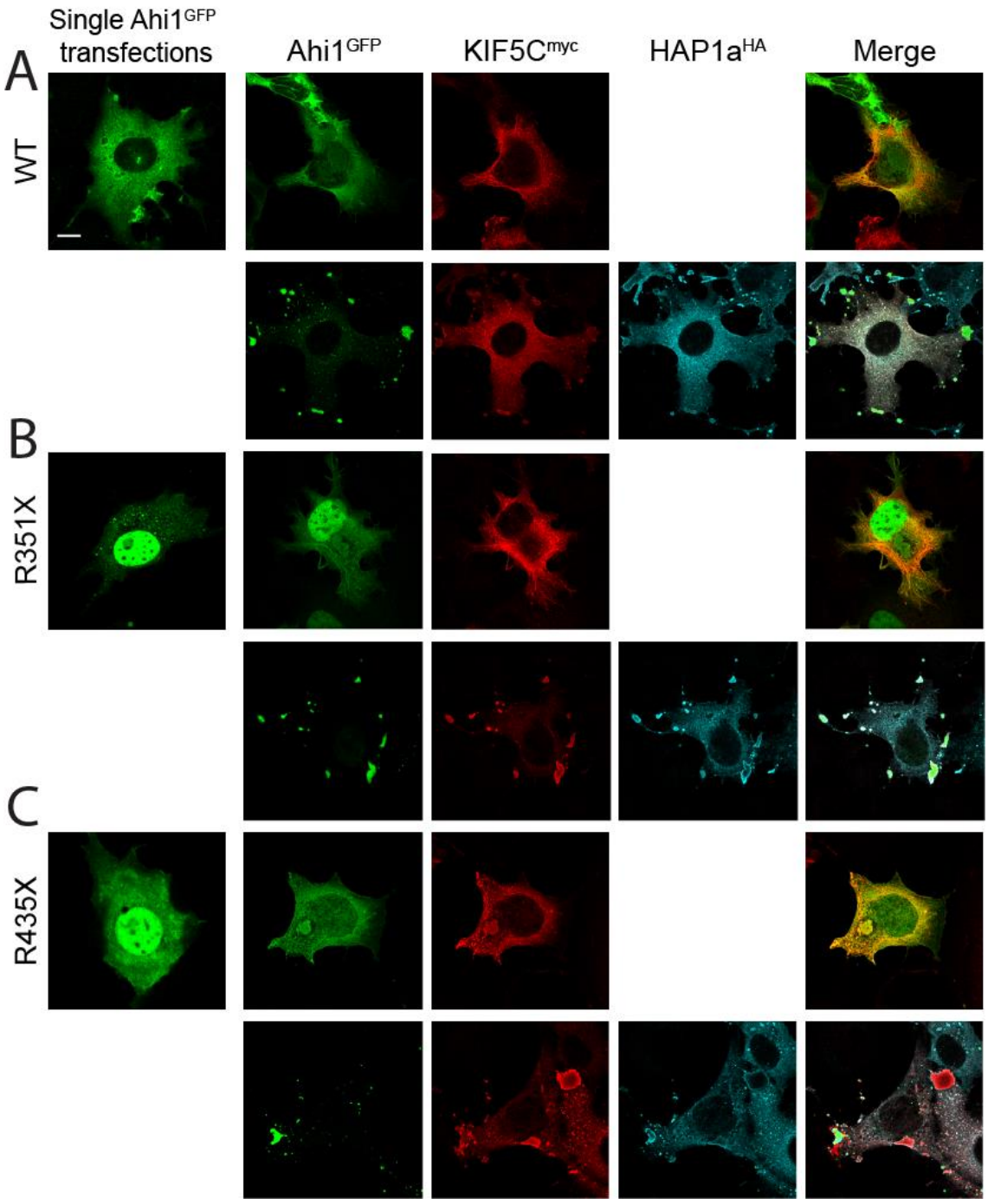

Figure continues over the page.

-

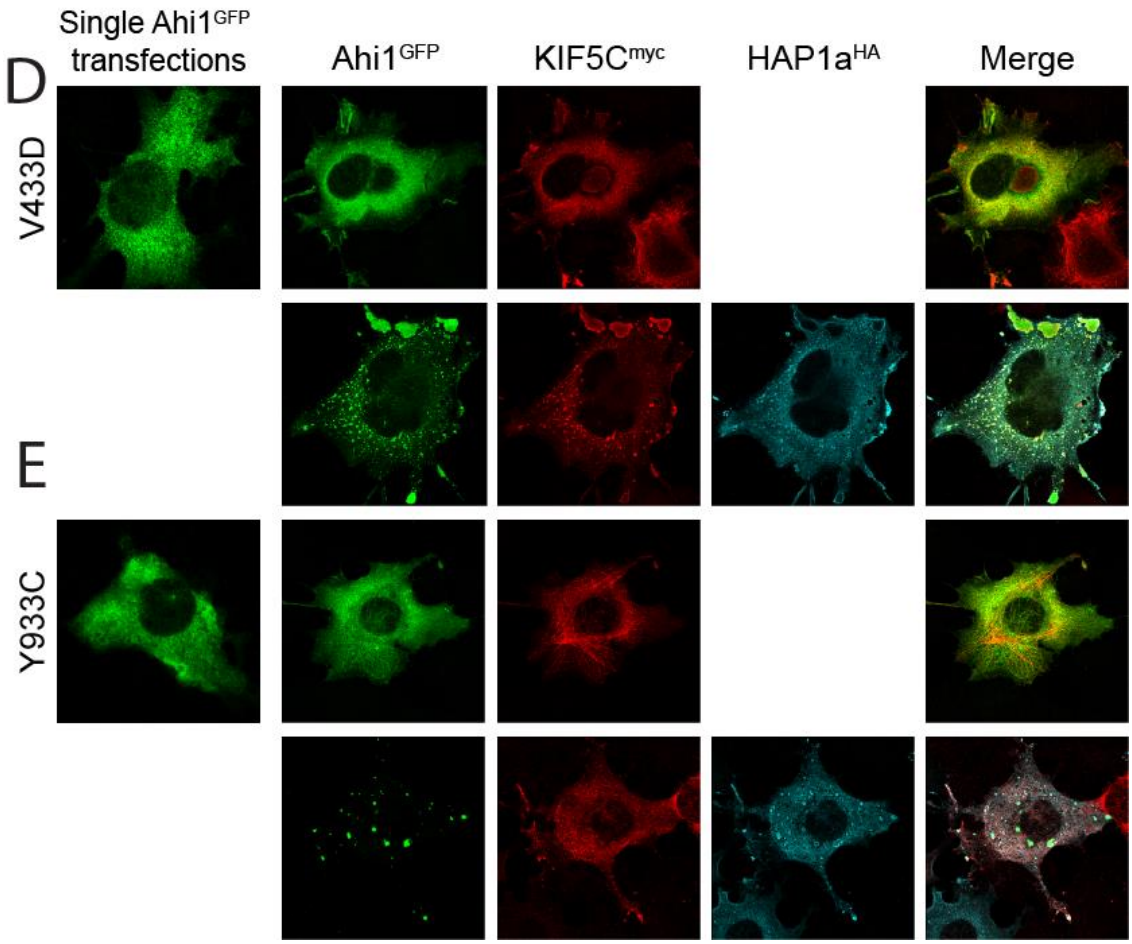

Figure 5.17: Ahi1 ASD mutants are trafficked by KIF5C in a HAP1-dependent manner.

Transfected COS-7 cells were fixed and immunostained against the expressed fusion protein tags before being imaged using confocal microscopy. **(A)** Cytosolic localisation of WT hAhi1^{GFP} alone (single transfection). Coexpression of WT hAhi1^{GFP} and KIF5C^{myc} does not interfere with KIF5C^{myc} microtubule staining. WT hAhi1^{GFP} is not redistributed and trafficked with KIF5C^{myc} (upper panels). A triple transfection of KIF5C^{myc}, HAP1A^{HA} and WT Ahi1^{GFP} results in all 3 proteins colocalising and HAP1A^{HA} and Ahi1^{GFP} positive clusters being trafficking to the cell membrane (lower panels). **(B-E)** Cytosolic/nuclear localisation of mutant Ahi1^{GFP} constructs alone (single transfections). Coexpression of mutant Ahi1^{GFP} constructs and KIF5C^{myc} does not interfere with KIF5C^{myc} microtubule staining. Mutant Ahi1^{GFP} constructs are not redistributed and trafficked with KIF5C^{myc} (upper panels). A triple transfection of KIF5C^{myc}, HAP1A^{HA} and Ahi1^{GFP} mutants results in all 3 proteins colocalising and HAP1A^{HA} and mutant Ahi1^{GFP} positive clusters being trafficking to the cell membrane along microtubules by KIF5C^{myc} (lower panels). Scale bar, 20µm.

5.3 Discussion

The data described in this chapter demonstrates that Ahi1, the protein mutated in the neurodevelopmental disorder Joubert syndrome (JS) and associated with neuropsychiatric phenotypes, interacts strongly with the trafficking molecule HAP1. This chapter reveals that the two proteins form a novel trafficking complex with KIF5 which exists *in vivo* in rodent brain. The trafficking of Ahi1 by KIF5C was shown to be dependent on HAP1. Irrespective of this trafficking complex, both overexpression and knockdown of Ahi1 did not alter surface levels of $GABA_A$Rs at inhibitory synapses, a mechanism known to be regulated by HAP1 and KIF5C (Twelvetrees et al., 2010). Nevertheless, endogenous Ahi1 was shown to be present at both inhibitory and excitatory synapses suggesting the protein may have an as yet unknown function in synaptic trafficking and transmission. Interestingly, Ahi1 ASD associated mutants can still interact with HAP1 and be trafficked by KIF5C. This points towards the mutations having more subtle effects on Ahi1 signalling and regulation rather than effecting its protein-protein interactions. In addition, knockdown of Ahi1 results in altered dendritic morphology a finding consistent with the defects in brain development observed in patients with JS.

5.3.1 Dissecting the Ahi1 HAP1 interaction

Since confirming the interaction between Ahi1 and HAP1 in the experiments described here, based on the original findings from Sheng and colleagues (Sheng et al., 2008), a number of papers have illustrated a robust interaction between Ahi1 and HAP1 (Niu et al., 2011; Tuz et al., 2013; Weng et al., 2013). Experiments carried out here have mapped the interaction between Ahi1 and HAP1 using HAP1 N-terminal truncations. Ahi1 was found to interact with the first coiled-coil domain (CC1) of HAP1 (aa169-205), this is consistent with findings from Tuz and colleagues (Tuz et al., 2013). Ahi1 therefore, either interacts directly with CC1 of HAP1 or the CC1 is required to make a HAP1 tertiary structure that allows Ahi1 to bind. Recently, others have attempted to map the binding of HAP1 onto Ahi1 using Ahi1 truncations (Sheng et al., 2008; Tuz et al., 2013; Weng et al., 2013). Sheng and colleagues initially showed a truncated version of mAhi1 (aa1-284) could still interact with HAP1 although to a lesser extent than WT Ahi1. Furthermore, unlike WT Ahi1, this truncation could not stabilise HAP1 protein levels (Sheng et al., 2008). A more recent publication from the same research group used GST fusion proteins and demonstrates the same N-

terminal truncation (aa1-284) bound very weakly to HAP1. This group also reported that Ahi1 protein fragments containing just the WD40 domain (aa262-795) or just the C-terminus and the SH3 domain (aa651-1047) could still interact with full-length HAP1 (Weng et al., 2013). Intriguingly, a yeast two-hybrid (Y2H) study has demonstrated that this is not the case for hAhi1. The results from this study clearly show that aa141-434 of hAhi1 (corresponding to the mouse aa1-284) robustly interact with HAP1. It is also shown that the WD40 domain and the C-terminal SH3 containing domain protein fragments do not interact with HAP1 (Tuz et al., 2013). These results contradict the mAhi1 mapping data. The species discrepancy in how Ahi1 interacts with HAP1 implies there could be differences in other Ahi1 protein-protein interactions between human and mouse. This raises important considerations when using mouse systems to study Ahi1 function, especially when studying human disease-associated mutations. However, the HAP1 binding site for Ahi1 illustrated here remains consistent for both mouse and human Ahi1 proteins.

The Y2H study also showed that the human specific N-terminal CC domain of Ahi1 alone (aa1-140) could not interact with HAP1 (Tuz et al., 2013). Results presented here have shown that the human Ahi1 autism mutant truncations aa1-351 (R351X) and aa1-455 (R435X) can still interact with HAP1. Taken together with the Y2H data these results indirectly map the HAP1 binding site on Ahi1 to aa212-351. It is interesting that common JS causing mutations, that are also associated with ASD, generate short Ahi1 fragments that still interact with HAP1. Perhaps these mutations encode truncated proteins that behave like dominant-negative constructs binding to HAP1 and disrupting its neuronal function. It would be interesting to carry out further experiments to explore this hypothesis.

5.3.2 Ahi1 in neuronal receptor trafficking and neuropsychiatric disorders

The strong interaction between HAP1 and Ahi1 coupled with their enrichment in the same brain regions pointed towards Ahi1 functioning with HAP1 or being implicated in the same molecular pathways. Indeed, it was exciting to hypothesise that Ahi1, with its many signalling domains, might regulate the $GABA_AR$ trafficking function of HAP1 (Twelvetrees et al., 2010). It could be speculated that defects in Ahi1, as seen in patients with JS, might dysregulate HAP1 function leading to disrupted inhibitory transmission and a pathological imbalance between neuronal excitation and

inhibition (Smith and Kittler, 2010). Demonstrating a regulatory role for Ahi1 in the E/I balance could have begun to provide an explanation for why altered Ahi1 expression results in neuropsychiatric and depressive phenotypes in human patients and animal models (Lotan et al., 2013; Ren et al., 2014; Retuerto et al., 2008; Torri et al., 2010; Xu et al., 2010). However, from the data presented in this chapter it appears this hypothesis is not the case. It can be concluded that Ahi1 does not impact the trafficking and recycling of $GABA_AR$s at the inhibitory synapse, using the methods described here. Neither overexpression nor knockdown of Ahi1, to manipulate Ahi1 signalling pathways, affected the levels of surface $GABA_AR$-γ2 clusters in hippocampal neuronal cultures.

Alternatively, it is possible that the experiments carried out in this chapter did not produce dramatic enough changes in Ahi1 protein levels to observe effects on synaptic trafficking. Ahi1 and HAP1 have been reported to stabilise each other (Sheng et al., 2008; Tuz et al., 2013; Xu et al., 2010). In Ahi1 KO tissue HAP1 protein levels are reduced compared to control and vice versa. In the RNAi experiments described here, perhaps the 55% loss of Ahi1 was not sufficient to disrupt the protein levels or regulation of HAP1 and hence, no effect was observed on $GABA_AR$ trafficking. However, the immunofluorescence assay used to quantify $GABA_AR$ trafficking may also not have been sensitive enough to detect subtle changes in surface receptors. Unfortunately, due to the limitations of neuronal transfection, assays could only be designed in this way at the single cell level.

It would be interesting to study how total loss of Ahi1 impacts $GABA_AR$ trafficking using an Ahi1 KO mouse model. These experiments would hopefully be consistent with the results observed here rather than lack of complete knockdown in the RNAi system masking an Ahi1 dependent $GABA_AR$ trafficking effect. Notably, the finding here that Ahi1 overexpression also has no impact on $GABA_AR$ trafficking points towards $GABA_AR$ trafficking being independent of Ahi1 rather than the RNAi system being inefficient. The availability of Ahi1 KO neurons would also allow biochemical surface biotinylation experiments to be carried out. This protocol purifies surface proteins from a total cell population so levels of a particular membrane protein between control and sample neurons can be measured. This experiment would provide an alternative method for investigating surface $GABA_AR$s and support any immunofluorescence results.

Others have attempted to identify HAP1-dependent mechanisms that are regulated by Ahi1 with more success. Indeed, one group have investigated how Ahi1 is implicated in the trafficking of the neurotrophic receptor TrkB. When activated, TrkB is internalised to bring about signalling events, it is then either recycled or degraded. HAP1 and Ahi1 appear to have a role in stabilising these internalised TrkB receptors. Sheng and colleagues initially showed that levels of TrkB were destabilised in HAP1 KO tissue and that RNAi against Ahi1 decreased HAP1 protein levels and hence, TrkB levels (Sheng et al., 2008). The group then studied neuronal specific Ahi1 cKO mice and revealed both HAP1 and TrkB protein levels were reduced in the hypothalamus. Specifically, the level of internalised TrkB protein was decreased in Ahi1 KO brain stem cells and was shown to be due to dysregulated endocytic sorting resulting in the rapid degradation of TrkB by lysosomes. Loss of Ahi1 was shown to disrupt an Ahi1/HAP1/Hrs complex that would normally stabilise internalised TrkB receptors for recycling (Xu et al., 2010).

TrkB receptor signalling is known to play a critical role in depressive neuropsychiatric disorders; reduced levels of TrkB and its ligands are detected in patients with SCZ and mood disorders. In addition, altered BDNF signalling, the neurotrophin ligand for TrkB, contributes to the progression of FXS and patients suffering from psychiatric disorders respond well to drugs that target TrkB receptors and their signalling pathways (Angelucci et al., 2005; Castrén and Castrén, 2014; Gupta et al., 2013; Ray et al., 2014). Therefore, the disrupted endocytic trafficking of TrkB in Ahi1 KO tissues suggests a mechanism for the neuropsychiatric phenotypes seen in JS patients. Importantly, Ahi1 deficiency in these mice lead to depressive and anxiolytic behaviour (Lotan et al., 2013; Ren et al., 2014; Xu et al., 2010). In line with this, Ahi1 has been shown to interact with the 5-HT_{2c} serotonin receptor (5-HT_{2c}R) and also promote degradation of the internalised receptors through the lysosomal pathway (Wang et al., 2012). Interestingly, serotonin receptors are the target for many antipsychotic drugs. Therefore, although a role for Ahi1 in $GABA_A$R trafficking has not been revealed other reports suggest that the role of Ahi1 in the trafficking of neuronal receptors may be contributing to JS pathogenesis and the neuropsychiatric behaviours observed.

5.3.3 An excitatory role for Ahi1

Unravelling a role for Ahi1 in synaptic function and neurotransmission is a tempting idea to explain some of the more complex cognitive phenotypes observed in JS

(Ferland et al., 2004; Holroyd et al., 1991; Joubert et al., 1969; Ozonoff et al., 1999; Xu et al., 2010). If Ahi1 is not impacting on GABAergic synapses at the level of trafficking $GABA_A$Rs then perhaps Ahi1 is playing a role at excitatory synapses. It would be interesting to carry out electrophysiological recording on neurons with altered Ahi1 expression to see if these neurons have disrupted inhibitory or excitatory transmission. Indeed, the data presented here shows that both overexpressed $Ahi1^{GFP}$ and endogenous Ahi1 colocalise with excitatory synaptic markers within dendrites. Furthermore, endogenous Ahi1 can be seen within dendritic spines. Intriguingly, these membrane protrusions, which compartmentalise excitatory synaptic structures for enhanced neurotransmission, show many similarities to primary non-motile cilia (Nechipurenko et al., 2013). Ahi1 has previously been described to localise and function within this protruding cell organelle. Both spines and cilia show parallels in their signalling mechanisms, protein composition, structural plasticity and their fundamental roles are ultimately similar, to sense and transduce extracellular cues into the cell (Nechipurenko et al., 2013). With this in mind, perhaps Ahi1 plays a similar role at dendritic spines to its described role at cilia.

The main function of Ahi1 within primary cilia is within the transition zone (TZ) (Hsiao et al., 2009; Lancaster et al., 2011b). This is the region at the junction between the distal end of the mother centriole, which forms the base of the cilia often known as the basal body, and the cilium itself. Super-resolution imaging has recently confirmed that Ahi1 is present in the TZ (Lee et al., 2014). Ahi1 is recruited to the TZ during ciliogenesis and is thought to function as a molecular component of the ciliary gate. The ciliary gate is considered to be a physical barrier that can be seen by electron microscopy and blocks the free exchange of soluble and plasma membrane cilia components with the rest of the cell. These gatekeeper molecules control the entry and exit of proteins into the cilia and regulate intraflagellar transport (Reiter et al., 2012). A similar diffusion barrier has been proposed for dendritic spines; with the constricted spine neck and comparable gatekeeper proteins being required to restrict movement of signalling molecules between the spine and the dendrite. Perhaps Ahi1 could function as a gatekeeper protein at spines as it does in cilia. It would be interesting to carry out super-resolution microscopy on Ahi1 in spines to see if it localises to the spine neck or forms ring structures. In addition, Ahi1 has been shown to interact with the small GTPase Rab8a and be critical in the delivery of vesicles targeted to the primary cilia (Hsiao et al., 2009). Rab8a is also required for the

synaptic delivery of AMPA receptors during LTP and constitutive receptor recycling, therefore, perhaps Ahi1 could be functioning in this trafficking event (Ng and Tang, 2008). A simple extension of the experiments presented here would be to study the role of Ahi1 in AMPA receptor trafficking using similar methods.

Via its interaction with HAP1, Ahi1 could also be implicated in cytoskeletal regulation at dendritic spines. HAP1 can bind to the Rac1 GEF kalirin-7 (Colomer, 1997), which activates the global actin regulator Rac1. Kalirin-7 is thought to be important in regulating the cytoskeleton at excitatory synapses and in dendritic spine morphology (Penzes and Jones, 2008) but the significance of its interaction with HAP1 and a possible role for Ahi1 in this complex has not been described.

5.3.4 Ahi1 and neuronal development

Loss of function mutations in human Ahi1 results in JS. Patients present with brain malformations including abnormal cerebellar development and axonal decussation highlighting the important of Ahi1 in neuronal development (Ferland et al., 2004). Ahi1 KO mice have a reduced cerebellum size due to failure of neuronal proliferation and defects in midline fusion consistent with the malformations observed in humans (Lancaster et al., 2011a). The use of RNA interference (RNAi) against Ahi1 in IMCD3 cells resulted in reduced primary cilia formation. Both cells stably expressing or transiently transfected with Ahi1 shRNA showed a decrease in the percentage of ciliated cells. This result was also confirmed in $Ahi1^{-/-}$ mouse embryonic fibroblasts (MEFs) (Hsiao et al., 2009). Defects in ciliogenesis are commonly associated with poor cell development as critical developmental signalling pathway such as Hedgehog and Wnt signalling required primary cilia (Lee and Gleeson, 2010; Waters and Beales, 2011). Taken together, this data points towards Ahi1 being required for normal neuronal development with loss of Ahi1 resulting in lack of neuronal proliferation and growth, probably due to impaired cilia formation.

It is therefore intriguing that Ahi1 knockdown in hippocampal neurons using an RNAi approach demonstrated here results in increased neuronal architecture and dendritic complexity. Knockdown of Ahi1 in DIV10 neurons for 4 days resulted in neurons being significantly more complex, having significantly longer dendrites with more branch points. The discrepancies between this data and previously published work, which has suggested loss of Ahi1 has a negative impact on neuronal development, could be due

to differences in experimental design. Here, an RNAi approach looked at acute knockdown of Ahi1 in single cultured neurons. It is not surprising that loss of Ahi1 in this way impacted differently on neuronal development when compared to *in vivo* brain studies in humans with Ahi1 mutations and germline Ahi1 KO mice studies (Ferland et al., 2004; Lancaster et al., 2011a). A more comparable experiment carried out by Weng and colleagues revealed cultured Ahi1 KO hypothalamic neurons had significantly reduced dendritic length compared to WT control cells (Weng et al., 2013). However, these neurons may still have been displaying dendritic defects due to total loss of Ahi1 throughout development. Furthermore, the morphology experiments carried out here examined the cell autonomous effects of Ahi1 knockdown at a stage when dendritic structure has already developed. In the hypothalamic neuron experiment (Weng et al., 2013) the changes in signalling due to loss of Ahi1 in the whole neuronal culture may account for the differences in the dendritic length findings. The results presented here show that Ahi1 is required for maintenance of dendritic arborisation, a result that has possibly been masked in previous studies using Ahi1 KO neurons due to the strong developmental defects observed.

To understand more about how acute knockdown of Ahi1 affects dendritic morphology it would be interesting to see if primary cilia formation is disrupted following RNAi treatment at the time point examined in this chapter. This experiment would shed light on whether cilia signalling plays a role in the increased dendritic complexity observed. In addition, investigating the dendritic effects of Ahi1 knockdown in young neurons might provide more information about how loss of Ahi1 at different time points impacts on dendritic development.

There have been no previous reports of the impact acute Ahi1 knockdown has on dendritic morphology. One possible explanation for the increased dendritic complexity observed here involves Ahi1 regulating HAP1 trafficking. HAP1A has been shown to interact with KLC and be trafficked to neurite tips (McGuire et al., 2006; Rong et al., 2006). KLC is part of the conventional anterograde microtubule motor kinesin. At neurite tips HAP1A promotes neurite outgrowth by stabilising internalised TrkA for downstream signalling. Indeed, loss of HAP1 expression using RNAi lead to reduced HAP1 in neurite tips, decreased levels of internalised TrkA and reduced neurite outgrowth. Phosphorylation of HAP1A has been shown to decrease its

associated with KLC reducing its localisation at neurite tips and inhibiting outgrowth (Rong et al., 2006). It could be hypothesised that Ahi1, as a HAP1 adaptor protein, promotes the recruitment of a kinase to HAP1A resulting in phosphorylation leading to the uncoupling of HAP1A from kinesin as a form of neurite outgrowth regulation. Therefore, when Ahi1 expression is reduced following RNAi, the regulation of HAP1 phosphorylation is lost, leaving HAP1A predominantly dephosphorylated, coupled to motors and trafficked to the neurite tip resulting in extension. This model could explain the increased dendritic complexity observed here when Ahi1 expression is decreased. Indeed, in a more recent study, NGF treatment was shown to induce dephosphorylation of HAP1A and reduce the amount of Ahi1 bound to HAP1A (Weng et al., 2013). This is consistent with the notion that Ahi1 could negatively regulate HAP1 trafficking and neurite outgrowth.

In contrast, the reduction of neurite length and brain volume observed with prolonged total loss of Ahi1 function (Ferland et al., 2004; Lancaster et al., 2011a; Weng et al., 2013) could be due to loss of Ahi1 promoting TrkB degradation (Xu et al., 2010), a critical receptor required for dendritic path finding and neuronal development. Alternatively, it could be due to the long-term loss of Ahi1 destabilising HAP1 expression, as previously shown (Sheng et al., 2008), therefore impacting on HAP1's function in TrkA and BDNF trafficking, two other vital pathways in dendritic maturation (Rong et al., 2006; Wu et al., 2010).

In summary, the results presented in this chapter explore the neuronal role of Ahi1 in an attempt to elucidate how loss of function mutations in Ahi1 can result in the neuropsychiatric phenotypes associated with JS. These results demonstrate an interaction between Ahi1 and HAP1 and map the Ahi1 binding site to the first CC domain of HAP1. This interaction led to the discovery of a novel Ahi1/HAP1/KIF5 trafficking complex that exists in brain. In light of this complex, the role of Ahi1 in the trafficking of $GABA_A$Rs at inhibitory synapses was investigated, however, although Ahi1 is present at inhibitory synapses, it does not appear to impact on $GABA_A$R surface stability. All the same, a synaptic role for Ahi1 is an exciting prospect to explain the behavioural defects observed in patients with JS. Ahi1 was shown to localise to excitatory synapses and be present in dendritic spines; its potential roles at excitatory synapses have been discussed. Finally, data reported here illustrates a new role for Ahi1 in the maintenance of dendritic complexity and a speculative model of a

mechanism involving the regulation of HAP1 phosphorylation has been suggested. Taken together, understanding the function of Ahi1 at synapses and in neuronal development, two key mechanisms in the pathogenesis of many neuropsychiatric disorders, may shed light on why *Ahi1* has been associated with ASD, SCZ and depressive phenotypes.

Chapter 6

Final Discussion

6.1 Summary

Synapses are vital for normal neuronal communication and for many years scientists have been attempting to understand their significance in neurological disease pathogenesis. Indeed, synapses have been shown to be disrupted in more than 100 brain disorders (Grant, 2012). Likewise, anatomical studies of post-mortem brains and more recently advanced imaging has illuminated an important role for correct neuronal connectivity and dendritic morphology in neurological disease (Harvey et al., 1993; Karlsgodt et al., 2008; Kulkarni and Firestein, 2012; Raymond et al., 1996; Ruiz et al., 2013). Attention has therefore been given to understanding the molecular mechanisms of synaptic dysfunction and altered connectivity in pathological conditions. Genome-wide genetic screening has identified a multitude of candidate disease-associated genes that converge on synaptic or dendritic pathways (Berg and Geschwind, 2012; Grant, 2012; Hall et al., 2015; Koleske, 2013). This plethora of disease-associated genes has provided scientists with a huge range of targets to research in an attempt to illuminate the underlying mechanisms of neuropsychiatric disorders. Using a combination of molecular, biochemical and imaging techniques this thesis has explored the role of two neuropsychiatric disorder-associated genes in an attempt to understand their involvement in such conditions.

Firstly, Chapter 3 described a novel role for CYFIP1 (Schenck et al., 2001) in synaptic morphology and dendritic complexity. CYFIP1 is encoded by a gene strongly associated with ASD and SCZ through CNV (Table 3.1). CYFIP1 and its homologue CYFIP2, a less well studied protein encoded by a genomic region that has also been identified as a susceptibility locus for SCZ and ADHD (Arcos-Burgos et al., 2004; Gurling et al., 2001), were both shown to be localised to dendritic spines and enriched at excitatory synapses. Overexpression of both proteins to model genetic microduplication of the genes led to alterations in dendritic complexity and spine morphology. Likewise, CYFIP1 haploinsufficiency, a model of microdeletion, resulted in more immature spines and reduced dendritic complexity. Interestingly, overexpression and haploinsufficiency of CYFIP1 has opposing effects on dendritic

complexity but the same effect on spine morphology highlighting the fact that CYFIP1 must play different roles in the regulation of these vital neuronal structures. Live imaging experiments revealed that F-actin assembly was enhanced in haploinsufficient neurons implying that altered CYFIP1 levels dysregulate actin dynamics and this may contribute to the disrupted spine morphology observed when CYFIP1 gene dosage was altered. Overexpression of CYFIP1 was also shown to impact on the stability of inhibitory synapses resulting in a loss of gephyrin clusters and surface $GABA_A$Rs. Intriguingly, overexpression of CYFIP1 also resulted in an increase in excitatory scaffold clusters suggesting that increased CYFIP1 protein levels could be impacting on the E/I balance of neuronal activity. This highlights another novel mechanism in which CYFIP1 might be acting on the synapse causing neuronal dysfunction.

The second results chapter of this thesis used a genetic approach (Curtis, 2012) to identify novel variants in CYFIP1 and determine if they were associated with SCZ. CYFIP1 was shown to be significantly associated with SCZ due to an accumulation of rare potentially functionally-damaging variants identified within the gene in a cohort of SCZ patients compared to unaffected controls. Indeed, one particular SNP in CYFIP1 at position 15:22963816 was shown to be significantly associated with SCZ. Five candidate CYFIP1 SCZ-associated SNPs were selected on the basis that they may disrupt functionally critical CYFIP1 protein interactions. The SNPs were genotyped in an independent SCZ case-control cohort, however, none yielded a significant association. Functional analysis of these five CYFIP1 variants in cell biological assays revealed that individual SNPs did not appear to alter the synaptic localisation of CYFIP1 or its interactions with a member of the WRC. CYFIP1 KO models were also characterised within Chapter 4 and provide the first description of systems where complete loss of CYFIP1 has been studied. Initial observations from these models revealed complete loss of CYFIP1 appeared to reduce cell viability in fast dividing MEF cells and postnatal deletion of CYFIP1 in CA1 hippocampal neurons altered dendritic complexity.

Lastly, in the final results chapter Ahi1, a protein known to be mutated in the neurodevelopmental disorder Joubert's syndrome (JS) and associated with ASD and depression, was shown to colocalise with excitatory and inhibitory synaptic markers. A novel trafficking complex involving Ahi1 with the inhibitory synaptic trafficking

adaptor protein HAP1 and the motor KIF5 was identified in brain. The binding site of Ahi1 was mapped to the first coiled-coil domain of HAP1. Although Ahi1 has been implicated in a myriad of trafficking pathways, Ahi1 did not appear to alter the $GABA_AR$ trafficking function of HAP1 (Twelvetrees et al., 2010) and likewise had no direct effect on the trafficking of $GABA_ARs$ to the membrane. However, knockdown of Ahi1 resulted in defects in dendritic complexity consistent with disrupted neuronal development observed in JS (Ferland et al., 2004). Finally, Ahi1 ASD associated mutations (Dixon-Salazar et al., 2004; Ferland et al., 2004; Retuerto et al., 2008; Yu et al., 2013) did not alter the ability of Ahi1 to interact with HAP1. That said, the synaptic localisation of Ahi1 revealed in Chapter 5 points towards a synaptic role for Ahi1 that may be disrupted by ASD associated mutations which requires further investigation.

Together, the results presented in this thesis shed more light on the function of two neuropsychiatric disease associated proteins and provides increasing evidence of a critical role for disrupted synaptic function and altered dendritic complexity in the etiology of neuropsychiatric disorders such as ASD and SCZ.

6.2 Regulation of synapse and dendritic morphology

The formation and maintenance of neuronal connectivity is critical for normal brain function. Dendrites and dendritic spines undergo a process of dynamic development extending and contracting before finally becoming stabilised in the adult brain. Loss or alterations in dendritic arbour and synapse stability are major contributing factors to the pathology of neuropsychiatric disorders. This altered synaptic connectivity is thought to contribute to the impaired cognition, memory and social behaviours that characterise these disorders (Kulkarni and Firestein, 2012).

Regulation of the cytoskeleton is at the heart of maintaining dendritic and spine stability for normal neuronal communication. Dynamic actin turnover within dendritic spines is vital for their constantly changing morphology during development and plasticity and for maintaining the integrity of the synapse and the stability of receptors in the membrane (Bellot et al., 2014; Frost et al., 2010b; Hanley, 2014; Hotulainen and Hoogenraad, 2010). As global regulators of the actin cytoskeleton this heavily implicates RhoGTPases in the maintenance of spine and dendritic

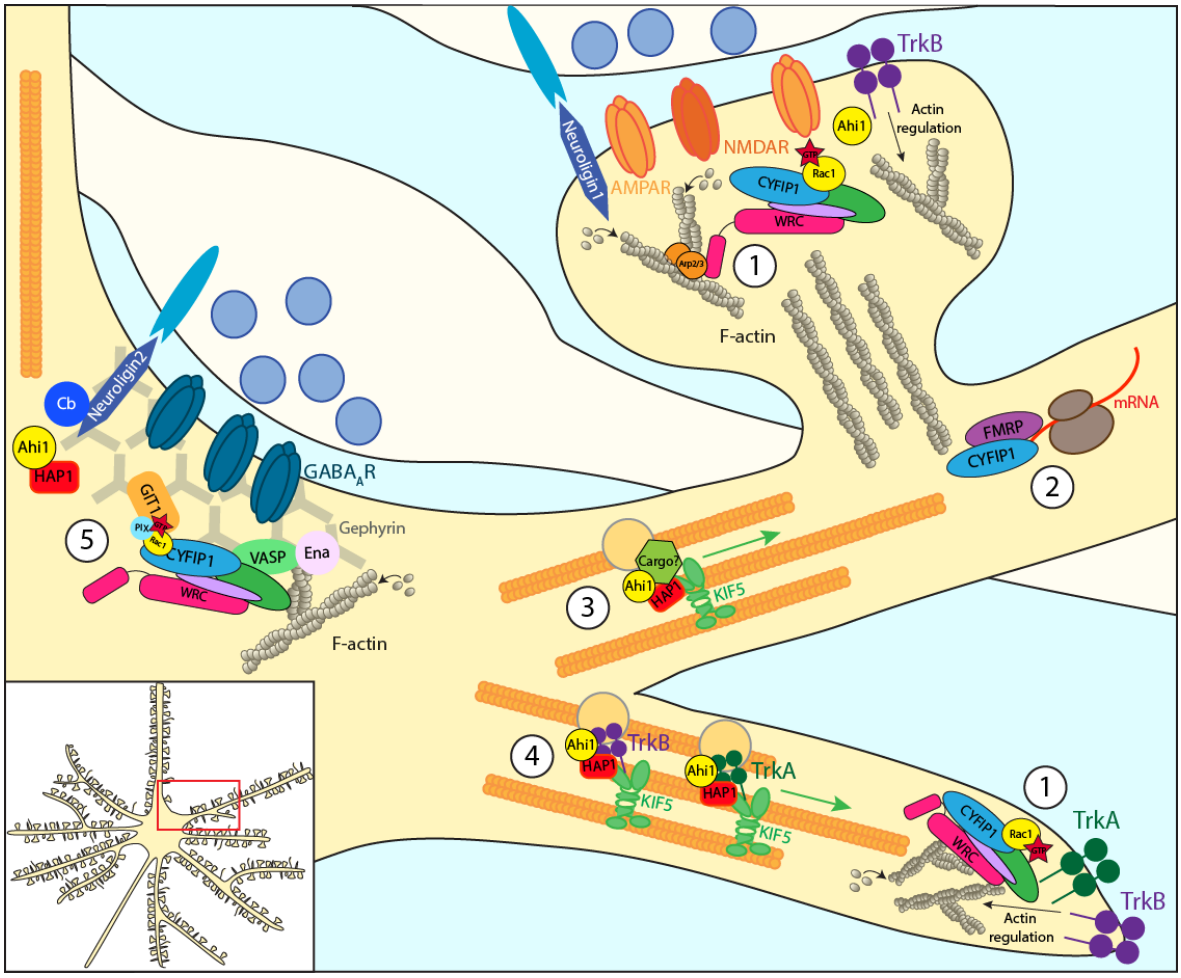

Figure 6.1: CYFIP1 and Ahi1 in the regulation of dendritic morphology and synapse stability

Diagram of the potential roles outlined in this thesis for CYFIP1 and Ahi1 in the regulation of dendritic and spine morphology. Protein interactions indicated by direct contacts or overlaps between shapes. **(1)** BDNF signalling via TrkB is known to regulate actin dynamics and promote Rac1 activation during spine plasticity changes and dendritic outgrowth. The WRC is a downstream effector of active Rac1 which brings about actin branching and polymerisation via activating Arp2/3. Rac1 likely signals to the WRC via CYFIP1 in dendritic spines and neurite tips to regulate morphology and F-actin turnover. **(2)** Additionally, CYFIP1 is known to form complex with FMRP and e1F4e to regulate the local protein translation of FMRP target mRNA such as PSD95 and Arc at the base of spines. Correct expression of these mRNA is vital for spine stability. **(3)** Delivery of protein cargo from the soma to distal regions is necessary to replenish proteins for dendritic growth and stabilisation. An Ahi1/HAP1/KIF5 trafficking complex could play a role in this function with Ahi1 being an adaptor for dendrite specific cargo. **(4)** Ahi1 and HAP1 are found in a complex with TrkB while HAP1 is known to interact with TrkA. The Ahi1/HAP1/KIF5 trafficking complex may also transport these neurotrophic receptors and regulate their membrane expression thus regulating dendritic outgrowth. **(5)** Finally, CYFIP1 is enriched at inhibitory synapses and likely regulates actin dynamics here. The WRC is probably tethered to gephyrin via a recently identified interaction

with Ena and VASP. Alternatively, CYFIP1 could recruit the WRC to Rac1 which is locally activated by the GEF βPIX tethered to the inhibitory synapse by GIT1. Ahi1 is also known to be present at excitatory and inhibitory synapses but its function within these compartments is still unknown.

morphology (Auer et al., 2011). In particular, Rac1 is required for spine stability as introduction of a Rac1 DN into hippocampal neurons in slices results in progressive spine loss (Nakayama et al., 2000). Among the downstream targets of Rac1 is WAVE, which as part of the WRC stimulates Arp2/3 activity bringing about actin nucleation and branch formation from existing actin filaments (Eden et al., 2002). WAVE1 localises to dendritic spines and is critical for spine stability as knockdown or total loss of WAVE1 reduced spine density (Kim et al., 2006; Soderling et al., 2007). Activated Rac1 signals to the WRC via CYFIP1 placing CYFIP1 right at the centre of this vital pathway for spine stability (Chen et al., 2010b). It is not surprising this thesis reports that altered CYFIP1 expression levels severely impact on spine morphology. Furthermore, recruitment and activation of Rac1 is essential for inhibitory synapse stability (Smith et al., 2014). As CYFIP1 and the WRC are downstream effectors of active Rac1 it is likely CYFIP1 is playing a key role in actin regulation at the inhibitory synapses too. The enrichment of CYFIP1 at the inhibitory synapse and the altered gephyrin and $GABA_AR$ clusters following CYFIP1 overexpression presented here support this idea.

Likewise, although development and maintenance of dendritic morphology relies heavily on MT dynamics, actin turnover is essential for membrane outgrowth and remodelling during neuronal development (Jan and Jan, 2010). Rac1 is known to play a critical role in neuronal outgrowth as Rac1 deficient cerebellar granule cells show impaired neurite extension and axon formation. Loss of Rac1 resulted in loss of WAVE recruitment to growth cones. This lead to reduced lamellipodia formation and actin dynamics which could be partially rescued by membrane targeted WAVE (Tahirovic et al., 2010). The presence of CYFIP1 is also necessary for the Rac1 induced membrane activity of WAVE (Steffen et al., 2004). It is likely these proteins all play key roles in the regulation of actin remodelling required during dendritic extension, thus, potentially explaining why altered CYFIP1 levels impact on dendritic morphology as described here. Alternatively, as CYFIP1 interacts with Rac1 solely in its active form (Kobayashi et al., 1998) then it could be hypothesised that CYFIP1 sequesters active Rac1 away from its critical roles in dendrite and spine stability.

Interestingly, BDNF signalling via TrkB is known to have a crucial role in spine and dendritic stability (Cohen-Cory et al., 2010; Gupta et al., 2013). Indeed, two-photon imaging of transfected cells within the visual cortex showed overexpression of BDNF

induced increased dendritic branching in neighbouring cells (Horch and Katz, 2002). In the postsynaptic neuron many actin regulatory pathways central to spine stabilisation are modulated by BDNF. TrkB signalling increases the localisation of cortactin to spines where it can recruit Arp2/3 and bring about actin turnover and spine stability (Iki et al., 2005). TrkB signalling can also activate PAK via Rac1. Active PAK promotes LIMK1 activity resulting in increased inhibitory phosphorylation of cofilin which blocks actin depolymerisation, promotes spine enlargement and stabilisation (Dong et al., 2012; Rust et al., 2010). It is likely that CYFIP1 is playing a role in these pathways. For example, increased levels of CYFIP1 could be sequestering Rac1 away from this BDNF induced cofilin regulation resulting in destabilised immature spines as shown here in Chapter 3. Furthermore, others have suggested BDNF treatment, shifts CYFIP1 from a protein translation regulatory complex with FMRP to the WRC complex where it can bring about actin turnover and regulate spine structure (De Rubeis et al., 2013).

Chapter 5 discussed how mutations or disrupted expression of Ahi1 might impact on its role with HAP1 in the stabilisation of internalised TrkB (Xu et al., 2010) leading to altered TrkB degradation. In this way, Ahi1 could also be implicated in BDNF induced spine and dendrite stability. Furthermore, it has been demonstrated here that Ahi1 and HAP1 form a neuronal trafficking complex with the kinesin motor KIF5. Disrupting dendritic trafficking inhibits the ability of neurons to replenish proteins and sustain dendritic structure, therefore, has devastating effects on dendritic development, maintenance and stability. For example, loss of KIF5 by RNAi in hippocampal neurons resulted in reduced dendritic development due to a decline in the delivery of key trophic signalling receptors to the membrane (Hoogenraad et al., 2005). Ahi1 may be involved with HAP1 in the regulation of KIF5 specific cargo necessary for synaptic function or dendritic development however, it has been shown here not to alter the membrane trafficking of $GABA_A$Rs, a known cargo of HAP1 and KIF5 (Twelvetrees et al., 2010). Perhaps Ahi1 is involved in the HAP1 dependent trafficking of TrkA to growing neurite tips or perhaps Ahi1 and HAP1 are implicated in the trafficking of TrkB as both proteins are known to regulate its degradation (Rong et al., 2006; Xu et al., 2010). Both TrkA and TrkB are important in neuronal development. Indeed, ablation of TrkB receptors leads to shrinkage of cortical excitatory neuronal dendrites (Xu et al., 2000).

Finally, as well as components synthesised in the soma being trafficked to distal regions for dendritic growth and maintenance, local protein synthesis is also vital for the replenishment of molecular structures to maintain spine and dendritic integrity (Jan and Jan, 2010). Loss of local mRNA regulation has been shown to alter the expression levels of synaptic proteins and disrupts synapse development (Bassell and Warren, 2008). PSD95 mRNA is known to accumulate along dendrites and at synapses (Zalfa et al., 2007). PSD95 mRNA translation has been directly visualised recently in dendrites and spines at the single molecular level and was shown to be disrupted in a mouse model of FXS. The altered expression of such a key PSD protein is thought to contribute to the immature spine phenotype observed in FXS (Ifrim et al., 2015). Local translation is also necessary to cope with the extra protein synthesis burden induced upon neuronal activity and plasticity changes. Arc (activity-regulated cytoskeletal associated protein) mRNA is another dendritically targeted mRNA that accumulates at activated synapses in response to stimuli such as BDNF (Steward and Worley, 2001). Correct Arc expression has been shown to be vital for synaptic plasticity and the regulation of actin dynamics (Guzowski et al., 2000; Plath et al., 2006). Reduced Arc levels occluded BDNF induced LTP and decreases F-actin formation in spines (Messaoudi et al., 2007). Interestingly, both PSD95 and Arc are FMRP target mRNAs. CYFIP1 is known to regulate the expression of FMRP targets as it forms a translational repressor complex with eIF4e (Napoli et al., 2008). Therefore, the spine and dendritic morphology defects observed here when CYFIP1 dosage is altered could be the result of misregulated local protein translation of genes such as PSD95 and Arc. Indeed, others have shown disrupted Arc protein levels in CYFIP1 haploinsufficient mice (De Rubeis et al., 2013).

Taken together, the data in this thesis supports a role for CYFIP1 and Ahi1 in the regulation of dendritic stability and a role for CYFIP1 in regulating spine dynamics. The underlying mechanisms are still not fully understood however, the pathways suggested to be involved in this discussion are summarised in Figure 6.1. Additionally, the data here suggests genetic mutations or alterations in the expression of CYFIP1 or Ahi1 may disrupt this normal dendritic and spine morphology which could be contributing to the pathogenesis of neuropsychiatric disorders associated with these genes.

6.3 Genetic risk for psychiatric disorders: convergence on synaptic pathways

The chief motivation for studying psychiatric genetics is to identify the biological processes involved in the pathogenesis of these conditions, in an attempt to understand more about the disorders and potentially reveal novel therapeutic targets. From this type of research, it is emerging that many of the genes associated with disorders such as SCZ, ASD, MR and ID are converging on the same pathways; in particular the regulation of synapse stability and plasticity (Berg and Geschwind, 2012; Hall et al., 2015). Numerous synaptic scaffold molecules have been implicated in neuropsychiatric disorders such as the SHANK proteins which are integral to the excitatory PSD and the NL adhesion proteins which promote synapse formation and stability (Guilmatre et al., 2014; Südhof, 2008). Indeed, mutations in over 200 genes encoding PSD proteins are known to result in over 130 human brain disorders (Grant, 2012). Additionally, risk genes are also known to converge on regulators of synaptic actin dynamics. Mutations associated with MR are found in PAK3, translocations in DISC1 underlie familial SCZ and genetic variations in oligophrenin1 are associated with SCZ, all these protein are known to impact on actin dynamics (Hayashi et al., 2004; Hayashi-Takagi et al., 2010; Ito et al., 2010).

This thesis has shed light on the biological roles of two genes, CYFIP1 and Ahi1, which have both been linked to neuropsychiatric disorders via CNVs and rare single nucleotide risk variants (Table 3.1) (Amann-Zalcenstein et al., 2006; Brett et al., 2014; Ingason et al., 2010; Retuerto et al., 2008; Rivero et al., 2010; Torri et al., 2010). With the mounting evidence that synaptic function is intimately connected to the pathogenesis of neuropsychiatric disorders it is not surprising that both proteins have been shown here to be colocalised with synapses. Indeed, data presented in this thesis strongly suggests CYFIP1 is involved in the regulation of actin at dendritic spines and is critical for normal spine morphology. Thus, CYFIP1 is another psychiatric disease-associated gene that can be added to the list converging on regulators of synaptic actin dynamics. Furthermore, the effect CYFIP1 overexpression has on inhibitory and excitatory synaptic clusters points towards CYFIP1 functioning in the regulation of the E/I balance. This is another synaptic regulatory pathway onto which neuropsychiatric disease associated genes such as *PTEN*, *TSC1* and *CNTNAP2* appear to be converging (Bateup et al., 2013; Luikart et al., 2011; Peñagarikano et al., 2011; Südhof, 2008). Further work will be required to determine if the synaptic localisation

of Ahi1 implicates the protein in synaptic regulation.

Many neuropsychiatric disorders are now being coined synaptopathies due to the vast numbers of synaptic genes implicated in these disorders and the observations from anatomical studies (Grant, 2012). It is hoped that by grouping disorders in this way, based on common molecular pathways, the most significant targets for therapeutic intervention will and are beginning to be uncovered. That said, many of the emerging pathways appear to be proving challenging drug targets. Indeed, there have been few, if any novel drugs developed to target psychiatric disorders in the last 40 years (Geschwind and State, 2015). One issue seems to be that modulating pathways such as regulators of actin dynamics would have vast off-target effects in other brain and bodily regions. However, generating drugs to target one particular pathway could be far too simplistic. Data in this thesis reveals that dendritic morphology is also disrupted when expression of both Ahi1 and CYFIP1 is altered. Furthermore, Ahi1 may also impact trafficking mechanisms although a precise cargo has not been resolved in this study. Numerous other factors have been put forward to contribute to the pathogenesis of neuropsychiatric disorders such as altered connectivity and trafficking defects as suggested here, altered nutrition and oxidative stress, inflammation and environmental factors (Compart, 2013). Therefore, like cancer treatments, personalised medicine is becoming increasingly popular for the treatment of psychiatric disorders in an attempt to combat the combination of pathogenic factors involved (Hamilton, 2015). It appears that coupling genetic sequencing to reveal affected genes with combination therapies is a more realistic approach. It seems clear that research is moving into the era of complexity and that all angles of neuronal dysfunction must be considered to fully understand disease pathogenesis and design novel therapies.

As a final comment it remains a puzzling question in the field as to why, when there is such a lot of genetic and mechanistic overlap in the factors contributing to neuropsychiatric disorders, the actual characteristics of the disorders themselves can manifest so differently in humans. For example, how is it that disrupted spine and dendritic morphology as well as genetic alterations in synaptic proteins are considered pathological mechanisms of both ASD and SCZ and yet the onset and clinical appearances of these two disorders are very distinct? This question remains to be answered. Almost certainly, neuropsychiatric phenotypes are modified by the

patient's genetic background, the time of dysfunction onset and experiences throughout life. As mentioned above the answers probably lie within the complexities of each individual disorder and with continued research getting to grips with this question may become achievable.

6.4 Future directions

It is evident that the mechanisms by which CYFIP1 brings about morphological changes in neurons still remains to be fully elucidated. Others have attempted to investigate this by using CYFIP1 deletion mutants that either disrupt the interaction between CYFIP1 and NAP1 or eIF4e. These mutations uncouple the actin regulation and translational regulation roles of CYFIP1 respectively. The group showed that both pathways were important for CYFIP1's role in spine formation as neither mutant could rescue the immature spine phenotype observed in CYFIP1 knockdown conditions (De Rubeis et al., 2013). It would be interesting to carry out similar experiments to determine which functions of CYFIP1 are important in maintaining dendritic complexity. A recent paper has shown that rapamycin an inhibitor of the mTOR pathway can rescue dendritic morphology defects observed in CYFIP1 knock-in mice (Oguro-Ando et al., 2014). The mTOR pathway promotes protein synthesis therefore, this points towards the role of CYFIP1 in the regulation of protein translation being important in regulating dendritic morphology but the precise mechanism is still to be determined. Importantly, identifying if there is a CYFIP1-dependent actin involvement in this process would enhance our understanding of this pathway.

It is shown here that constitutive haploinsufficiency in CYFIP1 led to a decrease in dendritic complexity in DIV14 cultured neurons (experiment carried out by Dr. Manav Pathania) while postnatal cKO of CYFIP1 in neurons increased basal dendritic complexity in adult CA1 pyramidal cells. These opposing results suggest CYFIP1 may play different roles during dendritic development and maintenance. Currently, others have profiled CYFIP1 expression during development but not addressed CYFIP1 function at different developmental time points (Bonaccorso et al., 2015; De Rubeis et al., 2013). Using the genetic models characterised here and the power of different Cre drivers to conditionally KO CYFIP1 at various developmental time points it would be interesting to try and determine whether CYFIP1 has distinct functions during neuron development and maintenance. As an alternative hypothesis perhaps the loss

of CYFIP1 in non-neuronal cells in the constitutive haploinsufficient model explains the differences between the dendritic complexity patterns of the two genotypes. Altered astrocyte function is known to impact on dendritic morphology in neuropsychiatric disorders (Molofsky et al., 2012; Sloan and Barres, 2014). Therefore, exploring the role of CYFIP1 in astrocytes and how altered CYFIP1 expression in these cells might impact on dendritic morphology is an intriguing question.

Experiments in Chapter 3 demonstrate that overexpression of CYFIP1 has opposing effects on the cluster size of excitatory and inhibitory synaptic structural molecules. The role of CYFIP1 in regulating excitatory and inhibitory synaptic size and number warrants much further examination. Indeed, the CYFIP mutants that uncouple its role in actin and translation could be again used to determine which of CYFIP1's functions cause these effects. The data presented here suggests that CYFIP1 overexpression may upset the E/I balance and it would be interesting to confirm this hypothesis electrophysiologically. Additionally, looking at how synaptic clusters are effected in the haploinsufficient neurons may also help illuminate how CYFIP1 is involved in synapse stability. Considerable research has focussed on the role of CYFIP1 in dendritic and spine morphology and how this might provide a mechanism for the genetic association of *Cyfip1* with ASD and SCZ (Bozdagi et al., 2012; Oguro-Ando et al., 2014; De Rubeis et al., 2013). Unravelling a role for CYFIP1 in maintaining the E/I balance links CYFIP1 to another mechanistic pathway which is increasingly being thought to underlie neuropsychiatric disorders such as ASD, epilepsy and TS (Bateup et al., 2013; Gkogkas et al., 2013; Luikart et al., 2011; Peñagarikano et al., 2011).

The function of CYFIP1 at the inhibitory synapse is totally unexplored. Does CYFIP1 play a role in regulating actin dynamics at these synapses? Although actin is known be important at the excitatory synapse (Bellot et al., 2014) far less is known about how actin dynamics regulate the inhibitory synapse however, this is an emerging field. Some studies suggest that actin is involved in both the movements of gephyrin (Hanus et al., 2006; Kirsch and Betz, 1995) and the trafficking of $GABA_A$Rs (Graziane et al., 2009; Meyer et al., 2000). Recently, Rac1 was shown to be recruited to inhibitory synapses via a protein complex involving GIT1 and βPIX and this recruitment was necessary for synapse stability (Smith et al., 2014). It would be interesting to know if CYFIP1 and the WRC can act downstream of Rac1 in this pathway. Preliminary data not discussed in this thesis shows that CYFIP1 can be coimmunoprecipitated with

GIT1 and βPIX when overexpressed in cell lines. Furthermore, a Mena/VASP protein complex is found at inhibitory synapses (Giesemann et al., 2003) which has recently been shown to interact with and cooperatively regulate the WRC (Chen et al., 2014b), highlighting that CYFIP1 and the WRC may indeed function at inhibitory synapses. Defects in inhibitory synapse structure and function are strongly associated with epilepsy which has been shown to be associated with CNV of the CYFIP1 region of the genome (de Kovel et al., 2010). Moreover, CYFIP1 mRNA and protein levels have recently been shown to be upregulated in temporal lobe tissue of patients with temporal lobe epilepsy (Huang and Chen, 2015). These findings support an as yet unknown role for CYFIP1 in inhibitory synaptic function.

Attempts have been made in Chapter 4 of this thesis to characterise novel CYFIP1 KO systems. These KO models provide an excellent platform to unpick the biological functions of CYFIP1. *In vitro* experiments have shown that CYFIP1 is vital in the regulation of WAVE and Arp2/3 activity (Chen et al., 2010b) however, little is known about how this regulation impacts on cellular function. In CYFIP1 KO MEFs the role of CYFIP1 in cell division and migration could be explored similarly to experiments carried out in other WRC protein KO or knockdown cells (Dubielecka et al., 2011; Steffen et al., 2004). CYFIP1 KO systems also provide a powerful tool for studying the effects of the SCZ-associated CYFIP1 variants identified in this study. Rescue experiments comparing the mutant variants to WT could be carried out to determine whether the variants alter CYFIP1 function both in neurons and MEFs. Alternatively, overexpression experiments with the mutants could be performed to study the impact of CYFIP1 disease associated variants on synapses. Similar experiments have recently been carried out for novel SHANK2 SCZ-associated variants (Peykov et al., 2015).

Finally, there is still much to be understood about the role of Ahi1 in neurons. The finding that Ahi1 forms a novel trafficking complex in brain with HAP1 and KIF5 raises the possibility of future research opportunities. Although here it is shown that Ahi1 is not involved in the trafficking of $GABA_A$Rs, Chapter 5 has demonstrated this protein is localised to excitatory and inhibitory synapses. Perhaps Ahi1 is involved in the trafficking of different cargo. A screen for novel of Ahi1 interacting proteins using immunoprecipitation from brain lysate and mass spectrometry analysis to reveal the interacting proteins would provide new avenues to study. Furthermore, Ahi1 is known to impact on cilia stability (Hsiao et al., 2009) and cilia have been compared to spines

(Nechipurenko et al., 2013). It would be very interesting to determine if altered Ahi1 levels or Ahi1 autism mutants could impact on spine morphology, a phenotype widely considered in ASD pathology. Finally, here Ahi1 knockdown is shown to disrupt dendritic complexity. Determining what role Ahi1 plays in the regulation of dendritic complexity and whether this role is developmentally regulated would be an exciting prospect. After all, JS, the condition caused by loss of Ahi1, is a neurodevelopmental disorder. As previously discussed, validating whether the trafficking of TrkA or TrkB receptors are involved would be of great interest.

Chapter 7

Bibliography

Abekhoukh, S., and Bardoni, B. (2014). CYFIP family proteins between autism and intellectual disability: links with Fragile X syndrome. Front. Cell. Neurosci. *8*, 81.

Allison, D.W., Gelfand, V.I., Spector, I., and Craig, A.M. (1998). Role of actin in anchoring postsynaptic receptors in cultured hippocampal neurons: differential attachment of NMDA versus AMPA receptors. J. Neurosci. *18*, 2423–2436.

Alvarez, V. a, and Sabatini, B.L. (2007). Anatomical and physiological plasticity of dendritic spines. Annu. Rev. Neurosci. *30*, 79–97.

Amann-Zalcenstein, Avidan, Kanyas, Ebstein, Kohn, Hamdan, Ben-Asher, Karni, Mujaheed, Segman, et al. (2006). AHI1, a pivotal neurodevelopmental gene, and C6orf217 are associated with susceptibility to schizophrenia. Eur. J. Hum. Genet. *14*, 1111–1119.

Andreasen, N.C. (1995). Symptoms, signs, and diagnosis of schizophrenia. Lancet *346*, 477–481.

Angelucci, F., Brenè, S., and Mathé, A.A. (2005). BDNF in schizophrenia, depression and corresponding animal models. Mol. Psychiatry *10*, 345–352.

Anitei, Stange, Parshina, Baust, Schenck, Raposo, Kirchhausen, and Hoflack (2010). Protein complexes containing CYFIP/Sra/PIR121 coordinate Arf1 and Rac1 signalling during clathrin-AP-1-coated carrier biogenesis at the TGN. Nat. Publ. Gr. *12*, 330–340.

Antonelli, R., Pizzarelli, R., Pedroni, A., Fritschy, J.-M., Del Sal, G., Cherubini, E., and Zacchi, P. (2014). Pin1-dependent signalling negatively affects GABAergic transmission by modulating neuroligin2/gephyrin interaction. Nat. Commun. *5*, 5066.

Aoto, J., Martinelli, D.C., Malenka, R.C., Tabuchi, K., and Südhof, T.C. (2013). Presynaptic neurexin-3 alternative splicing trans-synaptically controls postsynaptic AMPA receptor trafficking. Cell *154*, 75–88.

Aoto, J., Földy, C., Ilcus, S.M.C., Tabuchi, K., and Südhof, T.C. (2015). Distinct circuit-dependent functions of presynaptic neurexin-3 at GABAergic and glutamatergic synapses. Nat. Neurosci. *18*, 997–1007.

Arancibia-Cárcamo, Yuen, Muir, Lumb, Michels, Saliba, Smart, Yan, Kittler, and Moss (2009). Ubiquitin-dependent lysosomal targeting of GABA(A) receptors regulates neuronal inhibition. Proc. Natl. Acad. Sci. U. S. A. *106*, 17552–17557.

Arcos-Burgos, M., Castellanos, F.X., Pineda, D., Lopera, F., Palacio, J.D., Palacio,

L.G., Rapoport, J.L., Berg, K., Bailey-Wilson, J.E., and Muenke, M. (2004). Attention-deficit/hyperactivity disorder in a population isolate: linkage to loci at 4q13.2, 5q33.3, 11q22, and 17p11. Am. J. Hum. Genet. *75*, 998–1014.

Arnold, S.E., Franz, B.R., Gur, R.C., Gur, R.E., Shapiro, R.M., Moberg, P.J., and Trojanowski, J.Q. (1995). Smaller neuron size in schizophrenia in hippocampal subfields that mediate cortical-hippocampal interactions. Am. J. Psychiatry *152*, 738–748.

Arons, M.H., Thynne, C.J., Grabrucker, A.M., Li, D., Schoen, M., Cheyne, J.E., Boeckers, T.M., Montgomery, J.M., and Garner, C.C. (2012). Autism-Associated Mutations in ProSAP2/Shank3 Impair Synaptic Transmission and Neurexin-Neuroligin-Mediated Transsynaptic Signaling. J. Neurosci. *32*, 14966–14978.

Auer, Hausott, and Klimaschewski (2011). Rho GTPases as regulators of morphological neuroplasticity. Ann. Anat. *193*, 259–266.

Awapara, J., Landua, A.J., Fuerst, R., and Seale, B. (1950). Free gamma-aminobutyric acid in brain. J. Biol. Chem. *187*, 35–39.

Ayalon, G., and Stern-Bach, Y. (2001). Functional assembly of AMPA and kainate receptors is mediated by several discrete protein-protein interactions. Neuron *31*, 103–113.

Bae, J., Sung, B.H., Cho, I.H., Kim, S.-M., and Song, W.K. (2012). NESH regulates dendritic spine morphology and synapse formation. PLoS One *7*, e34677.

Bagni, C., and Greenough, W.T. (2005). From mRNP trafficking to spine dysmorphogenesis: the roots of fragile X syndrome. Nat. Rev. Neurosci. *6*, 376–387.

Bailey, A., Le Couteur, A., Gottesman, I., Bolton, P., Simonoff, E., Yuzda, E., and Rutter, M. (1995). Autism as a strongly genetic disorder: evidence from a British twin study. Psychol. Med. *25*, 63–77.

Banker, G., and Goslin, K. (1998). Culture Nerve Cells, second edition (Cellular and Molecular Neuroscience) (The MIT Press).

Bannai, H., Lévi, S., Schweizer, C., Inoue, T., Launey, T., Racine, V., Sibarita, J.-B., Mikoshiba, K., and Triller, A. (2009). Activity-dependent tuning of inhibitory neurotransmission based on GABAAR diffusion dynamics. Neuron *62*, 670–682.

Bansal, V., Libiger, O., Torkamani, A., and Schork, N.J. (2010). Statistical analysis strategies for association studies involving rare variants. Nat. Rev. Genet. *11*, 773–785.

Bardoni, B., Mandel, J.L., and Fisch, G.S. (2000). FMR1 gene and fragile X syndrome. Am. J. Med. Genet. *97*, 153–163.

Barrow, S.L., Constable, J.R., Clark, E., El-Sabeawy, F., McAllister, A.K., and Washbourne, P. (2009). Neuroligin1: a cell adhesion molecule that recruits PSD-95 and NMDA receptors by distinct mechanisms during synaptogenesis. Neural Dev. *4*, 17.

Bartlett, W.P., and Banker, G.A. (1984). An electron microscopic study of the development of axons and dendrites by hippocampal neurons in culture. I. Cells which develop without intercellular contacts. J. Neurosci. *4*, 1944–1953.

Bassell, G.J., and Warren, S.T. (2008). Fragile X syndrome: loss of local mRNA regulation alters synaptic development and function. Neuron *60*, 201–214.

Bateup, H.S., Johnson, C.A., Denefrio, C.L., Saulnier, J.L., Kornacker, K., and Sabatini, B.L. (2013). Excitatory/inhibitory synaptic imbalance leads to hippocampal hyperexcitability in mouse models of tuberous sclerosis. Neuron *78*, 510–522.

Bats, C., Groc, L., and Choquet, D. (2007). The interaction between Stargazin and PSD-95 regulates AMPA receptor surface trafficking. Neuron *53*, 719–734.

Bedford, F.K., Kittler, J.T., Muller, E., Thomas, P., Uren, J.M., Merlo, D., Wisden, W., Triller, A., Smart, T.G., and Moss, S.J. (2001). GABA(A) receptor cell surface number and subunit stability are regulated by the ubiquitin-like protein Plic-1. Nat. Neurosci. *4*, 908–916.

Bellone, C., and Mameli, M. (2012). mGluR-Dependent Synaptic Plasticity in Drug-Seeking. Front. Pharmacol. *3*, 159.

Bellot, A., Guivernau, B., Tajes, M., Bosch-Morató, M., Valls-Comamala, V., and Muñoz, F.J. (2014). The structure and function of actin cytoskeleton in mature glutamatergic dendritic spines. Brain Res. *1573*, 1–16.

Belmonte, M.K., Allen, G., Beckel-Mitchener, A., Boulanger, L.M., Carper, R.A., and Webb, S.J. (2004). Autism and abnormal development of brain connectivity. J. Neurosci. *24*, 9228–9231.

Ben-Ari, Y. (2002). Excitatory actions of gaba during development: the nature of the nurture. Nat. Rev. Neurosci. *3*, 728–739.

Ben-Ari, Y. (2014). The GABA excitatory/inhibitory developmental sequence: a personal journey. Neuroscience *279*, 187–219.

Benes, F.M., Sorensen, I., and Bird, E.D. (1991). Reduced neuronal size in posterior hippocampus of schizophrenic patients. Schizophr. Bull. *17*, 597–608.

Berg, J.M., and Geschwind, D.H. (2012). Autism genetics: searching for specificity and convergence. Genome Biol. *13*, 247.

Berkel, S., Marshall, C.R., Weiss, B., Howe, J., Roeth, R., Moog, U., Endris, V., Roberts, W., Szatmari, P., Pinto, D., et al. (2010). Mutations in the SHANK2 synaptic scaffolding gene in autism spectrum disorder and mental retardation. Nat. Genet. *42*, 489–491.

Berkel, S., Tang, W., Treviño, M., Vogt, M., Obenhaus, H.A., Gass, P., Scherer, S.W., Sprengel, R., Schratt, G., and Rappold, G.A. (2012). Inherited and de novo SHANK2 variants associated with autism spectrum disorder impair neuronal morphogenesis and physiology. Hum. Mol. Genet. *21*, 344–357.

Betz, H., Kuhse, J., Schmieden, V., Laube, B., Kirsch, J., and Harvey, R.J. (1999). Structure and functions of inhibitory and excitatory glycine receptors. Ann. N. Y. Acad. Sci. *868*, 667–676.

Bhattacharyya, S., Biou, V., Xu, W., Schlüter, O., and Malenka, R.C. (2009). A critical role for PSD-95/AKAP interactions in endocytosis of synaptic AMPA receptors. Nat. Neurosci. *12*, 172–181.

Bienvenu, O.J., Davydow, D.S., and Kendler, K.S. (2011). Psychiatric "diseases" versus behavioral disorders and degree of genetic influence. Psychol. Med. *41*, 33–40.

Bittel, D.C., Kibiryeva, N., and Butler, M.G. (2006). Expression of 4 genes between chromosome 15 breakpoints 1 and 2 and behavioral outcomes in Prader-Willi syndrome. Pediatrics *118*, e1276–e1283.

Blanpied, T.A., Kerr, J.M., and Ehlers, M.D. (2008). Structural plasticity with preserved topology in the postsynaptic protein network. Proc. Natl. Acad. Sci. U. S. A. *105*, 12587–12592.

Bloom, F.E., and Iversen, L.L. (1971). Localizing 3H-GABA in nerve terminals of rat cerebral cortex by electron microscopic autoradiography. Nature *229*, 628–630.

Blundell, J., Tabuchi, K., Bolliger, M.F., Blaiss, C.A., Brose, N., Liu, X., Südhof, T.C., and Powell, C.M. (2009). Increased anxiety-like behavior in mice lacking the inhibitory synapse cell adhesion molecule neuroligin 2. Genes. Brain. Behav. *8*, 114–126.

Bogdan, S., Grewe, O., Strunk, M., Mertens, A., and Klämbt, C. (2004). Sra-1 interacts with Kette and Wasp and is required for neuronal and bristle development in Drosophila. Development *131*, 3981–3989.

Bogdanov, Y., Michels, G., Armstrong-Gold, C., Haydon, P.G., Lindstrom, J., Pangalos, M., and Moss, S.J. (2006). Synaptic GABAA receptors are directly recruited from their extrasynaptic counterparts. EMBO J. *25*, 4381–4389.

Bonaccorso, C.M., Spatuzza, M., Di Marco, B., Gloria, A., Barrancotto, G., Cupo, A., Musumeci, S.A., D'Antoni, S., Bardoni, B., and Catania, M. V (2015). Fragile X mental retardation protein (FMRP) interacting proteins exhibit different expression patterns during development. Int. J. Dev. Neurosci. *42*, 15–23.

Bongmba, O.Y.N., Martinez, L.A., Elhardt, M.E., Butler, K., and Tejada-Simon, M. V (2011). Modulation of dendritic spines and synaptic function by Rac1: a possible link to Fragile X syndrome pathology. Brain Res. *1399*, 79–95.

Bourne, J.N., and Harris, K.M. (2008). Balancing structure and function at hippocampal dendritic spines. Annu. Rev. Neurosci.

Bourne, J.N., Sorra, K.E., Hurlburt, J., and Harris, K.M. (2007). Polyribosomes are increased in spines of CA1 dendrites 2 h after the induction of LTP in mature rat hippocampal slices. Hippocampus *17*, 1–4.

Bozdagi, O., Sakurai, T., Dorr, N., Pilorge, M., Takahashi, N., and Buxbaum, J.D. (2012). Haploinsufficiency of cyfip1 produces fragile x-like phenotypes in mice. PLoS One *7*, e42422.

Brady, M.L., and Jacob, T.C. (2015). Synaptic localization of α5 GABA (A) receptors via gephyrin interaction regulates dendritic outgrowth and spine maturation. Dev. Neurobiol.

Breitsprecher, D., and Goode, B.L. (2013). Formins at a glance. J. Cell Sci. *126*, 1–7.

Brett, M., McPherson, J., Zang, Z.J., Lai, A., Tan, E.-S., Ng, I., Ong, L.-C., Cham, B., Tan, P., Rozen, S., et al. (2014). Massively parallel sequencing of patients with intellectual disability, congenital anomalies and/or autism spectrum disorders with a targeted gene panel. PLoS One *9*, e93409.

Brickley, S.G., and Mody, I. (2012). Extrasynaptic GABA(A) receptors: their function in the CNS and implications for disease. Neuron *73*, 23–34.

Broadbelt, K., Byne, W., and Jones, L.B. (2002). Evidence for a decrease in basilar dendrites of pyramidal cells in schizophrenic medial prefrontal cortex. Schizophr. Res. *58*, 75–81.

Brown, V., Small, K., Lakkis, L., Feng, Y., Gunter, C., Wilkinson, K.D., and Warren, S.T. (1998). Purified recombinant Fmrp exhibits selective RNA binding as an intrinsic property of the fragile X mental retardation protein. J. Biol. Chem. *273*, 15521–15527.

Brown, V., Jin, P., Ceman, S., Darnell, J.C., O'Donnell, W.T., Tenenbaum, S.A., Jin, X., Feng, Y., Wilkinson, K.D., Keene, J.D., et al. (2001). Microarray identification of FMRP-associated brain mRNAs and altered mRNA translational profiles in fragile X syndrome. Cell *107*, 477–487.

Burette, A.C., Lesperance, T., Crum, J., Martone, M., Volkmann, N., Ellisman, M.H., and Weinberg, R.J. (2012). Electron tomographic analysis of synaptic ultrastructure. J. Comp. Neurol. *520*, 2697–2711.

Burnside, R.D., Pasion, R., Mikhail, F.M., Carroll, A.J., Robin, N.H., Youngs, E.L., Gadi, I.K., Keitges, E., Jaswaney, V.L., Papenhausen, P.R., et al. (2011). Microdeletion/microduplication of proximal 15q11.2 between BP1 and BP2: a susceptibility region for neurological dysfunction including developmental and language delay. Hum. Genet. *130*, 517–528.

Caesar, M., Felk, S., Aasly, J.O., and Gillardon, F. (2015). Changes in actin dynamics and F-actin structure both in synaptoneurosomes of LRRK2(R1441G) mutant mice and in primary human fibroblasts of LRRK2(G2019S) mutation carriers. Neuroscience *284*, 311–324.

Campellone, K.G., and Welch, M.D. (2010). A nucleator arms race: cellular control of actin assembly. Nat. Rev. Mol. Cell Biol. *11*, 237–251.

Castrén, M.L., and Castrén, E. (2014). BDNF in fragile X syndrome. Neuropharmacology *76 Pt C*, 729–736.

Chanda, S., Aoto, J., Lee, S.-J., Wernig, M., and Südhof, T.C. (2015). Pathogenic mechanism of an autism-associated neuroligin mutation involves altered AMPA-receptor trafficking. Mol. Psychiatry.

Chao, H.-T., Chen, H., Samaco, R.C., Xue, M., Chahrour, M., Yoo, J., Neul, J.L., Gong, S., Lu, H.-C., Heintz, N., et al. (2010). Dysfunction in GABA signalling mediates autism-like stereotypies and Rett syndrome phenotypes. Nature *468*, 263–269.

Charrier, C., Ehrensperger, M.-V., Dahan, M., Lévi, S., and Triller, A. (2006). Cytoskeleton regulation of glycine receptor number at synapses and diffusion in the plasma membrane. J. Neurosci. *26*, 8502–8511.

Charrier, C., Joshi, K., Coutinho-Budd, J., Kim, J.-E., Lambert, N., de Marchena, J., Jin, W.-L., Vanderhaeghen, P., Ghosh, A., Sassa, T., et al. (2012). Inhibition of SRGAP2 function by its human-specific paralogs induces neoteny during spine maturation. Cell *149*, 923–935.

Charych, E.I., Yu, W., Miralles, C.P., Serwanski, D.R., Li, X., Rubio, M., and De Blas, A.L. (2004). The brefeldin A-inhibited GDP/GTP exchange factor 2, a protein involved in vesicular trafficking, interacts with the beta subunits of the GABA receptors. J. Neurochem. *90*, 173–189.

Charych, E.I., Liu, F., Moss, S.J., and Brandon, N.J. (2009). GABA(A) receptors and their associated proteins: implications in the etiology and treatment of schizophrenia and related disorders. Neuropharmacology *57*, 481–495.

Chater, T.E., and Goda, Y. (2014). The role of AMPA receptors in postsynaptic mechanisms of synaptic plasticity. Front. Cell. Neurosci. *8*, 401.

Chen, B., Brinkmann, K., Chen, Z., Pak, C.W., Liao, Y., Shi, S., Henry, L., Grishin, N. V, Bogdan, S., and Rosen, M.K. (2014a). The WAVE regulatory complex links diverse receptors to the actin cytoskeleton. Cell *156*, 195–207.

Chen, S.X., Tari, P.K., She, K., and Haas, K. (2010a). Neurexin-neuroligin cell adhesion complexes contribute to synaptotropic dendritogenesis via growth stabilization mechanisms in vivo. Neuron *67*, 967–983.

Chen, X.J., Squarr, A.J., Stephan, R., Chen, B., Higgins, T.E., Barry, D.J., Martin, M.C., Rosen, M.K., Bogdan, S., and Way, M. (2014b). Ena/VASP proteins cooperate with the WAVE complex to regulate the actin cytoskeleton. Dev. Cell *30*, 569–584.

Chen, Z., Borek, D., Padrick, S.B., Gomez, T.S., Metlagel, Z., Ismail, A.M., Umetani, J., Billadeau, D.D., Otwinowski, Z., and Rosen, M.K. (2010b). Structure and control of the actin regulatory WAVE complex. Nature *468*, 533–538.

Cheng, D., Hoogenraad, C.C., Rush, J., Ramm, E., Schlager, M.A., Duong, D.M., Xu, P., Wijayawardana, S.R., Hanfelt, J., Nakagawa, T., et al. (2006). Relative and absolute quantification of postsynaptic density proteome isolated from rat forebrain and cerebellum. Mol. Cell. Proteomics *5*, 1158–1170.

Chesarone, M.A., DuPage, A.G., and Goode, B.L. (2010). Unleashing formins to

remodel the actin and microtubule cytoskeletons. Nat. Rev. Mol. Cell Biol. *11*, 62–74.

Chih, B., Afridi, S.K., Clark, L., and Scheiffele, P. (2004). Disorder-associated mutations lead to functional inactivation of neuroligins. Hum. Mol. Genet. *13*, 1471–1477.

Chih, B., Engelman, H., and Scheiffele, P. (2005). Control of excitatory and inhibitory synapse formation by neuroligins. Science *307*, 1324–1328.

Chih, B., Gollan, L., and Scheiffele, P. (2006). Alternative splicing controls selective trans-synaptic interactions of the neuroligin-neurexin complex. Neuron *51*, 171–178.

Cho, K.O., Hunt, C.A., and Kennedy, M.B. (1992). The rat brain postsynaptic density fraction contains a homolog of the Drosophila discs-large tumor suppressor protein. Neuron *9*, 929–942.

Choi, J., Ko, J., Racz, B., Burette, A., Lee, J.-R., Kim, S., Na, M., Lee, H.W., Kim, K., Weinberg, R.J., et al. (2005). Regulation of dendritic spine morphogenesis by insulin receptor substrate 53, a downstream effector of Rac1 and Cdc42 small GTPases. J. Neurosci. *25*, 869–879.

Cohen-Cory, S., Kidane, A.H., Shirkey, N.J., and Marshak, S. (2010). Brain-derived neurotrophic factor and the development of structural neuronal connectivity. Dev. Neurobiol. *70*, 271–288.

Colomer, V. (1997). Huntingtin-associated protein 1 (HAP1) binds to a Trio-like polypeptide, with a rac1 guanine nucleotide exchange factor domain. Hum. Mol. Genet. *6*, 1519–1525.

Comery, T.A., Harris, J.B., Willems, P.J., Oostra, B.A., Irwin, S.A., Weiler, I.J., and Greenough, W.T. (1997). Abnormal dendritic spines in fragile X knockout mice: maturation and pruning deficits. Proc. Natl. Acad. Sci. U. S. A. *94*, 5401–5404.

Compart, P.J. (2013). The Pathophysiology of Autism. Glob. Adv. Heal. Med. *2*, 32–37.

Consortium, I.S. (2008). Rare chromosomal deletions and duplications increase risk of schizophrenia. Nature *455*, 237–241.

Corbetta, S., Gualdoni, S., Ciceri, G., Monari, M., Zuccaro, E., Tybulewicz, V.L.J., and de Curtis, I. (2009). Essential role of Rac1 and Rac3 GTPases in neuronal development. FASEB J. *23*, 1347–1357.

Craddock, N., Jones, L., Jones, I.R., Kirov, G., Green, E.K., Grozeva, D., Moskvina, V., Nikolov, I., Hamshere, M.L., Vukcevic, D., et al. (2010). Strong genetic evidence for a selective influence of GABAA receptors on a component of the bipolar disorder phenotype. Mol. Psychiatry *15*, 146–153.

Craig, A.M., and Kang, Y. (2007). Neurexin-neuroligin signaling in synapse development. Curr. Opin. Neurobiol. *17*, 43–52.

Crestani, F., Lorez, M., Baer, K., Essrich, C., Benke, D., Laurent, J.P., Belzung, C.,

Fritschy, J.M., Lüscher, B., and Mohler, H. (1999). Decreased GABAA-receptor clustering results in enhanced anxiety and a bias for threat cues. Nat. Neurosci. *2*, 833–839.

Cui-Wang, T., Hanus, C., Cui, T., Helton, T., Bourne, J., Watson, D., Harris, K.M., and Ehlers, M.D. (2012). Local zones of endoplasmic reticulum complexity confine cargo in neuronal dendrites. Cell *148*, 309–321.

Curtis, D. (2011). Assessing the contribution family data can make to case-control studies of rare variants. Ann. Hum. Genet. *75*, 630–638.

Curtis, D. (2012). A rapid method for combined analysis of common and rare variants at the level of a region, gene, or pathway. Adv. Appl. Bioinform. Chem. *5*, 1–9.

D'Angelo, A., and Franco, B. (2009). The dynamic cilium in human diseases. Pathogenetics *2*, 3.

Dailey, M.E., and Smith, S.J. (1996). The dynamics of dendritic structure in developing hippocampal slices. J. Neurosci. *16*, 2983–2994.

Darnell, J.C., Van Driesche, S.J., Zhang, C., Hung, K.Y.S., Mele, A., Fraser, C.E., Stone, E.F., Chen, C., Fak, J.J., Chi, S.W., et al. (2011). FMRP stalls ribosomal translocation on mRNAs linked to synaptic function and autism. Cell *146*, 247–261.

Davis, G.A., and Bloom, F.E. (1973). Isolation of synaptic junctional complexes from rat brain. Brain Res. *62*, 135–153.

Dejanovic, B., and Schwarz, G. (2014). Neuronal nitric oxide synthase-dependent S-nitrosylation of gephyrin regulates gephyrin clustering at GABAergic synapses. J. Neurosci. *34*, 7763–7768.

Dejanovic, B., Semtner, M., Ebert, S., Lamkemeyer, T., Neuser, F., Lüscher, B., Meier, J.C., and Schwarz, G. (2014). Palmitoylation of gephyrin controls receptor clustering and plasticity of GABAergic synapses. PLoS Biol. *12*, e1001908.

Derivery, E., and Gautreau, A. (2010). Generation of branched actin networks: assembly and regulation of the N-WASP and WAVE molecular machines. Bioessays *32*, 119–131.

Derry, J.M., Ochs, H.D., and Francke, U. (1994). Isolation of a novel gene mutated in Wiskott-Aldrich syndrome. Cell *78*, 635–644.

Dixon-Salazar, T., Silhavy, J.L., Marsh, S.E., Louie, C.M., Scott, L.C., Gururaj, A., Al-Gazali, L., Al-Tawari, A.A., Kayserili, H., Sztriha, L., et al. (2004). Mutations in the AHI1 gene, encoding jouberin, cause Joubert syndrome with cortical polymicrogyria. Am. J. Hum. Genet. *75*, 979–987.

Doering, Kane, Hsiao, Yao, Shi, Slowik, Dhagat, Scott, Ault, Page-McCaw, et al. (2008). Species differences in the expression of Ahi1, a protein implicated in the neurodevelopmental disorder Joubert syndrome, with preferential accumulation to stigmoid bodies. J. Comp. Neurol. *511*, 238–256.

Doherty, D. (2009). Joubert syndrome: insights into brain development, cilium biology, and complex disease. Semin. Pediatr. Neurol. *16*, 143–154.

Dong, Q., Ji, Y.-S., Cai, C., and Chen, Z.-Y. (2012). LIM kinase 1 (LIMK1) interacts with tropomyosin-related kinase B (TrkB) and Mediates brain-derived neurotrophic factor (BDNF)-induced axonal elongation. J. Biol. Chem. *287*, 41720–41731.

Doornbos, M., Sikkema-Raddatz, B., Ruijvenkamp, C. a L., Dijkhuizen, T., Bijlsma, E.K., Gijsbers, A.C.J., Hilhorst-Hofstee, Y., Hordijk, R., Verbruggen, K.T., Kerstjens-Frederikse, W.S. (Mieke), et al. (2009). Nine patients with a microdeletion 15q11.2 between breakpoints 1 and 2 of the Prader-Willi critical region, possibly associated with behavioural disturbances. Eur. J. Med. Genet. *52*, 108–115.

Duan, X., Chang, J.H., Ge, S., Faulkner, R.L., Kim, J.Y., Kitabatake, Y., Liu, X., Yang, C.-H., Jordan, J.D., Ma, D.K., et al. (2007). Disrupted-In-Schizophrenia 1 regulates integration of newly generated neurons in the adult brain. Cell *130*, 1146–1158.

Dubielecka, P.M., Ladwein, K.I., Xiong, X., Migeotte, I., Chorzalska, A., Anderson, K. V, Sawicki, J.A., Rottner, K., Stradal, T.E., and Kotula, L. (2011). Essential role for Abi1 in embryonic survival and WAVE2 complex integrity. Proc. Natl. Acad. Sci. U. S. A. *108*, 7022–7027.

Dumoulin, A., Triller, A., and Kneussel, M. (2009). Cellular transport and membrane dynamics of the glycine receptor. Front. Mol. Neurosci. *2*, 28.

Durand, C.M., Betancur, C., Boeckers, T.M., Bockmann, J., Chaste, P., Fauchereau, F., Nygren, G., Rastam, M., Gillberg, I.C., Anckarsäter, H., et al. (2007). Mutations in the gene encoding the synaptic scaffolding protein SHANK3 are associated with autism spectrum disorders. Nat. Genet. *39*, 25–27.

Durand, C.M., Perroy, J., Loll, F., Perrais, D., Fagni, L., Bourgeron, T., Montcouquiol, M., and Sans, N. (2012). SHANK3 mutations identified in autism lead to modification of dendritic spine morphology via an actin-dependent mechanism. Mol. Psychiatry *17*, 71–84.

Dutertre, S., Becker, C.-M., and Betz, H. (2012). Inhibitory glycine receptors: an update. J. Biol. Chem. *287*, 40216–40223.

Earnheart, J.C., Schweizer, C., Crestani, F., Iwasato, T., Itohara, S., Mohler, H., and Lüscher, B. (2007). GABAergic control of adult hippocampal neurogenesis in relation to behavior indicative of trait anxiety and depression states. J. Neurosci. *27*, 3845–3854.

Ebrahimi, S., and Okabe, S. (2014). Structural dynamics of dendritic spines: molecular composition, geometry and functional regulation. Biochim. Biophys. Acta *1838*, 2391–2398.

Eden, S., Rohatgi, R., Podtelejnikov, A. V, Mann, M., and Kirschner, M.W. (2002). Mechanism of regulation of WAVE1-induced actin nucleation by Rac1 and Nck. Nature *418*, 790–793.

Ehrlich, I., Klein, M., Rumpel, S., and Malinow, R. (2007). PSD-95 is required for activity-driven synapse stabilization. Proc. Natl. Acad. Sci. U. S. A. *104*, 4176–4181.

El-Husseini, A.E., Schnell, E., Chetkovich, D.M., Nicoll, R.A., and Bredt, D.S. (2000). PSD-95 involvement in maturation of excitatory synapses. Science *290*, 1364–1368.

Elias, and Nicoll (2007). Synaptic trafficking of glutamate receptors by MAGUK scaffolding proteins. Trends Cell Biol. *17*, 343–352.

Elias, G.M., Funke, L., Stein, V., Grant, S.G., Bredt, D.S., and Nicoll, R.A. (2006). Synapse-specific and developmentally regulated targeting of AMPA receptors by a family of MAGUK scaffolding proteins. Neuron *52*, 307–320.

Engelender, S., Sharp, A.H., Colomer, V., Tokito, M.K., Lanahan, A., Worley, P., Holzbaur, E.L., and Ross, C.A. (1997). Huntingtin-associated protein 1 (HAP1) interacts with the p150Glued subunit of dynactin. Hum. Mol. Genet. *6*, 2205–2212.

Erlander, M.G., Tillakaratne, N.J., Feldblum, S., Patel, N., and Tobin, A.J. (1991). Two genes encode distinct glutamate decarboxylases. Neuron *7*, 91–100.

Esmailzadeh, S., and Jiang, X. (2011). AHI-1: a novel signaling protein and potential therapeutic target in human leukemia and brain disorders. Oncotarget *2*, 918–934.

Essrich, C., Lorez, M., Benson, J.A., Fritschy, J.M., and Lüscher, B. (1998). Postsynaptic clustering of major GABAA receptor subtypes requires the gamma 2 subunit and gephyrin. Nat. Neurosci. *1*, 563–571.

Feil, R., Wagner, J., Metzger, D., and Chambon, P. (1997). Regulation of Cre recombinase activity by mutated estrogen receptor ligand-binding domains. Biochem. Biophys. Res. Commun. *237*, 752–757.

Feil, S., Valtcheva, N., and Feil, R. (2009). Inducible Cre mice. Methods Mol. Biol. *530*, 343–363.

Feng, Y., Absher, D., Eberhart, D.E., Brown, V., Malter, H.E., and Warren, S.T. (1997). FMRP associates with polyribosomes as an mRNP, and the I304N mutation of severe fragile X syndrome abolishes this association. Mol. Cell *1*, 109–118.

Ferland, Eyaid, Collura, Tully, Hill, Al-Nouri, Al-Rumayyan, Topcu, Gascon, Bodell, et al. (2004). Abnormal cerebellar development and axonal decussation due to mutations in AHI1 in Joubert syndrome. Nat. Genet. *36*, 1008–1013.

Fiala, J.C., Spacek, J., and Harris, K.M. (2002). Dendritic spine pathology: cause or consequence of neurological disorders? Brain Res. Brain Res. Rev. *39*, 29–54.

Fischer, M., Kaech, S., Wagner, U., Brinkhaus, H., and Matus, A. (2000). Glutamate receptors regulate actin-based plasticity in dendritic spines. Nat. Neurosci. *3*, 887–894.

Flores, C.E., Nikonenko, I., Mendez, P., Fritschy, J.-M., Tyagarajan, S.K., and Muller, D. (2015). Activity-dependent inhibitory synapse remodeling through gephyrin phosphorylation. Proc. Natl. Acad. Sci. U. S. A. *112*, E65–E72.

Föcking, M., Lopez, L.M., English, J.A., Dicker, P., Wolff, A., Brindley, E., Wynne, K., Cagney, G., and Cotter, D.R. (2014). Proteomic and genomic evidence implicates the postsynaptic density in schizophrenia. Mol. Psychiatry.

Follit, J.A., Li, L., Vucica, Y., and Pazour, G.J. (2010). The cytoplasmic tail of fibrocystin contains a ciliary targeting sequence. J. Cell Biol. *188*, 21–28.

Frazer, K.A., Murray, S.S., Schork, N.J., and Topol, E.J. (2009). Human genetic variation and its contribution to complex traits. Nat. Rev. Genet. *10*, 241–251.

Frost, N.A., Shroff, H., Kong, H., Betzig, E., and Blanpied, T.A. (2010a). Single-molecule discrimination of discrete perisynaptic and distributed sites of actin filament assembly within dendritic spines. Neuron *67*, 86–99.

Frost, N.A., Kerr, J.M., Lu, H.E., and Blanpied, T.A. (2010b). A network of networks: cytoskeletal control of compartmentalized function within dendritic spines. Curr. Opin. Neurobiol. *20*, 578–587.

Fuchs, C., Abitbol, K., Burden, J.J., Mercer, A., Brown, L., Iball, J., Anne Stephenson, F., Thomson, A.M., and Jovanovic, J.N. (2013). GABA(A) receptors can initiate the formation of functional inhibitory GABAergic synapses. Eur. J. Neurosci. *38*, 3146–3158.

Gallagher, M.J., Ding, L., Maheshwari, A., and Macdonald, R.L. (2007). The GABAA receptor alpha1 subunit epilepsy mutation A322D inhibits transmembrane helix formation and causes proteasomal degradation. Proc. Natl. Acad. Sci. U. S. A. *104*, 12999–13004.

Galy, A., Schenck, A., Sahin, H.B., Qurashi, A., Sahel, J.-A., Diebold, C., and Giangrande, A. (2011). CYFIP dependent actin remodeling controls specific aspects of Drosophila eye morphogenesis. Dev. Biol. *359*, 37–46.

Garey, L.J., Ong, W.Y., Patel, T.S., Kanani, M., Davis, A., Mortimer, A.M., Barnes, T.R., and Hirsch, S.R. (1998). Reduced dendritic spine density on cerebral cortical pyramidal neurons in schizophrenia. J. Neurol. Neurosurg. Psychiatry *65*, 446–453.

Gassmann, M., and Bettler, B. (2012). Regulation of neuronal GABA(B) receptor functions by subunit composition. Nat. Rev. Neurosci. *13*, 380–394.

Gaugler, T., Klei, L., Sanders, S.J., Bodea, C.A., Goldberg, A.P., Lee, A.B., Mahajan, M., Manaa, D., Pawitan, Y., Reichert, J., et al. (2014). Most genetic risk for autism resides with common variation. Nat. Genet. *46*, 881–885.

Gauthier, J., Champagne, N., Lafrenière, R.G., Xiong, L., Spiegelman, D., Brustein, E., Lapointe, M., Peng, H., Côté, M., Noreau, A., et al. (2010). De novo mutations in the gene encoding the synaptic scaffolding protein SHANK3 in patients ascertained for schizophrenia. Proc. Natl. Acad. Sci. U. S. A. *107*, 7863–7868.

Gauthier, L.R., Charrin, B.C., Borrell-Pagès, M., Dompierre, J.P., Rangone, H., Cordelières, F.P., De Mey, J., MacDonald, M.E., Lessmann, V., Humbert, S., et al. (2004). Huntingtin controls neurotrophic support and survival of neurons by

enhancing BDNF vesicular transport along microtubules. Cell *118*, 127–138.

Gautier, J.J., Lomakina, M.E., Bouslama-Oueghlani, L., Derivery, E., Beilinson, H., Faigle, W., Loew, D., Louvard, D., Echard, A., Alexandrova, A.Y., et al. (2011). Clathrin is required for Scar/Wave-mediated lamellipodium formation. J. Cell Sci. *124*, 3414–3427.

Gautreau, A., Ho, H.H., Li, J., Steen, H., Gygi, S.P., and Kirschner, M.W. (2004). Purification and architecture of the ubiquitous Wave complex. Proc. Natl. Acad. Sci. U. S. A. *101*, 4379–4383.

Geschwind, D.H., and Levitt, P. (2007). Autism spectrum disorders: developmental disconnection syndromes. Curr. Opin. Neurobiol. *17*, 103–111.

Geschwind, D.H., and State, M.W. (2015). Gene hunting in autism spectrum disorder: on the path to precision medicine. Lancet Neurol.

Ghani, M., Pinto, D., Lee, J.H., Grinberg, Y., Sato, C., Moreno, D., Scherer, S.W., Mayeux, R., St George-Hyslop, P., and Rogaeva, E. (2012). Genome-wide survey of large rare copy number variants in Alzheimer's disease among Caribbean hispanics. G3 (Bethesda). *2*, 71–78.

Giannone, G., Mondin, M., Grillo-Bosch, D., Tessier, B., Saint-Michel, E., Czöndör, K., Sainlos, M., Choquet, D., and Thoumine, O. (2013). Neurexin-1β binding to neuroligin-1 triggers the preferential recruitment of PSD-95 versus gephyrin through tyrosine phosphorylation of neuroligin-1. Cell Rep. *3*, 1996–2007.

Gibson, J.R., Huber, K.M., and Südhof, T.C. (2009). Neuroligin-2 deletion selectively decreases inhibitory synaptic transmission originating from fast-spiking but not from somatostatin-positive interneurons. J. Neurosci. *29*, 13883–13897.

Giesemann, T., Schwarz, G., Nawrotzki, R., Berhörster, K., Rothkegel, M., Schlüter, K., Schrader, N., Schindelin, H., Mendel, R.R., Kirsch, J., et al. (2003). Complex formation between the postsynaptic scaffolding protein gephyrin, profilin, and Mena: a possible link to the microfilament system. J. Neurosci. *23*, 8330–8339.

Giuffrida, R., Musumeci, S., D'Antoni, S., Bonaccorso, C.M., Giuffrida-Stella, A.M., Oostra, B.A., and Catania, M.V. (2005). A reduced number of metabotropic glutamate subtype 5 receptors are associated with constitutive homer proteins in a mouse model of fragile X syndrome. J. Neurosci. *25*, 8908–8916.

Gkogkas, C.G., Khoutorsky, A., Ran, I., Rampakakis, E., Nevarko, T., Weatherill, D.B., Vasuta, C., Yee, S., Truitt, M., Dallaire, P., et al. (2013). Autism-related deficits via dysregulated eIF4E-dependent translational control. Nature *493*, 371–377.

Glantz, L.A., and Lewis, D.A. (2000). Decreased dendritic spine density on prefrontal cortical pyramidal neurons in schizophrenia. Arch. Gen. Psychiatry *57*, 65–73.

Graf, E.R., Zhang, X., Jin, S.-X., Linhoff, M.W., and Craig, A.M. (2004). Neurexins induce differentiation of GABA and glutamate postsynaptic specializations via neuroligins. Cell *119*, 1013–1026.

Grant, S.G.N. (2012). Synaptopathies: diseases of the synaptome. Curr. Opin. Neurobiol. *22*, 522–529.

Gray, E.G. (1959). Axo-somatic and axo-dendritic synapses of the cerebral cortex. J. Anat. *93*, 420–433.

Graziane, N.M., Yuen, E.Y., and Yan, Z. (2009). Dopamine D4 Receptors Regulate GABAA Receptor Trafficking via an Actin/Cofilin/Myosin-dependent Mechanism. J. Biol. Chem. *284*, 8329–8336.

Guilmatre, A., Huguet, G., Delorme, R., and Bourgeron, T. (2014). The emerging role of SHANK genes in neuropsychiatric disorders. Dev. Neurobiol. *74*, 113–122.

Gupta, V.K., You, Y., Gupta, V.B., Klistorner, A., and Graham, S.L. (2013). TrkB Receptor Signalling: Implications in Neurodegenerative, Psychiatric and Proliferative Disorders. Int. J. Mol. Sci. *14*, 10122–10142.

Gurling, H.M., Kalsi, G., Brynjolfson, J., Sigmundsson, T., Sherrington, R., Mankoo, B.S., Read, T., Murphy, P., Blaveri, E., McQuillin, A., et al. (2001). Genomewide genetic linkage analysis confirms the presence of susceptibility loci for schizophrenia, on chromosomes 1q32.2, 5q33.2, and 8p21-22 and provides support for linkage to schizophrenia, on chromosomes 11q23.3-24 and 20q12.1-11.23. Am. J. Hum. Genet. *68*, 661–673.

Guzowski, J.F., Lyford, G.L., Stevenson, G.D., Houston, F.P., McGaugh, J.L., Worley, P.F., and Barnes, C.A. (2000). Inhibition of activity-dependent arc protein expression in the rat hippocampus impairs the maintenance of long-term potentiation and the consolidation of long-term memory. J. Neurosci. *20*, 3993–4001.

Hall, J., Trent, S., Thomas, K.L., O'Donovan, M.C., and Owen, M.J. (2015). Genetic risk for schizophrenia: convergence on synaptic pathways involved in plasticity. Biol. Psychiatry *77*, 52–58.

Hamilton, S.P. (2015). The promise of psychiatric pharmacogenomics. Biol. Psychiatry *77*, 29–35.

Han, K., Chen, H., Gennarino, V.A., Richman, R., Lu, H.-C., and Zoghbi, H.Y. (2014). Fragile X-like behaviors and abnormal cortical dendritic spines in Cytoplasmic FMR1 interacting protein 2 mutant mice. Hum. Mol. Genet.

Han, K., Chen, H., Gennarino, V.A., Richman, R., Lu, H.-C., and Zoghbi, H.Y. (2015). Fragile X-like behaviors and abnormal cortical dendritic spines in Cytoplasmic FMR1-interacting protein 2-mutant mice. Hum. Mol. Genet. *24*, 1813–1823.

Hanley, J.G. (2014). Actin-dependent mechanisms in AMPA receptor trafficking. Front. Cell. Neurosci. *8*, 381.

Hanley, and Henley (2005). PICK1 is a calcium-sensor for NMDA-induced AMPA receptor trafficking. EMBO J. *24*, 3266–3278.

Hanus, C., Ehrensperger, M.-V., and Triller, A. (2006). Activity-dependent

movements of postsynaptic scaffolds at inhibitory synapses. J. Neurosci. *26*, 4586–4595.

Harvey, I., Ron, M.A., Du Boulay, G., Wicks, D., Lewis, S.W., and Murray, R.M. (1993). Reduction of cortical volume in schizophrenia on magnetic resonance imaging. Psychol. Med. *23*, 591–604.

Harvey, K., Duguid, I.C., Alldred, M.J., Beatty, S.E., Ward, H., Keep, N.H., Lingenfelter, S.E., Pearce, B.R., Lundgren, J., Owen, M.J., et al. (2004). The GDP-GTP exchange factor collybistin: an essential determinant of neuronal gephyrin clustering. J. Neurosci. *24*, 5816–5826.

Harvey, R.J., Topf, M., Harvey, K., and Rees, M.I. (2008). The genetics of hyperekplexia: more than startle! Trends Genet. *24*, 439–447.

Hayashi, M.L., Choi, S.-Y., Rao, B.S.S., Jung, H.-Y., Lee, H.-K., Zhang, D., Chattarji, S., Kirkwood, A., and Tonegawa, S. (2004). Altered cortical synaptic morphology and impaired memory consolidation in forebrain- specific dominant-negative PAK transgenic mice. Neuron *42*, 773–787.

Hayashi-Takagi, A., Takaki, M., Graziane, N., Seshadri, S., Murdoch, H., Dunlop, A.J., Makino, Y., Seshadri, A.J., Ishizuka, K., Srivastava, D.P., et al. (2010). Disrupted-in-Schizophrenia 1 (DISC1) regulates spines of the glutamate synapse via Rac1. Nat. Neurosci. *13*, 327–332.

Heasman, and Ridley (2008). Mammalian Rho GTPases: new insights into their functions from in vivo studies. Nat. Rev. Mol. Cell Biol. *9*, 690–701.

Hering, H., and Sheng, M. (2001). Dendritic spines: structure, dynamics and regulation. Nat. Rev. Neurosci. *2*, 880–888.

Hering, H., Lin, C.-C., and Sheng, M. (2003). Lipid rafts in the maintenance of synapses, dendritic spines, and surface AMPA receptor stability. J. Neurosci. *23*, 3262–3271.

Hill, T.C., and Zito, K. (2013). LTP-induced long-term stabilization of individual nascent dendritic spines. J. Neurosci. *33*, 678–686.

Hill, J.J., Hashimoto, T., and Lewis, D.A. (2006). Molecular mechanisms contributing to dendritic spine alterations in the prefrontal cortex of subjects with schizophrenia. Mol. Psychiatry *11*, 557–566.

Hines, R.M., Wu, L., Hines, D.J., Steenland, H., Mansour, S., Dahlhaus, R., Singaraja, R.R., Cao, X., Sammler, E., Hormuzdi, S.G., et al. (2008). Synaptic imbalance, stereotypies, and impaired social interactions in mice with altered neuroligin 2 expression. J. Neurosci. *28*, 6055–6067.

Ho, H.-Y.H., Rohatgi, R., Lebensohn, A.M., Le Ma, Li, J., Gygi, S.P., and Kirschner, M.W. (2004). Toca-1 mediates Cdc42-dependent actin nucleation by activating the N-WASP-WIP complex. Cell *118*, 203–216.

Hoeffer, C.A., Sanchez, E., Hagerman, R.J., Mu, Y., Nguyen, D. V, Wong, H., Whelan, A.M., Zukin, R.S., Klann, E., and Tassone, F. (2012). Altered mTOR signaling and enhanced CYFIP2 expression levels in subjects with fragile X syndrome. Genes. Brain. Behav. *11*, 332–341.

Holroyd, S., Reiss, A.L., and Bryan, R.N. (1991). Autistic features in Joubert syndrome: a genetic disorder with agenesis of the cerebellar vermis. Biol. Psychiatry *29*, 287–294.

Honkura, N., Matsuzaki, M., Noguchi, J., Ellis-Davies, G.C.R., and Kasai, H. (2008). The subspine organization of actin fibers regulates the structure and plasticity of dendritic spines. Neuron *57*, 719–729.

Hoogenraad, C.C., Milstein, A.D., Ethell, I.M., Henkemeyer, M., and Sheng, M. (2005). GRIP1 controls dendrite morphogenesis by regulating EphB receptor trafficking. Nat. Neurosci. *8*, 906–915.

Hoon, M., Bauer, G., Fritschy, J.-M., Moser, T., Falkenburger, B.H., and Varoqueaux, F. (2009). Neuroligin 2 controls the maturation of GABAergic synapses and information processing in the retina. J. Neurosci. *29*, 8039–8050.

Horch, H.W., and Katz, L.C. (2002). BDNF release from single cells elicits local dendritic growth in nearby neurons. Nat. Neurosci. *5*, 1177–1184.

Horton, A.C., Rácz, B., Monson, E.E., Lin, A.L., Weinberg, R.J., and Ehlers, M.D. (2005). Polarized secretory trafficking directs cargo for asymmetric dendrite growth and morphogenesis. Neuron *48*, 757–771.

Hotulainen, P., and Hoogenraad, C.C. (2010). Actin in dendritic spines: connecting dynamics to function. J. Cell Biol. *189*, 619–629.

Hotulainen, P., Llano, O., Smirnov, S., Tanhuanpää, K., Faix, J., Rivera, C., and Lappalainen, P. (2009). Defining mechanisms of actin polymerization and depolymerization during dendritic spine morphogenesis. J. Cell Biol. *185*, 323–339.

Hsiao, Tong, Westfall, Ault, Page-McCaw, and Ferland (2009). Ahi1, whose human ortholog is mutated in Joubert syndrome, is required for Rab8a localization, ciliogenesis and vesicle trafficking. Hum. Mol. Genet. *18*, 3926–3941.

Hsiao, Y.-C., Tuz, K., and Ferland, R.J. (2012). Trafficking in and to the primary cilium. Cilia *1*, 4.

Huang, Y., and Chen, Y. (2015). Up-Regulated Cytoplasmic FMRP-interacting protein 1 in Intractable Temporal Lobe Epilepsy Patients and a Rat Model. Int. J. Neurosci. 1–28.

Huber, K.M., Gallagher, S.M., Warren, S.T., and Bear, M.F. (2002). Altered synaptic plasticity in a mouse model of fragile X mental retardation. Proc. Natl. Acad. Sci. U. S. A. *99*, 7746–7750.

Huguet, G., Ey, E., and Bourgeron, T. (2013). The genetic landscapes of autism

spectrum disorders. Annu. Rev. Genomics Hum. Genet. *14*, 191–213.

Hutsler, J.J., and Zhang, H. (2010). Increased dendritic spine densities on cortical projection neurons in autism spectrum disorders. Brain Res. *1309*, 83–94.

Iacoangeli, A., Rozhdestvensky, T.S., Dolzhanskaya, N., Tournier, B., Schütt, J., Brosius, J., Denman, R.B., Khandjian, E.W., Kindler, S., and Tiedge, H. (2008a). On BC1 RNA and the fragile X mental retardation protein. Proc. Natl. Acad. Sci. U. S. A. *105*, 734–739.

Iacoangeli, A., Rozhdestvensky, T.S., Dolzhanskaya, N., Tournier, B., Schütt, J., Brosius, J., Denman, R.B., Khandjian, E.W., Kindler, S., and Tiedge, H. (2008b). Reply to Bagni: On BC1 RNA and the fragile X mental retardation protein. Proc. Natl. Acad. Sci. U. S. A. *105*, E29.

Ifrim, M.F., Williams, K.R., and Bassell, G.J. (2015). Single-Molecule Imaging of PSD-95 mRNA Translation in Dendrites and Its Dysregulation in a Mouse Model of Fragile X Syndrome. J. Neurosci. *35*, 7116–7130.

Iki, J., Inoue, A., Bito, H., and Okabe, S. (2005). Bi-directional regulation of postsynaptic cortactin distribution by BDNF and NMDA receptor activity. Eur. J. Neurosci. *22*, 2985–2994.

Ingason, A., Sigmundsson, T., Steinberg, S., Sigurdsson, E., Haraldsson, M., Magnusdottir, B.B., Frigge, M.L., Kong, A., Gulcher, J., Thorsteinsdottir, U., et al. (2007). Support for involvement of the AHI1 locus in schizophrenia. Eur. J. Hum. Genet. *15*, 988–991.

Ingason, A., Giegling, I., Cichon, S., Hansen, T., Rasmussen, H.B., Nielsen, J., Jürgens, G., Muglia, P., Hartmann, A.M., Strengman, E., et al. (2010). A large replication study and meta-analysis in European samples provides further support for association of AHI1 markers with schizophrenia. Hum. Mol. Genet. *19*, 1379–1386.

Ingason, A., Kirov, G., Giegling, I., Hansen, T., Isles, A.R., Jakobsen, K.D., Kristinsson, K.T., le Roux, L., Gustafsson, O., Craddock, N., et al. (2011). Maternally derived microduplications at 15q11-q13: implication of imprinted genes in psychotic illness. Am. J. Psychiatry *168*, 408–417.

Innocenti, M., Zucconi, A., Disanza, A., Frittoli, E., Areces, L.B., Steffen, A., Stradal, T.E.B., Di Fiore, P.P., Carlier, M.-F., and Scita, G. (2004). Abi1 is essential for the formation and activation of a WAVE2 signalling complex. Nat. Cell Biol. *6*, 319–327.

Irie, M., Hata, Y., Takeuchi, M., Ichtchenko, K., Toyoda, A., Hirao, K., Takai, Y., Rosahl, T.W., and Südhof, T.C. (1997). Binding of neuroligins to PSD-95. Science *277*, 1511–1515.

Irwin, S.A., Patel, B., Idupulapati, M., Harris, J.B., Crisostomo, R.A., Larsen, B.P., Kooy, F., Willems, P.J., Cras, P., Kozlowski, P.B., et al. (2001). Abnormal dendritic spine characteristics in the temporal and visual cortices of patients with fragile-X syndrome: a quantitative examination. Am. J. Med. Genet. *98*, 161–167.

Ismail, A.M., Padrick, S.B., Chen, B., Umetani, J., and Rosen, M.K. (2009). The WAVE regulatory complex is inhibited. Nat. Struct. Mol. Biol. *16*, 561–563.

Ito, H., Morishita, R., Shinoda, T., Iwamoto, I., Sudo, K., Okamoto, K., and Nagata, K. (2010). Dysbindin-1, WAVE2 and Abi-1 form a complex that regulates dendritic spine formation. Mol. Psychiatry *15*, 976–986.

Jacob, T.C., Bogdanov, Y.D., Magnus, C., Saliba, R.S., Kittler, J.T., Haydon, P.G., and Moss, S.J. (2005). Gephyrin regulates the cell surface dynamics of synaptic GABAA receptors. J. Neurosci. *25*, 10469–10478.

Jacobs, S., and Doering, L.C. (2010). Astrocytes prevent abnormal neuronal development in the fragile x mouse. J. Neurosci. *30*, 4508–4514.

Jaffe, A.B., and Hall, A. (2005). Rho GTPases: biochemistry and biology. Annu. Rev. Cell Dev. Biol. *21*, 247–269.

Jan, Y.-N., and Jan, L.Y. (2010). Branching out: mechanisms of dendritic arborization. Nat. Rev. Neurosci. *11*, 316–328.

Jiang, Y.-H., and Ehlers, M.D. (2013). Modeling autism by SHANK gene mutations in mice. Neuron *78*, 8–27.

Jiang, Hanna, Kaouass, Girard, and Jolicoeur (2002). Ahi-1, a novel gene encoding a modular protein with WD40-repeat and SH3 domains, is targeted by the Ahi-1 and Mis-2 provirus integrations. J. Virol. *76*, 9046–9059.

Jönsson, S.A., Luts, A., Guldberg-Kjaer, N., and Ohman, R. (1999). Pyramidal neuron size in the hippocampus of schizophrenics correlates with total cell count and degree of cell disarray. Eur. Arch. Psychiatry Clin. Neurosci. *249*, 169–173.

Joubert, M., Eisenring, J.J., and Andermann, F. (1968). Familial dysgenesis of the vermis: a syndrome of hyperventilation, abnormal eye movements and retardation. Neurology *18*, 302–303.

Joubert, M., Eisenring, J.J., Robb, J.P., and Andermann, F. (1969). Familial agenesis of the cerebellar vermis. A syndrome of episodic hyperpnea, abnormal eye movements, ataxia, and retardation. Neurology *19*, 813–825.

Kang, H., and Schuman, E.M. (1996). A requirement for local protein synthesis in neurotrophin-induced hippocampal synaptic plasticity. Science *273*, 1402–1406.

Kang, Y., Zhang, X., Dobie, F., Wu, H., and Craig, A.M. (2008). Induction of GABAergic postsynaptic differentiation by alpha-neurexins. J. Biol. Chem. *283*, 2323–2334.

Karlsgodt, K.H., Sun, D., Jimenez, A.M., Lutkenhoff, E.S., Willhite, R., van Erp, T.G.M., and Cannon, T.D. (2008). Developmental disruptions in neural connectivity in the pathophysiology of schizophrenia. Dev. Psychopathol. *20*, 1297–1327.

Kasai, H., Fukuda, M., Watanabe, S., Hayashi-Takagi, A., and Noguchi, J. (2010). Structural dynamics of dendritic spines in memory and cognition. Trends Neurosci.

33, 121–129.

Kaufmann, W.E., and Moser, H.W. (2000). Dendritic anomalies in disorders associated with mental retardation. Cereb. Cortex *10*, 981–991.

Kawano, Y., Yoshimura, T., Tsuboi, D., Kawabata, S., Kaneko-Kawano, T., Shirataki, H., Takenawa, T., and Kaibuchi, K. (2005). CRMP-2 is involved in kinesin-1-dependent transport of the Sra-1/WAVE1 complex and axon formation. Mol. Cell. Biol. *25*, 9920–9935.

Kelleher, R.J., Govindarajan, A., Jung, H.-Y., Kang, H., and Tonegawa, S. (2004). Translational control by MAPK signaling in long-term synaptic plasticity and memory. Cell *116*, 467–479.

Keller, C.A., Yuan, X., Panzanelli, P., Martin, M.L., Alldred, M., Sassoè-Pognetto, M., and Lüscher, B. (2004). The gamma2 subunit of GABA(A) receptors is a substrate for palmitoylation by GODZ. J. Neurosci. *24*, 5881–5891.

Kennedy, M.B., Beale, H.C., Carlisle, H.J., and Washburn, L.R. (2005). INTEGRATION OF BIOCHEMICAL SIGNALLING IN SPINES. *6*, 423–434.

Kerr, J.M., and Blanpied, T.A. (2012). Subsynaptic AMPA receptor distribution is acutely regulated by actin-driven reorganization of the postsynaptic density. J. Neurosci. *32*, 658–673.

Kim, C.H., and Lisman, J.E. (1999). A role of actin filament in synaptic transmission and long-term potentiation. J. Neurosci. *19*, 4314–4324.

Kim, C.H., and Lisman, J.E. (2001). A labile component of AMPA receptor-mediated synaptic transmission is dependent on microtubule motors, actin, and N-ethylmaleimide-sensitive factor. J. Neurosci. *21*, 4188–4194.

Kim, and Sheng (2004). PDZ domain proteins of synapses. Nat. Rev. Neurosci. *5*, 771–781.

Kim, I.H., Racz, B., Wang, H., Burianek, L., Weinberg, R., Yasuda, R., Wetsel, W.C., and Soderling, S.H. (2013). Disruption of Arp2/3 Results in Asymmetric Structural Plasticity of Dendritic Spines and Progressive Synaptic and Behavioral Abnormalities. J. Neurosci. *33*, 6081–6092.

Kim, Y., Sung, J.Y., Ceglia, I., Lee, K.-W., Ahn, J.-H., Halford, J.M., Kim, A.M., Kwak, S.P., Park, J.B., Ho Ryu, S., et al. (2006). Phosphorylation of WAVE1 regulates actin polymerization and dendritic spine morphology. Nature *442*, 814–817.

Kins, S., Betz, H., and Kirsch, J. (2000). Collybistin, a newly identified brain-specific GEF, induces submembrane clustering of gephyrin. Nat. Neurosci. *3*, 22–29.

Kirov, G., Pocklington, A.J., Holmans, P., Ivanov, D., Ikeda, M., Ruderfer, D., Moran, J., Chambert, K., Toncheva, D., Georgieva, L., et al. (2012). De novo CNV analysis implicates specific abnormalities of postsynaptic signalling complexes in the pathogenesis of schizophrenia. Mol. Psychiatry *17*, 142–153.

Kirsch, J., and Betz, H. (1995). The postsynaptic localization of the glycine receptor-associated protein gephyrin is regulated by the cytoskeleton. J. Neurosci. *15*, 4148–4156.

Kitamura, T., Kitamura, Y., Yonezawa, K., Totty, N.F., Gout, I., Hara, K., Waterfield, M.D., Sakaue, M., Ogawa, W., and Kasuga, M. (1996). Molecular cloning of p125Nap1, a protein that associates with an SH3 domain of Nck. Biochem. Biophys. Res. Commun. *219*, 509–514.

Kittler, Thomas, Tretter, Bogdanov, Haucke, Smart, and Moss (2004). Huntingtin-associated protein 1 regulates inhibitory synaptic transmission by modulating gamma-aminobutyric acid type A receptor membrane trafficking. Proc. Natl. Acad. Sci. U. S. A. *101*, 12736–12741.

Kittler, Chen, Honing, Bogdanov, McAinsh, Arancibia-Carcamo, Jovanovic, Pangalos, Haucke, Yan, et al. (2005). Phospho-dependent binding of the clathrin AP2 adaptor complex to GABAA receptors regulates the efficacy of inhibitory synaptic transmission. Proc. Natl. Acad. Sci. U. S. A. *102*, 14871–14876.

Kittler, Chen, Kukhtina, Vahedi-Faridi, Gu, Tretter, Smith, McAinsh, Arancibia-Carcamo, Saenger, et al. (2008). Regulation of synaptic inhibition by phospho-dependent binding of the AP2 complex to a YECL motif in the GABAA receptor gamma2 subunit. Proc. Natl. Acad. Sci. U. S. A. *105*, 3616–3621.

Kittler, J.T., Delmas, P., Jovanovic, J.N., Brown, D.A., Smart, T.G., and Moss, S.J. (2000). Constitutive endocytosis of GABAA receptors by an association with the adaptin AP2 complex modulates inhibitory synaptic currents in hippocampal neurons. J. Neurosci. *20*, 7972–7977.

Kneussel, M., Brandstätter, J.H., Laube, B., Stahl, S., Müller, U., and Betz, H. (1999). Loss of postsynaptic GABA(A) receptor clustering in gephyrin-deficient mice. J. Neurosci. *19*, 9289–9297.

Knuesel, I., Mastrocola, M., Zuellig, R.A., Bornhauser, B., Schaub, M.C., and Fritschy, J.M. (1999). Short communication: altered synaptic clustering of GABAA receptors in mice lacking dystrophin (mdx mice). Eur. J. Neurosci. *11*, 4457–4462.

Kobayashi, K., Kuroda, S., Fukata, M., Nakamura, T., Nagase, T., Nomura, N., Matsuura, Y., Yoshida-Kubomura, N., Iwamatsu, a, and Kaibuchi, K. (1998). p140Sra-1 (specifically Rac1-associated protein) is a novel specific target for Rac1 small GTPase. J. Biol. Chem. *273*, 291–295.

Koleske, A.J. (2013). Molecular mechanisms of dendrite stability. Nat. Rev. Neurosci. *14*, 536–550.

Kolomeets, N.S., Orlovskaya, D.D., Rachmanova, V.I., and Uranova, N.A. (2005). Ultrastructural alterations in hippocampal mossy fiber synapses in schizophrenia: a postmortem morphometric study. Synapse *57*, 47–55.

Körber, C., Richter, A., Kaiser, M., Schlicksupp, A., Mükusch, S., Kuner, T., Kirsch, J.,

and Kuhse, J. (2012). Effects of distinct collybistin isoforms on the formation of GABAergic synapses in hippocampal neurons. Mol. Cell. Neurosci. *50*, 250–259.

Kornau, H.C., Schenker, L.T., Kennedy, M.B., and Seeburg, P.H. (1995). Domain interaction between NMDA receptor subunits and the postsynaptic density protein PSD-95. Science *269*, 1737–1740.

Köster, F., Schinke, B., Niemann, S., and Hermans-Borgmeyer, I. (1998). Identification of shyc, a novel gene expressed in the murine developing and adult nervous system. Neurosci. Lett. *252*, 69–71.

de Kovel, C.G.F., Trucks, H., Helbig, I., Mefford, H.C., Baker, C., Leu, C., Kluck, C., Muhle, H., von Spiczak, S., Ostertag, P., et al. (2010). Recurrent microdeletions at 15q11.2 and 16p13.11 predispose to idiopathic generalized epilepsies. Brain *133*, 23–32.

Kowalczyk, S., Winkelmann, A., Smolinsky, B., Förstera, B., Neundorf, I., Schwarz, G., and Meier, J.C. (2013). Direct binding of GABAA receptor β2 and β3 subunits to gephyrin. Eur. J. Neurosci. *37*, 544–554.

Kriebel, M., Metzger, J., Trinks, S., Chugh, D., Harvey, R.J., Harvey, K., and Volkmer, H. (2011). The cell adhesion molecule neurofascin stabilizes axo-axonic GABAergic terminals at the axon initial segment. J. Biol. Chem. *286*, 24385–24393.

Kristiansen, L. V, Beneyto, M., Haroutunian, V., and Meador-Woodruff, J.H. (2006). Changes in NMDA receptor subunits and interacting PSD proteins in dorsolateral prefrontal and anterior cingulate cortex indicate abnormal regional expression in schizophrenia. Mol. Psychiatry *11*, 737–747, 705.

Kroes, H.Y., van Zon, P.H. a, van de Putte, D.F., Nelen, M.R., Nievelstein, R.J., Wittebol-Post, D., van Nieuwenhuizen, O., Mancini, G.M.S., van der Knaap, M.S., Kwee, M.L., et al. (2008). DNA analysis of AHI1, NPHP1 and CYCLIN D1 in Joubert syndrome patients from the Netherlands. Eur. J. Med. Genet. *51*, 24–34.

Krueger, D.D., Tuffy, L.P., Papadopoulos, T., and Brose, N. (2012). The role of neurexins and neuroligins in the formation, maturation, and function of vertebrate synapses. Curr. Opin. Neurobiol. *22*, 412–422.

Kulkarni, V.A., and Firestein, B.L. (2012). The dendritic tree and brain disorders. Mol. Cell. Neurosci. *50*, 10–20.

Kullmann, D.M., Ruiz, A., Rusakov, D.M., Scott, R., Semyanov, A., and Walker, M.C. (2005). Presynaptic, extrasynaptic and axonal GABAA receptors in the CNS: where and why? Prog. Biophys. Mol. Biol. *87*, 33–46.

Kunda, P., Craig, G., Dominguez, V., and Baum, B. (2003). Abi, Sra1, and Kette control the stability and localization of SCAR/WAVE to regulate the formation of actin-based protrusions. Curr. Biol. *13*, 1867–1875.

Kushima, I., Nakamura, Y., Aleksic, B., Ikeda, M., Ito, Y., Shiino, T., Okochi, T., Fukuo, Y., Ujike, H., Suzuki, M., et al. (2012). Resequencing and association analysis of the

KALRN and EPHB1 genes and their contribution to schizophrenia susceptibility. Schizophr. Bull. *38*, 552–560.

Kvajo, M., McKellar, H., Drew, L.J., Lepagnol-Bestel, A.-M., Xiao, L., Levy, R.J., Blazeski, R., Arguello, P.A., Lacefield, C.O., Mason, C.A., et al. (2011). Altered axonal targeting and short-term plasticity in the hippocampus of Disc1 mutant mice. Proc. Natl. Acad. Sci. U. S. A. *108*, E1349–E1358.

Kwon, H.-B., and Sabatini, B.L. (2011). Glutamate induces de novo growth of functional spines in developing cortex. Nature *474*, 100–104.

Labonté, D., Thies, E., and Kneussel, M. (2014). The kinesin KIF21B participates in the cell surface delivery of γ2 subunit-containing GABAA receptors. Eur. J. Cell Biol. *93*, 338–346.

Lal, D., Ruppert, A.-K., Trucks, H., Schulz, H., de Kovel, C.G., Kasteleijn-Nolst Trenité, D., Sonsma, A.C.M., Koeleman, B.P., Lindhout, D., Weber, Y.G., et al. (2015). Burden analysis of rare microdeletions suggests a strong impact of neurodevelopmental genes in genetic generalised epilepsies. PLoS Genet. *11*, e1005226.

Lambrechts, A., Gevaert, K., Cossart, P., Vandekerckhove, J., and Van Troys, M. (2008). Listeria comet tails: the actin-based motility machinery at work. Trends Cell Biol. *18*, 220–227.

Lancaster, M. a, Louie, C.M., Silhavy, J.L., Sintasath, L., Decambre, M., Nigam, S.K., Willert, K., and Gleeson, J.G. (2009). Impaired Wnt-beta-catenin signaling disrupts adult renal homeostasis and leads to cystic kidney ciliopathy. Nat. Med. *15*, 1046–1054.

Lancaster, M.A., Gopal, D.J., Kim, J., Saleem, S.N., Silhavy, J.L., Louie, C.M., Thacker, B.E., Williams, Y., Zaki, M.S., and Gleeson, J.G. (2011a). Defective Wnt-dependent cerebellar midline fusion in a mouse model of Joubert syndrome. Nat. Med. *17*, 726–731.

Lancaster, M.A., Schroth, J., and Gleeson, J.G. (2011b). Subcellular spatial regulation of canonical Wnt signalling at the primary cilium. Nat. Cell Biol. *13*, 700–707.

Landis, D.M., and Reese, T.S. (1983). Cytoplasmic organization in cerebellar dendritic spines. J. Cell Biol. *97*, 1169–1178.

Leblond, C.S., Heinrich, J., Delorme, R., Proepper, C., Betancur, C., Huguet, G., Konyukh, M., Chaste, P., Ey, E., Rastam, M., et al. (2012). Genetic and functional analyses of SHANK2 mutations suggest a multiple hit model of autism spectrum disorders. PLoS Genet. *8*, e1002521.

Lee, J.A., and Lupski, J.R. (2006). Genomic rearrangements and gene copy-number alterations as a cause of nervous system disorders. Neuron *52*, 103–121.

Lee, J.H., and Gleeson, J.G. (2010). The role of primary cilia in neuronal function. Neurobiol. Dis. *38*, 167–172.

Lee, S.H., and Dominguez, R. (2010). Regulation of actin cytoskeleton dynamics in cells. Mol. Cells *29*, 311–325.

Lee, V., and Maguire, J. (2014). The impact of tonic GABAA receptor-mediated inhibition on neuronal excitability varies across brain region and cell type. Front. Neural Circuits *8*, 3.

Lee, K., Kim, Y., Lee, S.-J., Qiang, Y., Lee, D., Lee, H.W., Kim, H., Je, H.S., Südhof, T.C., and Ko, J. (2013). MDGAs interact selectively with neuroligin-2 but not other neuroligins to regulate inhibitory synapse development. Proc. Natl. Acad. Sci. U. S. A. *110*, 336–341.

Lee, T., Winter, C., Marticke, S.S., Lee, A., and Luo, L. (2000). Essential roles of Drosophila RhoA in the regulation of neuroblast proliferation and dendritic but not axonal morphogenesis. Neuron *25*, 307–316.

Lee, Y.L., Santé, J., Comerci, C.J., Cyge, B., Menezes, L.F., Li, F.-Q., Germino, G.G., Moerner, W.E., Takemaru, K.-I., and Stearns, T. (2014). Cby1 promotes Ahi1 recruitment to a ring-shaped domain at the centriole-cilium interface and facilitates proper cilium formation and function. Mol. Biol. Cell.

Lein, E.S., Hawrylycz, M.J., Ao, N., Ayres, M., Bensinger, A., Bernard, A., Boe, A.F., Boguski, M.S., Brockway, K.S., Byrnes, E.J., et al. (2007). Genome-wide atlas of gene expression in the adult mouse brain. Nature *445*, 168–176.

Lepagnol-Bestel, A.M., Kvajo, M., Karayiorgou, M., Simonneau, M., and Gogos, J.A. (2013). A Disc1 mutation differentially affects neurites and spines in hippocampal and cortical neurons. Mol. Cell. Neurosci. *54*, 84–92.

Leroux, M.R. (2007). Taking vesicular transport to the cilium. Cell *129*, 1041–1043.

Lévi, S., Grady, R.M., Henry, M.D., Campbell, K.P., Sanes, J.R., and Craig, A.M. (2002). Dystroglycan is selectively associated with inhibitory GABAergic synapses but is dispensable for their differentiation. J. Neurosci. *22*, 4274–4285.

Lévi, S., Logan, S.M., Tovar, K.R., and Craig, A.M. (2004). Gephyrin is critical for glycine receptor clustering but not for the formation of functional GABAergic synapses in hippocampal neurons. J. Neurosci. *24*, 207–217.

Levy, D., Ronemus, M., Yamrom, B., Lee, Y., Leotta, A., Kendall, J., Marks, S., Lakshmi, B., Pai, D., Ye, K., et al. (2011). Rare de novo and transmitted copy-number variation in autistic spectrum disorders. Neuron *70*, 886–897.

Lewis, D.A., and Lieberman, J.A. (2000). Catching up on schizophrenia: natural history and neurobiology. Neuron *28*, 325–334.

Li, X.J., and Li (2005). HAP1 and intracellular trafficking. Trends Pharmacol. Sci. *26*, 1–3.

Li, R.-W., Yu, W., Christie, S., Miralles, C.P., Bai, J., Loturco, J.J., and De Blas, A.L. (2005). Disruption of postsynaptic GABA receptor clusters leads to decreased

GABAergic innervation of pyramidal neurons. J. Neurochem. *95*, 756–770.

Li, S.H., Gutekunst, C.A., Hersch, S.M., and Li, X.J. (1998). Interaction of huntingtin-associated protein with dynactin P150Glued. J. Neurosci. *18*, 1261–1269.

Li, S.H., Li, H., Torre, E.R., and Li, X.J. (2000). Expression of huntingtin-associated protein-1 in neuronal cells implicates a role in neuritic growth. Mol. Cell. Neurosci. *16*, 168–183.

Li, X.J., Li, S.H., Sharp, A.H., Nucifora, F.C., Schilling, G., Lanahan, A., Worley, P., Snyder, S.H., and Ross, C.A. (1995). A huntingtin-associated protein enriched in brain with implications for pathology. Nature *378*, 398–402.

Li, Y., Chin, L.-S., Levey, A.I., and Li, L. (2002). Huntingtin-associated protein 1 interacts with hepatocyte growth factor-regulated tyrosine kinase substrate and functions in endosomal trafficking. J. Biol. Chem. *277*, 28212–28221.

Liang, J., Xu, W., Hsu, Y.-T., Yee, A.X., Chen, L., and Südhof, T.C. (2015). Conditional neuroligin-2 knockout in adult medial prefrontal cortex links chronic changes in synaptic inhibition to cognitive impairments. Mol. Psychiatry.

Liao, L., Park, S.K., Xu, T., Vanderklish, P., and Yates, J.R. (2008). Quantitative proteomic analysis of primary neurons reveals diverse changes in synaptic protein content in fmr1 knockout mice. Proc. Natl. Acad. Sci. U. S. A. *105*, 15281–15286.

Lim, E.T., Raychaudhuri, S., Sanders, S.J., Stevens, C., Sabo, A., MacArthur, D.G., Neale, B.M., Kirby, A., Ruderfer, D.M., Fromer, M., et al. (2013). Rare complete knockouts in humans: population distribution and significant role in autism spectrum disorders. Neuron *77*, 235–242.

von der Lippe, C., Rustad, C., Heimdal, K., and Rødningen, O.K. 15q11.2 microdeletion - seven new patients with delayed development and/or behavioural problems. Eur. J. Med. Genet. *54*, 357–360.

Liu, D., Bei, D., Parmar, H., and Matus, A. (2000). Activity-regulated, cytoskeleton-associated protein (Arc) is essential for visceral endoderm organization during early embryogenesis. Mech. Dev. *92*, 207–215.

Lotan, A., Lifschytz, T., Slonimsky, A., Broner, E.C., Greenbaum, L., Abedat, S., Fellig, Y., Cohen, H., Lory, O., Goelman, G., et al. (2013). Neural mechanisms underlying stress resilience in Ahi1 knockout mice: relevance to neuropsychiatric disorders. Mol. Psychiatry.

Lotan, A., Lifschytz, T., Lory, O., Goelman, G., and Lerer, B. (2014). Amygdalar disconnectivity could underlie stress resilience in the Ahi1 knockout mouse: conclusions from a resting-state functional MRI study. Mol. Psychiatry *19*, 144.

Louie, and Gleeson (2005). Genetic basis of Joubert syndrome and related disorders of cerebellar development. Hum. Mol. Genet. *14 Spec No*, R235–R242.

Louie, C.M., Caridi, G., Lopes, V.S., Brancati, F., Kispert, A., Lancaster, M.A.,

Schlossman, A.M., Otto, E.A., Leitges, M., Gröne, H.-J., et al. (2010). AHI1 is required for photoreceptor outer segment development and is a modifier for retinal degeneration in nephronophthisis. Nat. Genet. *42*, 175–180.

Lu, J., Karadsheh, M., and Delpire, E. (1999). Developmental regulation of the neuronal-specific isoform of K-Cl cotransporter KCC2 in postnatal rat brains. J. Neurobiol. *39*, 558–568.

Lu, J., Helton, T.D., Blanpied, T.A., Rácz, B., Newpher, T.M., Weinberg, R.J., and Ehlers, M.D. (2007). Postsynaptic positioning of endocytic zones and AMPA receptor cycling by physical coupling of dynamin-3 to Homer. Neuron *55*, 874–889.

Luikart, B.W., Schnell, E., Washburn, E.K., Bensen, A.L., Tovar, K.R., and Westbrook, G.L. (2011). Pten knockdown in vivo increases excitatory drive onto dentate granule cells. J. Neurosci. *31*, 4345–4354.

Luján, R., Roberts, J.D., Shigemoto, R., Ohishi, H., and Somogyi, P. (1997). Differential plasma membrane distribution of metabotropic glutamate receptors mGluR1 alpha, mGluR2 and mGluR5, relative to neurotransmitter release sites. J. Chem. Neuroanat. *13*, 219–241.

Luscher, Fuchs, and Kilpatrick (2011a). GABAA receptor trafficking-mediated plasticity of inhibitory synapses. Neuron *70*, 385–409.

Luscher, B., Shen, Q., and Sahir, N. (2011b). The GABAergic deficit hypothesis of major depressive disorder. Mol. Psychiatry *16*, 383–406.

Lüscher, C., and Huber, K.M. (2010). Group 1 mGluR-dependent synaptic long-term depression: mechanisms and implications for circuitry and disease. Neuron *65*, 445–459.

MacGillavry, H.D., Song, Y., Raghavachari, S., and Blanpied, T.A. (2013). Nanoscale scaffolding domains within the postsynaptic density concentrate synaptic AMPA receptors. Neuron *78*, 615–622.

Machesky, L.M., and Insall, R.H. Scar1 and the related Wiskott-Aldrich syndrome protein, WASP, regulate the actin cytoskeleton through the Arp2/3 complex. Curr. Biol. *8*, 1347–1356.

Machesky, L.M., Mullins, R.D., Higgs, H.N., Kaiser, D.A., Blanchoin, L., May, R.C., Hall, M.E., and Pollard, T.D. (1999). Scar, a WASp-related protein, activates nucleation of actin filaments by the Arp2/3 complex. Proc. Natl. Acad. Sci. U. S. A. *96*, 3739–3744.

Madrigal, I., Rodríguez-Revenga, L., Xunclà, M., and Milà, M. (2012). 15q11.2 microdeletion and FMR1 premutation in a family with intellectual disabilities and autism. Gene *508*, 92–95.

Makino, H., and Malinow, R. (2009). AMPA receptor incorporation into synapses during LTP: the role of lateral movement and exocytosis. Neuron *64*, 381–390.

Maletic-Savatic, M., Malinow, R., and Svoboda, K. (1999). Rapid dendritic morphogenesis in CA1 hippocampal dendrites induced by synaptic activity. Science *283*, 1923–1927.

Manolio, T.A., Collins, F.S., Cox, N.J., Goldstein, D.B., Hindorff, L.A., Hunter, D.J., McCarthy, M.I., Ramos, E.M., Cardon, L.R., Chakravarti, A., et al. (2009). Finding the missing heritability of complex diseases. Nature *461*, 747–753.

Mantamadiotis, T., Lemberger, T., Bleckmann, S.C., Kern, H., Kretz, O., Martin Villalba, A., Tronche, F., Kellendonk, C., Gau, D., Kapfhammer, J., et al. (2002). Disruption of CREB function in brain leads to neurodegeneration. Nat. Genet. *31*, 47–54.

Mao, L., Takamiya, K., Thomas, G., Lin, D.-T., and Huganir, R.L. (2010). GRIP1 and 2 regulate activity-dependent AMPA receptor recycling via exocyst complex interactions. Proc. Natl. Acad. Sci. U. S. A. *107*, 19038–19043.

Marchionni, I., Kasap, Z., Mozrzymas, J.W., Sieghart, W., Cherubini, E., and Zacchi, P. (2009). New insights on the role of gephyrin in regulating both phasic and tonic GABAergic inhibition in rat hippocampal neurons in culture. Neuroscience *164*, 552–562.

Maric, H.-M., Mukherjee, J., Tretter, V., Moss, S.J., and Schindelin, H. (2011). Gephyrin-mediated γ-aminobutyric acid type A and glycine receptor clustering relies on a common binding site. J. Biol. Chem. *286*, 42105–42114.

Marini, C., Cecconi, A., Contini, E., Pantaleo, M., Metitieri, T., Guarducci, S., Giglio, S., Guerrini, R., and Genuardi, M. (2013). Clinical and genetic study of a family with a paternally inherited 15q11-q13 duplication. Am. J. Med. Genet. A *161A*, 1459–1464.

Marshall, W.F. (2008). Basal bodies platforms for building cilia. Curr. Top. Dev. Biol. *85*, 1–22.

Martinez-Quiles, N., Rohatgi, R., Antón, I.M., Medina, M., Saville, S.P., Miki, H., Yamaguchi, H., Takenawa, T., Hartwig, J.H., Geha, R.S., et al. (2001). WIP regulates N-WASP-mediated actin polymerization and filopodium formation. Nat. Cell Biol. *3*, 484–491.

Matsuzaki, M. (2007). Factors critical for the plasticity of dendritic spines and memory storage. Neurosci. Res. *57*, 1–9.

McAllister, A.K., Lo, D.C., and Katz, L.C. (1995). Neurotrophins regulate dendritic growth in developing visual cortex. Neuron *15*, 791–803.

McAllister, A.K., Katz, L.C., and Lo, D.C. (1997). Opposing roles for endogenous BDNF and NT-3 in regulating cortical dendritic growth. Neuron *18*, 767–778.

McCarroll, S.A. (2008). Extending genome-wide association studies to copy-number variation. Hum. Mol. Genet. *17*, R135–R142.

McCarroll, S.A., Feng, G., and Hyman, S.E. (2014). Genome-scale neurogenetics:

methodology and meaning. Nat. Neurosci. *17*, 756–763.

McGuire, J.R., Rong, Li, and Li, X.J. (2006). Interaction of Huntingtin-associated protein-1 with kinesin light chain: implications in intracellular trafficking in neurons. J. Biol. Chem. *281*, 3552–3559.

Mellor, H. (2010). The role of formins in filopodia formation. Biochim. Biophys. Acta *1803*, 191–200.

Meng, J., Meng, Y., Hanna, A., Janus, C., and Jia, Z. (2005). Abnormal Long-Lasting Synaptic Plasticity and Cognition in Mice Lacking the Mental Retardation Gene Pak3. *25*, 6641–6650.

Meng, Y., Zhang, Y., Tregoubov, V., Janus, C., Cruz, L., Jackson, M., Lu, W.Y., MacDonald, J.F., Wang, J.Y., Falls, D.L., et al. (2002). Abnormal spine morphology and enhanced LTP in LIMK-1 knockout mice. Neuron *35*, 121–133.

Menna, E., Zambetti, S., Morini, R., Donzelli, A., Disanza, A., Calvigioni, D., Braida, D., Nicolini, C., Orlando, M., Fossati, G., et al. (2013). Eps8 controls dendritic spine density and synaptic plasticity through its actin-capping activity. EMBO J. *32*, 1730–1744.

Merikangas, A.K., Corvin, A.P., and Gallagher, L. (2009). Copy-number variants in neurodevelopmental disorders: promises and challenges. Trends Genet. *25*, 536–544.

Messaoudi, E., Kanhema, T., Soulé, J., Tiron, A., Dagyte, G., da Silva, B., and Bramham, C.R. (2007). Sustained Arc/Arg3.1 synthesis controls long-term potentiation consolidation through regulation of local actin polymerization in the dentate gyrus in vivo. J. Neurosci. *27*, 10445–10455.

Meyer, D.K., Olenik, C., Hofmann, F., Barth, H., Leemhuis, J., Brünig, I., Aktories, K., and Nörenberg, W. (2000). Regulation of somatodendritic GABAA receptor channels in rat hippocampal neurons: evidence for a role of the small GTPase Rac1. J. Neurosci. *20*, 6743–6751.

Meyer, G., Kirsch, J., Betz, H., and Langosch, D. (1995). Identification of a gephyrin binding motif on the glycine receptor beta subunit. Neuron *15*, 563–572.

Migaud, M., Charlesworth, P., Dempster, M., Webster, L.C., Watabe, A.M., Makhinson, M., He, Y., Ramsay, M.F., Morris, R.G., Morrison, J.H., et al. (1998). Enhanced long-term potentiation and impaired learning in mice with mutant postsynaptic density-95 protein. Nature *396*, 433–439.

Migeotte, I., Omelchenko, T., Hall, A., and Anderson, K. V (2010). Rac1-dependent collective cell migration is required for specification of the anterior-posterior body axis of the mouse. PLoS Biol. *8*, e1000442.

Miki, H., Miura, K., and Takenawa, T. (1996). N-WASP, a novel actin-depolymerizing protein, regulates the cortical cytoskeletal rearrangement in a PIP2-dependent manner downstream of tyrosine kinases. EMBO J. *15*, 5326–5335.

Miki, H., Suetsugu, S., and Takenawa, T. (1998). WAVE, a novel WASP-family protein involved in actin reorganization induced by Rac. EMBO J. *17*, 6932–6941.

Miller, P.S., and Aricescu, A.R. (2014). Crystal structure of a human GABAA receptor. Nature *512*, 270–275.

Minshew, N.J., and Keller, T.A. (2010). The nature of brain dysfunction in autism: functional brain imaging studies. Curr. Opin. Neurol. *23*, 124–130.

Möhler, H. (2006). GABA(A) receptor diversity and pharmacology. Cell Tissue Res. *326*, 505–516.

Molofsky, A. V, Krencik, R., Krenick, R., Ullian, E.M., Ullian, E., Tsai, H., Deneen, B., Richardson, W.D., Barres, B.A., and Rowitch, D.H. (2012). Astrocytes and disease: a neurodevelopmental perspective. Genes Dev. *26*, 891–907.

Montgomery, Zamorano, and Garner (2004). MAGUKs in synapse assembly and function: an emerging view. Cell. Mol. Life Sci. *61*, 911–929.

Moretti, P., and Zoghbi, H.Y. (2006). MeCP2 dysfunction in Rett syndrome and related disorders. Curr. Opin. Genet. Dev. *16*, 276–281.

Moritz, O.L., Tam, B.M., Hurd, L.L., Peränen, J., Deretic, D., and Papermaster, D.S. (2001). Mutant rab8 Impairs docking and fusion of rhodopsin-bearing post-Golgi membranes and causes cell death of transgenic Xenopus rods. Mol. Biol. Cell *12*, 2341–2351.

Moss, S.J., and Smart, T.G. (2001). Constructing inhibitory synapses. Nat. Rev. Neurosci. *2*, 240–250.

Muddashetty, R.S., Kelić, S., Gross, C., Xu, M., and Bassell, G.J. (2007). Dysregulated metabotropic glutamate receptor-dependent translation of AMPA receptor and postsynaptic density-95 mRNAs at synapses in a mouse model of fragile X syndrome. J. Neurosci. *27*, 5338–5348.

Muir, Arancibia-Carcamo, MacAskill, Smith, Griffin, and Kittler (2010). NMDA receptors regulate GABAA receptor lateral mobility and clustering at inhibitory synapses through serine 327 on the γ2 subunit. Proc. Natl. Acad. Sci. U. S. A. *107*, 16679–16684.

Murk, K., Wittenmayer, N., Michaelsen-Preusse, K., Dresbach, T., Schoenenberger, C.-A., Korte, M., Jockusch, B.M., and Rothkegel, M. (2012). Neuronal profilin isoforms are addressed by different signalling pathways. PLoS One *7*, e34167.

Nachury, M. V, Loktev, A. V, Zhang, Q., Westlake, C.J., Peränen, J., Merdes, A., Slusarski, D.C., Scheller, R.H., Bazan, J.F., Sheffield, V.C., et al. (2007). A core complex of BBS proteins cooperates with the GTPase Rab8 to promote ciliary membrane biogenesis. Cell *129*, 1201–1213.

Nair, D., Hosy, E., Petersen, J.D., Constals, A., Giannone, G., Choquet, D., and Sibarita, J.-B. (2013). Super-resolution imaging reveals that AMPA receptors inside

synapses are dynamically organized in nanodomains regulated by PSD95. J. Neurosci. *33*, 13204–13224.

Nakajima, K., Yin, X., Takei, Y., Seog, D.-H., Homma, N., and Hirokawa, N. (2012). Molecular Motor KIF5A Is Essential for GABAA Receptor Transport, and KIF5A Deletion Causes Epilepsy. Neuron *76*, 945–961.

Nakamura, Wood, Patton, Jaafari, Henley, Mellor, and Hanley (2011). PICK1 inhibition of the Arp2/3 complex controls dendritic spine size and synaptic plasticity. EMBO J. *30*, 719–730.

Nakayama, A.Y., Harms, M.B., and Luo, L. (2000). Small GTPases Rac and Rho in the maintenance of dendritic spines and branches in hippocampal pyramidal neurons. J. Neurosci. *20*, 5329–5338.

Napoli, I., Mercaldo, V., Boyl, P.P., Eleuteri, B., Zalfa, F., De Rubeis, S., Di Marino, D., Mohr, E., Massimi, M., Falconi, M., et al. (2008). The fragile X syndrome protein represses activity-dependent translation through CYFIP1, a new 4E-BP. Cell *134*, 1042–1054.

Nechipurenko, I. V, Doroquez, D.B., and Sengupta, P. (2013). Primary cilia and dendritic spines: different but similar signaling compartments. Mol. Cells *36*, 288–303.

Neer, E.J., Schmidt, C.J., Nambudripad, R., and Smith, T.F. (1994). The ancient regulatory-protein family of WD-repeat proteins. Nature *371*, 297–300.

Negishi, and Katoh (2005). Rho family GTPases and dendrite plasticity. Neuroscientist *11*, 187–191.

Newey, S.E., Velamoor, V., Govek, E., and Aelst, L. Van (2004). Rho GTPases , Dendritic Structure , and Mental Retardation. 58–74.

Ng, E.L., and Tang, B.L. (2008). Rab GTPases and their roles in brain neurons and glia. Brain Res. Rev. *58*, 236–246.

Ng, J., Nardine, T., Harms, M., Tzu, J., Goldstein, A., Sun, Y., Dietzl, G., Dickson, B.J., and Luo, L. (2002). Rac GTPases control axon growth, guidance and branching. Nature *416*, 442–447.

Niell, C.M., Meyer, M.P., and Smith, S.J. (2004). In vivo imaging of synapse formation on a growing dendritic arbor. Nat. Neurosci. *7*, 254–260.

Nishimura, Y., Martin, C.L., Vazquez-Lopez, A., Spence, S.J., Alvarez-Retuerto, A.I., Sigman, M., Steindler, C., Pellegrini, S., Schanen, N.C., Warren, S.T., et al. (2007). Genome-wide expression profiling of lymphoblastoid cell lines distinguishes different forms of autism and reveals shared pathways. Hum. Mol. Genet. *16*, 1682–1698.

Niu, Huang, Wang, Rao, Kong, Xu, Li, Yang, and Sheng (2011). Brainstem Hap1-Ahi1 is involved in insulin-mediated feeding control. FEBS Lett. *585*, 85–91.

Niu, S., Wang, H., Huang, Z., Rao, X., Cai, X., Liang, T., Xu, J., Xu, X., and Sheng, G.

(2012). Expression changes of hypothalamic Ahi1 in mice brain: implication in sensing insulin signaling. Mol. Biol. Rep. *39*, 9697–9705.

Nusser, Z., Sieghart, W., Benke, D., Fritschy, J.M., and Somogyi, P. (1996). Differential synaptic localization of two major gamma-aminobutyric acid type A receptor alpha subunits on hippocampal pyramidal cells. Proc. Natl. Acad. Sci. U. S. A. *93*, 11939–11944.

Oguro-Ando, a, Rosensweig, C., Herman, E., Nishimura, Y., Werling, D., Bill, B.R., Berg, J.M., Gao, F., Coppola, G., Abrahams, B.S., et al. (2014). Increased CYFIP1 dosage alters cellular and dendritic morphology and dysregulates mTOR. Mol. Psychiatry.

Oh, W.C., Hill, T.C., and Zito, K. (2013). Synapse-specific and size-dependent mechanisms of spine structural plasticity accompanying synaptic weakening. Proc. Natl. Acad. Sci. U. S. A. *110*, E305–E312.

Olsen, R.W., and Sieghart, W. (2008). International Union of Pharmacology. LXX. Subtypes of gamma-aminobutyric acid(A) receptors: classification on the basis of subunit composition, pharmacology, and function. Update. Pharmacol. Rev. *60*, 243–260.

Ozonoff, S., Williams, B.J., Gale, S., and Miller, J.N. (1999). Autism and autistic behavior in Joubert syndrome. J. Child Neurol. *14*, 636–641.

Padrick, S.B., and Rosen, M.K. (2010). Physical mechanisms of signal integration by WASP family proteins. Annu. Rev. Biochem. *79*, 707–735.

Paluszkiewicz, S.M., Martin, B.S., and Huntsman, M.M. (2011). Fragile X syndrome: the GABAergic system and circuit dysfunction. Dev. Neurosci. *33*, 349–364.

Papadopoulos, T., and Soykan, T. (2011). The role of collybistin in gephyrin clustering at inhibitory synapses: facts and open questions. Front. Cell. Neurosci. *5*, 11.

Papadopoulos, T., Korte, M., Eulenburg, V., Kubota, H., Retiounskaia, M., Harvey, R.J., Harvey, K., O'Sullivan, G.A., Laube, B., Hülsmann, S., et al. (2007). Impaired GABAergic transmission and altered hippocampal synaptic plasticity in collybistin-deficient mice. EMBO J. *26*, 3888–3899.

Papadopoulos, T., Eulenburg, V., Reddy-Alla, S., Mansuy, I.M., Li, Y., and Betz, H. (2008). Collybistin is required for both the formation and maintenance of GABAergic postsynapses in the hippocampus. Mol. Cell. Neurosci. *39*, 161–169.

Papadopoulos, T., Schemm, R., Grubmüller, H., and Brose, N. (2015). Lipid binding defects and perturbed synaptogenic activity of a Collybistin R290H mutant that causes epilepsy and intellectual disability. J. Biol. Chem. *290*, 8256–8270.

Park, M., Salgado, J.M., Ostroff, L., Helton, T.D., Robinson, C.G., Harris, K.M., and Ehlers, M.D. (2006). Plasticity-induced growth of dendritic spines by exocytic trafficking from recycling endosomes. Neuron *52*, 817–830.

Parrish, J.Z., Emoto, K., Kim, M.D., and Jan, Y.N. (2007). Mechanisms that regulate establishment, maintenance, and remodeling of dendritic fields. Annu. Rev. Neurosci. *30*, 399–423.

Patapoutian, A., and Reichardt, L.F. (2001). Trk receptors: mediators of neurotrophin action. Curr. Opin. Neurobiol. *11*, 272–280.

Patrizi, A., Viltono, L., Frola, E., Harvey, K., Harvey, R.J., and Sassoè-Pognetto, M. (2012). Selective localization of collybistin at a subset of inhibitory synapses in brain circuits. J. Comp. Neurol. *520*, 130–141.

Peça, J., Feliciano, C., Ting, J.T., Wang, W., Wells, M.F., Venkatraman, T.N., Lascola, C.D., Fu, Z., and Feng, G. (2011). Shank3 mutant mice display autistic-like behaviours and striatal dysfunction. Nature *472*, 437–442.

Peden, D.R., Petitjean, C.M., Herd, M.B., Durakoglugil, M.S., Rosahl, T.W., Wafford, K., Homanics, G.E., Belelli, D., Fritschy, J.-M., and Lambert, J.J. (2008). Developmental maturation of synaptic and extrasynaptic GABAA receptors in mouse thalamic ventrobasal neurones. J. Physiol. *586*, 965–987.

Peñagarikano, O., Abrahams, B.S., Herman, E.I., Winden, K.D., Gdalyahu, A., Dong, H., Sonnenblick, L.I., Gruver, R., Almajano, J., Bragin, A., et al. (2011). Absence of CNTNAP2 leads to epilepsy, neuronal migration abnormalities, and core autism-related deficits. Cell *147*, 235–246.

Peng, J., Kim, M.J., Cheng, D., Duong, D.M., Gygi, S.P., and Sheng, M. (2004). Semiquantitative proteomic analysis of rat forebrain postsynaptic density fractions by mass spectrometry. J. Biol. Chem. *279*, 21003–21011.

Penzes, P., and Jones, K.A. (2008). Dendritic spine dynamics--a key role for kalirin-7. Trends Neurosci. *31*, 419–427.

Penzes, Cahill, Jones, Vanleeuwen, and Woolfrey (2011). Dendritic spine pathology in neuropsychiatric disorders. Nat. Neurosci. *14*, 285–293.

Penzes, P., Johnson, R.C., Sattler, R., Zhang, X., Huganir, R.L., Kambampati, V., Mains, R.E., and Eipper, B.A. (2001). The neuronal Rho-GEF Kalirin-7 interacts with PDZ domain-containing proteins and regulates dendritic morphogenesis. Neuron *29*, 229–242.

Perrais, D., and Ropert, N. (1999). Effect of zolpidem on miniature IPSCs and occupancy of postsynaptic GABAA receptors in central synapses. J. Neurosci. *19*, 578–588.

Petrini, E.M., and Barberis, A. (2014). Diffusion dynamics of synaptic molecules during inhibitory postsynaptic plasticity. Front. Cell. Neurosci. *8*, 300.

Peykov, S., Berkel, S., Schoen, M., Weiss, K., Degenhardt, F., Strohmaier, J., Weiss, B., Proepper, C., Schratt, G., Nöthen, M.M., et al. (2015). Identification and functional characterization of rare SHANK2 variants in schizophrenia. Mol. Psychiatry.

Pfeiffer, F., Graham, D., and Betz, H. (1982). Purification by affinity chromatography of the glycine receptor of rat spinal cord. J. Biol. Chem. *257*, 9389–9393.

Pilpel, and Segal (2005). Rapid WAVE dynamics in dendritic spines of cultured hippocampal neurons is mediated by actin polymerization. J. Neurochem. *95*, 1401–1410.

Pinto, D., Pagnamenta, A.T., Klei, L., Anney, R., Merico, D., Regan, R., Conroy, J., Magalhaes, T.R., Correia, C., Abrahams, B.S., et al. (2010). Functional impact of global rare copy number variation in autism spectrum disorders. Nature *466*, 368–372.

Pittman, A.J., Gaynes, J.A., and Chien, C.-B. (2010). nev (cyfip2) is required for retinal lamination and axon guidance in the zebrafish retinotectal system. Dev. Biol. *344*, 784–794.

Pizzarelli, R., and Cherubini, E. (2011). Alterations of GABAergic signaling in autism spectrum disorders. Neural Plast. *2011*, 297153.

Plath, N., Ohana, O., Dammermann, B., Errington, M.L., Schmitz, D., Gross, C., Mao, X., Engelsberg, A., Mahlke, C., Welzl, H., et al. (2006). Arc/Arg3.1 is essential for the consolidation of synaptic plasticity and memories. Neuron *52*, 437–444.

Poirier, Y., Kozak, C., and Jolicoeur, P. (1988). Identification of a common helper provirus integration site in Abelson murine leukemia virus-induced lymphoma DNA. J. Virol. *62*, 3985–3992.

Pollard, T.D. (1986). Rate constants for the reactions of ATP- and ADP-actin with the ends of actin filaments. J. Cell Biol. *103*, 2747–2754.

Pollard, T.D. (2007). Regulation of actin filament assembly by Arp2/3 complex and formins. Annu. Rev. Biophys. Biomol. Struct. *36*, 451–477.

Pollard, T.D., and Cooper, J.A. (2009). Actin, a central player in cell shape and movement. Science *326*, 1208–1212.

Pollitt, A.Y., and Insall, R.H. (2009). WASP and SCAR/WAVE proteins: the drivers of actin assembly. J. Cell Sci. *122*, 2575–2578.

Pontrello, C.G., Sun, M.-Y., Lin, A., Fiacco, T.A., DeFea, K.A., and Ethell, I.M. (2012). Cofilin under control of β-arrestin-2 in NMDA-dependent dendritic spine plasticity, long-term depression (LTD), and learning. Proc. Natl. Acad. Sci. U. S. A. *109*, E442–E451.

Poulopoulos, A., Aramuni, G., Meyer, G., Soykan, T., Hoon, M., Papadopoulos, T., Zhang, M., Paarmann, I., Fuchs, C., Harvey, K., et al. (2009). Neuroligin 2 drives postsynaptic assembly at perisomatic inhibitory synapses through gephyrin and collybistin. Neuron *63*, 628–642.

Poulopoulos, A., Soykan, T., Tuffy, L.P., Hammer, M., Varoqueaux, F., and Brose, N. (2012). Homodimerization and isoform-specific heterodimerization of neuroligins.

Biochem. J. *446*, 321–330.

Pruitt, K.D., Brown, G.R., Hiatt, S.M., Thibaud-Nissen, F., Astashyn, A., Ermolaeva, O., Farrell, C.M., Hart, J., Landrum, M.J., McGarvey, K.M., et al. (2014). RefSeq: an update on mammalian reference sequences. Nucleic Acids Res. *42*, D756–D763.

Puram, S. V, and Bonni, A. (2013). Cell-intrinsic drivers of dendrite morphogenesis. Development *140*, 4657–4671.

Purcell, S.M., Moran, J.L., Fromer, M., Ruderfer, D., Solovieff, N., Roussos, P., O'Dushlaine, C., Chambert, K., Bergen, S.E., Kähler, A., et al. (2014). A polygenic burden of rare disruptive mutations in schizophrenia. Nature *506*, 185–190.

Purpura, D.P. (1974). Dendritic spine "dysgenesis" and menPurpura, D.P. (1974). Dendritic spine "dysgenesis" and mental retardation. Science (New York, N.Y.) 186, 1126–1128.tal retardation. Science *186*, 1126–1128.

Radyushkin, K., Hammerschmidt, K., Boretius, S., Varoqueaux, F., El-Kordi, A., Ronnenberg, A., Winter, D., Frahm, J., Fischer, J., Brose, N., et al. (2009). Neuroligin-3-deficient mice: model of a monogenic heritable form of autism with an olfactory deficit. Genes. Brain. Behav. *8*, 416–425.

Rakeman, A.S., and Anderson, K. V (2006). Axis specification and morphogenesis in the mouse embryo require Nap1, a regulator of WAVE-mediated actin branching. Development *133*, 3075–3083.

Ramón y Cajal, S. (1888). Estructura de los centros nerviosos de las aves. Rev. Trim. Histol. Norm. Pat. *1*, 1–10.

Ray, M.T., Shannon Weickert, C., and Webster, M.J. (2014). Decreased BDNF and TrkB mRNA expression in multiple cortical areas of patients with schizophrenia and mood disorders. Transl. Psychiatry *4*, e389.

Raymond, G. V, Bauman, M.L., and Kemper, T.L. (1996). Hippocampus in autism: a Golgi analysis. Acta Neuropathol. *91*, 117–119.

Reiter, J.F., Blacque, O.E., and Leroux, M.R. (2012). The base of the cilium: roles for transition fibres and the transition zone in ciliary formation, maintenance and compartmentalization. EMBO Rep. *13*, 608–618.

Ren, L., Qian, X., Zhai, L., Sun, M., Miao, Z., Li, J., and Xu, X. (2014). Loss of Ahi1 impairs neurotransmitter release and causes depressive behaviors in mice. PLoS One *9*, e93640.

Retuerto, A., Cantor, Gleeson, Ustaszewska, Schackwitz, Pennacchio, and Geschwind (2008). Association of common variants in the Joubert syndrome gene (AHI1) with autism. Hum. Mol. Genet. *17*, 3887–3896.

Ribeiro, S., Napoli, I., White, I.J., Parrinello, S., Flanagan, A.M., Suter, U., Parada, L.F., and Lloyd, A.C. (2013). Injury signals cooperate with Nf1 loss to relieve the tumor-suppressive environment of adult peripheral nerve. Cell Rep. *5*, 126–136.

Ridley, A.J., Paterson, H.F., Johnston, C.L., Diekmann, D., and Hall, A. (1992). The small GTP-binding protein rac regulates growth factor-induced membrane ruffling. Cell *70*, 401–410.

Ripke, S., Neale, B.M., Corvin, A., Walters, J.T.R., Farh, K.-H., Holmans, P.A., Lee, P., Bulik-Sullivan, B., Collier, D.A., Huang, H., et al. (2014). Biological insights from 108 schizophrenia-associated genetic loci. Nature *511*, 421–427.

Rivero, O., Reif, A., Sanjuán, J., Moltó, M.D., Kittel-Schneider, S., Nájera, C., Töpner, T., and Lesch, K.-P. (2010). Impact of the AHI1 gene on the vulnerability to schizophrenia: a case-control association study. PLoS One *5*, e12254.

Roberts, E., and Frankel, S. (1950). gamma-Aminobutyric acid in brain: its formation from glutamic acid. J. Biol. Chem. *187*, 55–63.

Rocca, Martin, Jenkins, and Hanley (2008). Inhibition of Arp2/3-mediated actin polymerization by PICK1 regulates neuronal morphology and AMPA receptor endocytosis. Nat. Cell Biol. *10*, 259–271.

Rocca, D.L., Amici, M., Antoniou, A., Suarez, E.B., Halemani, N., Murk, K., McGarvey, J., Jaafari, N., Mellor, J.R., Collingridge, G.L., et al. (2013). The small GTPase Arf1 modulates Arp2/3-mediated actin polymerization via PICK1 to regulate synaptic plasticity. Neuron *79*, 293–307.

Roche, K.W., Standley, S., McCallum, J., Dune Ly, C., Ehlers, M.D., and Wenthold, R.J. (2001). Molecular determinants of NMDA receptor internalization. Nat. Neurosci. *4*, 794–802.

Rong, Li, and Li, X.J. (2007a). Regulation of intracellular HAP1 trafficking. J. Neurosci. Res. *85*, 3025–3029.

Rong, J., McGuire, J.R., Fang, Z.-H., Sheng, G., Shin, J.-Y., Li, S.-H., and Li, X.-J. (2006). Regulation of intracellular trafficking of huntingtin-associated protein-1 is critical for TrkA protein levels and neurite outgrowth. J. Neurosci. *26*, 6019–6030.

Rong, J., Li, S., Sheng, G., Wu, M., Coblitz, B., Li, M., Fu, H., and Li, X.-J. (2007b). 14-3-3 protein interacts with Huntingtin-associated protein 1 and regulates its trafficking. J. Biol. Chem. *282*, 4748–4756.

Rossman, K.L., Der, C.J., and Sondek, J. (2005). GEF means go: turning on RHO GTPases with guanine nucleotide-exchange factors. Nat. Rev. Mol. Cell Biol. *6*, 167–180.

Roussignol, G., Ango, F., Romorini, S., Tu, J.C., Sala, C., Worley, P.F., Bockaert, J., and Fagni, L. (2005). Shank expression is sufficient to induce functional dendritic spine synapses in aspiny neurons. J. Neurosci. *25*, 3560–3570.

Rubeis, D., and Bagni (2011). Regulation of molecular pathways in the Fragile X Syndrome: insights into Autism Spectrum Disorders. J. Neurodev. Disord. *3*, 257–269.

De Rubeis, S., and Buxbaum, J.D. (2015). Recent advances in the genetics of autism spectrum disorder. Curr. Neurol. Neurosci. Rep. *15*, 36.

De Rubeis, S., Pasciuto, E., Li, K.W., Fernández, E., Di Marino, D., Buzzi, A., Ostroff, L.E., Klann, E., Zwartkruis, F.J.T., Komiyama, N.H., et al. (2013). CYFIP1 coordinates mRNA translation and cytoskeleton remodeling to ensure proper dendritic spine formation. Neuron *79*, 1169–1182.

Rudelli, R.D., Brown, W.T., Wisniewski, K., Jenkins, E.C., Laure-Kamionowska, M., Connell, F., and Wisniewski, H.M. (1985). Adult fragile X syndrome. Clinico-neuropathologic findings. Acta Neuropathol. *67*, 289–295.

Ruiz, S., Birbaumer, N., and Sitaram, R. (2013). Abnormal Neural Connectivity in Schizophrenia and fMRI-Brain-Computer Interface as a Potential Therapeutic Approach. Front. Psychiatry *4*, 17.

Rust, M.B., Gurniak, C.B., Renner, M., Vara, H., Morando, L., Görlich, A., Sassoè-Pognetto, M., Banchaabouchi, M. Al, Giustetto, M., Triller, A., et al. (2010). Learning, AMPA receptor mobility and synaptic plasticity depend on n-cofilin-mediated actin dynamics. EMBO J. *29*, 1889–1902.

Saiepour, L., Fuchs, C., Patrizi, A., Sassoè-Pognetto, M., Harvey, R.J., and Harvey, K. (2010). Complex role of collybistin and gephyrin in GABAA receptor clustering. J. Biol. Chem. *285*, 29623–29631.

Sala, C., and Segal, M. (2014). Dendritic spines: the locus of structural and functional plasticity. Physiol. Rev. *94*, 141–188.

Sala, C., Piëch, V., Wilson, N.R., Passafaro, M., Liu, G., and Sheng, M. (2001). Regulation of dendritic spine morphology and synaptic function by Shank and Homer. Neuron *31*, 115–130.

Saller, E., Tom, E., Brunori, M., Otter, M., Estreicher, A., Mack, D.H., and Iggo, R. (1999). Increased apoptosis induction by 121F mutant p53. EMBO J. *18*, 4424–4437.

Sander, B., Tria, G., Shkumatov, A. V, Kim, E.-Y., Grossmann, J.G., Tessmer, I., Svergun, D.I., and Schindelin, H. (2013). Structural characterization of gephyrin by AFM and SAXS reveals a mixture of compact and extended states. Acta Crystallogr. D. Biol. Crystallogr. *69*, 2050–2060.

Sans, N., Vissel, B., Petralia, R.S., Wang, Y.-X., Chang, K., Royle, G.A., Wang, C.-Y., O'Gorman, S., Heinemann, S.F., and Wenthold, R.J. (2003). Aberrant formation of glutamate receptor complexes in hippocampal neurons of mice lacking the GluR2 AMPA receptor subunit. J. Neurosci. *23*, 9367–9373.

Sarmiere, P.D., and Bamburg, J.R. (2004). Regulation of the neuronal actin cytoskeleton by ADF/cofilin. J. Neurobiol. *58*, 103–117.

Sato, D., Lionel, A.C., Leblond, C.S., Prasad, A., Pinto, D., Walker, S., O'Connor, I., Russell, C., Drmic, I.E., Hamdan, F.F., et al. (2012). SHANK1 Deletions in Males with Autism Spectrum Disorder. Am. J. Hum. Genet. *90*, 879–887.

Scheiffele, P., Fan, J., Choih, J., Fetter, R., and Serafini, T. (2000). Neuroligin expressed in nonneuronal cells triggers presynaptic development in contacting axons. Cell *101*, 657–669.

Schenck, A., Bardoni, B., Moro, A., Bagni, C., and Mandel, J.L. (2001). A highly conserved protein family interacting with the fragile X mental retardation protein (FMRP) and displaying selective interactions with FMRP-related proteins FXR1P and FXR2P. Proc. Natl. Acad. Sci. U. S. A. *98*, 8844–8849.

Schenck, A., Bardoni, B., Langmann, C., Harden, N., Mandel, J.L., and Giangrande, A. (2003). CYFIP/Sra-1 controls neuronal connectivity in Drosophila and links the Rac1 GTPase pathway to the fragile X protein. Neuron *38*, 887–898.

Schenck, A., Qurashi, A., Carrera, P., Bardoni, B., Diebold, C., Schejter, E., Mandel, J.-L., and Giangrande, A. (2004). WAVE/SCAR, a multifunctional complex coordinating different aspects of neuronal connectivity. Dev. Biol. *274*, 260–270.

Schmeisser, M.J., Ey, E., Wegener, S., Bockmann, J., Stempel, a V., Kuebler, A., Janssen, A.-L., Udvardi, P.T., Shiban, E., Spilker, C., et al. (2012). Autistic-like behaviours and hyperactivity in mice lacking ProSAP1/Shank2. Nature *486*, 256–260.

Schork, N.J., Murray, S.S., Frazer, K.A., and Topol, E.J. (2009). Common vs. rare allele hypotheses for complex diseases. Curr. Opin. Genet. Dev. *19*, 212–219.

Schumann, C.M., Hamstra, J., Goodlin-Jones, B.L., Lotspeich, L.J., Kwon, H., Buonocore, M.H., Lammers, C.R., Reiss, A.L., and Amaral, D.G. (2004). The amygdala is enlarged in children but not adolescents with autism; the hippocampus is enlarged at all ages. J. Neurosci. *24*, 6392–6401.

Scott, Reuter, and Luo (2003). Small GTPase Cdc42 is required for multiple aspects of dendritic morphogenesis. J. Neurosci. *23*, 3118–3123.

Sebat, J., Lakshmi, B., Malhotra, D., Troge, J., Lese-Martin, C., Walsh, T., Yamrom, B., Yoon, S., Krasnitz, A., Kendall, J., et al. (2007). Strong association of de novo copy number mutations with autism. Science *316*, 445–449.

Selemon, L.D., Rajkowska, G., and Goldman-Rakic, P.S. (1995). Abnormally high neuronal density in the schizophrenic cortex. A morphometric analysis of prefrontal area 9 and occipital area 17. Arch. Gen. Psychiatry *52*, 805–818; discussion 819–820.

Setou, M., Seog, D.-H., Tanaka, Y., Kanai, Y., Takei, Y., Kawagishi, M., and Hirokawa, N. (2002). Glutamate-receptor-interacting protein GRIP1 directly steers kinesin to dendrites. Nature *417*, 83–87.

Shen, K., and Scheiffele, P. (2010). Genetics and cell biology of building specific synaptic connectivity. Annu. Rev. Neurosci. *33*, 473–507.

Sheng, M., and Kim, E. (2011). The postsynaptic organization of synapses. Cold Spring Harb. Perspect. Biol. *3*.

Sheng, Xu, Lin, Wang, Rong, Cheng, Peng, Jiang, and Li (2008). Huntingtin-associated protein 1 interacts with Ahi1 to regulate cerebellar and brainstem development in mice. J. Clin. Invest. *118*, 2785–2795.

Shepherd, J.D., and Huganir, R.L. (2007). The cell biology of synaptic plasticity: AMPA receptor trafficking. Annu. Rev. Cell Dev. Biol. *23*, 613–643.

Shi, Z., Liang, N., Xu, W., Li, K., Sheng, G., Liu, J., Xu, A., Li, X.J., and Wu, D. (2009). Expression, purification, crystallization and preliminary X-ray crystallographic analysis of the SH3 domain of human AHI1. Acta Crystallogr. Sect. F. Struct. Biol. Cryst. Commun. *65*, 361–363.

Shishido, E., Aleksic, B., and Ozaki, N. (2014). Copy-number variation in the pathogenesis of autism spectrum disorder. Psychiatry Clin. Neurosci. *68*, 85–95.

Sholl, D.A. (1953). Dendritic organization in the neurons of the visual and motor cortices of the cat. J. Anat. *87*, 387–406.

Siddiqui, T.J., and Craig, A.M. (2011). Synaptic organizing complexes. Curr. Opin. Neurobiol. *21*, 132–143.

Siekevitz, P. (1985). The postsynaptic density: a possible role in long-lasting effects in the central nervous system. Proc. Natl. Acad. Sci. U. S. A. *82*, 3494–3498.

Silva, J.M., Ezhkova, E., Silva, J., Heart, S., Castillo, M., Campos, Y., Castro, V., Bonilla, F., Cordon-Cardo, C., Muthuswamy, S.K., et al. (2009). Cyfip1 Is a Putative Invasion Suppressor in Epithelial Cancers. Cell *137*, 1047–1061.

Simms, Hynes, Eley, Inglis, Chaudhry, Dawe, and Sayer (2011). Modelling a ciliopathy: Ahi1 knockdown in model systems reveals an essential role in brain, retinal, and renal development. Cell. Mol. Life Sci.

Skarnes, W.C., Rosen, B., West, A.P., Koutsourakis, M., Bushell, W., Iyer, V., Mujica, A.O., Thomas, M., Harrow, J., Cox, T., et al. (2011). A conditional knockout resource for the genome-wide study of mouse gene function. Nature *474*, 337–342.

Sloan, S.A., and Barres, B.A. (2014). Mechanisms of astrocyte development and their contributions to neurodevelopmental disorders. Curr. Opin. Neurobiol. *27*, 75–81.

Slonimsky, A., Levy, I., Kohn, Y., Rigbi, A., Ben-Asher, E., Lancet, D., Agam, G., and Lerer, B. (2010). Lymphoblast and brain expression of AHI1 and the novel primate-specific gene, C6orf217, in schizophrenia and bipolar disorder. Schizophr. Res. *120*, 159–166.

Smart, T.G., and Paoletti, P. (2012). Synaptic neurotransmitter-gated receptors. Cold Spring Harb. Perspect. Biol. *4*.

Smith, and Kittler (2010). The cell biology of synaptic inhibition in health and disease. Curr. Opin. Neurobiol. *20*, 550–556.

Smith, K., Muir, J., Rao, Y., Browarski, M., Gruenig, M., Sheehan, D., Haucke, V., and Kittler, J. (2012). Stabilization of GABAA Receptors at Endocytic Zones Is Mediated

by an AP2 Binding Motif within the GABAA Receptor 3 Subunit. J. Neurosci. *32*, 2485–2498.

Smith, K.R., Davenport, E.C., Wei, J., Li, X., Pathania, M., Vaccaro, V., Yan, Z., and Kittler, J.T. (2014). GIT1 and βPIX Are Essential for GABAA Receptor Synaptic Stability and Inhibitory Neurotransmission. Cell Rep. *9*, 298–310.

Snapper, S.B., Takeshima, F., Antón, I., Liu, C.H., Thomas, S.M., Nguyen, D., Dudley, D., Fraser, H., Purich, D., Lopez-Ilasaca, M., et al. (2001). N-WASP deficiency reveals distinct pathways for cell surface projections and microbial actin-based motility. Nat. Cell Biol. *3*, 897–904.

Soderling, S.H., Guire, E.S., Kaech, S., White, J., Zhang, F., Schutz, K., Langeberg, L.K., Banker, G., Raber, J., and Scott, J.D. (2007). A WAVE-1 and WRP signaling complex regulates spine density, synaptic plasticity, and memory. J. Neurosci. *27*, 355–365.

Soltau, M., Berhörster, K., Kindler, S., Buck, F., Richter, D., and Kreienkamp, H.-J. (2004). Insulin receptor substrate of 53 kDa links postsynaptic shank to PSD-95. J. Neurochem. *90*, 659–665.

Sommer, B., Köhler, M., Sprengel, R., and Seeburg, P.H. (1991). RNA editing in brain controls a determinant of ion flow in glutamate-gated channels. Cell *67*, 11–19.

Specht, C.G., Izeddin, I., Rodriguez, P.C., El Beheiry, M., Rostaing, P., Darzacq, X., Dahan, M., and Triller, A. (2013). Quantitative nanoscopy of inhibitory synapses: counting gephyrin molecules and receptor binding sites. Neuron *79*, 308–321.

Spruston, N. (2008). Pyramidal neurons: dendritic structure and synaptic integration. Nat. Rev. Neurosci. *9*, 206–221.

Srivastava, D.P., Woolfrey, K.M., Jones, K.A., Anderson, C.T., Smith, K.R., Russell, T.A., Lee, H., Yasvoina, M. V, Wokosin, D.L., Ozdinler, P.H., et al. (2012). An autism-associated variant of Epac2 reveals a role for Ras/Epac2 signaling in controlling basal dendrite maintenance in mice. PLoS Biol. *10*, e1001350.

St Clair, D., Blackwood, D., Muir, W., Carothers, A., Walker, M., Spowart, G., Gosden, C., and Evans, H.J. (1990). Association within a family of a balanced autosomal translocation with major mental illness. Lancet *336*, 13–16.

Stamatakou, E., Marzo, A., Gibb, A., and Salinas, P.C. (2013). Activity-dependent spine morphogenesis: a role for the actin-capping protein eps8. J. Neurosci. *33*, 2661–2670.

Star, E.N., Kwiatkowski, D.J., and Murthy, V.N. (2002). Rapid turnover of actin in dendritic spines and its regulation by activity. Nat. Neurosci. *5*, 239–246.

Stefansson, H., Rujescu, D., Cichon, S., Pietiläinen, O.P.H., Ingason, A., Steinberg, S., Fossdal, R., Sigurdsson, E., Sigmundsson, T., Buizer-Voskamp, J.E., et al. (2008). Large recurrent microdeletions associated with schizophrenia. Nature *455*, 232–236.

Stefansson, H., Meyer-Lindenberg, A., Steinberg, S., Magnusdottir, B., Morgen, K., Arnarsdottir, S., Bjornsdottir, G., Walters, G.B., Jonsdottir, G.A., Doyle, O.M., et al. (2014). CNVs conferring risk of autism or schizophrenia affect cognition in controls. Nature *505*, 361–366.

Steffen, A., Rottner, K., Ehinger, J., Innocenti, M., Scita, G., Wehland, J., and Stradal, T.E.B. (2004). Sra-1 and Nap1 link Rac to actin assembly driving lamellipodia formation. EMBO J. *23*, 749–759.

Stein, V., House, D.R.C., Bredt, D.S., and Nicoll, R.A. (2003). Postsynaptic density-95 mimics and occludes hippocampal long-term potentiation and enhances long-term depression. J. Neurosci. *23*, 5503–5506.

Steiner, P., Higley, M.J., Xu, W., Czervionke, B.L., Malenka, R.C., and Sabatini, B.L. (2008). Destabilization of the postsynaptic density by PSD-95 serine 73 phosphorylation inhibits spine growth and synaptic plasticity. Neuron *60*, 788–802.

Ster, J., Steuble, M., Orlando, C., Diep, T.-M., Akhmedov, A., Raineteau, O., Pernet, V., Sonderegger, P., and Gerber, U. (2014). Calsyntenin-1 regulates targeting of dendritic NMDA receptors and dendritic spine maturation in CA1 hippocampal pyramidal cells during postnatal development. J. Neurosci. *34*, 8716–8727.

Steward, O., and Worley, P.F. (2001). Selective targeting of newly synthesized Arc mRNA to active synapses requires NMDA receptor activation. Neuron *30*, 227–240.

Südhof (2008). Neuroligins and neurexins link synaptic function to cognitive disease. Nature *455*, 903–911.

Suetsugu, S., Miki, H., and Takenawa, T. (1999). Identification of two human WAVE/SCAR homologues as general actin regulatory molecules which associate with the Arp2/3 complex. Biochem. Biophys. Res. Commun. *260*, 296–302.

Suetsugu, S., Miki, H., Yamaguchi, H., and Takenawa, T. (2001). Requirement of the basic region of N-WASP/WAVE2 for actin-based motility. Biochem. Biophys. Res. Commun. *282*, 739–744.

Suetsugu, S., Hattori, M., Miki, H., Tezuka, T., Yamamoto, T., Mikoshiba, K., and Takenawa, T. (2002). Sustained activation of N-WASP through phosphorylation is essential for neurite extension. Dev. Cell *3*, 645–658.

Sullivan, P.F., Kendler, K.S., and Neale, M.C. (2003). Schizophrenia as a complex trait: evidence from a meta-analysis of twin studies. Arch. Gen. Psychiatry *60*, 1187–1192.

Sumita, K., Sato, Y., Iida, J., Kawata, A., Hamano, M., Hirabayashi, S., Ohno, K., Peles, E., and Hata, Y. (2007). Synaptic scaffolding molecule (S-SCAM) membrane-associated guanylate kinase with inverted organization (MAGI)-2 is associated with cell adhesion molecules at inhibitory synapses in rat hippocampal neurons. J. Neurochem. *100*, 154–166.

Tabuchi, K., Blundell, J., Etherton, M.R., Hammer, R.E., Liu, X., Powell, C.M., and

Südhof, T.C. (2007). A neuroligin-3 mutation implicated in autism increases inhibitory synaptic transmission in mice. Science *318*, 71–76.

Tahirovic, S., Hellal, F., Neukirchen, D., Hindges, R., Garvalov, B.K., Flynn, K.C., Stradal, T.E., Chrostek-Grashoff, A., Brakebusch, C., and Bradke, F. (2010). Rac1 regulates neuronal polarization through the WAVE complex. J. Neurosci. *30*, 6930–6943.

Takahashi, H., Katayama, K., Sohya, K., Miyamoto, H., Prasad, T., Matsumoto, Y., Ota, M., Yasuda, H., Tsumoto, T., Aruga, J., et al. (2012). Selective control of inhibitory synapse development by Slitrk3-PTPδ trans-synaptic interaction. Nat. Neurosci. *15*, 389–398.

Takenawa, and Suetsugu (2007). The WASP–WAVE protein network: connecting the membrane to the cytoskeleton. Nat. Rev. Mol. Cell Biol. *8*, 37–48.

Tam, G.W.C., Redon, R., Carter, N.P., and Grant, S.G.N. (2009). The role of DNA copy number variation in schizophrenia. Biol. Psychiatry *66*, 1005–1012.

Tam, G.W.C., van de Lagemaat, L.N., Redon, R., Strathdee, K.E., Croning, M.D.R., Malloy, M.P., Muir, W.J., Pickard, B.S., Deary, I.J., Blackwood, D.H.R., et al. (2010). Confirmed rare copy number variants implicate novel genes in schizophrenia. Biochem. Soc. Trans. *38*, 445–451.

Tan, H.-Y., Callicott, J.H., and Weinberger, D.R. (2007). Dysfunctional and compensatory prefrontal cortical systems, genes and the pathogenesis of schizophrenia. Cereb. Cortex *17 Suppl 1*, i171–i181.

Tavalin, S.J., Colledge, M., Hell, J.W., Langeberg, L.K., Huganir, R.L., and Scott, J.D. (2002). Regulation of GluR1 by the A-kinase anchoring protein 79 (AKAP79) signaling complex shares properties with long-term depression. J. Neurosci. *22*, 3044–3051.

Terunuma, M., Xu, J., Vithlani, M., Sieghart, W., Kittler, J., Pangalos, M., Haydon, P.G., Coulter, D.A., and Moss, S.J. (2008). Deficits in phosphorylation of GABA(A) receptors by intimately associated protein kinase C activity underlie compromised synaptic inhibition during status epilepticus. J. Neurosci. *28*, 376–384.

Ting, J.T., Peça, J., and Feng, G. (2012). Functional consequences of mutations in postsynaptic scaffolding proteins and relevance to psychiatric disorders. Annu. Rev. Neurosci. *35*, 49–71.

Torri, Akelai, Lupoli, Sironi, Amann-Zalcenstein, Fumagalli, Fiume, D., Ben-Asher, Kanyas, Cagliani, et al. (2010). Fine mapping of AHI1 as a schizophrenia susceptibility gene: from association to evolutionary evidence. FASEB J. *24*, 3066–3082.

Tretter, V., Jacob, T.C., Mukherjee, J., Fritschy, J.-M., Pangalos, M.N., and Moss, S.J. (2008). The clustering of GABA(A) receptor subtypes at inhibitory synapses is facilitated via the direct binding of receptor alpha 2 subunits to gephyrin. J. Neurosci. *28*, 1356–1365.

Tretter, V., Revilla-Sanchez, R., Houston, C., Terunuma, M., Havekes, R., Florian, C., Jurd, R., Vithlani, M., Michels, G., Couve, A., et al. (2009). Deficits in spatial memory correlate with modified {gamma}-aminobutyric acid type A receptor tyrosine phosphorylation in the hippocampus. Proc. Natl. Acad. Sci. U. S. A. *106*, 20039–20044.

Tretter, V., Kerschner, B., Milenkovic, I., Ramsden, S.L., Ramerstorfer, J., Saiepour, L., Maric, H.-M., Moss, S.J., Schindelin, H., Harvey, R.J., et al. (2011). Molecular basis of the γ-aminobutyric acid A receptor α3 subunit interaction with the clustering protein gephyrin. J. Biol. Chem. *286*, 37702–37711.

Triller, A., Cluzeaud, F., Pfeiffer, F., Betz, H., and Korn, H. (1985). Distribution of glycine receptors at central synapses: an immunoelectron microscopy study. J. Cell Biol. *101*, 683–688.

Truett, G.E., Heeger, P., Mynatt, R.L., Truett, A.A., Walker, J.A., and Warman, M.L. (2000). Preparation of PCR-quality mouse genomic DNA with hot sodium hydroxide and tris (HotSHOT). Biotechniques *29*, 52, 54.

Tu, J.C., Xiao, B., Naisbitt, S., Yuan, J.P., Petralia, R.S., Brakeman, P., Doan, A., Aakalu, V.K., Lanahan, A.A., Sheng, M., et al. (1999). Coupling of mGluR/Homer and PSD-95 complexes by the Shank family of postsynaptic density proteins. Neuron *23*, 583–592.

Turrigiano, G. (2011). Too many cooks? Intrinsic and synaptic homeostatic mechanisms in cortical circuit refinement. Annu. Rev. Neurosci. *34*, 89–103.

Tuz, K., Hsiao, Y.-C., Juárez, O., Shi, B., Harmon, E.Y., Phelps, I.G., Lennartz, M.R., Glass, I.A., Doherty, D., and Ferland, R.J. (2013). The Joubert syndrome-associated missense mutation (V443D) in the Abelson-helper integration site 1 (AHI1) protein alters its localization and protein-protein interactions. J. Biol. Chem. *288*, 13676–13694.

Twelvetrees, Yuen, Arancibia-Carcamo, Macaskill, Rostaing, Lumb, Humbert, Triller, Saudou, and Yan (2010). Delivery of GABAARs to Synapses Is Mediated by HAP1-KIF5 and Disrupted by Mutant Huntingtin. Neuron *65*, 53–65.

Tyagarajan, S.K., and Fritschy, J.-M. (2014). Gephyrin: a master regulator of neuronal function? Nat. Rev. Neurosci. *15*, 141–156.

Tyagarajan, S.K., Ghosh, H., Yévenes, G.E., Nikonenko, I., Ebeling, C., Schwerdel, C., Sidler, C., Zeilhofer, H.U., Gerrits, B., Muller, D., et al. (2011a). Regulation of GABAergic synapse formation and plasticity by GSK3beta-dependent phosphorylation of gephyrin. Proc. Natl. Acad. Sci. U. S. A. *108*, 379–384.

Tyagarajan, S.K., Ghosh, H., Harvey, K., and Fritschy, J.-M. (2011b). Collybistin splice variants differentially interact with gephyrin and Cdc42 to regulate gephyrin clustering at GABAergic synapses. J. Cell Sci. *124*, 2786–2796.

Tyagarajan, S.K., Ghosh, H., Yévenes, G.E., Imanishi, S.Y., Zeilhofer, H.U., Gerrits,

B., and Fritschy, J.-M. (2013). Extracellular signal-regulated kinase and glycogen synthase kinase 3β regulate gephyrin postsynaptic aggregation and GABAergic synaptic function in a calpain-dependent mechanism. J. Biol. Chem. *288*, 9634–9647.

Valnegri, P., Puram, S. V, and Bonni, A. (2015). Regulation of dendrite morphogenesis by extrinsic cues. Trends Neurosci. *38*, 439–447.

Vardi, N., Zhang, L.L., Payne, J.A., and Sterling, P. (2000). Evidence that different cation chloride cotransporters in retinal neurons allow opposite responses to GABA. J. Neurosci. *20*, 7657–7663.

Varoqueaux, F., Jamain, S., and Brose, N. (2004). Neuroligin 2 is exclusively localized to inhibitory synapses. Eur. J. Cell Biol. *83*, 449–456.

Vessey, and Karra (2007). More than just synaptic building blocks: scaffolding proteins of the post-synaptic density regulate dendritic patterning. J. Neurochem. *102*, 324–332.

Wang, H., Bedford, F.K., Brandon, N.J., Moss, S.J., and Olsen, R.W. (1999). GABA(A)-receptor-associated protein links GABA(A) receptors and the cytoskeleton. Nature *397*, 69–72.

Wang, H., Huang, Z., Huang, L., Niu, S., Rao, X., Xu, J., Kong, H., Yang, J., Yang, C., Wu, D., et al. (2012). Hypothalamic Ahi1 mediates feeding behavior through interaction with 5-HT2C receptor. J. Biol. Chem. *287*, 2237–2246.

Wang, H.-F., Shih, Y.-T., Chen, C.-Y., Chao, H.-W., Lee, M.-J., and Hsueh, Y.-P. (2011). Valosin-containing protein and neurofibromin interact to regulate dendritic spine density. J. Clin. Invest. *121*, 4820–4837.

Waters, A.M., and Beales, P.L. (2011). Ciliopathies: an expanding disease spectrum. Pediatr. Nephrol. *26*, 1039–1056.

Wearne, S.L., Rodriguez, A., Ehlenberger, D.B., Rocher, A.B., Henderson, S.C., and Hof, P.R. (2005). New techniques for imaging, digitization and analysis of three-dimensional neural morphology on multiple scales. Neuroscience *136*, 661–680.

Weng, L., Lin, Y.-F., Li, A.L., Wang, C.-E., Yan, S., Sun, M., Gaertig, M.A., Mitha, N., Kosaka, J., Wakabayashi, T., et al. (2013). Loss of Ahi1 affects early development by impairing BM88/Cend1-mediated neuronal differentiation. J. Neurosci. *33*, 8172–8184.

Westfall, Hoyt, Liu, Hsiao, Pierce, Page-McCaw, and Ferland (2010). Retinal degeneration and failure of photoreceptor outer segment formation in mice with targeted deletion of the Joubert syndrome gene, Ahi1. J. Neurosci. *30*, 8759–8768.

Whissell, P.D., Lecker, I., Wang, D.-S., Yu, J., and Orser, B.A. (2014). Altered expression of δGABAA receptors in health and disease. Neuropharmacology.

White, J.K., Gerdin, A.-K., Karp, N.A., Ryder, E., Buljan, M., Bussell, J.N., Salisbury, J., Clare, S., Ingham, N.J., Podrini, C., et al. (2013). Genome-wide generation and

systematic phenotyping of knockout mice reveals new roles for many genes. Cell *154*, 452–464.

Willert, K., and Nusse, R. (1998). Beta-catenin: a key mediator of Wnt signaling. Curr. Opin. Genet. Dev. *8*, 95–102.

Wu, L.L., and Zhou, X.F. (2009). Huntingtin associated protein 1 and its functions. Cell Adh. Migr. *3*, 71–76.

Wu, L.L., Fan, Y., Li, S., Li, X.-J., and Zhou, X.-F. (2010). Huntingtin-associated protein-1 interacts with pro-brain-derived neurotrophic factor and mediates its transport and release. J. Biol. Chem. *285*, 5614–5623.

Wu, X., Wu, Z., Ning, G., Guo, Y., Ali, R., Macdonald, R.L., De Blas, A.L., Luscher, B., and Chen, G. (2012). γ-Aminobutyric acid type A (GABAA) receptor α subunits play a direct role in synaptic versus extrasynaptic targeting. J. Biol. Chem. *287*, 27417–27430.

Wuchter, J., Beuter, S., Treindl, F., Herrmann, T., Zeck, G., Templin, M.F., and Volkmer, H. (2012). A comprehensive small interfering RNA screen identifies signaling pathways required for gephyrin clustering. J. Neurosci. *32*, 14821–14834.

Xiang, S., Nichols, J., Rajagopalan, K. V, and Schindelin, H. (2001). The crystal structure of Escherichia coli MoeA and its relationship to the multifunctional protein gephyrin. Structure *9*, 299–310.

Xiang, S., Kim, E.Y., Connelly, J.J., Nassar, N., Kirsch, J., Winking, J., Schwarz, G., and Schindelin, H. (2006). The crystal structure of Cdc42 in complex with collybistin II, a gephyrin-interacting guanine nucleotide exchange factor. J. Mol. Biol. *359*, 35–46.

Xu, Yang, Lin, Li, Cape, and Ressler (2010). Neuronal Abelson helper integration site-1 (Ahi1) deficiency in mice alters TrkB signaling with a depressive phenotype. Proc. Natl. Acad. Sci. U. S. A. *107*, 19126–19131.

Xu, B., Zang, K., Ruff, N.L., Zhang, Y.A., McConnell, S.K., Stryker, M.P., and Reichardt, L.F. (2000). Cortical degeneration in the absence of neurotrophin signaling: dendritic retraction and neuronal loss after removal of the receptor TrkB. Neuron *26*, 233–245.

Yan, C., Martinez-Quiles, N., Eden, S., Shibata, T., Takeshima, F., Shinkura, R., Fujiwara, Y., Bronson, R., Snapper, S.B., Kirschner, M.W., et al. (2003). WAVE2 deficiency reveals distinct roles in embryogenesis and Rac-mediated actin-based motility. EMBO J. *22*, 3602–3612.

Yang, Y., Higashimori, H., and Morel, L. (2013). Developmental maturation of astrocytes and pathogenesis of neurodevelopmental disorders. J. Neurodev. Disord. *5*, 22.

Yizhar, O., Fenno, L.E., Prigge, M., Schneider, F., Davidson, T.J., O'Shea, D.J., Sohal, V.S., Goshen, I., Finkelstein, J., Paz, J.T., et al. (2011). Neocortical

excitation/inhibition balance in information processing and social dysfunction. Nature *477*, 171–178.

Yoon, K.-J., Nguyen, H.N., Ursini, G., Zhang, F., Kim, N.-S., Wen, Z., Makri, G., Nauen, D., Shin, J.H., Park, Y., et al. (2014). Modeling a Genetic Risk for Schizophrenia in iPSCs and Mice Reveals Neural Stem Cell Deficits Associated with Adherens Junctions and Polarity. Cell Stem Cell *15*, 79–91.

Yu, T.W., Chahrour, M.H., Coulter, M.E., Jiralerspong, S., Okamura-Ikeda, K., Ataman, B., Schmitz-Abe, K., Harmin, D.A., Adli, M., Malik, A.N., et al. (2013). Using whole-exome sequencing to identify inherited causes of autism. Neuron *77*, 259–273.

Yu, W., Jiang, M., Miralles, C.P., Li, R.-W., Chen, G., and de Blas, A.L. (2007). Gephyrin clustering is required for the stability of GABAergic synapses. Mol. Cell. Neurosci. *36*, 484–500.

Yuste, R. (2015). The discovery of dendritic spines by Cajal. Front. Neuroanat. *9*, 18.

Zalfa, F., Giorgi, M., Primerano, B., Moro, A., Di Penta, A., Reis, S., Oostra, B., and Bagni, C. (2003). The fragile X syndrome protein FMRP associates with BC1 RNA and regulates the translation of specific mRNAs at synapses. Cell *112*, 317–327.

Zalfa, F., Eleuteri, B., Dickson, K.S., Mercaldo, V., De Rubeis, S., di Penta, A., Tabolacci, E., Chiurazzi, P., Neri, G., Grant, S.G.N., et al. (2007). A new function for the fragile X mental retardation protein in regulation of PSD-95 mRNA stability. Nat. Neurosci. *10*, 578–587.

Zhang (2005). A GIT1/PIX/Rac/PAK Signaling Module Regulates Spine Morphogenesis and Synapse Formation through MLC. J. Neurosci. *25*, 3379–3388.

Zhang, C., Atasoy, D., Araç, D., Yang, X., Fucillo, M. V, Robison, A.J., Ko, J., Brunger, A.T., and Südhof, T.C. (2010). Neurexins physically and functionally interact with GABA(A) receptors. Neuron *66*, 403–416.

Zhang, Y., Chen, K., Sloan, S.A., Bennett, M.L., Scholze, A.R., O'Keeffe, S., Phatnani, H.P., Guarnieri, P., Caneda, C., Ruderisch, N., et al. (2014). An RNA-Sequencing Transcriptome and Splicing Database of Glia, Neurons, and Vascular Cells of the Cerebral Cortex. J. Neurosci. *34*, 11929–11947.

Zhao, L., Wang, D., Wang, Q., Rodal, A.A., and Zhang, Y.Q. (2013a). Drosophila cyfip Regulates Synaptic Development and Endocytosis by Suppressing Filamentous Actin Assembly. PLoS Genet. *9*, e1003450.

Zhao, Q., Li, T., Zhao, X., Huang, K., Wang, T., Li, Z., Ji, J., Zeng, Z., Zhang, Z., Li, K., et al. (2013b). Rare CNVs and tag SNPs at 15q11.2 are associated with schizophrenia in the Han Chinese population. Schizophr. Bull. *39*, 712–719.

Zhou, J., and Parada, L.F. (2012). PTEN signaling in autism spectrum disorders. Curr. Opin. Neurobiol. *22*, 873–879.

Zhou, Q., Xiao, M., and Nicoll, R.A. (2001). Contribution of cytoskeleton to the

internalization of AMPA receptors. Proc. Natl. Acad. Sci. U. S. A. *98*, 1261–1266.

Zito, K., Scheuss, V., Knott, G., Hill, T., and Svoboda, K. (2009). Rapid functional maturation of nascent dendritic spines. Neuron *61*, 247–258.

Zuk, O., Schaffner, S.F., Samocha, K., Do, R., Hechter, E., Kathiresan, S., Daly, M.J., Neale, B.M., Sunyaev, S.R., and Lander, E.S. (2014). Searching for missing heritability: designing rare variant association studies. Proc. Natl. Acad. Sci. U. S. A. *111*, E455–E464.

van der Zwaag, B., Staal, W.G., Hochstenbach, R., Poot, M., Spierenburg, H.A., de Jonge, M. V, Verbeek, N.E., van 't Slot, R., van Es, M.A., Staal, F.J., et al. (2010). A co-segregating microduplication of chromosome 15q11.2 pinpoints two risk genes for autism spectrum disorder. Am. J. Med. Genet. B. Neuropsychiatr. Genet. *153B*, 960–966.

Appendix A

Dendritic morphology analysis

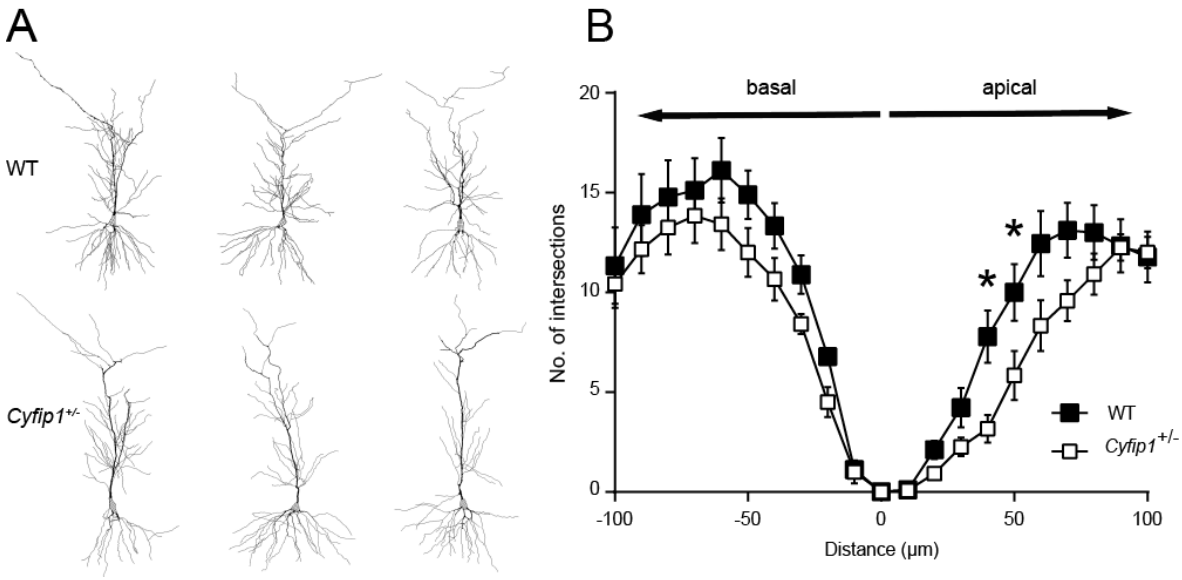

Figure A.1: Dendritic morphology of CA1 hippocampal neurons in adult CYFIP1$^{+/-}$ mice.

Golgi-stained CA1 neurons from *Cyfip1*$^{+/-}$ and WT littermate controls (P55–60) were traced to analyse dendritic morphology. **(A)** Example traces of *Cyfip1*$^{+/-}$ and WT neurons. **(B)** Sholl analysis indicates that *Cyfip1*$^{+/-}$ neurons are significantly less complex within 100µm from the soma, in the apical compartment and trending towards significance in the basal compartment, compared with WT control neurons (n=9–12 cells per condition, 22-way ANOVA, *p<0.05). *Experiment carried out by Dr. Manav Pathania.*

Appendix B

Schizophrenia screen data

Table B.1: Weighted burden analysis output for *Cyfip1* in the UK10K dataset

Locus	Unaffected Genotypes				Case Genotypes				Weight	Variant Effect	Allele Change	Residue Change	Functional Prediction	p value
	AA	AB	BB	MAF	AA	AB	BB	MAF						
22928169	982	0	0	0	1391	1	0	0.000359	24.98	non-synonymous	cTg/cCg	L/P	probably damaging	0.401
22928190	981	1	0	0.000509	1392	0	0	0	24.98	non-synonymous	tCc/tTc	S/F	probably damaging	0.234
22933663	950	32	0	0.016293	1355	37	0	0.01329	11.78	splice-site			unknown	0.394
22933749	981	1	0	0.000509	1392	0	0	0	12.49	splice-site			possibly damaging	0.234
22933848	982	0	0	0	1391	1	0	0.000359	24.98	non-synonymous	aCg/aTg	T/M	possibly damaging	0.401
22940721	979	3	0	0.001527	1391	1	0	0.000359	12.46	splice-site			unknown	0.172
22940807	982	0	0	0	1390	2	0	0.000718	24.96	non-synonymous	Cgc/Tgc	R/C	possibly damaging	0.235
22947019	982	0	0	0	1390	2	0	0.000718	24.96	non-synonymous	aGc/aAc	S/N	benign	0.235
22947045	982	0	0	0	1391	1	0	0.000359	24.98	non-synonymous	Cgc/Tgc	R/C	probably damaging	0.401
22954273	982	0	0	0	1391	1	0	0.000359	24.98	non-synonymous	Gcc/Acc	A/T	benign	0.401
22954276	982	0	0	0	1391	1	0	0.000359	24.98	non-synonymous	Atc/Gtc	I/V	possibly damaging	0.401
22954334	981	1	0	0.000509	1392	0	0	0	24.98	non-synonymous	cCg/cTg	P/L	benign	0.234
22955174	981	1	0	0.000509	1392	0	0	0	24.98	non-	aCg/aTg	T/M	possibly	0.234

										synonymous			damaging	
22956327	979	3	0	0.001527	1391	0	0	0	24.94	non-synonymous	Ccc/Tcc	P/S	unknown	0.039
22956358	982	0	0	0	1391	1	0	0.000359	24.98	non-synonymous	tCt/tTt	S/F	unknown	0.401
22960795	981	1	0	0.000509	1392	0	0	0	12.49	splice-site			probably damaging	0.234
22962425	982	0	0	0	1391	1	0	0.000359	12.49	splice-site			unknown	0.401
22962514	981	1	0	0.000509	1392	0	0	0	24.98	non-synonymous	cGc/cAc	R/H	possibly damaging	0.234
22963782	982	0	0	0	1391	1	0	0.000359	24.98	non-synonymous	Cgt/Agt	R/S	benign	0.401
22963816	982	0	0	0	1385	7	0	0.002514	24.85	non-synonymous	tAt/tGt	Y/C	benign	0.026
22963869	976	6	0	0.003055	1377	15	0	0.005388	24.56	non-synonymous	Ata/Gta	I/V	probably damaging	0.234
22969154	978	4	0	0.002037	1387	3	0	0.001079	12.43	splice-site			unknown	0.397
22969215	982	0	0	0	1391	1	0	0.000359	24.98	non-synonymous	cGg/cAg	R/Q	benign	0.401
22969251	982	0	0	0	1391	1	0	0.000359	24.98	non-synonymous	cGg/cAg	R/Q	possibly damaging	0.401
22969353	982	0	0	0	1391	1	0	0.000359	24.98	non-synonymous	tCt/tGt	S/C	probably damaging	0.401
22990053	981	1	0	0.000509	1392	0	0	0	12.49	splice-site			unknown	0.234
22990087	975	7	0	0.003564	1371	21	0	0.007543	24.41	non-synonymous	Ggc/Agc	G/S	benign	0.078
22990190	981	1	0	0.000509	1392	0	0	0	24.98	non-	gTc/gCc	V/A	benign	0.234

										synonymous				
22993010	982	0	0	0	1391	1	0	0.000359	12.49	splice-site			unknown	0.401
22993121	954	27	1	0.014766	1340	51	1	0.019037	23.3	non-synonymous	gCc/gTc	A/V	possibly damaging	0.266
22993158	981	1	0	0.000509	1392	0	0	0	12.49	splice-site			unknown	0.234
22997793	977	5	0	0.002546	1386	6	0	0.002155	12.38	splice-site			unknown	0.783
22999320	981	1	0	0.000509	1390	2	0	0.000718	12.47	splice-site			unknown	0.778
22999403	980	2	0	0.001018	1391	1	0	0.000359	24.94	non-synonymous	aTg/aCg	M/T	benign	0.373
22999408	981	1	0	0.000509	1392	0	0	0	24.98	non-synonymous	Gag/Cag	E/Q	possibly damaging	0.234
22999457	982	0	0	0	1391	1	0	0.000359	24.98	non-synonymous	cGc/cAc	R/H	benign	0.401
23000084	981	1	0	0.000509	1392	0	0	0	12.49	splice-site	Cct/Gct	P/A	benign	0.234
23000091	982	0	0	0	1390	2	0	0.000718	12.48	splice-site			unknown	0.235
23002876	982	0	0	0	1391	1	0	0.000359	12.49	splice-site			benign	0.401
23002888	982	0	0	0	1391	1	0	0.000359	24.98	non-synonymous	Atg/Gtg	M/V	benign	0.401

Output from SCOREASSOC for the analysis of *Cyfip1* using the narrow category of variants and treating SCZ subjects as cases. The table shows genotype counts, frequencies, weights and effects for each variant. The weighted scores were calculated for each subject and the means compared. Mean scores unaffected = 1.904, cases = 2.415, *p = 0.0487)